UNIVERSITÉ DE MONTRÉAL

BIOBASED PLA/PA11 BLENDS AND THE INCORPORATION OF CELLULOSE NANOCRYSTAL

VAHID HESHMATI

DÉPARTEMENT DE GÉNIE CHIMIQUE

ÉCOLE POLYTECHNIQUE DE MONTRÉAL

THÈSE PRÉSENTÉE EN VUE DE L'OBTENTION

DU DIPLÔME DE PHILOSOPHIAE DOCTOR

(GÉNIE CHIMIQUE)

MAI 2017

UNIVERSITÉ DE MONTRÉAL

ÉCOLE POLYTECHNIQUE DE MONTRÉAL

Cette thèse intitulée:

BIOBASED PLA/PA11 BLENDS AND THE INCORPORATION OF CELLULOSE NANOCRYSTAL

Présentée par : HESHMATI Vahid

en vue de l'obtention du diplôme de : Philosophiae Doctor

a été dûment acceptée par le jury d'examen constitué de :

M. CICOIRA Fabio, Ph. D., président

M. FAVIS Basil, Ph. D., membre et directeur de recherche

M. KAMAL Musa, Ph. D., membre et codirecteur de recherche

M. AJJI Abdellah, Ph. D., membre

M. RIEDL Bernard, Ph. D., membre

DEDICATION

To my Family

ACKNOWLEDGEMENTS

Firstly, I would like to express my sincere gratitude to my supervisor Prof. Basil Favis for the continuous support, motivation, and immense knowledge. I truly enjoyed the freedom you provided in my research endeavors. I would like to thank you for encouraging my teaching aspiration and for helping me to grow as a research scientist and a teacher. Your support, inspiration, advices and belief in me, made me less nervous when I started teaching in French.

I would like to thank my cosupervisor Prof. Musa Kamal for his insightful discussion particularly in the last two part of my work. Your advice on both research as well as on my career have been priceless.

Thanks to Prof. Fabio Cicoira, Prof. Abdellah Ajji and Prof. Bernard Riedl for taking part in my thesis committee.

A special word of thanks is owed to the polymer blend research group: Sepehr, Ata, Nima, Ebrahim, Ali and Jun. A deepest thanks goes to Ali for his insightful discussion and thoughtful opinion.

My special thanks goes to my best friends; Khashayar, Mahdi, Reza, Behzad, Peyman Y, Amisaeed, Saeed R, Farid and Hadi. I would never forget all the beautiful moments I had with you guys during years of my studies. I would also like to thank my friends: Hajer, El-mahdi, Raziyeh, Violete, Helia, Davood, Fatemeh, Teodoara, Ata, Shervin, Mounia, Amir, Amirhosein, Melissa, Krista, Reza, Marilyne and Richard. I greatly value your friendship and I deeply appreciate your help.

I would also like to thank the technical and administrative staff of the Chemical Engineering Department of Ecole Polytechnique de Montréal.

Most importantly to my parents: you have filled my life with love and compassion, you mean the world to me, thank you for all of your love and support. To my beloved sister: there is no friend better than a sister and there is no sister better than you. To my dear brothers: you are the purest form of love and friendship, thank you for being there for me, you are simply amazing. To dear Hamed: I am very grateful to have such a wonderful brother-in law, thank you for being part of our family.

RÉSUMÉ

Le mélange de polymère et la plastification sont connus comme deux stratégies majeures pour améliorer la ténacité du poly (acide lactique) (PLA). Cependant, l'étude de la combinaison de ces deux méthodes est absente de la littérature. Le mélange de PLA avec d'autres bioplastiques est une stratégie qui permet d'améliorer les propriétés mécaniques tout en conservant un aspect biomatériau. D'autre part, la plastification du PLA, a été la plus prometteuse pour améliorer la mobilité des chaînes du PLA. Cependant, le principal inconvénient de la plastification du PLA, est la baisse du module et de la résistance à la traction par rapport au PLA pur. L'incorporation de nano-inclusions solides dans un mélange polymère-polymère est une voie bien connue pour développer des matériaux avec un bon équilibre de ténacité/rigidité. Dans cette dissertation, la morphologie et les propriétés mécaniques des mélanges PLA/Polyamide 11 (PA11) et la localisation de la nanocellulose cristalline dans le mélange sont étudiés.

Dans la première partie de ce travail, une étude systématique de la tension interfaciale et du développement morphologique du PLA/PA11 est effectuée. Il a été démontré que la tension interfaciale dans les mélanges PLA/PA11 dans des conditions dynamiques mesurée par la technique du triangle de Neuman (3.2 mN/m) est nettement inférieure à celle mesurée dans des conditions statiques par la méthode de rupture du fil (5.8 mN/m) et la rétraction de fibre intégrée (5.4 mN/m). Dans des conditions de mélange dynamiques, les analyses morphologiques et thermiques indiquent sans ambiguïté que le système PLA/PA11 se comporte comme un système hautement interactif interfacialement compatibilisé. Il a été démontré que la mobilité restreinte de la chaîne de PLA est la raison principale de l'écart observé entre le comportement statique et dynamique des mélanges PLA/PA11. L'amélioration de la mobilité de la chaîne de PLA grâce à l'ajout de 5% de plastifiant PEO a entraîné une tension interfaciale significativement plus faible et même une coalescence supplémentaire supprimée sous un mélange dynamique à 30 et 40% de phase mineure. Ces résultats sont importants car ils indiquent clairement que, même si les polymères peuvent avoir des interactions interfaciales, une mobilité de chaîne suffisante est nécessaire pour que ces interactions entrent en jeu.

Dans la deuxième partie de ce projet, l'impact profond de la mobilité contrôlée de la chaîne de PLA sur les propriétés mécaniques des mélanges PLA/PA11 est étudié. Il a été démontré que l'amélioration de la ductilité du PLA améliorée suite à l'ajout d'une quantité optimale d'oxyde de

polyéthylène (PEO), affecte de manière significative les propriétés mécaniques des mélanges PLA/PA11. Dans le mélange (PLA-15PEO)/PA11 50/50 vol%, une amélioration remarquable des propriétés mécaniques est observée avec des spécimens démontrant 17.5 fois la résistance aux chocs du PLA pur et 3 fois celui du PA11 pur. En outre, une amélioration exceptionnelle de l'allongement à la rupture à 275% a été enregistrée pour le même mélange, contre 5% pour le PLA et 6% pour le PLA/PA11. Les rôles critiques de la concentration de PEO, la séparation des phases de PLA/PEO, les interactions interfaciales et la cavitation interfaciale en tant que paramètres principaux contrôlant ce comportement de renforcement sont discutés en détail. Contrairement au PEO, le PEG n'a aucun effet en tant que plastifiant sur le durcissement du mélange PLA/PA11. Ceci est attribué à une séparation de phase PLA/PEG à des concentrations inférieures de PEG que pour PEO. Ces résultats sont d'une importance significative car ils indiquent clairement que la mobilité contrôlée des chaîne de PLA grâce à l'utilisation d'une concentration optimale d'un plastifiant approprié est une approche hautement efficace pour le développement de mélanges PLA/PA11 à haute performance.

La troisième partie de ce travail présente, pour la première fois, la localisation thermodynamiquement stable des nanocristaux de cellulose (CNC) dans un mélange d'acide polylactique)/bio-polyamide11 (PA11) préparé avec une combinaison de dissolution du solvant, de coulée et de mélange à l'état fondu. La microscopie à force atomique (AFM) et l'analyse de rhéologie démontrent un niveau élevé de dispersion des CNC. Les CNC sont alimentés dans les mélanges à travers la préparation de mixtures PLA/CNC ou PA11/CNC par mélange à l'état fondu dans un mélangeur interne. Les particules CNC dans le mélange PLA/PA11 restent dans la phase PA11 lorsqu'elles sont ajoutées dans les mélanges à travers la mixture PA11/CNC. De manière significative, dans les systèmes ternaires dans lesquels les CNC sont introduits dans le mélange à travers la mixture PLA/CNC, les nanoparticules migrent de la phase de PLA qui est thermodynamiquement moins stable vers PA11, et ce indépendamment du fait que le PLA/PA11 forme une phase dispersée dans la matrice (PLA/PA11 70/30, 30/70 vol%) ou une morphologie co-continue (PLA/PA11 50/50 vol%). La localisation stable des CNC dans la phase PA11 est en accord avec les prédictions thermodynamiques. La morphologie de la phase dispersée n'est pratiquement pas affectée par l'addition de 3 wt% de CNC, ce qui est attribuée au niveau déjà faible de coalescence dans ces compositions. Cependant, l'addition de seulement 1 wt% de CNC au mélange co-continu PLA/PA11 50/50 vol%, avec le plus haut taux de coalescence, diminue

considérablement le diamètre de la taille des pores de 13 μm à 3 μm. Il a été supposé que la relaxation retardée des domaines PA11 remplis par les CNC, est à l'origine cette réduction de coalescence.

La dernière partie de ce travail rapporte le contrôle de la localisation stable des nano cristaux de cellulose (CNC) dans la phase PLA dans les mélanges PLA/PA11. Une stratégie de traitement versatile est optimisée en combinant l'homogénéisation-lyophilisation afin de préparer une mixture PEO/CNC. La mixture PEO/CNC préparé est par la suite incorporé dans des mélanges PLA/PA11 en utilisant deux stratégies de mélange différentes. La microscopie à force atomique (AFM) démontre une dispersion individuelle de nanoéchelle de CNC avec une épaisseur de 10-20 nm dans des mélanges PEO, PLA-PEO et (PLA-PEO)/A11 qui se situent dans la même gamme de nanoparticules CNC individuelles. Les particules CNC se localisent sélectivement dans la phase PA11 dans un système classique PLA/PA11/CNC ternaire. Cependant, les analyses SEM et AFM dans cette étude montrent la localisation stable presque exclusive des particules CNC revêtues de PEO dans la phase PLA, que la mixture PEO/CNC soit prémélangé avec PLA ou PA11. Il est suggéré que les fortes interactions entre les particules de CNC et PEO combinées à la miscibilité de PLA/PEO facilitent la localisation de la CNC recouverte de PEO dans la phase PLA. La localisation de 2 wt% de CNC dans la phase PLA-PEO diminue la taille des pores du mélange co-continu de 11 à 4 μm. Cependant, lorsque la CNC est sélectivement localisée dans la phase PA11, un plus grand effet de coalescence réduite est observé. Ceci est lié à une structure de réseau CNC plus développée dans le dernier cas au même chargement CNC. Les résultats de cette partie indiquent une stratégie pour la ségrégation de la CNC en PLA. Ainsi, il est possible d'avoir un degré élevé de contrôle sur la localisation CNC dans les mélanges PLA/PA11.

ABSTRACT

Polymer blending and plasticization are known as two major strategies in poly(lactic acid) (PLA) toughening. A combination of these two methods, however, is lacking in the literature. The blending of PLA with other bio-plastics is a strategy that allows for tuning the mechanical properties while still maintains a bio-material. PLA plasticization on the other hand has shown the greatest promise in enhancing PLA chain mobility. The main drawback of PLA plasticization, however, is the drop in the modulus and tensile strength compared to neat PLA. Incorporation of solid nano-inclusions into polymer-polymer blend is a well-known pathway for engineering materials with a good toughness/stiffness balance. In this dissertation, the morphology and mechanical properties of PLA/PA11 blends and the localization of crystalline nanocellulose in the blend are studied.

In the first part of this work, a systematic study of the interfacial tension and morphology development of PLA/PA11 is reported. It is shown that the interfacial tension in PLA/PA11 blends under dynamic conditions measured by the Neuman Triangle technique (3.2 mN/m) is significantly lower than that measured under static conditions by the breaking thread (5.8 mN/m) and imbedded fiber retraction (5.4 mN/m) methods. Under dynamic mixing conditions, morphological and thermal analysis unambiguously indicate that the PLA/PA11 system is behaving as a highly interacting interfacially compatibilized system. It is shown that the limited PLA chain mobility is the main reason for the observed discrepancy between the static and dynamic behavior of PLA/PA11 blends. Enhancing the PLA chain mobility through the addition of 5% PEO plasticizer results in a significantly lower interfacial tension and even further suppressed coalescence under dynamic mixing at 30 and 40 vol% minor phase. These results are important since they clearly indicate that even if polymers may have the potential for interfacial interactions, sufficient chain mobility is necessary in order for those interactions to come into play.

In the second part of this project, the profound impact of controlled PLA chain mobility on the mechanical properties of PLA/bio-PA11 blends, is studied. It is shown that enhanced PLA ductility due to the addition of an optimal amount of polyethylene oxide (PEO) significantly affects the mechanical properties of PLA/PA11 blends. In the (PLA-15PEO)/PA11 50/50 vol% blend a remarkable improvement in mechanical properties is observed with specimens

demonstrating 17.5 times the impact strength of the neat PLA and 3 times that of neat PA11. Also an exceptional improvement in elongation at break at 275% is found for the same blend, as compared to 5% for the PLA and 6 % for PLA/PA11. The critical roles of PEO concentration, PLA/PEO phase separation, interfacial interactions and interfacial debonding/cavitation as the main parameters controlling this toughening behavior are discussed in detail. In contrast to PEO, PEG as a plasticizer has no effect on the toughening of PLA/PA11 blend. This is attributed to a PLA/PEG phase separation at lower PEG concentrations than for PEO. These results are of significant importance since they clearly indicate that controlled PLA chain mobility through the use of an optimal concentration of an appropriate plasticizer is a highly effective approach towards the development of high performance PLA/PA11 blends.

The third part of this work presents, for the first time, the thermodynamically stable localization of cellulose nanocrystal (CNC) into poly (lactic acid)/bio-polyamide11 (PA11) blends prepared with a combination of solvent dissolution, casting and melt mixing. Atomic force microscopy (AFM) and rheology analysis demonstrate a high level of CNC dispersion using this technique. CNC is fed into the blends through prepared PLA/CNC or PA11/CNC mixtures via melt mixing in an internal mixer. CNC particles in the PLA/PA11 blend remain in the PA11 phase when they are added into the blends through the PA11/CNC mixture. Significantly, in the ternary systems in which CNCs are fed into the blend through the PLA/CNC mixture, the nanoparticles migrate from the less thermodynamically stable PLA phase toward PA11 irrespective of whether the PLA/PA11 forms a matrix/dispersed phase (PLA/PA11 70/30, 30/70 vol%) or a co-continuous morphology (PLA/PA11 50/50 vol%). The stable localization of CNC in the PA11 phase is in good agreement with thermodynamic predictions. The dispersed phase morphology is virtually unaffected by the addition of up to 3 wt% CNC which is attributed to the already low level of coalescence in these compositions. However, addition of only 1 wt% CNC to the PLA/PA11 50/50 vol% co-continuous blend, with the highest level of coalescence, dramatically diminishes the pore size diameter from 13 μm to 3 μm. It is postulated that the retarded relaxation of the CNC filled PA11 domains dominates this coalescence reduction.

The last part of this work, reports on the control of the stable localization of cellulose nanocrystal (CNC) in the PLA phase in melt processed poly (lactic acid) (PLA)/bio-polyamide11 (PA11) blends. A versatile processing strategy is optimized combining homogenization-freeze drying in order to prepare a PEO/CNC mixture. The prepared PEO/CNC mixture is then incorporated into

PLA/PA11 blends in two different mixing strategies. Atomic force microscopy (AFM) demonstrates an individual nano-scale dispersion of CNCs with a thickness of 10-20 nm in PEO, PLA-PEO and (PLA-PEO)/PA11 blends which is in the same range of individual CNC nanoparticles. CNC particles selectively localize in PA11 phase in a classic PLA/PA11/CNC ternary systems. However, SEM and AFM analysis in this study show the almost exclusive stable localization of the PEO-coated CNC particles in the PLA phase whether PEO/CNC mixture is premixed with PLA or PA11. It is suggested that the strong interactions between PEO and CNC particles combined with PLA/PEO miscibility facilitate the localization of PEO-coated CNC in the PLA phase. The localization of 2 wt% CNC in the PLA-PEO phase diminishes the pore size of the co-continuous blend from 11 to 4 μm. However, when CNC is selectively localized in the PA11 phase a more than double effect of reduced coalescence is observed. This is related to a more highly developed CNC network structure in the latter case at the same CNC loading. The results in this part indicates a strategy for the segregation of CNC into PLA. Thus, it is possible to have a high degree of control over CNC localization in PLA/PA11 blends.

TABLE OF CONTENTS

LIST OF TABLES

LIST OF FIGURES

LIST OF SYMBOLS AND ABBREVIATIONS

Symbols:

α	amplitude of distortion
Ca	Capillary number
μ	chemical potential
G^*	complex modulus
θ_e	contact angle
$h_{critical}$	Critical thickness of film between two drops in rupture
ρ	density of polymers
D	diameter
p	dispersed phase/matrix viscosity ratio
γ_i^d	dispersive component of surface tension
η_e	effective viscosity
N_1	first normal stress difference
χ_{AB}	Flory-Huggins interaction parameter
ω	frequency
G	Gibbs free energy
γ_{ij}/γ	interfacial tension
$G"$	loss modulus
M_w	molecular weight of the polymers
n	number of moles
γ_i^p	polar component of surface tension
P_c	probability of the droplet collision
R	radius

γ	shear rate
G'	storage modulus
γ	surface/interfacial tension
Ω	Tomotika function
η	viscosity
φ	volume fraction
η_0	zero shear viscosity

Abbreviations:

ABS	Acrylonitrile-butadiene-styrene
AFM	Atomic force microscopy
ATBC	Acetyl tri-n-butyl citrate
BT	Breaking thread
BBSA	N-Butylbenzene sulfonamide
CNC	Cellulose Nanocrystal
CNT	Carbon Nanotube
DMF	Dimethyleformamide
DSC	Differential scanning calorimetry
EPDM	Ethylene-propylene-diene terpolymer
EPR	Ethylene-propylene-rubber
EVA	Ethylene-co-vinyl acetate
FTIR	Fourier transform infrared spectroscopy
HDPE	High density polyethylene
HDT	Heat deflection temperature
HIPS	High Impact Polystyrene

HPH	High pressure homegenizer
IFR	Imbedded fiber retraction
MA	Maleic Anhydride
MCC	Micro Crystalline cellulose
NT	Neumann triangle
PA11	Polyamide 11
PA6	Polyamide 6
PBAT	Poly(butylene adipate-co-terephthalate)
PBS	Poly(butylene succinate)
PBT	Polybutylene terephthalate
PHB	Poly([(R)-3-hydroxybutyrate]
PHBV	Poly(3-hydroxybutyrate-co-3-hydroxyvalerate)
PC	Polycarbonate
PCL	Polycaprolactone
PDLA	Poly(D,L-lactic acid)
PE	Polyethylene
PEBA	Poly(ether-b-amide)
PEG	Polyethylene glycol
PEO	Poly(ethylene oxide)
PHBV	Poly(3-hydroxybutyrate-co-hydroxyvalerate)
PLA	Polylactide
PLLA	Poly(L-lactic acid)
PMMA	Polymethyl methacrylate
POE	Polyethylene-octene elastomer
PP	Polypropylene

PPD	Poly(para-dioxanone)
PPG	Poly(propylene glycol)
PS	Polystyrene
SAN	Styrene acrylonitrile resin
SBR	Styrene-butadiene rubber
SEB	Styrene-(ethylene-butylene) diblock
SEBS	Styrene-ethylene/butylene-styrene copolymer
SEM	Scanning electron microscopy
SMA	Styrene-maleic anhydride
TCP	1,2,3-trichloropropane
TEM	Transmission Electron Microscopy
THF	Tetrahydrofuran
TPS	Thermoplastic starch
TPU	Thermoplastic polyurethane

CHAPTER 1 INTRODUCTION AND OBJECTIVES

1.1 Introduction

Due to the environmental concerns and limited petroleum resources, the development of high performance biomaterials as a replacement for conventional petroleum based polymers has gathered significant interest in recent years [1], [2]. Bioplastics market is expected to grow at an annual growth rate of 10.8% between 2015 and 2020 [3]. High production cost and poor thermo-mechanical performance of bioplastics, however, limit their applications compared to the commodity polymers [3], [4].

Poly(lactic acid) (PLA) a biopolymer derived from renewable resources is known as one the most promising bio-plastic candidates [1], [5]. Apart from its biocompatibility, wide biological-medical application, compostability and its easier waste management, PLA has good mechanical properties (high strength and modulus) compared to those of many conventional polymers [5], [6]. However PLA suffers from inherent brittleness, poor impact strength, small deformation at break and low heat deflection temperature [5], [7]. Enhancing PLA mechanical properties using different strategies including plasticization, copolymerization and blending have been widely reported [2], [8]–[10]. PLA toughening, especially modification of impact toughness via melt blending with various bio and synthetic polymers such as poly(butylenes-succinate) [7], [11], poly(butylene adipate-co-terephtalate) [12], thermoplastic starch[13], polycaprolactone [13], polycarbonate [14] and polyethylene [15], [16] has received a lot of attention. In this area blending with other bioplastics is a versatile and efficient approach which allows tuning the mechanical properties while offers a completely biomaterial with a minimum carbon footprint [6], [12], [17].

Polyamide11 (PA11) being derived from castor oil is a high-performance, semi-crystalline biopolymer with interesting elongation at break and Izod impact strength [18], [19]. These properties are just those lacking in PLA. Moreover, due to the presence of polar functional groups in polyamides and polyesters, PA11 and PLA could potentially interact during blending [20], [21]. From this point of view a PLA/PA11 blend has the potential to generate a new biomaterial with unique advantages. Although both PLA and PA11 have been commercialized, only a few studies have been reported considering this unique system [6], [22]–[24]. In all of

these studies, many aspects of the morphology, coalescence, continuity development and interfacial properties of PLA/PA11 blends, remain unclear or contradictory.

Plasticization has long been known as an efficient approach in enhancing flexibility and ductility of glassy polymers. An efficient plasticizer for PLA, has to diminish dramatically the glass transition of PLA while being nonvolatile, non-toxic and should exhibit minimal migration during aging [10]. PEO has shown the greatest promise as a plasticizer for PLA, as it provides the highest increase in elongation at break with the minimal decrease in the tensile strength [7]. To the best of our knowledge, the combination of blending and plasticization in PLA toughening has not been studied in the literature.

The main drawback of PLA plasticization, however, is the drop in the modulus and tensile strength compared to neat PLA. Incorporation of solid nano-inclusions into polymer-polymer blend is a well known pathway for engineering materials with a reasonable toughness/stiffness balance [25]–[30]. However, controlling the morphology of polymer-polymer blends with solid inclusion is challenging. Not only the size, shape and interfacial characteristics of the polymer components but also the dispersion and localization of the nanoparticle have to be examined [27], [28], [30]. Desired properties of the final product define the nature and size of the solid particle in these composites. Therefore, in order to design a completely green ternary system, we are limited to biobased reinforcement.

Owing to their superior mechanical properties, low density, renewability and low cost, cellulose nanocrystal (CNC) offers the potential of generating new products [31]–[33]. With a young modulus higher than 100 GPa and a high specific surface area it has the potential to substantially enhance polymers properties at low content [33]. In recent years a lot of researches have been made to add CNC particles into polymers through solvent casting/evaporation or a combination of both [34]–[38]. Study the effect of controlled localization of CNC particles in polymer-polymer blends, however, is lacking in the literature.

Achieving a proper homogenous dispersion of CNC within a polymer matrix is the main challenge in preparation of CNC nanocomposites [31], [39]. Dispersing CNC in an adequate organic medium with respect to matrix has shown to be an effective processing alternative for polymer/CNC systems. However solvent dissolution technique is limited because only a few organic solvents provide high level of CNC dispersion. In addition this approach becomes much

more limited when applied to polymer-polymer blending due to the lack of common solvents. A combination of solvent dissolution and melt mixing could potentially ensure a good level of dispersion without degrading CNC particles in polymer blends. Another promising approach is the incorporating CNC particles into melt processed polymer blends through a mixture of a water soluble polymer and CNC which is miscible with one of the components [33], [40]–[42]. Exceptional dispersion of CNC particles in water-soluble polymers such as polyethylene oxide (PEO) has been reported [40], [43], [44]. Considering the aforementioned the main objectives of this work are presented in the following section.

1.2 Objectives

The main objective of this project is *to Study the morphology-properties relationship in biobased PLA/PA11 blends and the incorporation of cellulose nanocrystal (CNC).* The following specific objectives are thus defined as the main landmarks to achieve the main objective of this work:

- Study the morphology and interfacial development in PLA/PA11 biobased blends including the region of dual phase continuity.

- Examine the potential of enhanced PLA chain mobility through plasticization as a route to yield high performance mechanical properties in PLA/PA11 blends.

- Develop a technique to generate well dispersed cellulose nanocrystal (CNC) in PLA/PA11 bioblends through melt mixing and to examine the effect of selective localization of the CNC on the blend morphology.

- Develop a strategy to control the localization of finely dispersed CNC particles in the PLA phase in melt processed PLA/PA11 blends.

CHAPTER 2 LITERATURE REVIEW

2.1 Bioplastics

Governments commitment to decrease energy consumption and carbon dioxide emission, corporate environmental responsibilities and public attitude for "going green" have driven a lot of interest in biopolymers. Biopolymers are newly emerging plastics which are projected to completely replace commodity plastics. Bioplastics are generally categorized into three main groups:

a) Biobased or partially biobased polymers which are not biodegradable or compostable such as biopolyamide 11 (bio-PA11) or biopolyethylene (bio-PE).

b) Polymers which are biobased and biodegradable (or compostable) such as polyhydroxyalkanoate (PHA), starch and poly(lactic acid) PLA.

c) Petroleum-based polymers which are biodegradable (or compostable) such as poly(butylene succinate) PBS, poly(butylene adipate-co-terephthalate) PBAT and polycaprolactone (PCL).

According to ASTM D6866 standard, when a substantial part of carbons in a polymeric material is from renewable resources it is considered as a biopolymer. Biodegradable on the other hand refer to materials that degrades under specific conditions. Based on the ASTM D-6400 standard a biodegradable polymer undergoes 60% degradation in a lab within 180 days. According to EN 13432 standard this condition is 90% degradation threshold within 180 days.

In spite of the increasing production rate, biopolymers still comprise relatively small part of the global plastic production. The worldwide capacity of biobased plastics is expected to increase from 2.33 Mt in 2013 to 3.45 Mt in 2020 [4]. One of the most important bioplastics in terms of production capacity is PLA with 0.15 Mt which is estimated to increase to 0.8 Mt by 2020. Although enhancing the production capacity and improving production technology of biopolymers will possibly decrease their final cost, the poor mechanical performance of these polymers will still limit their applications. Brittleness, low barrier properties, low thermal stability, thermal degradability and processing window sensitivity are among the most important weaknesses of biopolymers [45]. Elongation at break and modulus and of some bioplastics are shown in Figure 2.1. Almost all biopolymer suffer from a low elongation at break or low modulus which limits their applications.

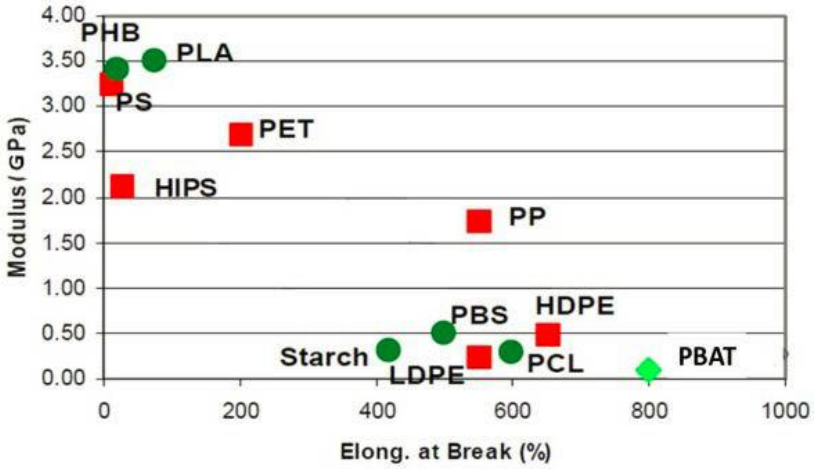

Figure 2.1. Elongation at break and modulus of some of bioplastics (Green symbols) and conventional polymers (red symbols).

2.1.1 Poly (lactic acid)

Poly(lactic acid) is a biodegradable/compostable aliphatic polyester, derived from renewable resources, which has gathered a lot of attention over the last decades mainly because of high modulus and tensile strength, reasonable price and availability in the market [5], [46]–[48]. Typically, PLA is a rigid semi-crystalline polymer with an elastic modulus of 2.5-4 GPa, a tensile strength of 50-70 MPa and an elongation at break of 2-6% [49]. PLA is one of the few biopolymers that has a tensile strength comparable with the conventional polymers such as polyethylene terephthalate (PET) and polystyrene (PS). The main drawback of PLA are low barrier properties, inherent brittleness (low impact strength and elongation at break) and low crystallization rate [46], [47]. Rasal et al. [8] and Anderson et al. [7] in separate studies reviewed different strategies for PLA toughening such as, plasticization, copolymerization, variation of the D and L ratio and blending with other biopolymers. PLA has a wide range of applications. Packaging is the major PLA application (nearly 70%) and the increase of other applications especially in fibers and fabrics is also expected, (see Table 2.1).

2.1.2 Polyamide 11 (PA11)

An excellent combination of chemical, mechanical and thermal properties has brought polyamide 11 as a promising polymer in the most industrial applications. PA11, a green polymer issued from castor oil, was firstly developed by ATOFINA chemical Inc in 1942. Rilsan (PA11),

2.1. Main applications of PLA [7].

sector	Percent of total production (2003)	Percent of total production (2020)
Packaging	55	20
Building	5	9
Agriculture	1	10
Transportation	3	20
Furniture	2	3
Houseware	6	8
Fibers and Fabrics	28	30

derived from vegetable oil is an engineering high performance biopolymer used in metal coatings, flexible pipes for offshore oilfield exploration or automotive applications [53]. PA11 possess superior mechanical properties including excellent resilience, acceptable tensile strength, exceptional dimensional stability and high impact strength [23]. It possesses easy processability and can be readily processed by blow molding, extrusion and injection molding. Moreover it has great thermal properties with the heat deflection temperature (HDT) of 135 °C [22]. PA11 shows outstanding feature exposing to water environment and regardless of the existence of amide groups, it has lower water adsorption characteristic than those of PA6 and PA66 due to the presence of long hydrocarbon chains in PA11 backbone [18]. The molecular structure of PA11 is presented in Figure 2.2.

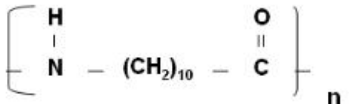

Figure 2.2. The molecular structure of PA11.

2.2 Polymer Blends

2.2.1 Thermodynamics of polymer blends

Thermodynamic of mixing of a binary polymer-polymer mixture is described by the Gibbs free energy of mixing:

$$\Delta G_m = RT\chi_{AB}\varphi_A\varphi_B + RT\left[\frac{\rho_A\varphi_A \ln \varphi_A}{M_{w_A}} + \frac{\rho_B\varphi_B \ln \varphi_B}{M_{w_B}}\right] \quad (2.1)$$

where ΔG_m is the Gibbs free energy of mixing, φ_i is the volume fraction of the components, χ_{AB} is the Flory-Huggins interaction parameter, M_{w_i} is the molecular weight of the polymers, ρ_i is the density of components, and T and R are the absolute temperature and gas constant, respectively. Therefore Gibbs free energy of mixing consists of the enthalpy of mixing (the first terms on the right side of the equation) and the entropy of mixing (the term in the bracket). Based on the Gibbs free energy of mixing, binary polymer mixtures are classified into three main groups: a) miscible polymer blends with $\Delta G_m < 0$ and $\partial^2 \Delta G/\partial \varphi^2 > 0$ over the whole composition range; b) partial miscible polymer blends which have $\Delta G_m < 0$ over the whole composition range but $\partial^2 \Delta G/\partial \varphi^2 > 0$ not in the entire compositions range; and c) immiscible polymer blends with $\Delta G_m > 0$ which is valid over the entire composition range. In immiscible polymer blends two separate phase are formed, while in miscible systems, both polymer show miscibility down to the molecular scale. The majority of polymer mixtures are immiscible due to the positive enthalpy of mixing and negligible entropy of mixing resulted by high molecular weights and a low degree of freedom of polymers. Therefore, most polymer mixtures have a positive Gibbs energy of mixing which results in immiscibility. Morphology of immiscible polymer blends substantially affects the final blend performance and need to be controlled in order to achieve the desire properties. Different possible morphologies in binary polymer systems and their potential properties are shown in Figure 2.3.

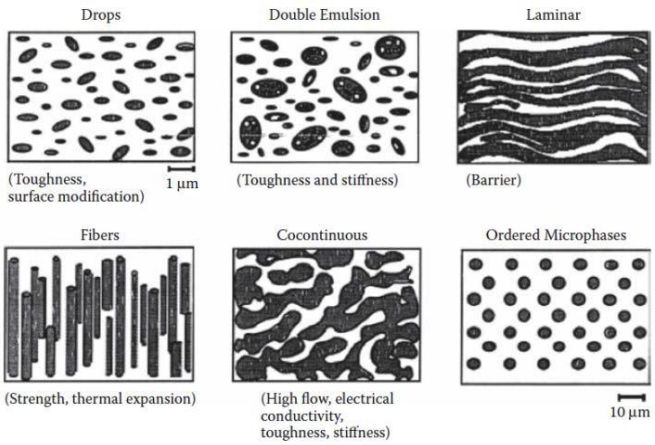

Figure 2.3. Different morphologies of binary polymer systems and their potential applications [54].

2.2.2 Interfacial Tension

Morphology development in immiscible polymer blends is substantially affected by the interfacial tension between the two components. By definition interfacial tension is a required reversible work to make an interfacial area by the unit area [55]. The rate of the change in the interfacial energy of a system with increasing the interfacial area can also be defined as the interfacial tension. Some of the relevant methods of measuring the interfacial tension between polymer pairs such as breaking thread, imbedded fiber retraction and in-situ Neumann triangle methods are briefly presented in the following sections.

2.2.3 Interfacial Tension Measurement From Surface Tension Data

The interfacial tension between two polymers or a polymer melt and a solid can be determined from the surface tension of the components. Good and Girifalco [56] used the work of adhesion concept to estimate the interfacial tension:

$$\gamma_{12} = \gamma_1 + \gamma_2 - W_a \tag{2.2}$$

In which γ_{12} is the interfacial tension between the two components, γ_1 and γ_2 stand for the surface tension of the component 1 and component 2, respectively, and W_a is the work of adhesion between the two components. By considering the concept of energy additivity and contribution of polar and dispersive components in the work of adhesion, Wu [57] presented the harmonic mean approach for system with low surface tensions:

$$\gamma_{12} = \gamma_1 + \gamma_2 - 4\left(\frac{\gamma_1^d \gamma_2^d}{\gamma_1^d + \gamma_2^d} + \frac{\gamma_1^p \gamma_2^p}{\gamma_1^p + \gamma_2^p}\right) \tag{2.3}$$

in which γ_i^d and γ_i^p are the dispersive and polar components of the surface tension, respectively. Wu [57] also found that the estimation of the interfacial tension between two materials with highly different polarity with the harmonic mean equation is not accurate. He estimated the work of adhesion based on the geometric mean approach in these systems. The interfacial tension estimated by the geometric mean equation is described as:

$$\gamma_{12} = \gamma_1 + \gamma_2 - 2\left(\sqrt{\gamma_1^d \gamma_2^d} + \sqrt{\gamma_1^p \gamma_2^p}\right) \tag{2.4}$$

2.2.4 The Breaking Thread Method

The breaking thread is a well known technique which has widely been used to estimate the

interfacial tension between a variety of different polymer pairs [58]. This method consists of heating a filament of the polymer with higher melting temperature sandwiched between two films of the other component and analyzing the evolution of the capillary instabilities. If a thread of a polymer is inserted into another polymer and heated until they melt, sinusoidal distortions start to grow exponentially at the surface of the thread until the thread breaks up into a number of small droplets. The tendency of two immiscible polymers to minimize the interfacial area induces these sinusoidal distortion and make them grow. Figure 2.4 shows a typical distortion of a thread of nylon 6 (PA6) in a polystyrene (PS) matrix.

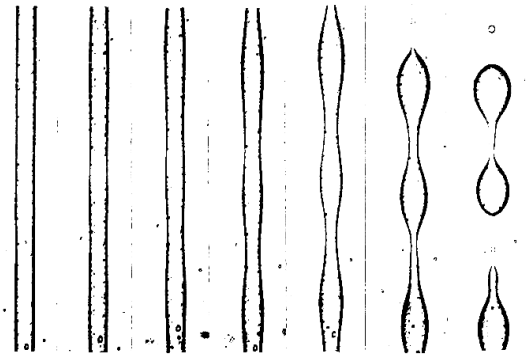

Figure 2.4. The distortion process of a PA6 thread with a 55 μm diameter sandwiched between two PS films at 230 ℃ [58].

The exponential growth of the amplitude of the sinusoidal distortions over time can be described by the Tomotika's model [59]:

$$\alpha = \alpha_0 e^{qt} \tag{2.5}$$

in which α_0 stands for the amplitude of the initial distortion and q is the growth rate and is determined by the following equation [60]:

$$q = \frac{\gamma_{12}\Omega(x,p)}{\eta_0 D_0} \tag{2.6}$$

where γ_{12} is the interfacial tension between two polymers, $\Omega(x,p)$ is a tabulated function, η_0 is the matrix zero shear viscosity, D_0 is the initial thread diameter. $\Omega(x,p)$ is a function of the viscosity ratio p of the thread with the matrix.

2.2.5 The Imbedded Fiber Retraction Method

This method is similar to the breaking thread technique, but here, due to its shorter length, the

imbedded thread will retract to a spherical shape instead of breaking up. In this method the ratio of the initial length with diameter of the fiber should be less than 12 [58], [61]. Figure 2.5 shows a representative retraction process of a PA6 short fiber embedded in a PS matrix. During this retraction, the short fiber first converts into a dumbbell-like form through a surface smoothing process, afterwards relaxes and retracts into a spherical shape [58]. The retraction process is induced by the interfacial tension between the thread and the matrix. Therefore the transformation of the thread into the sphere and also rheological characteristic can be employed to determine the interfacial tension.

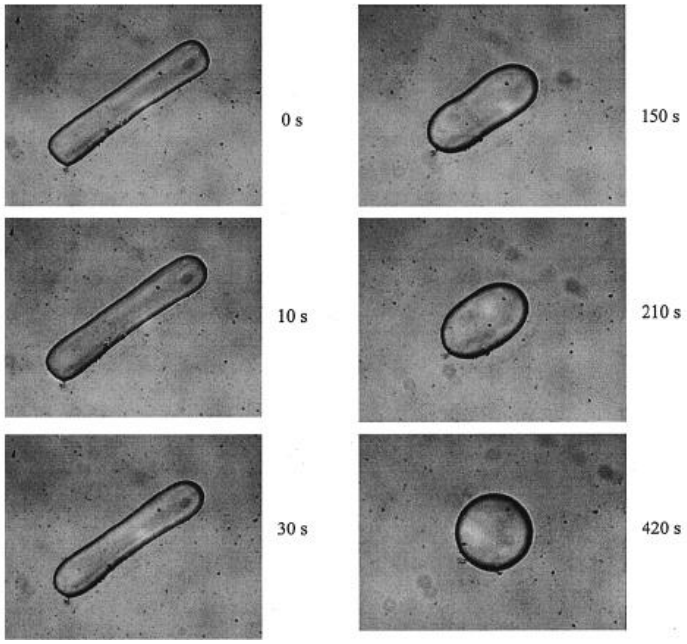

Figure 2.5. A typical retraction process of PA6 fiber imbedded in a PS matrix [58].

In this technique it is assumed that the fiber is a cylinder with a radius of *R* and hemispherical caps during the experiment. The effective radius *R* as a function of time (t) is estimated as the radius of a cylinder with equal length and volume as the fiber. The final expression for the evolution of the retraction process is described with the following equation:

$$\mathrm{f}\left(\frac{R}{R_0}\right) - \mathrm{f}\left(\frac{R_e}{R_0}\right) = t\,\frac{\gamma_{12}}{R_0\eta_e} \tag{2.7}$$

where R is the radius at time t, R_0 is the radius of the final spherical droplet, R_e is the fiber radius at $t=0$, γ_{12} is the interfacial tension, and η_e is the effective viscosity expressed by:

$$\eta_e = \frac{\eta_m + 1.7\eta_d}{2.7} \tag{2.8}$$

in which η_d and η_m are the zero shear viscosities of the fiber and matrix, respectively. The function *f* used in Equation (2.7) is expressed by the following equation developed by Cohen and Carriere [62], [63]:

$$\mathrm{f}(x) = \frac{3}{2}\ln\left(\frac{\sqrt{1+x+x^2}}{1-x}\right) + \frac{3^{1.5}}{2}\arctan\left(\sqrt{3}\,\frac{x}{2+x}\right) - \frac{x}{2} - \frac{4}{x^2} \tag{2.9}$$

where *x* is $R(t)/R_d$. Interfacial tension is estimated from the slope of the plot of $\mathrm{f}(R(t)/R_d) - \mathrm{f}(R(0)/R_d)$ versus time [58], [61].

2.2.6 Neumann Triangle Method

The Neumann triangle is another method that can provide quantitative information on the interfacial tension in immiscible polymer systems [64]–[66]. This approach is based on the geometrical examination of three phase contact between three immiscible polymers A, B and C which demonstrate partial wet morphology at equilibrium with a common line of contact (see Figure 2.6). In a ternary immiscible polymer blend with a partial wet morphology, the three spreading coefficients are negative [66]. The vector sum of the three interfacial tensions applying

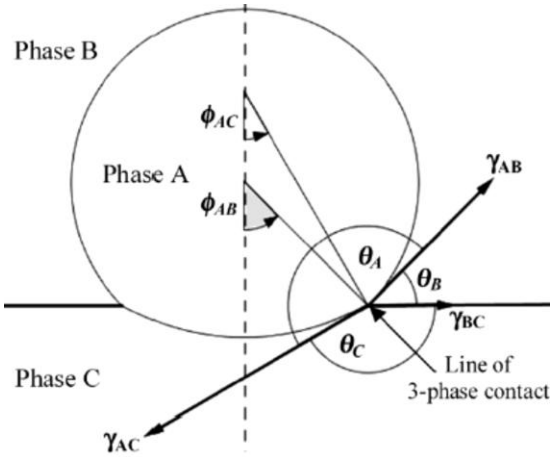

Figure 2.6. Geometrical parameters of a ternary blend with partial wet morphology. The angles Φ_{AC} and Φ_{AB} are used to estimate the θ_A, θ_B and θ_C contact angles between the components at the three phase contact line. The three interfacial tensions are γ_{AB}, γ_{AC} and γ_{BC} [66].

on the plane perpendicular to the three phase contact line, by neglecting the effect of the line tension, is equal to zero:

$$\vec{\gamma}_{AB} + \vec{\gamma}_{AC} + \vec{\gamma}_{BC} = \vec{0} \tag{2.10}$$

The three θ_A, θ_B and θ_C contact angles are defined by using the three tensions. It is thus possible to calculate ratios of the three interfacial tension using these angles, Γ_i :

$$\Gamma_A = \frac{\gamma_{AC}}{\gamma_{AB}} = \frac{\sin\theta_B}{\sin\theta_C},\ \Gamma_B = \frac{\gamma_{BC}}{\gamma_{AB}} = \frac{\sin\theta_A}{\sin\theta_C},\ \Gamma_C = \frac{\gamma_{BC}}{\gamma_{AC}} = \frac{\sin\theta_A}{\sin\theta_B} \tag{2.11}$$

Although the Neumann triangle technique gives relative values, it is possible to estimate absolute interfacial tensions when the value of at least one pair of the various interfacial tensions is known [66].

2.3 Morphology Development in Polymer Blends

Control of the morphology and interfacial properties is very crucial in the development of new multiphase polymer blends. In spite of the interfacial tension, phase compositions, processing conditions (shear rate, time and temperature) and rheological characteristics (viscosity and elasticity ratios) should be carefully controlled in multiphase systems in order to obtain the desire final performance. These days there is a growing attention in adjusting the interfacial energies, morphology and thus end properties of multicomponent systems. The phase structure obtained after compounding of binary immiscible polymers is usually categorized into two general morphology types: (1) matrix/dispersed phase morphology and (2) co-continuous phase structure (see Figure 2.7). In type (1) the dispersed phase can be in the shape of lamella, A-B-A droplet-in-droplet, particle or fiber structures as is shown in Figure 2.8 (a-1 to a-4) [67], [68]. The majority of commercial binary polymer blends have matrix-dispersed phase morphology [67]. This type of morphology is observed in low concentration of the minor phase. By increasing the concentration of the minor phase, the dispersed/matrix phase structure is converted to continuous morphology through droplets coalescence and reaching the percolation threshold. Further increase of minor phase concentration, results in co-continuity in which for a certain range of composition both phases are 100% continuous. At higher content of the minor phase, phase inversion results in once again the dispersed/matrix phase morphology. The development of matrix/dispersed phase morphology and the effect of different parameters such as viscosity ratio,

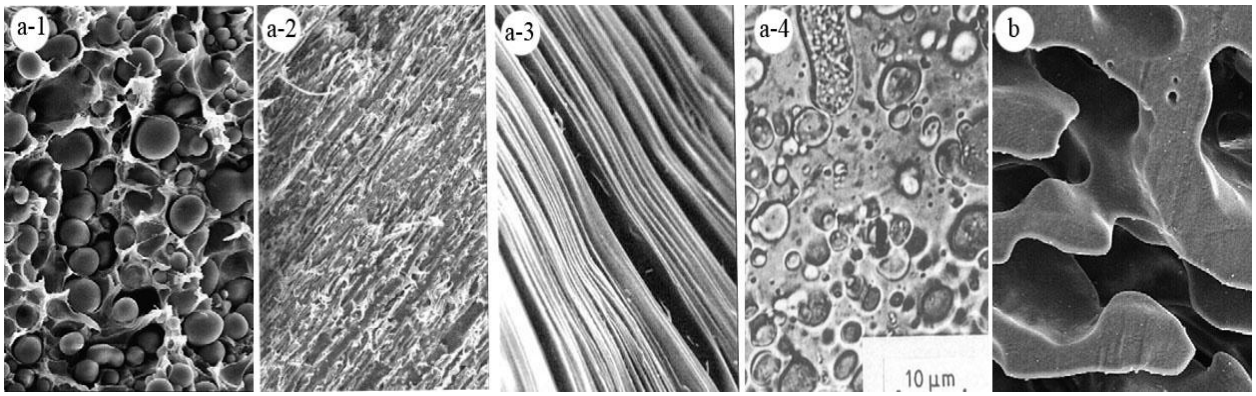

Figure 2.7. Different types of morphology in immiscible binary blends: a-1) matrix/dispersed particle structure a-2) matrix/fibre structure, a-3) lamellar structure, a-4) droplet-in-droplet morphology and b) Co-continuous morphology [67]–[69]

composition, interfacial tension, processing parameters, etc on this type of structure have been widely studied [70]–[73]. The co-continuous morphology has also gathered a lot of attentions for the last two decades [74]–[77]. In a binary polymer blend the competition between dispersed phase coalescence on one side and disintegration/breakup of the dispersed phase on other side defines the final blend morphology. Therefore a detailed understanding of the deformation-disintegration and coalescence phenomena is crucial in controlling the final blend morphology. These two competitive behavior will be discussed in the following sections.

2.3.1 Droplet breakup

Taylor studied, for the first time, the deformation and breakup of a single Newtonian droplet in a Newtonian matrix under elongational or shear flow field [78], [79]. He determined the maximum droplet diameter by balancing the maximum pressure difference in the droplet. He observed that at high elongation rates, the droplet transforms from a sphere to a thread and then breaks into a number of smaller droplets after stopping the flow. Taylor also found that the droplet breakup occurs when the ratio of the deforming viscous forces, applied by the flow field, to the restoring interfacial forces is higher than a critical value. He then demonstrated that the viscosity ratio ρ ($\eta_{droplet}/\eta_{matrix}$), capillary number and shear field control the droplet breakup. Capillary number, *Ca*, is described as the ratio of the viscous to the interfacial forces:

$$Ca = {\eta_m \dot{\gamma} R}/{\gamma_{12}} \tag{2.12}$$

and $$p = \eta_d/\eta_m \quad (2.13)$$

in which η_m is the matrix viscosity, $\dot{\gamma}$ is the shear rate, R is the droplet radius, γ_{12} is the interfacial tension and η_d and η_m are the viscosity of the droplet and matrix respectively. Small capillary number indicate low viscous forces compared to interfacial forces which leads to a steady state ellipsoidal form. By increasing the viscous forces, the capillary number reaches a critical value, Ca_{crit}, at which the breakup occurs. Taylor developed the following equation for Ca_{crit} under simple shear flow:

$$Ca_{crit} = {}^{1}/_{2}\ (\tfrac{16\rho+16}{19\rho+16}) \quad (2.14)$$

Grace et al. [80] developed the Taylor theory by studying the effect of the viscosity ratio on the Ca_{crit} for the both shear and elongational flow. The critical capillary number (Ca_{crit}) versus the viscosity ratio ρ ($\eta_{droplet}/\eta_{matrix}$) under shear and elongation flow fields for a Newtonian mixtures is shown in Figure 2.8 . The U-type dependence of droplet breakup as a function of the viscosity

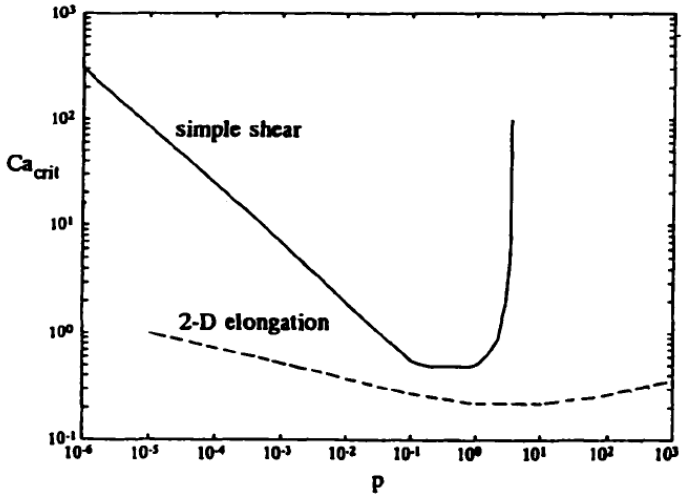

Figure 2.8. Critical capillary number as a function of the viscosity ratio under elongation and simple shear flow [80].

ratio as is shown in Figure 2.9 indicates that there are lower and upper limits for the viscosity ratio beyond which droplets are stable and no breakup happens [80]. It is evident in Figure 2.9 that Ca_{crit} for the elongational flow is always lower than that of the shear flow. The Ca_{crit} under shear flow exhibits a minimum of $0.25 < p < 1$. This imply that elongational flow is much more effective in droplet breakup compared to the shear flow. Moreover it is obvious that under simple

shear flow, the droplet break-up only happens when $\rho < 4$.

The effect of the viscosity ratio on the droplet break up and morphology of polymer blend has been studied as well [81], [82]. The results reveal a strong dependency of droplet size on the viscosity ratio under shear flow. Wu [82] demonstrated that in rubber-polyamide blends, the particle size increases as the viscosity ratio shift away from 1 (lower or higher). Favis et al. [81] studied the influence of the viscosity ratio on the morphology of polycarbonate/polypropylene binary blends. Figure 2.9 shows the effect of the viscosity ratio on the droplet size in binary blends of PC/PP under shear flow. They showed an increase of up to three to four times in the phase size with increasing the viscosity ratio of between 2 and 13. Moreover, they observed that a reduction in the dispersed phase size when the viscosity ratio is less than 1 with a minimum in the droplet size at the viscosity ratio of 0.25. This value is in line with the one reported by Taylor for a Newtonian droplet under shear flow as is shown in Figure 2.9.

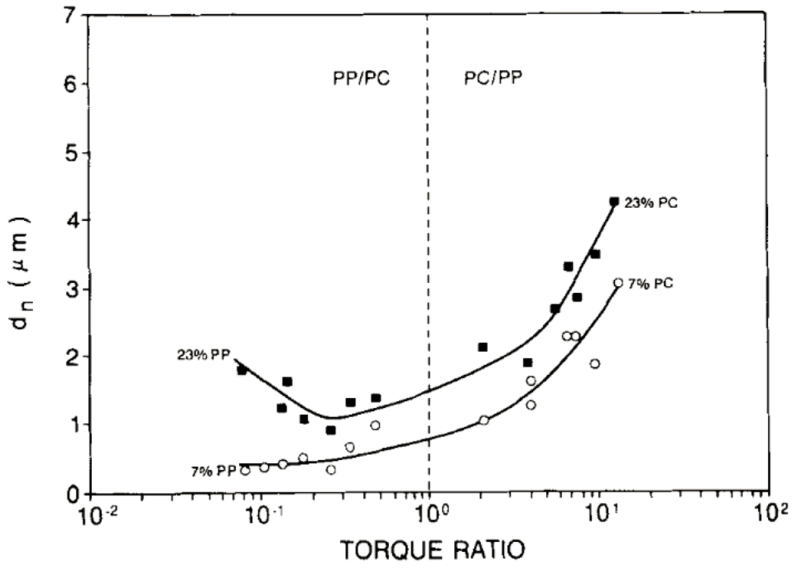

Figure 2.9. The effect of the torque ratio (viscosity ratio) on the dispersed phase size (d_n) in the blends of PC/PP

Wildes et al. [83] also examined the influence of the viscosity ratio on the particle size in a blend of styrene–acrylonitrile (SAN) and PC and observed a minimum phase size at a viscosity ratio of 0.4. Bhadane et al. [84] studied the effect of the viscosity ratio on the phase size in a PP/EPDM blend with low interfacial tension. They demonstrated that although a small change in the viscosity ratio does not affect the droplet size, a seven-time increase in the viscosity ratio

increases the phase size by a factor of 3 to 4. The effect of the viscosity ratio in elongational flow field has also been studied [83] [85]. Favis and Therrien [85] reported that under elongation flow field (twin screw extruder) droplet break up is less dependent on the viscosity ratio compared to the shear flow fields (using an internal mixer). Wildes et al. [83] also reported that SAN dispersed phase size in a PC/SAN blend mixed by a twin-screw extruder is independent of the viscosity ratio.

2.3.2 Phase Coalescence

Newtonian Coalescence. For a Newtonian mixture it has been reported that the required contact time for coalescence increases by increasing the droplet size, the matrix viscosity and also the density difference between the matrix and droplet. The droplets coalescence in a Newtonian mixture can be modeled as a three-step process as shown in Figure 2.10 [86]: (i) the droplets are brought close to one another by the flow field, (ii) the matrix film between the two droplets thins until the thickness of the film decreases to a critical value, (iii) the rupture of the interface and coalescence occurs. It has to be noted that the contact time in shear flow fields are very short. Thus the film must drain very fast for two droplets to coalesce.

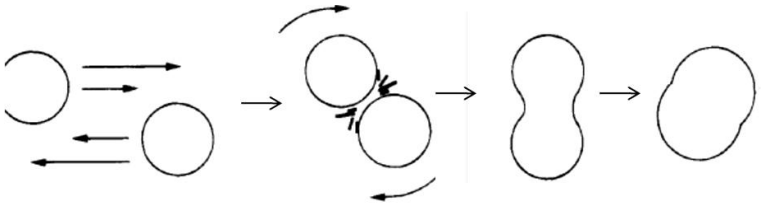

Figure 2.10. Schematic of flow induced coalescence of Newtonian drops. The droplets are brought close to one other by the shear flow field, and afterwards the matrix film between the droplets drains until the film ruptures and results in coalescence [86].

Coalescence in Polymer Blends. Generally, phase coalescence in polymer blends is divided into two major classes: static and dynamic processes [87], [88]. The former case is a quiescent process, whereby the minor phase/matrix structure grows in size in order to minimize the free energy of the system by decreasing the interfacial area. The latter case is a flow induced phenomena in which a balance between coalescence and droplet breakup determines the dispersed phase size [87]. Coalescence in polymer blends has been studied both theoretically and experimentally [73], [86], [89]–[93]. At equilibrium, Tokita [90] developed the following expression for the dispersed phase size:

$$D_e = \frac{24P_r\gamma_{12}}{\pi\tau}\ (\varphi + \frac{4P_rE_{DK}}{\pi\tau}\ \varphi^2) \quad (2.15)$$

where P_r is the collision probability, τ is the shear stress, φ is the minor phase composition, and E_{DK} is the bulk breaking energy of the minor phase. According to Tokita's theory the dispersed phase size decreases linearly with decreasing the interfacial tension and increasing the shear stress. The applicability of Tokita model is limited due to the lack in collision probability of droplets. Moreover the evaluation of other parameters in this model are also difficult [89]. Favis and Willis [73] presented a master curve of the dispersed phase size as a function of the minor phase concentration for several immiscible polymer pairs and expressed the following equation for the phase size as a function of compositions: $\varphi+k\varphi^2$. Therefore, coarsening and phase coalescence of the dispersed phase substantially increases with increasing the dispersed phase content in the blend. Elmendorp and Van der Vegt [93] demonstrated that collision is more likely to lead to coalescence if the minor phase is small and if the interface is very mobile. However it has been shown that this mobility is decreased with compatibilization in which interfacial modification leads to fewer droplet-droplet collision and much less coalescence. Compatibilization (through adding premade block copolymers or in-situ reaction) has been shown both theoretically and experimentally to be very efficient in stabilizing the blends morphology against phase coalescence [86], [92]. Lepers et al. [91] found that both interfacial tension reduction and diminished coalescence contribute almost equally in dropping the dispersed phase size in interfacially modified blends

A lot of coalescence studies in polymer blends have been carried out under quiescent conditions. Coalescence after blending is very important because processed polymer products are often annealed and phase coarsening may occur during annealing [86]. Under these conditions it has been reported that extent of coalescence in polymer blends significantly decreases if the viscosity of the matrix is higher than a critical value and if the dispersed phase concentration is below a critical value.

2.3.3 Continuity Development

In a binary polymer blend, as it was explained in the previous section, increase the composition of the minor phase increases the number of collisions and results in of coalescence between the particles of the dispersed phase. By increasing the composition of the dispersed phase at a certain concentration, the first connected pathway in the blend known as the percolation threshold point

forms [67], [94], (See Figure 2.12). According to the classic percolation theory, this percolation threshold is the onset of the formation of a long-range connected pathway in random systems [94]. The percolation threshold has been reported to occur at a volume fraction of 0.156 for a random distribution of mono-dispersed spherical particles [94]. Increase the concentration of the dispersed phase higher than percolation threshold, increases the levels of continuity in polymer blends until a fully-interconnected co-continuous structure is achieved as is shown in Figure 2.11. Co-continuous is described as a system in which each phase is 100% continuous in the blend. For a binary polymer mixture, co-continuity often takes place over a composition range. Thus it is also known as the dual phase continuity region [69]. Further increase in the content of the minor phase results in a transformation of the co-continuous morphology to the matrix/dispersed phase structure. It has been shown that the region of dual-phase continuity can be shifted to higher or lower concentration depending on the viscosity ratio and interfacial tension. Typically, in polymer blends, the continuous phase dominates the final properties, thus it

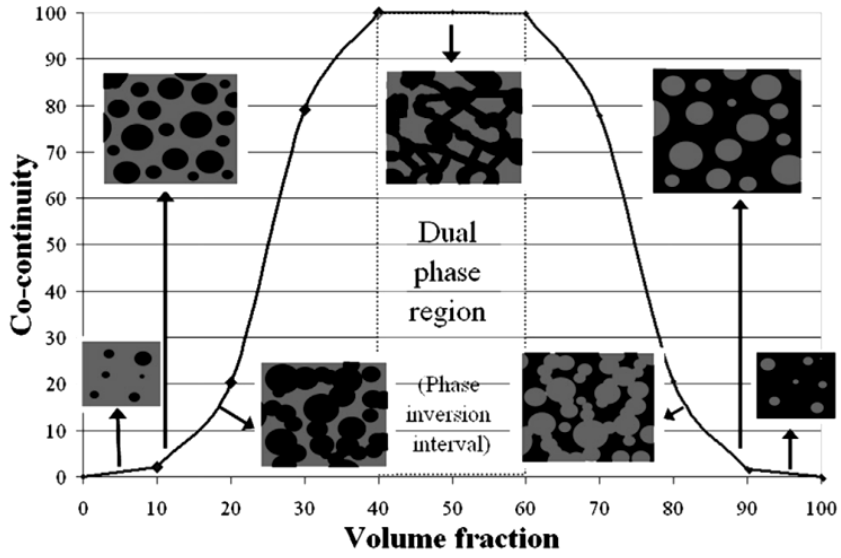

Figure 2.11. Schematic describing the continuity development in an immiscible binary polymer blend [94].

is believed that in co-continuous morphology both phases contribute equally to the material properties. Also, their interpenetrating assembly can possibly result in synergistic increase in specific properties. Thus, it is of particular interest to predict at which composition co-continuous morphology most probably can happen. Some theoretical and semi-empirical attempts have been made to determine the phase inversion composition in terms of processing conditions and material characteristics, (see Table 2.2).

Table 2.2. Predictive equations for the phase inversion composition, φ_i and φ_{PI} represent the phase inversion composition.

Theoretical	Viscosity dependent	$\frac{\varphi_1}{\varphi_2} = \frac{\eta_1}{\eta_2}$	η_i and ϕ_i are the zero shear viscosity and volume fraction of component i, respectively. [95]
		$\varphi_1 = \frac{\varphi_m + (1-\varphi_m)\left(\frac{\eta_1}{\eta_2}\right)^{1/[\eta]\varphi_m}}{1+\left(\frac{\eta_1}{\eta_2}\right)^{1/[\eta]\varphi_m}}$	$\varphi_m = 1-\varphi_c$ $[\eta]$ is intrinsic viscosity of matrix φ_c is the percolation threshold concentration.
		$\varphi_1 = \frac{\left(\frac{\eta_1}{\eta_2}\right)^2 \Omega^2\left(\frac{\eta_1}{\eta_2}\right)}{\left(\frac{\eta_1}{\eta_2}\right)^2 \Omega^2\left(\frac{\eta_1}{\eta_2}\right) + \Omega^2\left(1/\frac{\eta_1}{\eta_2}\right)}$	$\Omega\left(\frac{\eta_1}{\eta_2}, \lambda\right)$ is complex function of both the viscosity ratio and observed wavelength of the distortion in Tomotika's theory [96].
	Elasticity dependent	$\frac{\varphi_1}{\varphi_2} = \frac{\tan\delta_1(\omega)}{\tan\delta_2(\omega)}$ and $\frac{\varphi_1}{\varphi_2} = \frac{G_2'(\omega)}{G_1'(\omega)}$	G_i' and G_i'' are storage and loss moduli of component i (i=1,2), respectively and $\tan\delta = \frac{G_i''}{G_i'}$ [97].
Semi-empirical	Viscosity dependent	$\varphi_1 = \frac{1}{\left(\frac{\eta_1}{\eta_2}\right)^{1/z} + 1}$	z is a dependent parameter on the blend system that should be first evaluated for each system [98].
		$\frac{1}{\varphi_d} = 1.38 + 0.0213\left(\frac{\eta_m \dot{\gamma}}{\sigma} R_0\right)^{4.2}$	$\dot{\gamma}$ is the shear rate, R_0 the radius of the thread, η_m is the viscosity of the matrix, σ is the interfacial tension, φ_d is the volume fraction of the dispersed phase [99].
	Elasticity dependent	$\varphi_{PI} = -0.34\log\left(\Psi_{eff.G''}\right) + 0.67$	$\Psi_{eff.G''}$ is the effective elasticity ratio [100].

2.3.4 The Role of Interfacial Tension on Continuity Development

Interfacial tension plays an important role in polymer blend morphology. It has been demonstrated for different blends with different viscosity ratios and matrix viscosity that interfacial tension significantly affects the composition range of dual phase continuity [101]. The stability of elongated structure can be increased by low interfacial tension. Thus a wider range of

co-continuity can be obtained. Furthermore, the phase size is strongly dependent on the interfacial tension and typically reduction in interfacial tension leads to a drop in the dispersed phase size. Li et al. [102] conceptually elucidated this mechanism based on droplet versus thread (breakup) lifetime during melt process. They studied the effect of the blend interface type on the co-continuity and distinguished between three possible types of co-continuous microstructure. In immiscible but compatible binary polymer blends showing low interfacial tension (type I), the morphology characteristics and continuity development is dominated by mechanism of thread-thread coalescence. For immiscible binary systems with high interfacial tension (type II), co-continuity is controlled by droplet-droplet coalescence. The morphology of compatibilized ternary systems (type III) are in consistence with mechanism dominated by droplet-droplet c-oalescence, which is reduced but not totally inhibited by the compatibilizer. For type I, the droplet lifetime is proposed to be lower than the thread lifetime, whereas for type II and type III, the droplet lifetime is larger than the thread lifetime (See Figure 2.12).

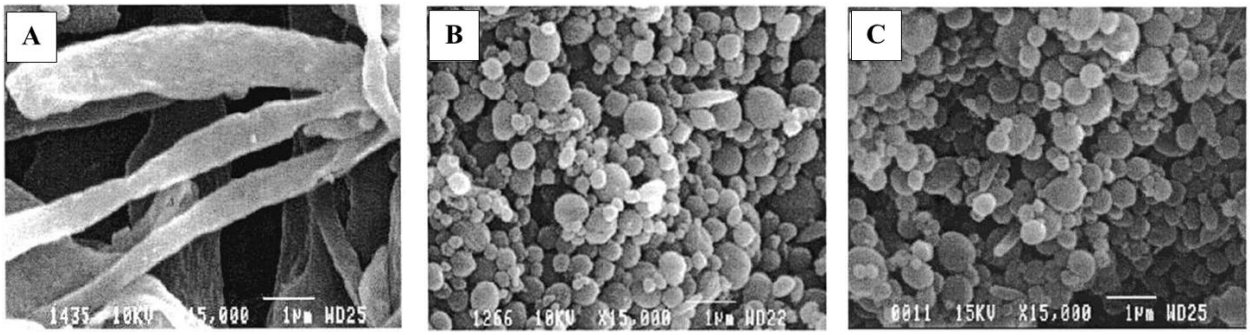

Figure 2.12. SEM photomicrographs of dispersed HDPE phase after matrix dissolution technique: (A) 5 HDPE/95 SEBS (type I); (B) 5 HDPE/95 PS (type II); (C) 5 HDPE/90 PS/20 SEBS (type III) [102].

2.3.5 Coarsening of Co-Continuous Morphology

Significantly coarsened structures at very short times under quiescent annealing have been reported for blends with co-continuous morphology [70], [75], [103]–[109]. Willemse et al. [103] observed that in a blend with dual phase continuity, when the composition of one of the components is much lower than the other, coarsening is attributed to a restructuring procedure including breakup and fiber retraction. At higher concentrations (> 30 vol %), coarsening in co-continuous morphology is believed to occur through retraction only. A number of studies have

demonstrated a linear phase size growth for the coarsening of co-continuous phases as a function of time in uncompatibilized blends that last for even hours of annealing [87], [108], [110]. Veenstra et al. [111] reported a linear increase in phase size with annealing time for co-continuous 50/50 wt% PP/PE, PE/PMMA and PS/PE blends. In a previous work from this laboratory linear phase coarsening with time was reported for different co-continuous PS/HDPE blends with a wide range of viscosity ratios and temperatures [87]. It was demonstrated that the coarsening rate of the average phase size by annealing time is governed by a capillary breakup process and a relation between pore size *R* and annealing time *t* was determined as:

$$R \sim kt \tag{2.16}$$

where *k* is the rate of coarsening expressed by:

$$k = \alpha_0 q = (\alpha_0/R_0)\frac{\sigma\Omega(\lambda,\rho)}{2\eta_c} \tag{2.17}$$

in which α_0/R_0 is the ratio of the original distortion amplitude to the thread radius, σ is the interfacial tension, η_c is the matrix viscosity, and $\Omega(\lambda,\rho)$ is the Tomotika function related to the viscosity ratio ρ ($\rho = \eta_d/\eta_c$ where η_d is the dispersed phase viscosity) and the dominant wavelength, λ.

Interfacial modification through addition of either premade block copolymers or insitu formed copolymers are usually effective in reduction of the interfacial tension and coalescence which results in morphology stabilization [77], [108], [110], [112], [113]. Omonov et al. [107] studied the phase coarsening and morphology stability of co-continuous uncompatibilized PS/PP and reactive amino-terminated polystyrene (PS-NH2)/Maleic anhydride grafted polypropylene (PP-MAh) blends during quiescent annealing. They observed a significant phase coarsening from micro to millimeter scale upon annealing of the un-modified 50/50 PS/PP model blends. For the in-situ interfacially modified (PS-NH2)/(PP-MAh) blends, however, coarsening reached a plateau after 10 min of annealing as is shown in Figure 2.13. Bell et al. [110] studied the stability of co-continuous morphologies in PS/PE, PS/PMMA and PS/SAN blends with and without copolymer. They found that properly chosen interfacial modifier can stop coarsening during static annealing. Yuan et al. [87] observed that although co-continuous PS/PP blends demonstrate a linear phase size growth, the compatibilized PS/PP blends show a nonlinear coarsening behavior as is presented in Figure 2.14. They explained that although the chief reason for coarsening process is a capillary pressure effect, the rate of phase growth is controlled by

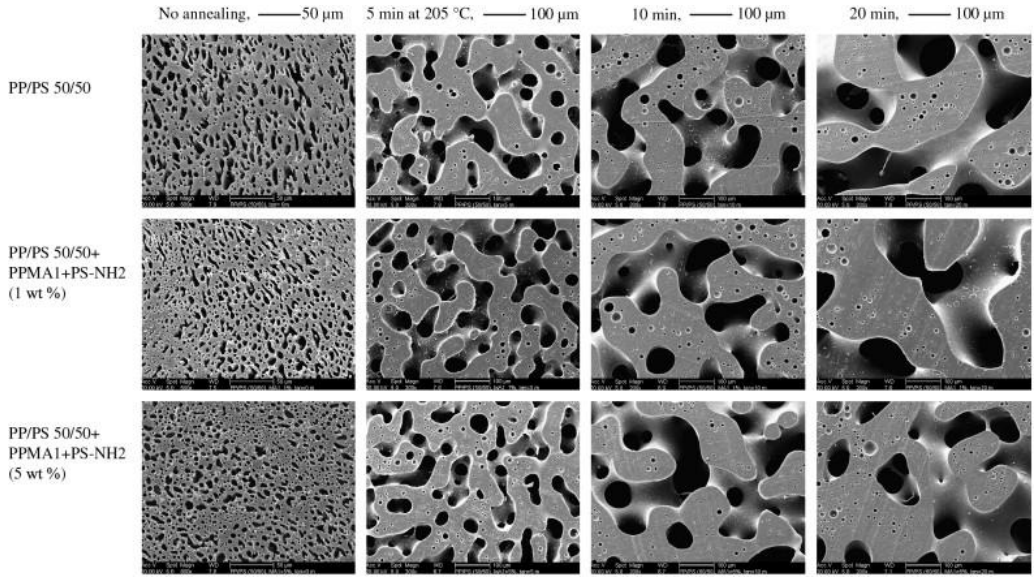

Figure 2.13. Phase coarsening during annealing of co-continuous PP/PS blend [107].

capillary instability effect where the thick thread cannot breakup by a capillary instability because of the abundant branches that continuously feed it. In the case of binary blends with interfacial reactions, dropping the interfacial tension diminishes capillary instability effects and thus will lead to a reduction in the phase growth. Moreover, capillary pressure effects are

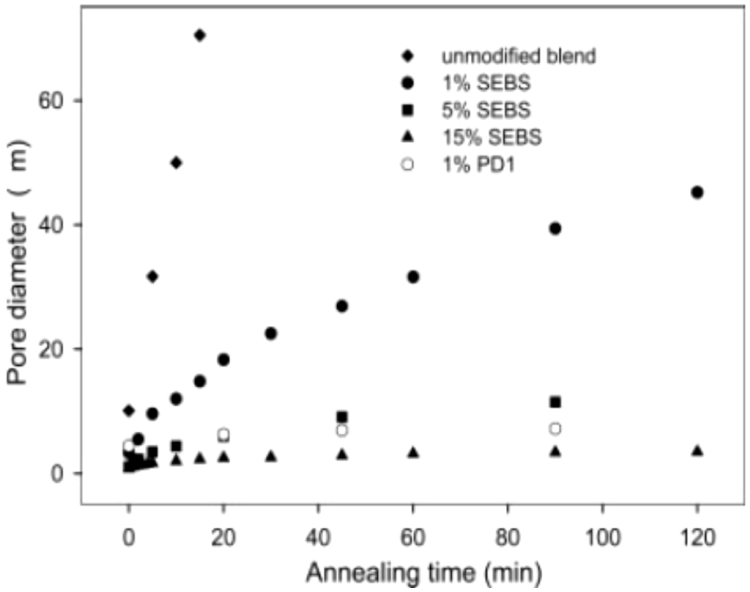

Figure 2.14. Pore size diameter as a function of annealing time for PS/PE 50/50 blends compatibilized with different concentrations of di-blcok and tri-blcok copolymers at 200 °C [108].

proportional to the interfacial tension and pore size polydispesity. Interfacial modification and interfacial reactions in an immiscible blend system renders the system less polydisperse in size [87].

2.4 Reactive Polymer Blends

In reactive polymer blends, in-situ compatibilization occurs due to the reaction between the two polymers with functional groups distributed randomly in polymers chains and end-functional polymers like polyesters or polyamides [114]. It is difficult, however, to define reactivity between two polymers with functional groups. This is mainly related to the lack of sensitivity of standard methods such as IR or NMR spectroscopy due the low concentration of functional groups along the polymer chain. In these cases, solvent extraction and determining the amount of formed copolymer by measuring the mass or using NMR and FTIR have been shown to be useful [115]–[117]. However, this method can result in inaccurate high values due to the incomplete extraction of unreacted polymer [114]. Size exclusion chromatography can also be used to determine the copolymer formation if a common solvent for both polymers can be found [118]. Interfacial reactions in polymer blends have been studied theoretically in the literature [119], [120]. Fredrickson [119] predicted that interfacial interactions in a polymer blend is described by a reaction rate constant:

$$k \approx DR_g((2R_g S_V) / \ln N) \tag{2.18}$$

in which D is the diffusion coefficient, R_g is the radius of gyration, N is the degree of polymerization and S_V is the ratio of interfacial area to total volume. Accordingly the interfacial reaction in polymer blends is controlled by the diffusion of the center of mass of functional chains in the polymer bulk towards the interface. Interfacial reactions under dynamic melt mixing and quiescent conditions have been extensively studied in the literature [114], [121]–[124]. Surprisingly reaction rate constant in the flow condition was found to be over 1000 times higher than that in the static bi-layer films [114], [121]. Reaction time at flat static interface is reported to be in the scale of hours [123]. Table 2.3 compares the interfacial reactions under static dynamic flow conditions. The interface of immiscible blends is constantly changing during melt mixing due to the droplet break-up and coalescence of the minor phase resulted by the flow field in a mixer [114], [121]. The amount of deformation is the largest in the first two minutes of the mixing in which the interfacial area rises by ~1000 time [125]. In addition to the increase in

interfacial area through deformation, the kinetic and amount of interfacial reaction may also be affected with convection due to flow [122]. Convection flow may increase the number of collisions at the interface and also enhance the accessibility of complementary functional groups near the interface [114]. Moreover due to the higher concentration of chain ends at the equilibrium interface [126], di-block copolymer formation is preferable over graft copolymer formation [127]. These di-block copolymers at the interface decrease the amount of

Table 2.3. Comparison of the rate of reaction under static and dynamic flow mixing.

	polymer 1/polymer 2 Mn1/Mn2 (kg/mol	conversion (time, min)	k_I (kg/mol.min)
Static film	PS-NH2/PMMA-An 17/15 ,[124]	0.092 (40)	12
	PS-NH2/PMMA-An 26/15, [121]	0.03 (60)	3.2
Melt mixing	PS-NH2/PMMA-An 15/12, [128]	0.43 (2)	4200
	PS-NH2/PMMA-An 26/15, [121]	0.20 (2)	5300

reaction by limiting the diffusion of other reactive chains [127]. Therefore interface is consider as a barrier against the formation of graft copolymers in static conditions. Generating fresh interface with dynamic mixing and interfacial roughening could reduce this effect [121].

2.5 PLA Toughening

PLA brittle nature limits its application where high toughness i.e. high impact strength and high plastic deformation is needed. Different strategies including plasticization, blending and copolymerization have been extensively used to compensate this gap [2], [8]–[10]. In this section, the plasticization and PLA blending are discussed with an emphasis on the PLA blends with other bio-polymers.

2.5.1 PLA Blending

Blending with various bio and synthetic polymers has been used to toughen PLA [7], [11]–[16]. In this area blending with other bioplastics is a versatile and efficient approach which allows tuning the mechanical properties while offers a completely biomaterial with minimum carbon footprint [6], [12], [17]. PCL and PBAT are probably the most used biopolymers in PLA blending. However, insignificant improvement in mechanical properties in PLA/PCL binary

blend has been reported. Hiljanen-Vaini et al. [129] reported a slight increase in elongation at break from 1.6 (neat PLA) to 9.6 % in PLA containing 20% PCL. Addition of compatibilizer to PCL/PLA binary blends, however, led to significant increase in elongation at break [129]. In another work it has been reported that elongation at break of PLA/PCL blend does not improve remarkably until 60 wt% and higher PCL concentration [130]. Maglio et al. [131] incorporated PLLA-PCL-PLLA triblock copolymer as an interfacial modifier in 30/70 wt% PCL/PLLA blends. An increase in elongation at break from 2% (binary blend) to 53% and notched Izod impact strength from 1.1 kJm^{-2} (binary) to 3.7 kJm^{-2} was reported. In-situ reactive compatibilization has also been used for PLA/PCL interface modification. Wang et al. [132] used a trans-esterification catalyst to prepare reactive blends of PLA and PCL. The elongation at break increased to 127% for reactive blend compared to 28% for non-reactive PLA/PCL binary blend. Jiang et al. studied the mechanical properties of PLA/PBAT blends. They found an increase in Izod impact strength from 2.6 KJm^{-2} for neat PLA to 4.4 kJm^{-2} in 20 wt% PBAT concentration. An improve of about 200% in elongation at break was also reported for PLA containing 20 wt% PBAT [133]. Kumar et al. [134] reported an improvement in impact strength from 21.9 to 50.34 J/m with the addition 25% PBAT to PLA. They also showed that addition of 5% glycidyl methacrylate (GMA) as reactive compatibilizer yielded much higher improvement in impact strength to 76.6 J/m compared to the binary blend and neat PLA. PLA blends with other biodegradable/renewable polymers such as poly(para-dioxanone) (PPD) [135], poly(butylene succinate) (PBS) [136], poly([(R)-3-hydroxybutyrate] (PHB) [137] and poly(3-hydroxybutyrate-co-3-hydroxyvalerate) (PHBV) [138] have also been studied. Table 2.4 compares the mechanical properties of PLA blended with different bio-polymers. PLA blends with synthetic polymers have also been widely explored. Melt blending of PLLA with linear low density polyethylene (LLDPE) results in significant increase in impact strength (490 ± 200 J/m vs 20 ± 2 J/m) [15]. Addition of 5 wt% PLLA-b-PE interfacial modifier to PLLA/LLDPE binary blends led to much better impact strength (760 ± 50 J/m vs 20 ± 2 J/m) due to the much better interfacial adhesion and LLDPE dispersion in PLA. They reported noticeable lower impact strength even in compatibilized HDPE/PLLA blends (64 ± 20 J/m) compared to those of LLDPE/PLLA blends. Choudhary et al. [142] studied the mechanical properties of PLA/Polypropylene (PP) blends. They reported a slight increase in impact strength from 12.76 for neat PLA to 37 for binary blends and a noticeable enhancement of tensile modulus (2302 ±

16 vs 1254 ± 55 MPa (neat PLA)).

Table 2.4. Mechanical properties of PLA blended with different biopolymers

Material	Elongation at break (%)		Tensile Modulus (GPa)		Impact strength	
	neat PLA	Blend	neat PLA	Blend	Neat PLA	Blend
PLA/PCL (30%) [139]	10	20	2.8	1.6	2 kJ/m^2	3.6 kJ/m^2
PLLA/PCL (20%) [140]	5	175	1.3	1.1	-	-
PLLA/PPD (20%) [135]	15	55	1.4	1.6	-	-
PLLA/PBS (50%) [136]	7.6	56	3.3	1.7	23.2 J/m	34.5 J/m
PLLA/PBSL*(10%) [11]	3	160	3	2.5	-	-
PLLA/PBSA**(25%) [141]	-	150	-	1.2	-	-
PLLA/PHBV(40%) [138]	5	7	2.4	1.5	-	-
PLLA/PHB (50%) [137]	-	4.4	-	2.7	-	-
PLA/PBAT(25%) [29]	4.2	120	2.1	1.7	22 J/m	31 J/m

*poly(butylene succinate-L-lactate) **poly(butylene succinate-co-butylene adipate)

PLA/PA11 blends. There are only a few studies reported in the literature considering PLA blend with any kind of polyamide or related polymers and as yet is not completely understood system [6], [22]–[24]. Stoclet et al. [22] investigated the morphology and mechanical properties of this unique system, melt blended by twin screw extrusion. They postulated that PLA/PA11 is a low interfacial tension system with rather good compatibility according to their SEM images of the cryo-fractured samples as shown in Figure 2.15. It is obvious that extraction of the PLA

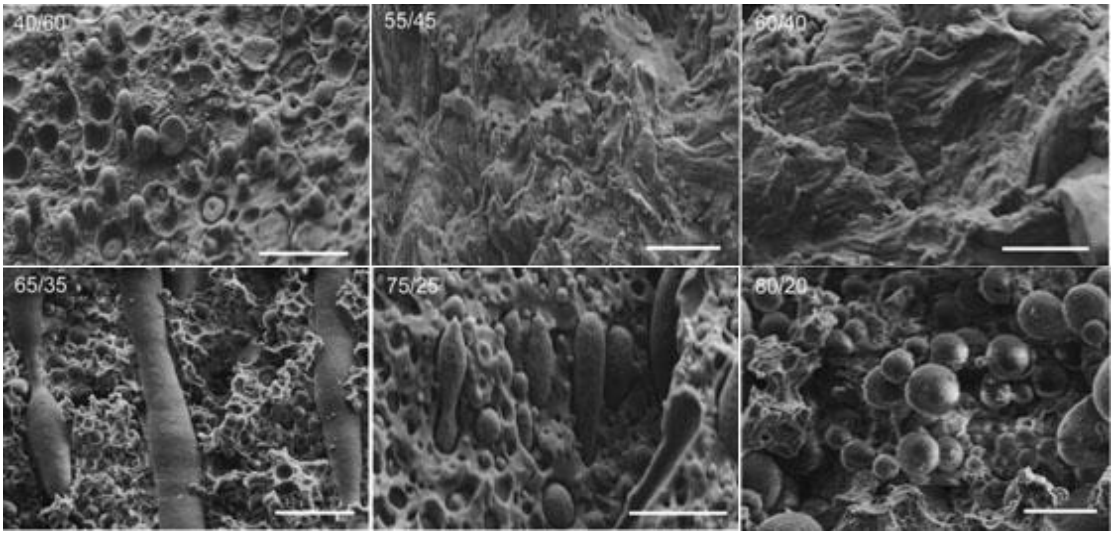

Figure 2.15. SEM images of the fracture surface of PLA/PA11 with different compositions. The scale bar is 5 μm [22].

dispersed phase in the blends is required. They, however, ascribed the rough fracture surface of samples in mid-compositions range to the co-continuous phases morphology. Dong et al. [23] studied the effect of localization of ethylene glycidyl methacrylate-graft-styrene-co-acrylonitrile (EGMA-g-AS) rubber particles in PLA or PA11 phases on the mechanical properties of PLA/PA11 blends. They observed a 78 and 5.2 fold increase in elongation at break and impact strength, respectively, in ternary blends in which EGMA-g-AS is predominantly dispersed in the PLA phase. They also showed that the addition of EGMA-G-AS did not change the dispersed phase morphology of PLA/PA11 blends. Patel et al. [24] studied the reactive compatibilization of PLA/PA11 in the presence of a titanium isopropoxide catalyst. No direct evidence of interfacial reaction was reported even in the presence of a high amount of catalyst and high temperatures. In all of these studies, many aspects of the morphology, coalescence, continuity development and interfacial properties of PLA/PA11 blends, remain unclear or contradictory.

2.5.2 PLA Plasticization

In order to improve the flexibility of glassy polymers, plasticization of the amorphous phase is an option. Poly(ethylene glycol) (PEG) [143], poly(ethylene oxide) [144], [145], citrate esters [146] and triacetine [147] are the most efficient plasticizers for PLA. Brittle ductile transition behavior in plasticized PLA occurs when T_g is decreased to 35 °C [148]. PEO has shown the greatest promise as a plasticizer for PLA, as it gives the highest increase in the elongation at break with the minimal decrease in the tensile strength [7]. Among the most interesting results, it has been shown that in most plasticized PLA systems, by increasing the plasticizer concentration, the PLA/plasticizer blends experience a phase separation at a certain plasticizer concentration depending on the plasticizer molecular weight and chain architecture [148]–[150]. Pillin et al. [150] studied the miscibility of PLA and PEGs with different molecular weights. They showed that phase separation is caused by the PLA crystallization which is increased for PEGs with lower molecular weight. Depletion of excessive amount of plasticizer from the growing PLA spherulites increases stiffness and decreases strain at break of plasticized PLA [148]. Jacobsen et al. [151] studied the effect of plasticizers such as glucosemonoesters, PEG and partial fatty acid esters on PLA flexibility. They showed that the elongation at break of PLA increased from 3.3 to 40% with the addition of 10 wt% PEG. Baiardo et al. [152] studied the effect of acetyl tri-n-butyl citrate(ATBC) and PEG plasticizers on mechanical properties of PLA. They demonstrated that in all systems increasing plasticizer concentration decreases PLA tensile modulus and tensile

strength while increases elongation at break. Their DSC analysis showed that the sudden changes in PLA plastic deformation occurs when T_g is around 35 °C. Kulinski et al. [153] demonstrated that PEG plasticizer increases PLA chain mobility resulting in a drop in the yield stress and an increase in the ability of amorphous PLA to plastic deformation. They also reported of about 20% elongation at break for PEG plasticized semicrystalline PLA at 10 wt% plasticizer consternation.

2.6 Polymer Nanocomposites

Nanotechnology is known as one of the most favored area of research and development in all technical disciplines including polymer science and technology. In polymer field, studies cover a broad range of subjects including miniemulsion particles, electrospun nanofibers, self-assembled polymer films, polymer-based biomaterials, nanoparticle drug delivery, imprint lithography, fuel cell electrode polymer bound catalysts, nanocomposites and polymer blends [154]. Polymer blends with solid inclusions is a traditional method in polymer processing. Basically the purpose of incorporation solid inclusion into polymer blends is achieving is enhancing electrical or mechanical properties. Considering the final properties, it is essential to predict and control the localization of the nanoparticles in the blend [27]–[30]. We will discuss this topic in more detail in the next section.

Solid-inclusions have diversified, involving, carbon nanotubes, titanium dioxide, aggregated and spherical silicas, micas, nanoclays, nanocellulose and etc. These solid inclusions have created new challenges as they vary by their size, their surface energy, their shape (fibers, platelets, spheres, needles) their agglomeration and dispersability depending on the processing conditions and possible surface modifications [155]. Owing to their superior mechanical properties, low density, biodegradability, renewability and low cost cellulose nanocrystal (CNC) offers the potential of generating new products when well dispersed in polymers [31]–[33]. High strength cellulose nanocrystal (CNC) are typically obtained from acid hydrolysis of cellulosic fibers and have a rod-like shape with a length of tens to hundreds nanometers and thickness of four to tens nanometers [31], [35], [156]. In recent years CNC has been successfully added to variety of polymers improving their thermo-mechanical performances. However incorporation of CNC nanoparticles into polymer blends has rarely been studied [17], [157].

2.6.1 Localization of Solid Inclusions in Polymer Blends

Morphology of immiscible polymer blends containing solid inclusion can be significantly different than that of the binary counterparts. Tuning the localization of solid-inclusion in either phases or at the interface of binary polymer blends is a key parameter in controlling the morphology and final properties.

2.6.1.1 Thermodynamic Effect

From a thermodynamic point of view, the localization of the nano-inclusion can qualitatively be estimated by comparing the surface tensions of the three components. Differences between the surface tensions defines the location where the CNC particles will be located after mixing. This can be estimated by the Young's equation [155]:

$$\omega = \frac{\gamma_{NCC-2} - \gamma_{NCC-1}}{\gamma_{12}} \tag{2.19}$$

where γ_{NCC-i} is the interfacial tension between the nano-inclusion and the polymer i, γ_{12} is the interfacial tension between the two polymers and ω is the wetting coefficeint. When $\omega < -1$ the CNC is only found in polymer 2. For value of $\omega > 1$ the particles are presented in polymer 1. If $-1 < \omega < 1$, the CNC is located at the interface of the two polymers. Interfacial tensions can be calculated based on the two main approaches, harmonic-mean:

$$\gamma_{ij} = \gamma_i + \gamma_j - 4\left[\frac{\gamma_i^d \gamma_j^d}{\gamma_i^d + \gamma_j^d} + \frac{\gamma_i^p \gamma_j^p}{\gamma_i^p + \gamma_j^p}\right] \tag{2.20}$$

and geometric-mean equations:

$$\gamma_{ij} = \gamma_i + \gamma_j - 2\left[\left(\gamma_i^d \gamma_j^d\right)^{1/2} + \left(\gamma_i^p \gamma_j^p\right)^{1/2}\right] \tag{2.21}$$

Elias et al. [88] found that by simultaneous mixing of all components, hydrophilic nanosilica were located in the PS phase while hydrophobic nanosilica were localized in the PP phase in PP/PS blends. These localizations were in line with the thermodynamic prediction of Young's model. Although Young's model have been able to predict the localization of nanoparticles, some researchers have reported discrepancy between experimental localization of nanoparticles and theoretical predictions [30], [158], [159]. The difference between melting points of polymers and also uncertainty in the surface tension data of components have been noted as the chief reasons for these discrepancies.

Changing the surface characteristic of nanoparticles has been shown to be an effective approach to alter the themodynamically stable localization of nanoparticles in binary polymer blends. Li et al. [160] studied the effect of interfacial tension and the presence of PP-g-maleic anhydride (PP-

g-MA) on the localization of Tio_2 nanoparticles in PP/PET blends. Their theoretical analysis predicted the thermodynamically stable localization of the Tio_2 particles in the PET phase irrespective of the sequence of addition in PP/PET blends without PP-g-MA. However in the presence of PP-g-MA they found the preferential localization of the Tio_2 particles in the PP phase. They explained that PP-g-MA adsorbs on the surface of nanoparticles by electronic donation and then becomes compatible with the PP phase. Similar observation was reported by Gultner et al.[161] for PC/SAN/carbon nanotubes (CNT) system. They demonstrated that the incorporation of N-phenylmaleimide styrene maleic anhydride (N-PSMA) changed the localization of CNTs and the electrical properties of co-continuous PC/SAN blends. In PC/SAN/CNTs systems CNTs particles were located in the PC phase irrespective of the sequence of mixing while after addition of the N-PSMA all the nanoparticles were resided in the miscible SAN/N-PSMA phase. Strong interaction between maleic anhydride groups (MA) of the N-PSMA and CNTs and miscibility of N-PSMA with SAN were reported to be the main reasons of changing the localization of CNTs from PC to the SAN/N-PSMA miscible phase. Bose et al. [162] were able to localize MWNT particles at the interface of PA6/ABS blends by adding styrene-maleic anhydride copolymer (SMA) to the blend. Their SEM analysis revealed the encapsulation of the SMA copolymer on the nanoparticles surface. In another study Liu et al. [163] demonstrated the thermodynamic stable localization of nanosilica particles in PP phase in PP/ethylene propylene rubber (EPR) blends. Addition of EPR-graft-maleic anhydride (EPR-g-MA) to the system, however, altered the localization from PP to EPR-g-MA phase. Chen et al. [164] were able to alter the localization of CNT particles from PC to acrylonitrile butadiene styrene (ABS) phase with the addition of 5 wt.% of ABS-g-MA to the ABS phase.

2.6.1.2 Kinetic Effects

Migration of particles is thermodynamically favored in order to decrease the free energy of system. Typically all of the theoretical predictions are valid as long as surface energy effects are dominant. In other words kinetic contributions during mixing process may rule out these equilibrium states [30], [155]. Kinetic contribution in particle migration is strongly affected by the viscosity changes, competitive adsorption/desorption of the two phases and also the sequence of addition of the blend components. In this section, the effect of different kinetic parameters on the migration and localization of solid particles in polymer blends will be reviewed.

The effect of sequence of addition. In most of the studies in which nanoparticles and both

polymers were fed into the mixing chamber simultaneously, a thermodynamically stable localization of nanoparticles has been found [25], [26], [165]–[169]. However, in the cases that nanoparticles are premixed with the less favored phase, different observations have been noted. Some researchers found the migration of nanoparticles from the less thermodynamically stable phase toward the favorable one while in many systems inhibited migration and nonstable localization has been reported [27], [30], [158], [161], [164], [170]–[172]. Baudouin et al. [158] observed that when CNT particles are fed into PA12/ethylene–acrylate (EA) copolymer blends, they selectively reside at their thermodynamically stable location at the interface while they remain in the PA12 when they are premixed with PA12.

The effect of viscosity. Viscosity is known as a strong kinetic barrier for nanoparticles migration toward stable localization. Taghizadeh et al. [30] reported that by blending a PCL/CNT masterbatch with TPS in an internal batch mixer carbon nanotube are located at the interface and in the PCL phase. However preparation of the samples with a twin-screw extruder led to a complete migration of nanotubes to the TPS phase as is shown in Figure 2.16. They postulate that in addition to the different flow filed in an internal mixer and an extruder, TPS viscosity drops in twin screw extruder which facilitate the migrations of the nanotubes toward the TPS phase.

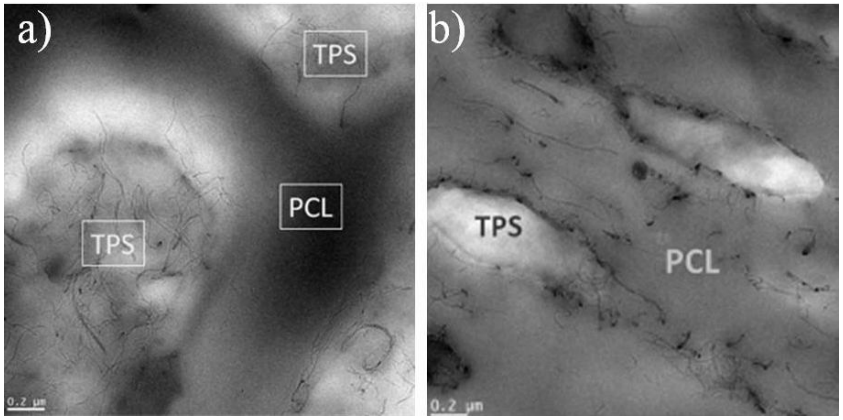

Figure 2.16. TEM images of PCL/TPS blends with 2 wt% CNT prepared by a PCL/CNT masterbatch. a) sample prepared in an twin-screw extruder; b) sample prepared in an internal mixer [30].

Figure 2.17 shows that hydrophobic silica particles localize completely at the interface of ethylene-co-vinyl acetate (EVA) phase in PP/EVA blends only when EVA has a low viscosity [159]. Jalali dil et al. [27], [28] in two separate studies, examined the effect of viscosity on the localization of nano and microsilica particles in PLA/PBAT low interfacial tension and PLA/PE

high interfacial tension systems as is shown in Figure 2.18. For the low interfacial tension PLA/PBAT system, nano and microsilica particles are located in the thermodynamically stable PBAT phase regardless of the PLA viscosity when they are fed into a PLA/PBAT melt. When

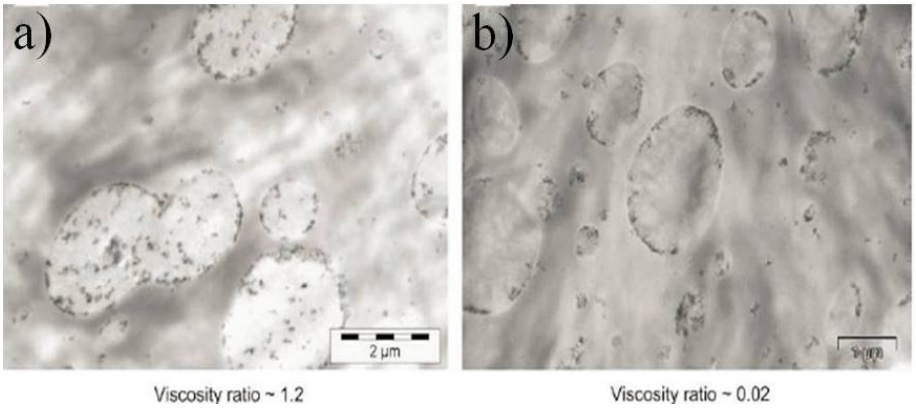

Figure 2.17. Localization of hydrophobic silica particles in EVA/PP blends: a) high viscosity EVA, b) low viscosity EVA [159].

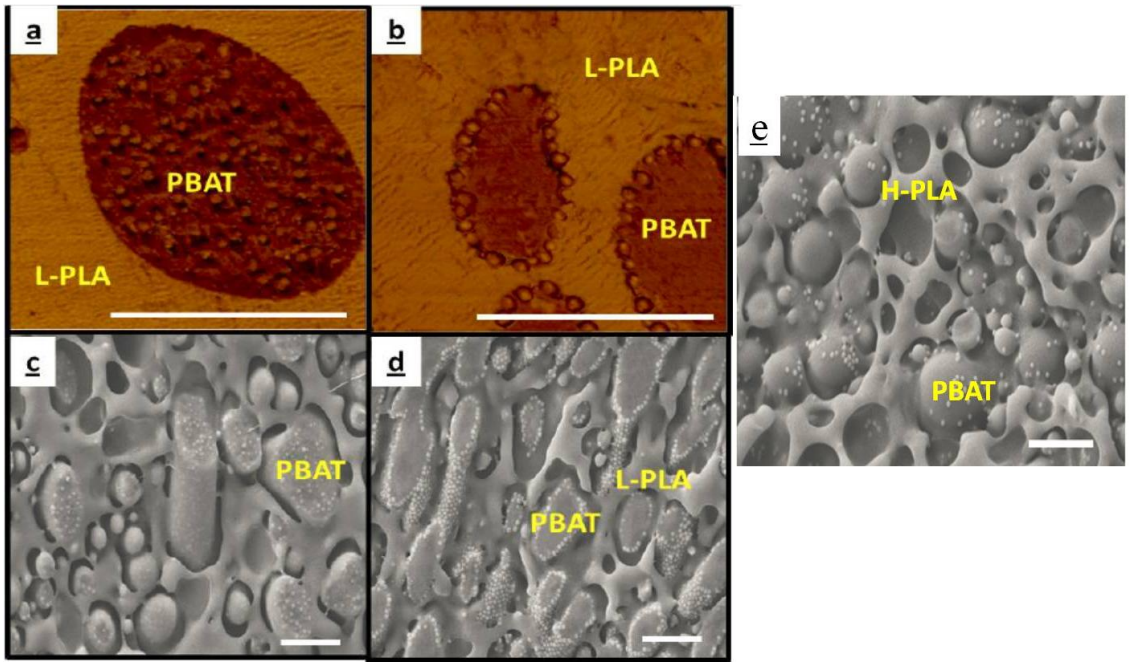

Figure 2.18. The effect of viscosity on the localization of 3 wt% nanosilica particles in PLA/PBAT 70/30 blends: a, c) AFM and SEM micrographs of sample in which nanoparticles were added to the low viscosity PLA (L-PLA)/PBAT melt, (b, d) AFM and SEM micrographs of sample in which nanoparticles were first premixed with low viscosity PLA (L-PLA) and e) SEM image of sample in which nanoparticles were first premixed with high viscosity PLA (H-PLA). The scale bar indicates 2 µm [27].

silica particle are mixed with the less favored PLA phase, however, they found that the migrations of microsilica particles strongly depends on the PLA viscosity, mixing shear rate and silica particle size. Nanosilica particles however are located at the PLA/PBAT interface regardless of the PLA viscosity. Low interfacial tension of PLA and PBAT was shown to be the reason of the stable localization of nanosilica at the interface. It was shown that in polymer blends with high interfacial tension, the thermodynamically stable localization of well dispersed nanoparticles is not significantly influenced by kinetic parameters such as sequence of mixing [28].

Effect of dispersion of particles. The increase in agglomerate strength of nanoparticles with decreasing the particle size makes it difficult to achieve a high level of nanoscale dispersion of nanoparticles [35]. Nanoparticle agglomeration not only affects the reinforcement efficacy of nanoparticles but also poor dispersion of nanoparticles may influence their transformation and localization in the binary polymer blends [173], [174]. Baudouin et al. [158] reported that agglomerated CNT particles were remained in the ethylene–acrylate (EA) phase while well dispersed CNT particles migrated toward their thermodynamically favored localization at the interface of PA6/EA blends. Goldel et al. [165] suggested that increasing the aspect ratio of individual nanoparticles increases the dependency of their localization on their state of dispersion. They proposed a so called “slim-fast-mechanism” (SFM) in which the only migration driving force for nanoparticle is the interface curvature as is presented in Figure 2.19. They explained that for high aspect ratio particles during the migration, the interface does not relax until the whole particle passes the interface. It means that the migration driving force does not change during the migrations of particles with high aspect ratio. However agglomeration decreases the aspect ratio of particles resulting in a decrease in the curvature of interface and migrations driving force.

2.6.2 Mechanisms of Particle Migration

The role of thermodynamic and kinetic parameters on the particles localization was discussed in previous sections. The way by which nanoparticles migrate from the less favored phase to the thermodynamically favored one by passing through the interface needs to be discussed. Elias et al. [159] proposed three major mechanism for the migration of nanoparticles from one phase toward other: The first possible mechanism is the Brownian motion of nanoparticles. However due to the high viscosity of polymer matrix, particles cannot migrate under static conditions in

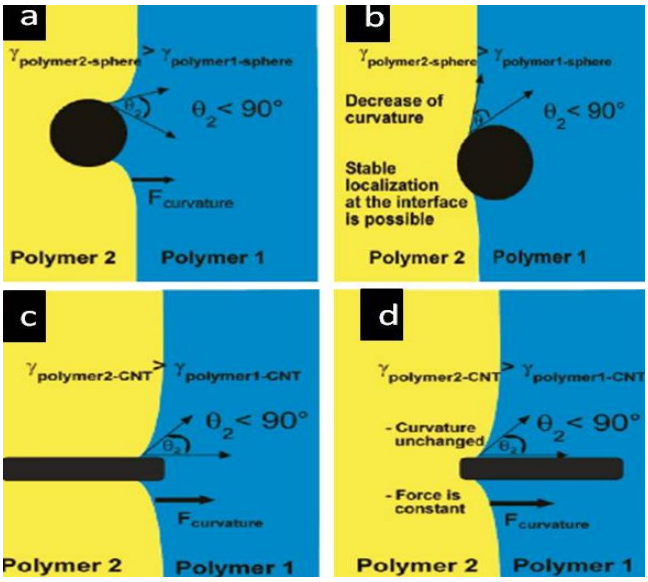

Figure 2.19. a ,b) low aspect ratio particle (or possible aggregated structure of high aspect ratio particles) at the blend interface during melt process. The interfacial curvature is able to relax and thus the driving force is diminishing during the migration, c, d) High aspect ratio particles at the blend interface. The interfacial curvature cannot relax when θ_2 is constant. Thus, the driving force does not change during the migration [165].

polymer melt. The second proposed mechanism is the shear induced movement. During mixing process, nanoparticles and droplet of the minor phase are subjected to numerous collision which may lead to transfer of nanoparticles from matrix to the dispersed phase. The frequency of collisions of nanoparticles moving under shear flow is expressed by the following equation:

$$C = \frac{8}{\pi}\,\dot{\gamma}\varphi \tag{2.22}$$

in which φ and $\dot{\gamma}$ are volume fraction of the considered dispersed phase (polymer droplets or particles) and shear rate, respectively, By considering the shear rate of 100 s^{-1} and φ = 1.5 vol% (in the case of nanoparticles), we would get C = 4 collision/second. If we consider φ = 20 vol% (in the case of polymer droplet), we would get C = 20 collision/second. It has to be noted that because of the small size of individual nanoparticles, they can easily rupture the polymer film trapped between them and polymer droplet compared to the case that two minor polymer droplet collide. The transfer of nanoparticles from matrix toward dispersed phase is not the only possible migration scenario. Another situation exists in which nanoparticles are embedded into the droplet of dispersed phase and tend to migrate toward matrix. It has been proposed that velocity gradient inside the droplet cause the nanoparticles to move across the interface and possibly migrate to

the matrix [155]. This mechanism, however, is not able to explain the effect of the size of nanoparticles, the effect of the components viscosity and thermodynamically instable localization of nano-inclusions observed in the literature [27], [161].

The third possibility is the nanoparticle trapping in the inter-droplet zone of two colliding dispersed polymer droplets. In this mechanism coalescence of dispersed phase has a great influence on the particle transfer from one phase to another. Size and deformability of dispersed polymer phase may influence the efficiency of this mechanism.

Recently Jalali dil et al. [27], [28] studied the migration mechanism of silica particles from the less thermodynamically stable phase toward the more favored interacting one in polymer blends with both high and low interfacial tensions. They studied the migration mechanism of the silica particles from the less thermodynamically stable phase toward the more favored interacting one in the both system. The contribution of the bulk migration, film draining and the migration at the interface were critically examined. Migration of silica particles (nano and micro) was described as a three–stage process: (a) migration from the bulk of the polymer 1 toward the interface, (b) draining of a thin film of polymer 1 between the interface and the particle and (c) passing through the interface. Figure 2.20 shows an schematic of these three steps. They reported a number of fascinating observations when kinetic effects are imposed by premixing of silica

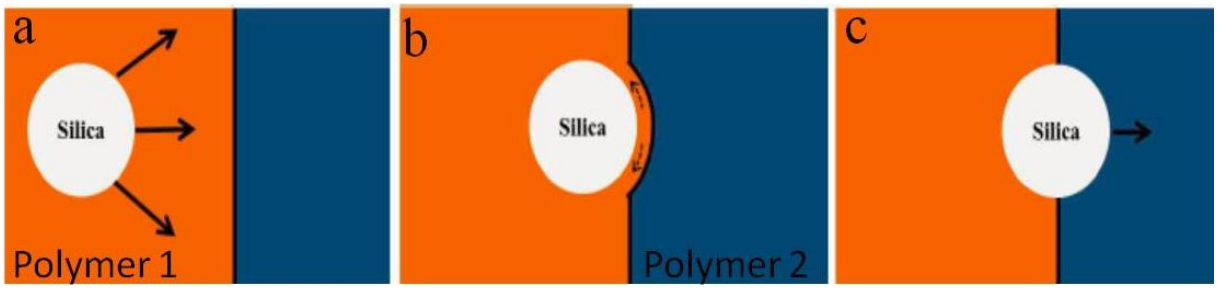

Figure 2.20. The migration mechanism of a silica particle from the less favored polymer1 toward the thermodynamically favored polymer2. Silica particles were fed into blends through a masterbacth of polymer1/silica particles: a) migration from the bulk of the polymer1 toward the interface, (b) draining of a thin film of polymer 1 between the interface and the particle and (c) passing through the interface [27], [28].

particles with the less favored polymer: (i) the migration of individually dispersed nanosilica particles from the bulk toward interface is not a limiting factor in neither low nor high interfacial tension polymer blends; (ii) film draining is a critical stage in the transfer of microsilica particles in polymer blends with both high and low interfacial tensions; (iii) the migration through the

interface is a critical step in the transfer of nano and microsilica in low interfacial tension polymer blends while it does not influence the localization of the particles in high interfacial tension polymer systems. A summary of the factors that control the transfer and localization of nano and microsilica particles in both low and high interfacial tension polymer blends is presented in Table 2.5.

Table 2.5. The parameters that control the transfer and localization of silica particles in both low and high interfacial tension polymer systems [32].

	High interfacial tension blends	Low interfacial tension blends
Microsilica	Film draining step	Film draining step Migration at the interface
Nanosilica	Film draining in the case of aggregation	Migration at the interface

Considering this kinetic control of particle movement, by quenching a polymer blend before attaining equilibrium, the particle localization can eventually be different than that predicted by thermodynamic theories. Hong et al. [175] studied the time dependent localization of nanoarticles in PBT/PS/organoclay ternary system. TEM micrographs of this system are shown in Figure 2.21. At the early stage of mixing process, 300 s, most clay particles are resided in the

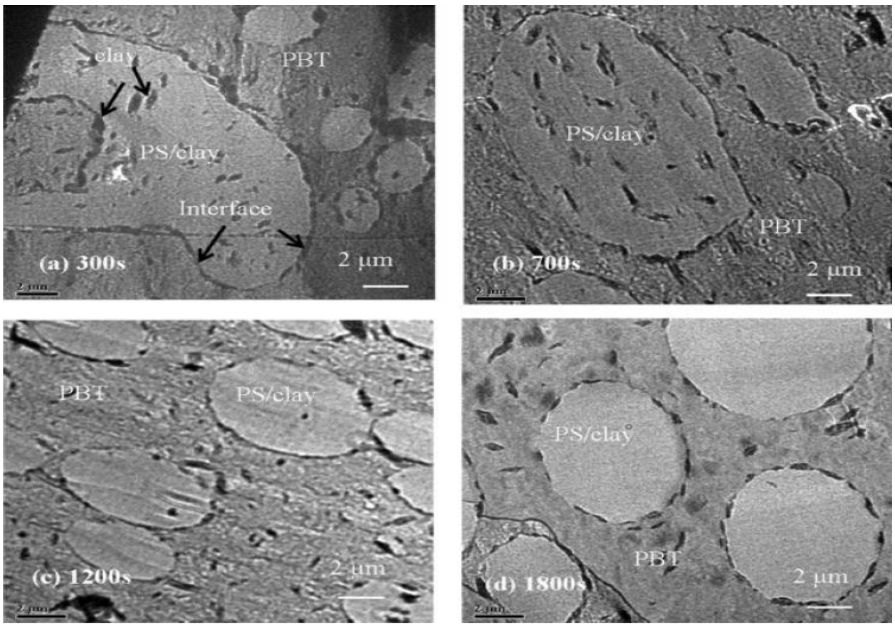

Figure 2.21. Migration of oraganoclay nanoparticles in PBT/PS blend by time at shear rate of 1 S^{-1}: a) 300 s b) 700 s c) 1200 s and d) 1800 s [175].

PS phase. After 700s, nanoparticles are located in both PS phase and at the interface. As 1200s, most of the particles migrate into the interface. At 1800s of mixing all of clay nanoparticles are located in the PBT phase and at the interface.

2.6.3 The Effect of Nanoinclusion on Morphology of Polymer Blends

Generally solid inclusions may change the morphology of polymer blends by increasing the compatibility of the blends components [168], [171], [176], coalescence suppression [25], [26], [177], [178] or changing the viscoelastic properties [155], [177], [178] of the phases. Specific interaction of the nano-inclusion and both polymers may lead to compatibility [171]. Moreover, changes of the viscosity ratio or even shape restriction of solid-inclusion can result in morphology alteration [159]. In this section we are going to discuss the effect of different localization of nanoparticles on the morphology of binary polymer blends.

2.6.4 Localization of Nanoparticles in Matrix

It is generally believed that segregation of nanoparticles within one phase only affects the kinetics of morphological evolution and does not expect to change the thermodynamic interactions between two polymers [179]. It was reported that selective localization of silica particles in the PP matrix decreases the dispersed phase size in PP/ethylene-octene copolymer (POE) blends [174]. Ashabi et al. [180] demonstrated that selective localization of OMMT nanoparticles in the PA6 phase of compatibilized PA6/SAN blends refines the co-continuous morphology as is shown in Figure 2.22. They attributed that to the role of exfoliated clay nanoparticles in inhibiting the phase coalescence and enhanced elasticity of the PA6 phase.

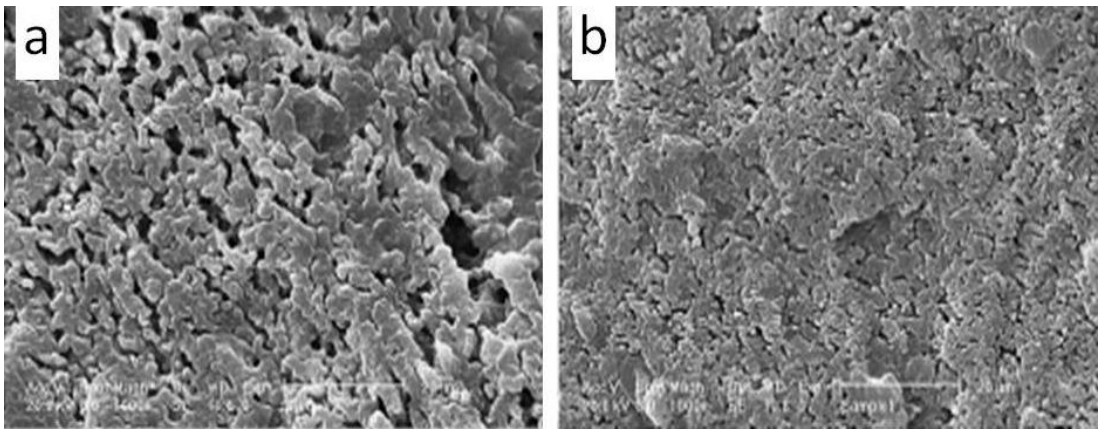

Figure 2.22. SEM photomicrographs of a) PA6/ABS/SANMA and b) comaptibilized PA6/ABS/5% OMMT [180].

The decrease in the dispersed phase size in polymer blends in the presence of solid inclusions localized in the matrix has been related to changes in the breakup-coalescence behavior through two major mechanisms: a) droplet-droplet coalescence is inhibited by nanoparticles which act as solid barriers at contact points [155], [171], [181]. b) reduced chain mobility around the nanoparticles which increases the viscoelastic properties of the matrix and drainage time of the matrix thin film separating the droplets of the dispersed phase [155], [174], [181]. Moreover, any changes in the matrix viscoelastic behavior might influence the droplet breakup process. Khatua et al. [182] found that, the exfoliated clay platelets located in polyamide6 matrix effectively prevent the coalescence of the poly(ethylene-ran-propylene) domains. Lee et al. [183] demonstrated that by addition of silica nanoparticles to co-continuous PP/polyolefin elastomer (POE) blends in the presence of maleated PP as a compatibilizer, a finer morphology consisting of elongated POE domains within the PP phase is obtained. They attributed that to the increase in the tendency of the PP phase to form the continuous phase by increasing the silica loading. Filippone et al. [177] observed a significant reduction in the size of PE dispersed phase in PA6/PE 75/25 blends, upon addition of small contents of organoclay nanoparticles which were selectively located in PA6 major phase. They postulated that nanoclay platelets act like solid-barriers which hinders the coalescence of colliding PE droplets during melt mixing. On the basis of these observation they proposed a schematic mechanism illustrating the role of the nanoparticle in coalescence suppression, Figure 2.23.

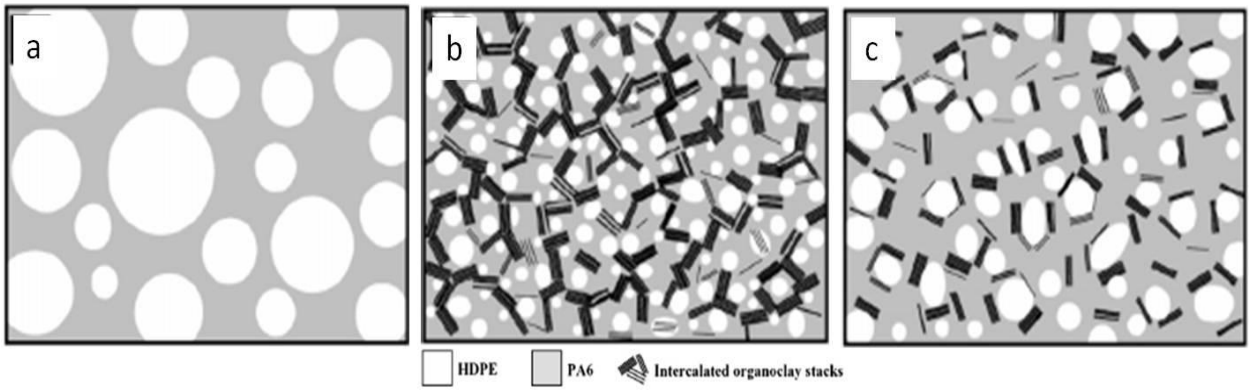

Figure 2.23. Schematic mechanism illustrating the role of the nanoparticle in coalescence suppression in binary PA6/HDPE blends [177].

2.6.5 Localization of Nanoparticles in the Dispersed Phase

In case of selective localization of nanoparticles in the dispersed phase, the increased viscosity and elasticity of the dispersed phase stabilizes irregularly-shaped domains which may eventually lead to stable co-continuous structures [25], [26], [177], [184]. Nuzzo et al. [26] found that the selective localization of three different nanoparticles including CNT, organoclay, organo-modified sepiolite in the PA11 phase converts the dispersed/matrix morphology to a stable highly continuous structure at a critical nanoparticle concentration in PA11/PLA blends. This observation was attributed to the retarded relaxation time of the PA11 dispersed phase due to the formation of a network structure of nanoparticles in PA11 phase. The localization of carbon black nanoparticles within PA6, in PA6/ABS blends led to an increase in the viscosity of PA6 phase and thus morphology conversion from matrix/dispersed to co-continuous [184] as is shown in Figure 2.24. In another study, Filippone et al. [177] reported that increasing the concentration of organoclay nanoparticles, preferentially located in PA6 dispersed phase in PA6/HDPE 25/75 blends, results in a high level of PA6 continuity. They attributed that to the rheological transition of PA6 phase from liquid- to solid-like behavior with increasing the nanoparticles content.

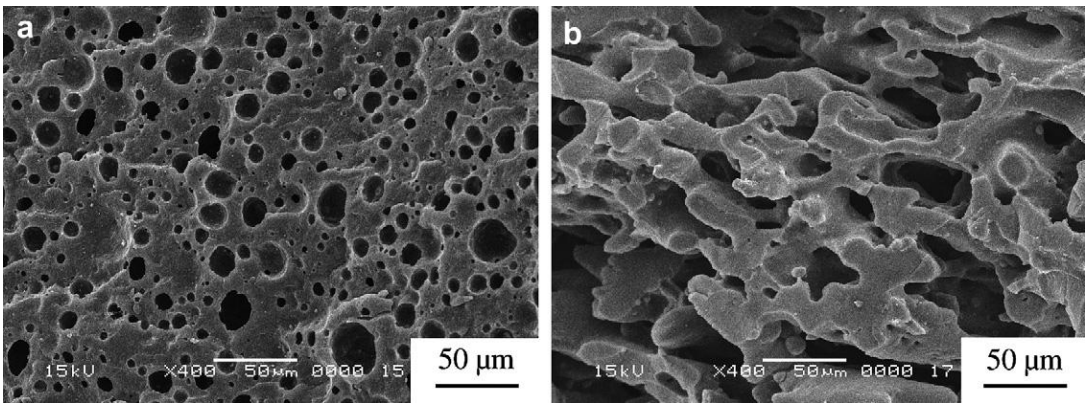

Figure 2.24. SEM micrographs of the PA6/ABS blends (40/60) a) without CB, PA6 extracted with formic acid; b) 7.5 phr CB, ABS was extracted by THF [184].

2.6.6 Localization of Nanoparticles at the Interface

Localization of nanoparticles at the interface of polymer blends may lead to a reduction in the dispersed phase size through two major mechanism [155], [181]: a) suppression coalescence resulted by the solid barrier effect of nanoparticles and b) compatbilization effect of nanoparticles on blends. In the first mechanism, nanoparticles form a solid shell around the dispersed phase which prevents the coalescence of colliding droplets of the dispersed phase.

Elias et al. [159] reported that although addition of 3 wt% of hydrophobic silica to PP/EVA 80/20 blends did not completely cover the interface of the dispersed phase, it decreased the dispersed phase size from 1.6 μm to 0.9 μm. Therefore small amount of interfacially located nanoparticles even lower than interfacial saturation concentration can diminish the dispersed phase size. The formation of a CNT solid shell around PA6 droplets in PA6/EA was shown to be effective in diminishing the droplet/droplet coalescence [158]. In the second mechanism interaction of nanoparticles with polymer components and the consequent reduction in the interfacial tension results in the blend compatibilization and decrease in the dispersed phase size. Fang et al. [185] proposed that strong interactions between polymers and nanoparticles immobilize polymer chains at the interface similar to a copolymer. Elias et al. [171] determined the interfacial tension between PP and PS with and without silica nanoparticles by using the Palierne's rheological model. They observed a reduction in the interfacial tension from 2.3 mN/m to 0.45 mN/m upon addition of 3 wt% of silica nanoparticles. A reduction in the volume average diameter of the PS dispersed phase from 6.5 μm to 1.7 μm upon addition of 3 wt% nanoparticle was reported. In another work a reduction of the interfacial tension from 0.94 mN/m for neat poly(ethylene-*co*-vinyl acetate) (EVA)/PP blends to 0.18 mN/m for EVA/PP blends with 3 wt% nanosilica was reported [168]. Salehyian et al. [186] reported that selective localization of 5 wt% organoclay at the PP/PS blends interface decreases the interfacial tension from 1.9 mN/m to 0.4 mN/m. Localization of multiwall carbon nanotube at the interface was reported to improve the interfacial adhesion and mechanical properties of poly (styrene-co-acrylonitrile)/poly(vinyl chloride) blends [187]. Jalali et al. [29] studied the effect of interracially assembly of nanosilica particles on the morphology of PLA/PBAT blends at PBAT compositions close to the co-continuity region (PLA/PBAT 70/30) and also within the co-continuity region (PLA/PBAT 50/50). They observed that localization of 1 wt% nanosilica particles at the PLA/PBAT interface, decreases the volume average diameter of the PBAT dispersed phase from 1.7 ± 0.25 μm to 1 ± 0.1 μm. They attributed that to the suppressed coalescence resulted by the nanoparticles. Interestingly, by further increase in the nanoparticle content to 3 wt%, the PBAT/PLA dispersed/matrix morphology changed to a highly continuous structure as can be seen in Figure 2.25. This observation was related to the rheological transitions in PLA/PBAT blends from a liquid- to a solid-like behavior. Moreover, although interfacial assembly of nanosilica particles did not change the co-continuous PLA/PBAT 50/50 morphology, the normalized interface length

increased from 0.54 ± 0.08 μm^{-1} for the pure PLA/PBAT 50/50 blend to 0.7 ± 0.06 μm^{-1} for the PLA/PBAT 50/50 with 3 wt% nanoparticles as is shown in Figure 2.26. They also proposed a conceptual model to explain the continuity development in PLA/PBAT 70/30 vol% blends and

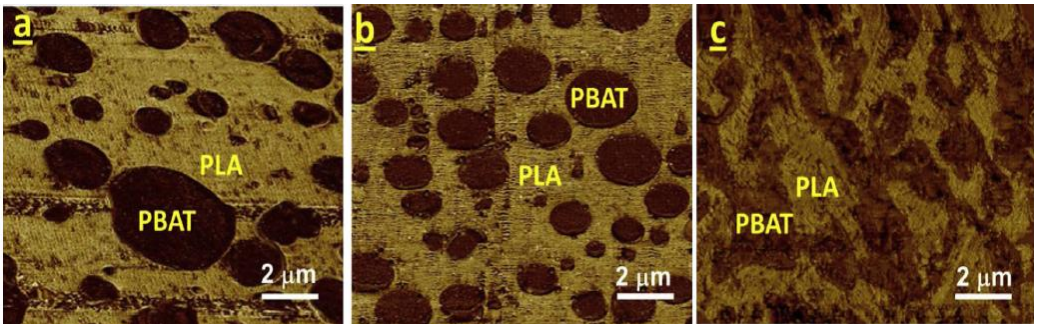

Figure 2.25. AFM micrographs of PLA/PBAT(70/30) blends with different nanosilica concentrations a) PLA/PBAT(70/30), b) PLA/PBAT(70/30) with 1 wt.% nanosilica, c) PLA/PBAT(70/30) with 3 wt.% nanosilica [29].

finer morphology in PLA/PBAT 50/50 vol% blends in the presence of nanosilica particles as is shown in Figure 2.27. They explained that during mixing due to the deformation of the PBAT fibers a fresh PLA/PBAT interface is formed. Transfer of nanosilica from the PLA phase to the fresh interface inhibits relaxation and breakup process of the PBAT fibers. The migration of nanosilica stabilizes the newly formed interface and prevents relaxation or breakup of the PBAT

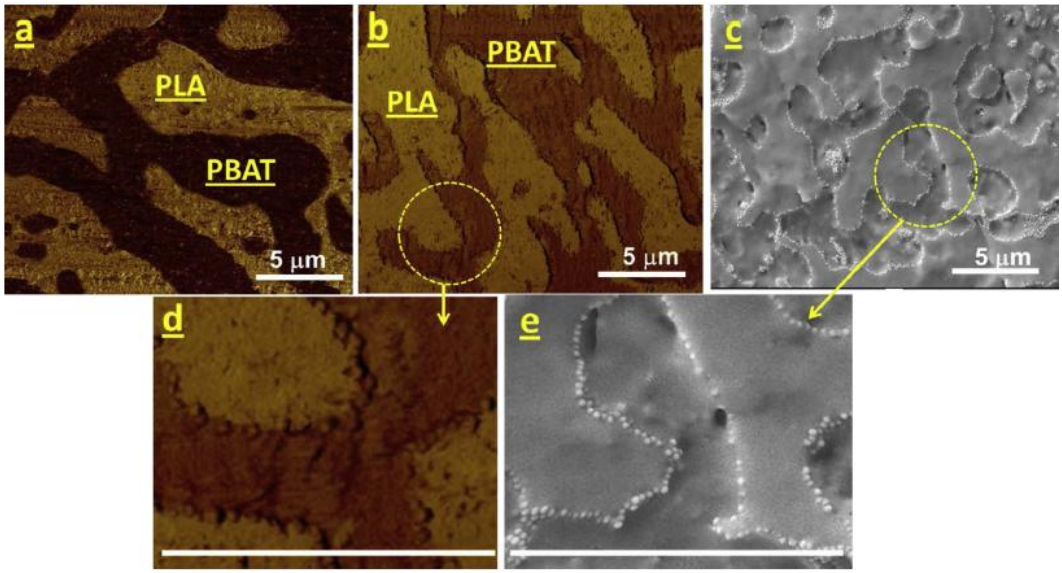

Figure 2.26. The effect of the interfacial assembly of silica particles on the morphology of PLA/PBAT 50/50: a) AFM micrograph of PLA/PBAT 50/50, b) AFM micrograph of PLA/PBAT 50/50 with 3 wt.% silica, c) SEM micrograph of a cryofractured surface of PLA/PBAT 50/50 with 3 wt.% silica, (d) and (e) are higher magnification of images (b) and (c), respectively. The white scale bar indicates 5 μm [29].

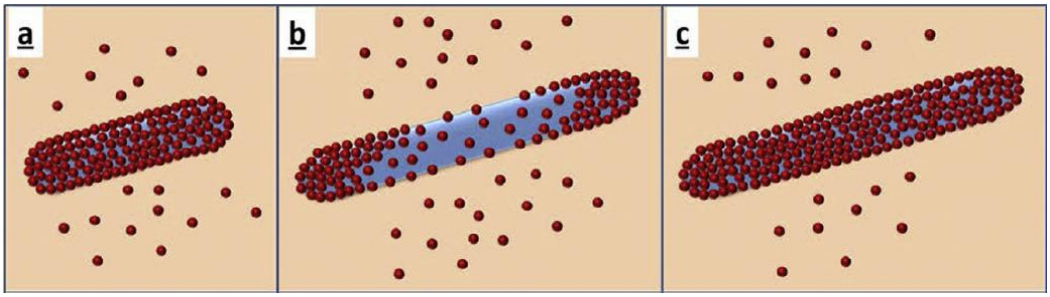

Figure 2.27. The co-continuity development in PLA/PBAT(70/30) with 3 wt.% interracially localized nanosilica particles: a) nanosilica particles cover a PBAT fiber interface b) formation of a fresh PLA/PBAT interface, (c) stabilization of the PBAT fiber due to transfer of nanosilica particles to the interface [29].

phase. This leads to a highly elongated fibrillar morphology which eventually results in a co-continuous morphology in the system. The finer co-continuous morphology was also assigned to the formation of more elongated PBAT phase. Trifkovic et al.[188] also reported a finer co-continuous morphology with an enhanced interfacial area resulted by the preferential localization of organoclay nanoparticles at the interface of a co-continuous PEO/LDPE blend. This was attributed to the compatibilization effect of organoclay particles.

2.7 Bionanocomposites

Biocomposites made of biofillers and bioplastic are ecofriendly materials known as green composites. The best known renewable resources for biofiller is cellulose. Cellulose nanocrystal is known as the second generation of cellulosic based fibers which has achieved a lot of attention.

2.7.1 Cellulose Nanocrystal (CNC)

Isolation of CNC. The major process for preparation of rigid rodlike nanoparticles known as CNC from cellulose microfibrils is based on acid hydrolysis [189]. Amorphous or non-crystalline regions of cellulose microfibrils are susceptible to acid attack, while crystalline regions with a higher resistance to acid hydrolysis remain intact [189], [190]. Hydrochloric and sulfuric acids are used widely in CNC isolation process. CNC particles prepared with hydrochloric acid hydrolysis have a limited dispersability and their suspension in water tends to flocculate. On the other hand, in CNC particles prepared with hydrolysis in sulfuric acid, charged surface sulfate esters resulted by reaction of sulfuric acid and hydroxyl groups of cellulose

facilitate their dispersion in water. The thermostability of CNC particles, however, decreases with introducing charged sulfate groups. Dufresne et al. [31] reported that the stability of CNC aqueous suspension depends on the CNC dimensions, their size polydispersity and their surface charge. In spite of the acid type, hydrolysis preparation conditions such as acid concentration, ultrasonic treatment time, temperature and time of hydrolysis are need to be optimized. Bondeson et al. [191] obtained CNC particles with length between 200 and 400 nm by using sulfuric acid of 63.5% (w/w) concentration for about 2 h. [189]. Beck-Candanedo et al. [192] studied the effect of time and sulfuric acid-to-cellulosic fiber ratio on CNC characteristics. They showed that longer hydrolysis time results in shorter CNC particles with narrower size distribution. Elazzouzi-Hafraoui et al. [193] studied the effect of hydrolysis temperature on the size distribution of CNC particles obtained by sulfuric acid (65%) hydrolysis of cotton fiber over 30 min. They demonstrated that increasing the hydrolysis temperature decreases the size of the nanoparticles. Cellulose whiskers are prepared from a variety of sources such as bacterial cellulose, hemp, sugar beet, sisal, ramie, cotton, microcrystalline cellulose (MCC), algal cellulose, tunicin and wood [39], [189], [190]. Figure 2.28 shows TEM images of some CNC particles derived from different sources.

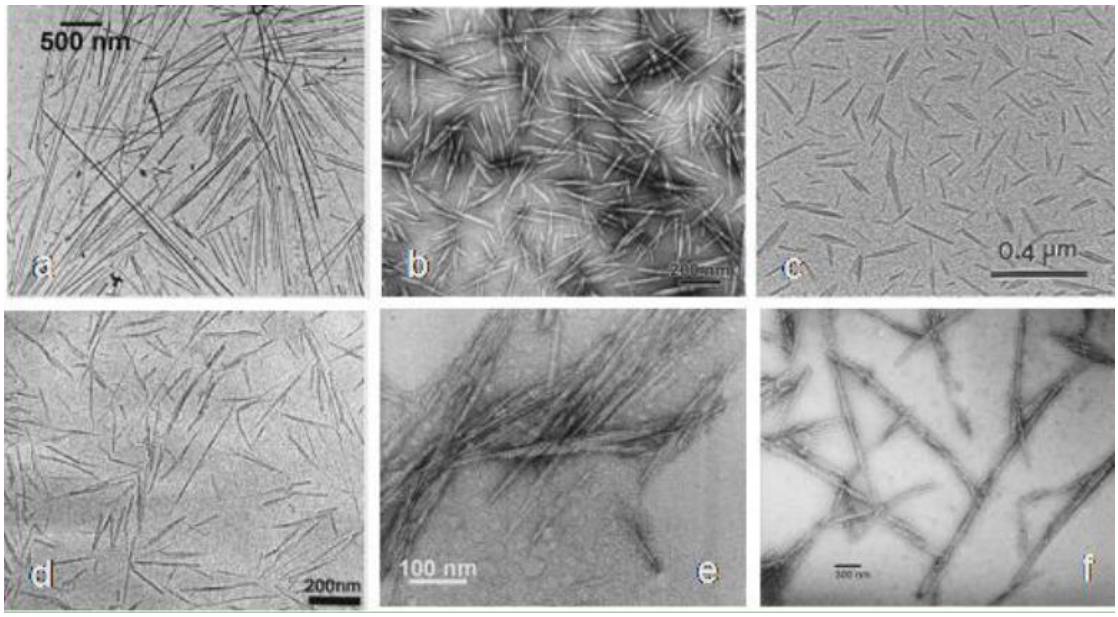

Figure 2.28. TEM images of CNC particles obtained with acid hydrolysis from different sources: a) tunicin, b) ramie, c) cotton, d) sugar beet, e) micro crystalline cellulose, and f) bacterial cellulose [190].

Shape and size. The dimensions of CNC particles strongly depends on the source of cellulosic material and the hydrolysis conditions. Microscopy (TEM, FE-SEM and AFM) and light scattering techniques are typically used for geometrical characterization of CNC particles [31]. AFM is a reliable technique in analyzing surface topography of CNC particles compared to the other microscopic techniques, such as TEM, in which beam sensitivity is a big challenge [156]. However, due to the tip-broadening effects AFM analysis may present rounded cross-section in cases that other shapes are expected. Typical dimensional characteristic of some CNC particles derived from different sources are presented in Table 2.6.

Table 2.6. dimensional characteristic of some CNC from different sources [189].

Cellulose type	Length (nm)	Cross section (nm)
MCC	35-265	3-48
Cotton linter	25-320	6-70
Ramie	150-250	6-8
Tunicate	100-1000	15-28
Hard wood	140-150	4-5
Sisal	100-500	3-5
Bacterial	100-1000	10-50

Mechanical properties. Some physical properties of CNC particles and some other widely used filler are compared in Table 2.7. The mechanical properties and surface area of CNC particles are in a good range that qualify them to be used as nano-reinforcement in polymer composites. Due to its low density, renewable nature, high potential for surface modification and renewable resources, CNC particles have become of great interest [194]–[196]. Compared to carbon nanotubes (CNT), which is one of the strongest known nanofiller, CNC particles have lower strength but the final costs of CNC particles are lower than that of CNTs, which makes CNC based nanomaterials more attractive for certain applications [194]. For instance, carbon

Table 2.7. Some physical properties of CNC particles compared to some other fillers [194], [196].

Filler	Density (g/cm^3)	Tensile strength (GPa)	Tensile Modulus (GPa)	Surface area (m^2/g)
Glass fiber	2.5	2-3.5	70	1
Clay	2.9	....	140-170	750
Carbon nano-tubes	1.7	11-63	150-500	100-1000
CNC	1.5	10	130-150	250

nanotubes (CNT) are made by methods such as thermal or plasma enhanced chemical vapor depositions or laser ablation which are very complex and expensive. However, CNC particles are produced with a relatively easy hydrolysis reactions with a lower cost [196].

2.7.2 Polymer/CNC Nanocomposites

Since the first announcement of using CNC in polymer composites by Favier et al. [197], CNC has gathered a lot of interests in the composites field. CNC particles have been incorporated into both bio and synthetic polymers such as poly(vinyl alcohol), poly(caprolactone), cellulose acetate butyrate, polypropylene, polyethylene, poly(oxyethylene), carboxymethyl cellulose, poly(vinyl acetate), poly(lactic acid), poly(hydroxyoctanoate), chitosan and starch based polymers [31], [189].

2.7.2.1 Processing Techniques

Processing methods have substantial effects on the final performance of CNC nanocomposites. Intrinsic properties of CNC particles, their surface characteristics (modified or not and charge type) and polymer matrix properties (degradation, dispersibility and solubility) have to be considered in choosing a proper processing technique [31], [189], [198]. Different strategies for homogeneous dispersion of CNC particles in a polymer matrix are summarized in Figure 2.29.

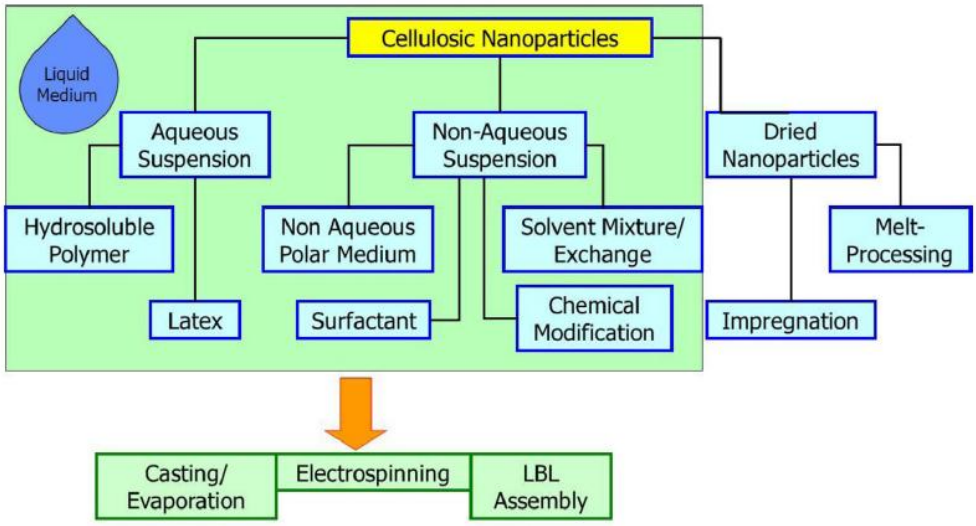

Figure 2.29. Different strategies in the processing of CNC nanocomposites [198].

Solvent dissolution-casting process. Solvent casting is known as the main method to transfer

CNC particles into a polymer matrix. Without surface modification, CNC particles have strong tendency to agglomerate and thus it is extremely difficult to disperse them in polymer matrices. This problem is even worse when CNC particles are dried and not in aqueous suspension before nanocomposite processing. Due to the hydrophilic nature of CNC particles, water is a favored processing medium which limits the choice of the matrix to water soluble polymers. The first alternative is therefore hydrophobic polymers which ensures a proper level of dispersion of CNC particles. After mixing the aqueous CNC suspension and polymer solution, a composite film can be prepared by casting/evaporation on teflon or propylene dishes, or freeze-drying followed by compression molding. Dispersing CNC particles in an appropriate (respect to matrix) organic solvent is the second alternative. This is typically possible by using a surfactant or chemical modification of CNC particles. Although the used of surfactant is a simple method, high concentration of surfactant required to coat the high surface area of CNC particles limits the use of this method in composite preparation. The surface chemical modification is the second approach to dispersed CNC particles in an organic medium. However it has been reported that chemical modification substantially decreases the mechanical performance of the final product. Freeze-dried CNC powder were successfully dispersed in organic solvents such as DMF [38], DMSO, formic acid and m-cresol without any surface modification [31], [189], [198].

Melt processing. Melt blending as an industrial processing technique has also been used in the preparation of CNC based nanocomposites. The process involves pumping an aqueous suspension of CNC coated with surfactant [189], or poly(vinyl alcohol) coated CNC [41] into PLA melt in an twin screw extruder. However, lack of compatibility was reported for these systems. Jiang et al. [199] introduced CNC particles into PHBV matrix in a twin-screw extruder by using PEO as the CNC carrier. High level of CNC agglomeration, however, was observed. Coating of CNC particles with polyamide 6 (PA6) [200] or PEO [33] prior to melt-blending was also shown to be effective in achieving a high level of CNC dispersion. Dried coated CNC particles were obtained by mixing of CNCs in a PEO/water or PA6/formic acid solution followed by freeze-drying or precipitation in water, respectively. A good level of dispersion of PEO-coated CNC particles in LDPE [33] and PA6-coated CNC in PA6 [200] were reported.

2.7.3 PLA/CNC and PA/CNC Nanocomposites

PLA has been widely used as a biopolymer matrix for CNC based biocomposites. Khoshkava et

al. [35] compared the surface energy interactions, work of adhesion and dispersibility of PLA/CNC and PP/CNC composites. They reported that PLA/CNC composites shows a higher work of adhesion and higher potential of dispersibility than PP/CNC composites due to the higher polarity of PLA compared to PP. Solvent/dissolution technique has been used more frequently in the process of PLA/CNC nanocomposites. Pei et al. [201] reported a good level of dispersion of silylated CNC particles in PLA matrix prepared with solution casting in chloroform. Oksman et al. [202] used a combined solvent dissolution/melt mixing approach to prepare PLA/CNC nanocomposites. PLA/CNC nanocomposites were made by pumping a CNC suspension in N-dimethylacetamide (DMAc)/0.5 wt.% lithium chloride (LiCl) into a PLA melt in a twin screw extruder followed by vacuum evaporation of the solvent. Improved CNC dispersion in PLA matrix was also reported when PEG was used as a processing aid. Bondeson et al. [41] used PVOH/CNC masterbatch to add CNC particles into PLA matrix prepared by melt mixing. Although a good level of dispersion of CNC in PVOH were obtained all nanoparticles remained in the PVOH phase due to the immiscibility of PLA and PVOH. No significant improvement in thermo-mechanical properties was observed which was attributed to the inadequate dispersion of the CNC in the PLA phase. Bagheriasl et al. [38] incorporated CNC particles into PLA matrix through a solution casting method in DMF. They showed that addition of up to 6 wt% CNC into PLA results in a significant increase in the complex viscosity and storage modulus of PLA/CNC nanocomposites.

There are only a few studies reported in the literature considering composites of CNC particles with any kind of polyamide or related polymers. That could be assigned to the low thermal stability of nanocellulose and high processing temperature (usually >230 ºC) of polyamides. Incorporation of cellulose fibers into PA11 is promising as PA11 exhibit lower melting point (190 ºC) than other nylons (except nylon 12). Correa et al. [200] coated the surface of CNC particles with PA6 in order to increase their thermal stability and prevent their aggregation in melt mixed CNC/PA6 nanocomposites. Their DSC and tensile results showed that PA6 coating was effective in increasing the thermal stability and improving the dispersion of CNC particles in PA6 matrix. Incorporation of only 1 wt% PA6-coated CNC led to an 45% increase in the elastic modulus of the PA6/CNC nanocomposites compared to neat PA6.

CHAPTER 3 ORGANIZATION OF THE ARTICLES

The results of the first part of the thesis are presented in Chapter 4 as the first article entitled "Morphology Development in Poly (Lactic Acid)/Polyamide11 biobased Blends: Chain Mobility and Interfacial Interactions". CHAPTER 4 is dedicated to study the morphology and interfacial development in PLA/PA11 biobased blends including the region of dual phase continuity. A variety of interfacial tension techniques including the contact angle, breaking thread, imbedded fiber retraction and in-situ Neumann triangle are studied. The morphology of the blend over the whole composition range is examined and the PLA phase continuity is determined using solvent-extraction gravimetry technique. The morphology stability during quiescent annealing in co-continuous blends is studied. A detailed analysis of the blend thermal and crystallization behavior is conducted. Finally, the addition of plasticizers to both PLA and PA11 is used to examine the influence of chain mobility on the interfacial interactions and morphology.

The Second article is entitled "High Performance Poly (Lactic Acid)/Bio-Polyamide11 through Controlled Chain Mobility" which is presented in CHAPTER 5. This article reports on the role of the controlled PLA chain mobility in developing high performance PLA/PA11 blend. By using an appropriate amount of a proper PLA plasticizer, it is shown that PA11 ability to enhance PLA mechanical properties is affected by the brittle nature of the PLA phase itself. Ternary (PLA-PEO)/PA11 systems demonstrate exceptional ductility at an optimum PEO composition leading to specimens with tremendous increase in the Izod impact strength and elongation at break. The relationship between mechanical properties and PLA/plasticizer phases separation is studied. Assembly of PLA spherulites in PLA/PEO blends with different PEO content after isothermal crystallization and distribution of PEO plasticizer in PLA spherulites is also examined with POM and SEM. Localization of the excessive amount of PEO plasticizer after phase separation in ternary (PLA-PEO/PA11) blends is studied with SEM and AFM.

CHAPTER 6 presents the third article entitled: "Cellulose nanocrystal in Poly (Lactic acid)/Polyamide11 Blends: Preparation, Morphology and Co-continuity". From the knowledge acquired on the morphology of binary PLA/PA11 from the first article, in this work, for the first time the effect of selective localization of cellulose nanocrystal (CNC) particles on the morphology of the PLA/PA11 blend is investigated. CNC is incorporated into PLA/PA11 blends

by a combination of solvent dissolution/melt mixing process. The effect of the kinetic parameters on the localization of CNC particles is studied and the experimental observation are compared with theoretical predictions. The effect of CNC loading on the PLA/PA11 with dispersed/matrix and co-continuous type morphology is also reported. Finally the stability of co-continuous PLA/PA11 50/50 vol% in the presence of 1 wt% CNC particles is examined.

CHAPTER 7 reports on a versatile approach to control the thermodynamically stable localization of CNC particles in melt mixed PLA/PA11 blends. The results are presented as the fourth paper entitled: "Tuning the Localization of Finely Dispersed Cellulose nanocrystal in Poly (Lactic acid)/Bio-Polyamide11 Blends". A high pressure homogenization followed by freeze drying method is utilized to prepare a PEO/CNC mixture. Desired amount of the prepared PEO/CNC mixture is then incorporated into PLA/PA11 blends with three different compositions in two different mixing strategies. SEM, AFM and rheology analysis are employed to evaluate the level of dispersion of CNCs in PEO and PLA. Localization of the nanoparticles in PLA/PA11 blends are examined with SEM and AFM. The effect of PEO-coated CNC particles on the PLA/PA11 blend morphology is examined and compared with the results obtained in the third article.

CHAPTER 4 ARTICLE 1: MORPHOLOGY DEVELOPMENT IN POLY (LACTIC ACID)/ POLYAMIDE11 BIOBASED BLENDS: CHAIN MOBILITY AND INTERFACIAL INTERACTIONS[1]

Vahid Heshmati , Ali M. Zolali and Basil D. Favis

CREPEC, Dept of Chemical Engineering, École Polytechnique de Montréal, Montreal, Canada

4.1 Abstract

In this study, the interfacial tension, morphology, PLA phase continuity and thermal behavior are studied for poly (lactic acid)/bio-polyamide11 blends. This blend combines the very unusual characteristics of high static interfacial tension, 5.8 ± 0.6 mN/m and 5.4 ± 0.4 mN/m as measured by the breaking thread (BT) and fiber retraction (FR) methods respectively, with the fine dispersed morphology and low level coalescence of a highly interacting system after melt mixing. The dispersed phase size at 1 vol% is 750 and 700 nm for dispersed PLA and PA11 respectively with no coalescence whatsoever up to 20 vol% minor phase. A coalescence study during annealing shows that the 50PLA-50PA11 blend behaves as if it were an interfacially modified system. Furthermore, the half time of crystallization of PA11 increases in the presence of PLA, an indication of significant interfacial interactions. A study using plasticizers for both PA11 and the PLA shows that this discrepancy between the static interfacial tension and the observed morphology after dynamic mixing can be attributed directly to the limited chain mobility of the stiff PLA molecule, particularly under quiescent conditions, which inhibits the available functional groups from reacting at the interface. Plasticized PLA in PLA-PA11 serves to significantly reduce the static interfacial tension as well as the phase size and coalescence in the dynamically mixed system at high concentrations of 30 and 40 vol% PLA. These results underline that the stiffness and borderline mobility of PLA chains can have a significant influence on its capacity for interfacial interactions and could be dependent on the flow conditions.

[1] Accepted in Polymer

4.2 Introduction

Poly (lactic acid) (PLA) is a biosourced polyester with unique properties such as high tensile strength and modulus. However, PLA suffers from an inherent brittleness, low deformation at break, low impact strength, and low crystallizability which limits its practical applications [1,2]. The blending of PLA with other polymers offers an effective approach to overcoming these weaknesses [2–5]. Polyamide11 (PA11), derived from castor oil, is a high-performance bio-polymer with good elongation at break and impact strength [3]. It has been widely recognized in the literature that due to the presence of polar functionality in polyamides and polyesters, interfacial reactions could potentially occur between these dissimilar chains during blending [6,7]. From this point of view a PLA/PA11 multiphase system has the potential for both complementary properties and interfacial interactions.

Only a few studies has been conducted so far on PLA/PA11 blends [3–5]. Stoclet et al. [3] investigated the morphology of PLA/PA11 by SEM analysis of cryo-fractured samples. Sub-micronic dispersed phase size was attributed to interfacial interactions in the blend. Patel et al. [4] studied the reactive compatibilization of PLA/PA11 in the presence of a titanium isopropoxide catalyst. No direct evidence of interfacial reaction was reported even in the presence of a high amount of catalyst and high temperatures. In another study the addition of ethylene glycidyl methacrylate-g-styrene-co-acrylonitrile (EGMA-G-AS) did not change the dispersed phase morphology of PLA/PA11 blends [5]. In all of these studies, many aspects of the morphology, coalescence, continuity development and interfacial properties of PLA/PA11 blends, remain unclear or contradictory.

The interfacial tension between polymers is one of the main parameters controlling the dispersed phase size and morphology of polymer blends. Among the different techniques, the breaking thread (BT) and imbedded fiber retraction (IFR) methods have been widely used to measure the interfacial tension between different polymer pairs [8,9]. In these techniques, interfacial tension is measured based on the amplitude of a fiber disintegration or fiber retraction in a matrix under static conditions [10]. Ihm et al. [8] and Lepers et al. [9] employed the BT method to measure the interfacial tension between PE/PET and PP/PET with SEBS-grafted-(MA) as the interfacial modifier, respectively. They reported a significant reduction in the interfacial tension in the modified systems compared to the unmodified ones. The direct measurement of interfacial

tension in polymer blends with the in-situ Neumann triangle (NT) technique has also been reported [10,11]. In this method, which is directly applied to the melt processed blend, the interfacial tension is determined based on the fact that in a ternary system with a partially wet morphology at equilibrium any point of the three phase contact balances the interfacial tension. By using the NT method Kim et al. [11] showed that the interfacial tension in PS-grafted-MA modified PS/PBT blends significantly decreased. Zhang et al. [10] measured the interfacial tension of PS/PBT, PS/PMMA and PMMA/PBT systems with the NT method and their results were in line with those obtained by the BT technique.

It is well known that both the interfacial tension and the dispersed phase size decreases with increasing interfacial interactions in reactive polymer blends [9,12]. The reduction of the dispersed phase size after interfacial modification is actually the result of a combination of effects: a reduced interfacial tension and reduced coalescence [9]. Generally, phase coalescence in polymer blends is divided into two major classes: static and dynamic processes [13]. The former case is a quiescent process, whereby the minor phase/matrix structure grows in size in order to minimize the free energy of the system by decreasing the interfacial area. The latter case is a flow induced phenomena in which a balance between coalescence and droplet breakup determines the dispersed phase size [13]. It has been demonstrated that inter-particle collisions are more likely to result in coalescence if the minor phase size is small and the interface is highly mobile [14]. However, this mobility decreases for interfacially modified blends where interfacial modification leads to fewer droplet-droplet contacts and therefore less coalescence occurs with increasing concentration [15].

This work aims to carry out a detailed examination of the morphology and interfacial development in PLA/PA11 biobased blends including the region of dual phase continuity. A variety of interfacial tension techniques, under static and dynamic conditions, will be studied and compared for this blend. Finally, the addition of plasticizers will be used to examine the influence of chain mobility on the interfacial interactions and morphology.

4.3 Experimental section

4.3.1 Materials

Three different grades of PLA (PLA 3001D (PLA1), PLA 2002D (PLA2) and PLA 3251D (PLA3)) were obtained from Natureworks. PA11 (Rilsan BMNO TL) and Poly(ethylene) oxide

(PEO) water-soluble polymer (POLYOX™ WSR-N10) were produced by Arkema and Dow, respectively. N-Butylbenzene sulfonamide (BBSA) was used as plasticizer for PA11. PLA and PA11 were dried at 80 °C and PEO was dried at 45 °C overnight before use. PLA-1 was used in all the work reported in this paper. PLA-2 and PLA-3 were used specifically for the viscosity ratio study.

4.3.2 Interfacial Tension

The contact angle [16], classical breaking thread (BT) [17], imbedded fiber retraction (IFR) [17] and in-situ Neumann-triangle (NT) [11] methods were used to measure the interfacial tension between PA11 and PLA at 200 °C.

4.3.2.1 Contact Angle

For surface energy measurements, PLA and PA11 granules were first dried in a vacuum oven at 60 and 80 °C for 48 h, respectively. Polymer films with a thickness of about 1mm were prepared by compression molding. The prepared films were washed with ethanol and distilled water and then dried in a vacuum oven over night. Surface energy and contact angle measurements of the polymer films were carried out with probe liquids. The details of the method are described elsewhere [16]. Briefly, the prepared films were placed in the test chamber and a drop, about 4-7 µl, of liquid probe was placed gently on the film. The drop evolution was monitored by a CCD camera. Images were taken every 40s until a stable drop shape was obtained. Smapera software (Coreco Inc, Canada) were used for image processing. The PLA/PA11 interfacial tension was calculated with the harmonic mean approach:

$$\gamma_{ij} = \gamma_i + \gamma_j - 4\left[\frac{\gamma_i^d \gamma_j^d}{\gamma_i^d + \gamma_j^d} + \frac{\gamma_i^p \gamma_j^p}{\gamma_i^p + \gamma_j^p}\right] \quad (4.1)$$

4.3.2.2 Breaking Thread (BT)

The BT method consists of heating a filament of the polymer with higher melting temperature sandwiched between two films of the other component and analyzing the evolution of capillary instabilities. PA11 threads with diameters of 30-60 µm were drawn from a molten PA11 granule. PLA films with thickness of about 0.3 mm were prepared by compression molding at 180 °C and 300 kPa under a nitrogen atmosphere. Before each test in order to remove the residual stress, both thread and films were annealed at 80 °C and 60 °C for 48 h, respectively. The thread of PA11 (L/D~300) sandwiched between two PLA films was enclosed between a glass slide and a

coverslip and heated at a rate of 20 °C/min to 200 °C in a Mettler FP-82HT hot-stage equipped with a Mettler FP-90 central processor placed under a Nikon Optiphot-2 microscope for direct observation. The development of the thread shape was recorded with a CCD camera mounted on the microscope. Streampix v.III and Visilog v.6.3 software were used to capture and analyze the digital images. All the tests were done under a constant purge of dry nitrogen. The interfacial tension was calculated using the following equation [17]:

$$\sigma = {}^{q\eta_m D_0}/_{\Omega_m} \tag{4.2}$$

in which q is the distortion growth rate obtained by the breaking thread, η_m is the matrix viscosity, D_0 is the initial diameter of the thread and Ω_m is a tabulated parameter.

4.3.2.3 Imbedded Fiber Retraction (IFR)

The IFR method is similar to the BT except that this method consists of studying the kinetics of retraction of a short fiber, in this case a short PA11 fiber between two PLA films. In contrast to the BT approach, IFR permits the measurement of the interfacial tension in a shorter time period. Thus one can prevent PLA and PA11 degradation during interfacial tension measurements. The sample preparation is the same as the BT method except that here a PA11 fiber with a length of 0.6-1.1 mm was sandwiched between two PLA films and heated at 200 °C. The retraction evolution of the PA11 fiber was then recorded and the same software as those used for the BT were employed to analyze the PA11 fiber retraction into a spherical droplet. The interfacial tension was determined by using the initial PA11 fiber diameter, its diameter during retraction, zero shear viscosities of PA11 and PLA and the diameter of the final droplet [17].

4.3.2.4 In situ Neumann Triangle Method (NT)

The BT and IFR methods cannot be used directly on melt-processed blends. Therefore the NT technique was used as an in-situ measurement of interfacial tension between PLA and PA11. This method is based on the fact that in a partially wet ternary system at equilibrium any point of three phase contact balances the interfacial tension [11]. In this study a PLA/PA11/PE ternary blend was used as the partially wet system. By conducting the NT technique on the micrographs of the PLA/PA11/PE blend morphology, the contact angles (θ_{PA11}, θ_{PLA} and θ_{PE}) and also the interfacial tension ratios ($\gamma_{(PA11/PLA)}/\gamma_{(PA11/PE)}$, $\gamma_{(PA11/PLA)}/\gamma_{(PLA/PE)}$, $\gamma_{(PLA/PE)}/(\gamma_{PA11/PE)}$) were calculated for at least 20 partially wet droplets at the interface. The PLA/PE and PA11/PE interfacial tensions were obtained by the BT method and the PLA/PA11 interfacial tension was

thus determined based on the interfacial tension ratios. The detailed procedure for the NT method is described elsewhere [11].

4.3.3 Blend Preparation

All samples were prepared by melt mixing in an internal batch mixer (Plasti-Corder, Brabender, with a total volume of 30 ml) with roller blades, under a flow of dry nitrogen. The rotor speed was maintained at 50 rpm and the processing temperature was set at 200 °C. The average shear rate in the mixing chamber at the processing conditions was considered as 25 s^{-1}. [18]. PLA and PA11 were dried at 80 °C and PEO at 40 °C in a vacuum oven for 24h before use.

4.3.4 Rheology Analysis

Disks of 1.2 mm thickness and 25 mm diameter were prepared by compression molding of all the samples at 200 °C and 300 kPa under a nitrogen atmosphere. All samples were dried in a vacuum oven at 80 °C for 24h before the rheological test. The rheological characterization was performed using a constant stress rheometer (Physica MCR 301, Anton Paar) in a parallel plate geometry with a diameter of 25 mm and a 1 mm gap at 200 °C under a constant high flow of dry nitrogen.

4.3.5 Solvent Extraction and Continuity of the PLA Phase

Extractions were carried out in a soxhlet extraction setup. The PLA phase was extracted with chloroform. After extraction, samples were dried under vacuum at 60°C. Extraction was repeated until the weight of the dried extracted samples did not change. In order to determine the extent of continuity of the PLA phase, a gravimetric analysis was applied, using the following equation:

$$\%\ continuity\ of\ P = \left(\frac{Wieght\ P_{initial} - Weight\ P_{final}}{Wieght\ P_{initial}}\right) * 100 \qquad (4.3)$$

where P is the PLA phase. $P_{initial}$ is the weight of PLA in the blend before extraction, while P_{final} is the weight of PLA remaining after selective extraction.

4.3.6 Microtomy and Scanning Electron Microscopy

In order to create a plane face, all samples were cryo-microtomed using a Leica-Jung RM2065 microtome equipped with a glass knife under liquid nitrogen conditions. After solvent extraction of the PLA phase with chloroform and coating with a 15 nm thick gold layer, the morphology was observed under a scanning electron microscope (SEM) (JSM 7600F, JEOL) at a voltage of 5kV.

4.3.7 Image Analysis

An image analyzer (SigmaScan Pro.V.5) with a digitizing table (Wacom) was used to measure the size of the minor phase for the dispersed phase/matrix blends and the specific interfacial area between PLA and PA11 for the co-continuous morphology. SEM images were used for each sample to measure the volume average diameter, d_v, and number average diameter, d_n, of the dispersed phase using an average number of 400 measurements. The specific interfacial area of the co-continuous blends, S, was determined using the following equation [19]:

$$S = P / A \tag{4.4}$$

where P is the interfacial perimeter of the PLA/PA11 interface and A is the area of the analyzed SEM image. The average pore diameter was determined using equation 4.5:

$$d = 4\emptyset_p / S \tag{4.5}$$

in which d is the average pore diameter, $\emptyset_p$ is the porous volume fraction and S is the specific interfacial area.

4.3.8 Matrix Dissolution Technique

In order to define the shape (droplet or fiber) of the PA11 dispersed phase during blending, the extraction of the PLA matrix was performed in chloroform followed by centrifugation and filtration. The detailed procedure for the dissolution method is described elsewhere [20].

4.3.9 Quiescent Annealing

In order to study the effect of static coalescence on the blend morphology, quiescent annealing was performed at 200°C for different time intervals with a hot plate press without applied pressure and under a blanket of dry nitrogen.

4.3.10 Differential Scanning Calorimetry

Thermal analysis of the blends were performed in a DSC Q1000, TA instruments, at a heating–cooling rate of ±10 °Cmin^{-1} in the temperature range of 25 °C to 210 °C. The degree of crystallinity of each component in the blends was also calculated using equation (6):

$$X_c = {(\Delta H_m - \Delta H_c)}/{\Delta H^0} \tag{4.6}$$

Where ΔH^0 is the enthalpy of melting of pure crystals, which is 93 J/g and 190 J/g for PLA and PA11, respectively.[21] For the iso-thermal crystallization the thermal history of each sample was first removed by a rapid heating cycle to 200 °C and holding it for 3 min. Then a fast

cooling cycle down to the desired crystallization temperature was applied. The samples were held at this temperature for about 20-30 min until no change in the heat flow was observed.

4.4 Results and Discussion

4.4.1 Rheological Characterization

The complex viscosities as a function of angular frequency for the three different PLA materials (PLA1, PLA2 and PLA3), PA11 and plasticized PLA1 with 5% PEO (PLA1-5PEO) are presented in Figure 4.1. As expected, increasing the molecular weight of PLA increases the complex viscosity. All polymer components show Newtonian behavior at low shear rates. The viscosity ratios (viscosity of dispersed phase/viscosity of matrix) of PLA1, PLA2, PLA3 and PLA1-5PEO with PA11 at the processing conditions (25 s^{-1}) are estimated as 1, 2.5, 0.1 and 0.6 respectively. The zero shear viscosities were calculated by fitting the Carreau-Yassuda model to the viscosity/shear rate data.

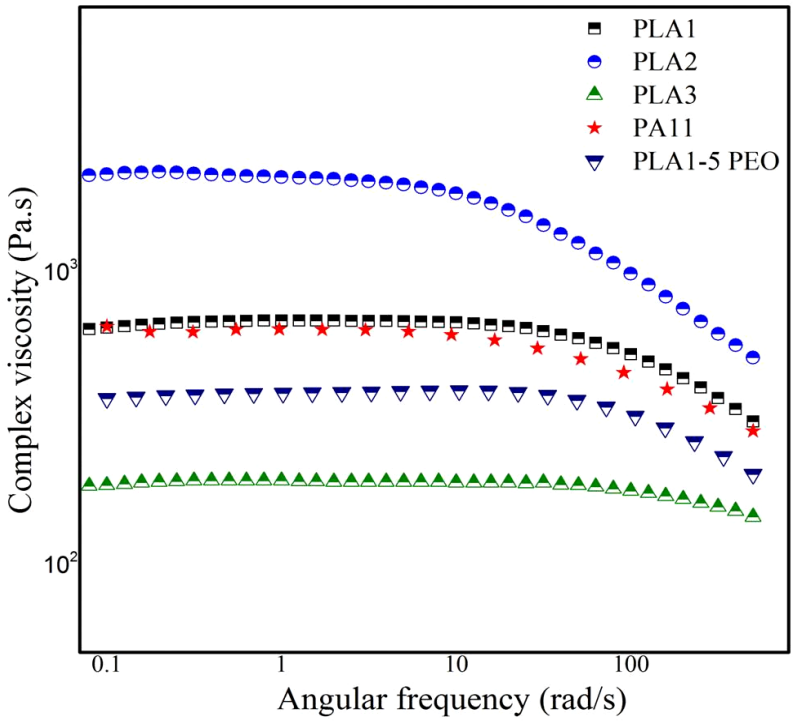

Figure 4.1. Complex viscosity of three different PLA samples (PLA1, PLA2 and PLA3), PLA1-5PEO and PA11 as a function of angular frequency.

4.4.2 PLA/PA11 Interfacial Tension

Contact angle method. The surface tension of PLA-1 was found to be $\gamma = 33.6 \pm 0.3$ mN/m at 200 °C with dispersive and polar contributions of $\gamma^d = 26.5 \pm 0.2$ and $\gamma^p = 7.1 \pm 0.1$ respectively. PA11 has a surface tension of $\gamma = 25.6 \pm 0.2$ mN/m at 200 °C with dispersive and polar contributions of $\gamma^d = 13 \pm 0.1$ and $\gamma^p = 12.6 \pm 0.1$ respectively. Using the harmonic mean equation, the interfacial tension between PLA-1 and PA11 was estimated to be 6.2 ± 0.6 mN/m at a melt blending temperature of 200 °C. Note that recently, the interfacial tension of the PLA/PA11 system was also measured by the contact angle method and was found to be very high as 13.05 mN/m [22] which is significantly different with our result. The differences between these values could potentially be due to differences in sample preparation and surface roughness [16]. In order to confirm the interfacial tension value, more work is carried out below.

Breaking Thread and Imbedded Fiber Retraction. For the BT method a typical sinusoidal PA11 thread distortion is observed in Figure 4.2-a. The interfacial tension of PLA/PA11 was found to be 5.8 ± 0.6 mN/m by this approach. For IFR method the retraction process of the PA11 fiber reaching an equilibrium spherical shape in the PLA matrix is shown in Figure 4.2-b and the interfacial tension obtained in this case is 5.4 ± 0.4 mN/m at 200 °C (10 replicates). The BT and IFR techniques, as well as the contact angle method, present the PLA/PA11 blend as a quite high interfacial tension system. Such a blend system would generally be expected to demonstrate high immiscibility, large dispersed phase sizes and high coalescence.

The Neumann Triangle method. The Neumann triangle method is another technique for measuring the PLA/PA11 interfacial tension that is very interesting since it can be applied directly to the melt mixed blends and hence provides an in-situ quantitative value [11]. In order to be able to apply the in-situ NT method, a ternary immiscible polymer blend must demonstrate at equilibrium a partially wet structure with a common line of contact. The interfacial tensions of each of the binary pairs can then be estimated. Although the NT method gives relative values, it is possible to determine the absolute value of interfacial tensions when the magnitude of at least one pair of the various components is known. Polyethylene (PE) was used as the third component because the PLA/PA11/PE blend forms a partially wet ternary immiscible system, Figure 4.2-c. The PLA/PE and PA11/PE interfacial tensions were measured by the BT method as 5 ± 0.4 mN/m and 6.1 ± 1 mN/m, respectively. Using the Neumann triangle technique the

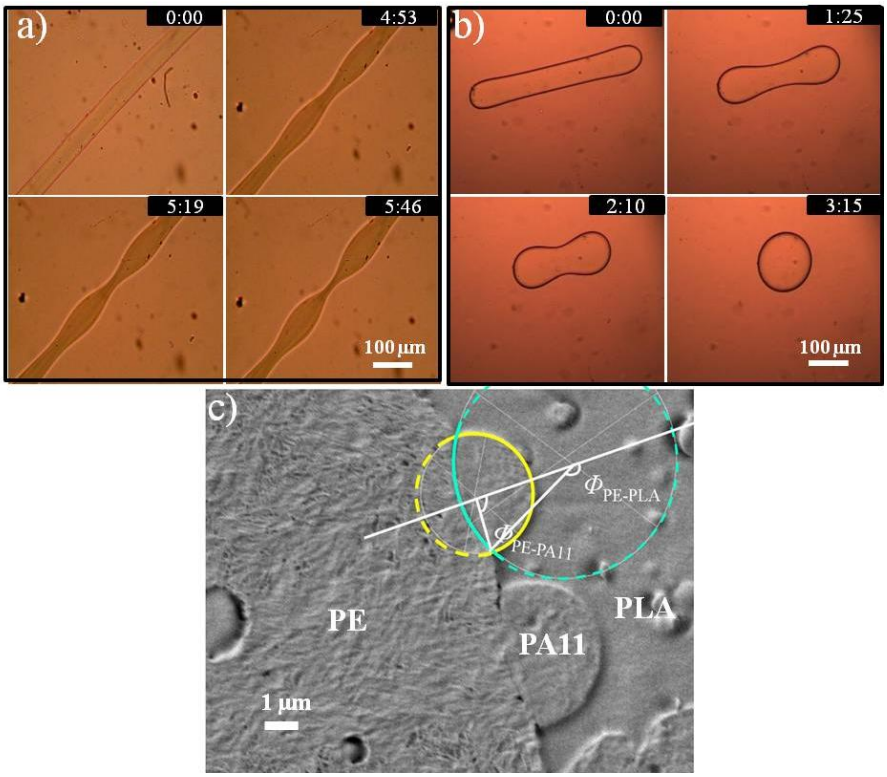

Figure 4.2. PLA-1/PA11 interfacial tension: a) Breaking Thread (BT) process of PA11 thread embedded in the PLA matrix (5.8 ± 0.6 mN/m), b), Imbedded Fiber Retraction process of a short fiber of PA11 in the matrix of PLA (5.4 ± 0.4 mN/m) and C) In-situ Newman triangle method: 3.2 ± 0.3 mN/m.

interfacial tension ratios were calculated directly for the PLA/PA11/PE 45/10/45 (vol%.) system. Figure 4.2-c shows an example of the geometric analysis used to determine the ratio of interfacial tensions. The interfacial tension value obtained under dynamic conditions for PLA/PA11 by the Neumann-triangle method is 3.2 ± 0.3 mN/m. This value is significantly lower than the 6.2 ± 0.6 mN/m, 5.8 ± 0.6 mN/m and 5.4 ± 0.4 mN/m values obtained by the contact angle, the breaking thread (BT) and the imbedded fiber retraction (IFR) methods, respectively.

The major discrepancy between the interfacial tensions obtained under static and dynamic conditions observed here for PLA1/PA11 is puzzling as it appears to indicate that the PLA/PA11 blend system behaves as a low interfacial tension system during dynamic mixing. One possible explanation for this behavior is the effect of elasticity on interfacial tension. It has been shown in a classic work [23] that a highly elastic matrix encapsulating a less elastic dispersed phase can

lead to a lower interfacial tension under dynamic conditions. In the present case, however, the PLA1 and PA11 elasticity values (taken using G') are virtually identical. The other possible explanation is that an interfacial reaction is taking place between PLA1 and PA11 under dynamic conditions that is not observed under static conditions. It is well known that PLA is a stiff chain with a characteristic ratio of 11.8 [24] while PA is more mobile with a characteristic ratio of 5.9 [25]. The validity of this latter explanation will now be explored throughout the rest of this paper.

Interfacial reactions carried out under dynamic melt mixing and quiescent conditions have been studied in the literature [26–30]. It has been shown in the literature that the reaction rate constant between reactive polymer pairs under flow conditions is over 1000 times higher than that between the static bi-layer films [26,27]. The reaction time at a flat static interface has been reported to be in the scale of hours [29]. Jeon et al. [27] compared the reaction rate constant (*k*) of a phthalic anhydride functionalized poly(methyl methacrylate) (PMMA-An) reacting with amine functionalized polystyrene (PS-NH_2) under static and dynamic conditions. They found that (*k*) increases from 3.2 (kg/mol.min) for the static flat film of PS-NH_2/PMMA-An to 5300 (kg/mol.min) for the melt mixed blend [27]. This effect has also been found in several other studies [30,31]. Moreover, the interface of immiscible blends is constantly changing during melt mixing due to the droplet break-up and coalescence of the minor phase resulting from the flow field in a mixer [26,27]. Due to the higher concentration of chain ends at the equilibrium interface [32], di-block copolymer formation is preferred over graft copolymer formation [33]. These di-block copolymers at the interface can also decrease the amount of reaction by limiting the diffusion of other reactive chains [33]. Generating fresh interface with dynamic mixing and interfacial roughening could reduce this effect [27]. In the case of the current system under study, differences in interfacial interactions under static and dynamic conditions would also be expected to be further exaggerated by the very high stiffness of the PLA chain.

4.4.3 Morphology and Continuity of PLA/PA11 Blends

Effect of composition. The SEM images of PLA1/PA11 blends at different compositions are shown in Figure 4.3. In order to increase the contrast, the PLA1 dispersed phase was extracted with chloroform. Selective extraction of the PA11 phase was impossible, however, due to good

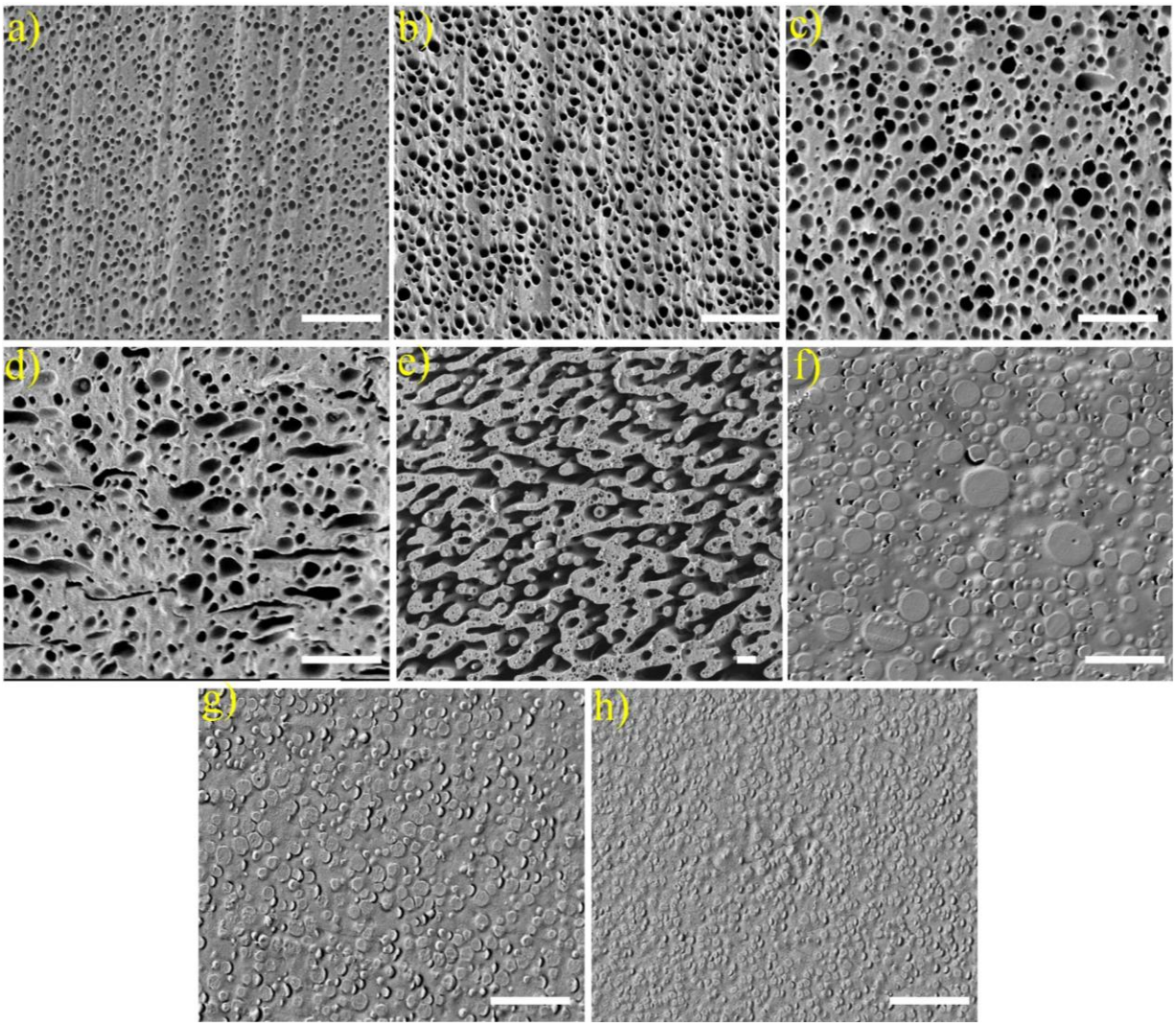

Figure 4.3. SEM images of the PLA1/PA11 blends at different compositions. PLA1/PA11 a) 20/80 b) 30/70, c) 40/60, d) 45/55, e) 50/50, f) 60/40, g) 70/30, h) 80/20 vol%. Note that the PLA1 phase was extracted using chloroform and the white bars indicate 10 μm.

topographical contrast it was still possible to distinguish the phases without PA11 extraction in the samples with PA11 as the dispersed phase. Micrographs a-c in Figure 4.3 suggest that PLA1 forms the dispersed phase in the PA11 matrix up to 45 vol% PLA1. Figure 4.4 shows the diameter of the minor phase as measured by image analysis over the entire composition range. At 1% minor phase, PLA in PA11 has a d_n of 700 nm and a d_v of 740 nm. PA11 in PLA at that same concentration has a d_n value of 690 nm and a d_v of 700 nm. The 1% composition value is important since it essentially indicates the no-coalescence baseline [9]. It is very interesting to note in Figure 4.4 that the PLA1 and PA11 minor phase sizes are virtually independent of

concentration right up to 20 vol% PLA1 or PA11. In other words, the coalescence is suppressed at these higher concentration and the dispersed phase size at 20 vol% is virtually identical to the 1 vol% minor phase size (absence of coalescence). The absence of coalescence over such a wide range of composition is generally taken as an indication of a highly interacting system. It is well known that coalescence can be significantly reduced or eliminated by controlling the level of interfacial interactions of the components of a polymer blend [34]. Both premade or insitu formed copolymers are believed to be able to significantly reduce the particle size at high minor

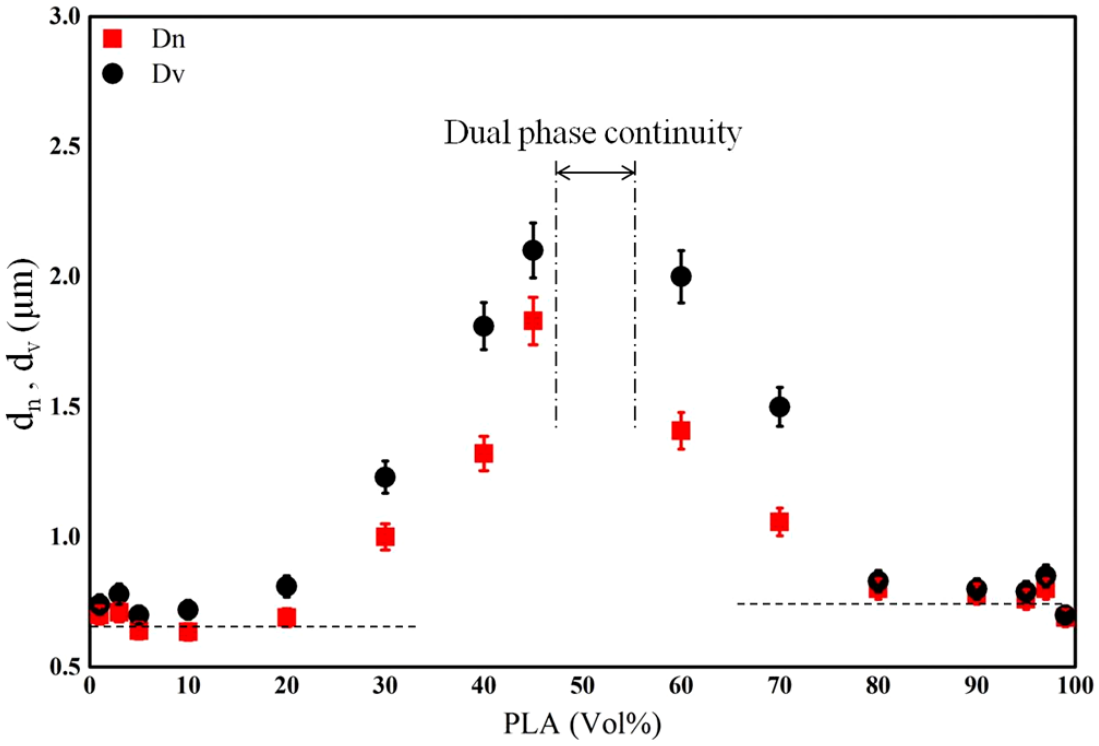

Figure 4.4. Volume average (●) and number average (■) diameters of the dispersed phase in PLA1/PA11 blends with different PLA1 compositions. The dashed lines show the "no-coalescence" baseline. The error bars are the standard deviation of the measured phase size.

phase concentrations [15,35,36]. Suppressed phase coalescence due to the high level of interfacial reactions has been reported as the main reason for the observation of a constant phase size of the minor phase up to 40 vol% of brominated poly(isobutylene-co-p-methylstyrene) (BIMSM) in BIMSM/PA reactive blends [36]. Tan et al. [35] reported that the introduction of reactive compatibilization to (PS)/amorphous PA (aPA) system results in a 60% reduction in the dispersed phase size compared to the non-reactive blend. Sundararaj et al. [15] investigated the

importance of insitu reactions at the interface of polymer blends on the coalescence during melt blending. They found that an insitu reaction during blending leads to suppressed coalescence, a smaller phase size and a narrower phase size distribution. Efficient phase size stabilization for end-functional polymers with only one functional group per chain are well known and have been reported [37,38]. In Figure 4.4, the PLA1 phase size significantly increases above 40 vol%. At 45 vol% PLA1 (Figure 4.3-d), particle–particle coalescence appears to lead to continuity effects. Finally at 50 vol% PLA1, the micrographs suggest that the blend reaches co-continuity with a significant number of PLA1 subinclusions in the PA11 phase.

In order to study the continuity development quantitatively, the PLA1 percentage continuity obtained by solvent extraction gravimetry analysis is shown in Figure 4.5. The continuity

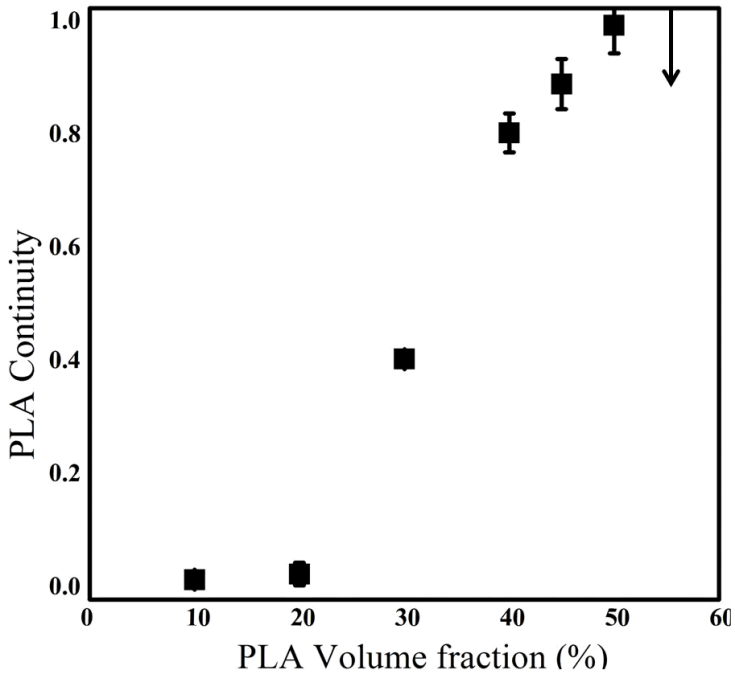

Figure 4.5. PLA1 phase continuity as a function of composition using solvent-extraction technique, the arrow indicates the disintegration concentration of PLA1 in the blend.

diagram confirms the microstructural image analysis from Figure 4.4. The PLA1/PA11 blend displays zero continuity up to 20 vol% PLA1. Continuity development develops above that concentration and a co-continuous morphology (100% dissolution of PLA1) is achieved at a composition of about 45-50 vol% PLA1. The extracted structure disintegrates at 55 vol% PLA1 indicated by an arrow in Figure 4.5. This is typically an indication of phase inversion. Thus, the

dual-phase continuity region appears to exist in the concentration range of 45 to 55 vol% PLA1, which correlates well with the morphology observations. This dual phase continuity region indicates a symmetry around the 50% composition value and hence indicates that there is no preferential tendency of either phase to encapsulate the other.

In order to better understand the continuity development in this system for the case where PA11 is the minor phase, PLA1 matrix dissolution was carried out on the PLA1/PA11: 95/05, 80/20, 60/40 and 55/45 vol% blends in Figure 4.6. This allows one to observe the shape of the dispersed PA11 phase (droplet or fiber) in the PLA1 matrix. Figures 4.6 a) and b) clearly show that the

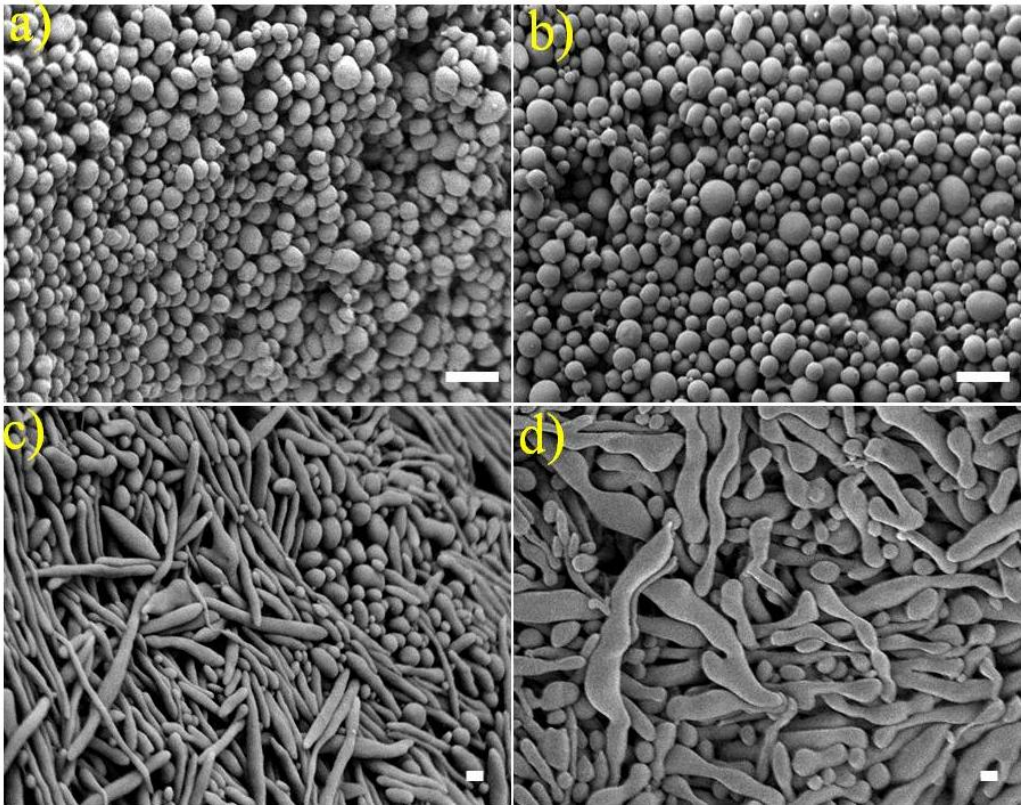

Figure 4.6. SEM micrographs of PA11 dispersed phase after PLA1 matrix dissolution. a) PLA1/PA11 95/05, b) PLA1/PA11 80/20 c) PLA1/PA11 60/40 d) PLA1/PA11 55/45 vol%. The white bars indicate 2 μm.

PA11 minor phase exists in the form of stable droplets at concentrations up to 20 vol.% PA11. Furthermore, the phase size of those PA11 droplets are very similar to that reported in Figure 4.4. Significant evidence of PA11 continuity is shown in Figures 4.6 c) and d) which, again is also in line with what was observed in Figure 4.4.

Taken all together, the phase size/composition dependence and continuity studies shown here indicate that the PLA/PA11 system is behaving as a highly interacting interfacially compatibilized system. Li et al. [20] refer to the characteristics of such a system as a Type III polymer blend which has been modified by an interfacial modifier. These type of blends show a minor phase in the form of droplets up to high concentrations with high percolation thresholds (indicating low level coalescence behavior) and achievement of co-continuity at high compositions with a narrow dual phase continuity region [20].

Effect of viscosity ratio: In order to study the effect of the viscosity ratio on the PLA/PA11 blend morphology three grades of PLA with different molecular weights, and hence different viscosities, were used (see Figure 4.1). The SEM images of the PLA/PA11 30/70 blends at various viscosity ratios are shown in Figure 4.7. Image analysis results reveal that the viscosity

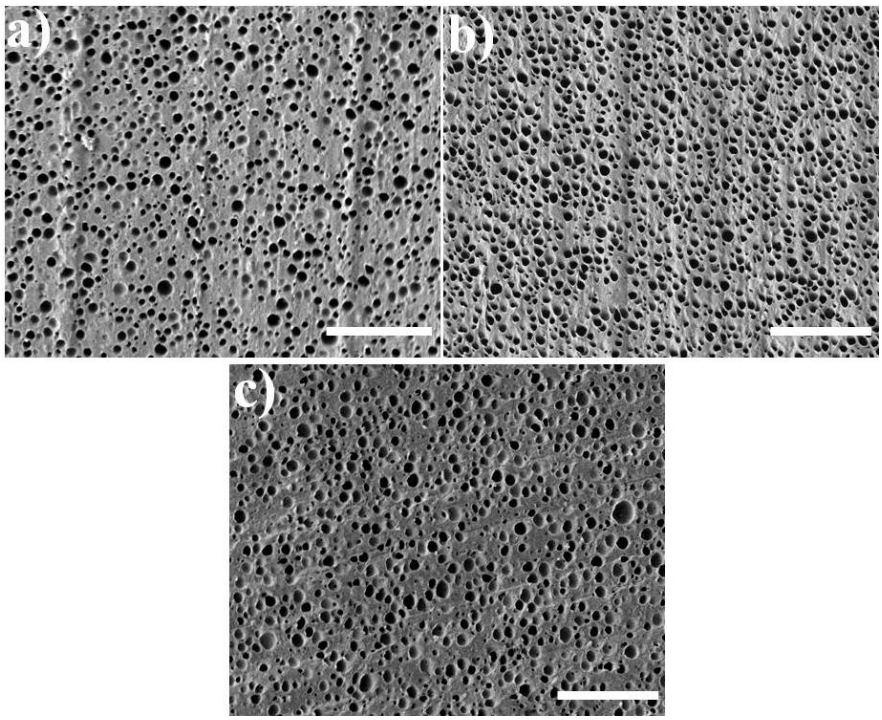

Figure 4.7. The effect of viscosity ratio on the morphology of the PLA/PA11 blend, PLA/PA11 30/70 vol%: a) $\eta_{PLA3/PA11}$ = 0.1 (d_v = 1.3 μm, d_n = 1.1 μm), b) $\eta_{PLA1/PA11}$ = 1 (d_v = 1.2 μm , d_n = 1 μm), c) $\eta_{PLA2/PA11}$ = 2.5 (d_v = 1.4 μm , d_n = 1.1 μm) . The white bars indicate 10 μm.

ratio, in the studied range, has practically no effect on the dispersed phase size. Although it has been reported that the viscosity ratio has a significant influence on the minor phase size in

immiscible polymer blends, it is well known that interfacially modified systems demonstrate much less dependence on this parameter [39].

Effect of quiescent annealing: In order to better understand the coalescence behavior of PLA/PA11 blends, quiescent annealing was undertaken. A co-continuous blend of PLA1/PA11 50/50 vol% prepared by dynamic mixing in the melt mixer as described above was subjected to quiescent annealing at 200 °C and the results are shown in Figures 4.8 and 4.9. Figure 4.9 shows the PLA pore size obtained by image analysis as a function of annealing time. It can be seen in Figure 4.9 that there is an increase in the PLA1/PA11 pore size from 13 ± 1 μm to 38 ± 3 μm over the first 30 min of annealing time. However, beyond that time, no significant phase

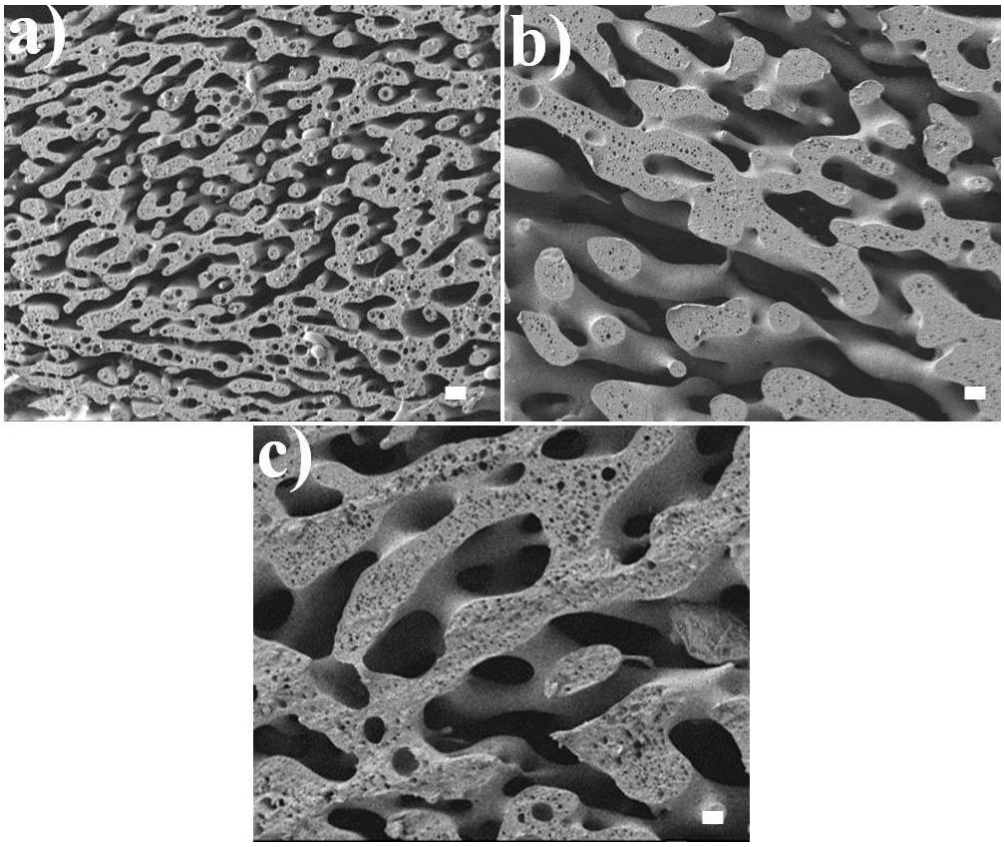

Figure 4.8. The effect of quiescent annealing at 200 ºC on the morphology of PLA1/PA11 50/50 vol% co-continuous blend : a) 0 min with average pore size of 13 μm ± 1, b) 30 min with average pore size of 38 ± 3 μm and c) 80 min with the average pore size of 46 ± 2 μm. The white bars indicate 10 μm.

growth is observed right up to 80 minutes of annealing. Multiple studies from this group have

shown that classic immiscible polymer systems typically show a linear increase in co-continuous phase size with time [13,40]. Compatibilized systems, typically demonstrate significantly reduced coarsening or even plateau behavior with time. Figure 4.9 also shows that the coarsening process of the co-continuous PLA1/PA11 blend occurs in two stages: a fast linear process at initial times of annealing and a second plateau-type behavior later. Since the coarsening of co-continuous structures has been theoretically related to the inhibited growth of Tomotika-like capillary instabilities [13], it is possible to present the coarsening curve that would have been

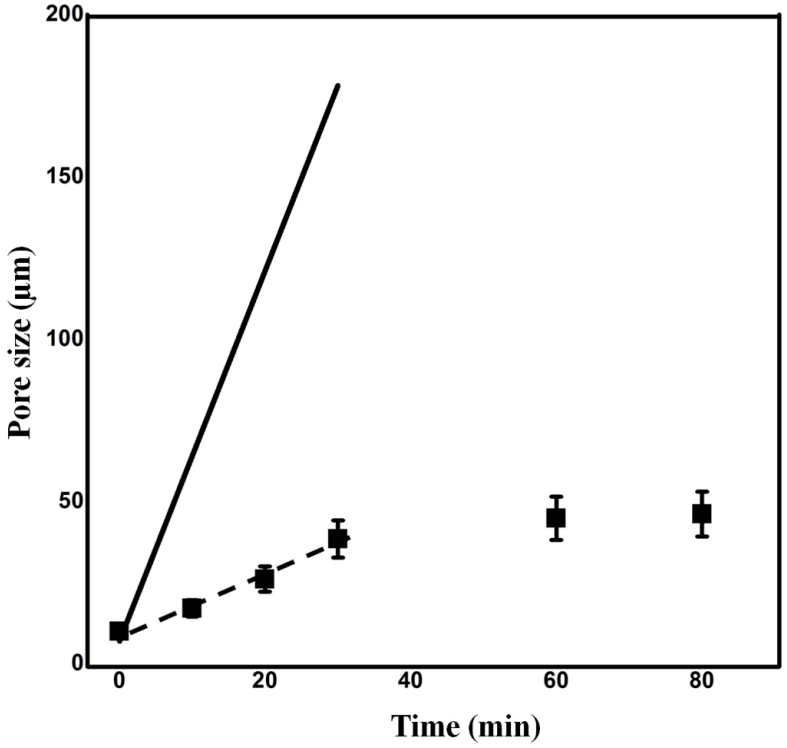

Figure 4.9. Pore size growth during quiescent annealing of the PLA1/PA11 50/50 vol% blend; Experimental ■ and solid line theoretical curve (solid line indicates the expected annealing behavior based on an interfacial tension of 5.8 ± 0.6 mN/m). The error bars represent the standard deviation of the measured phase size.

expected for a completely immiscible system of interfacial tension of 5.8 mN/m. This curve is shown by a solid line in Figure 4.9. Clearly the experimental annealing data for PLA1/PA11 from this study show all the characteristics of an interfacially modified system. Significantly reduced coalescence coarsening and even plateau behavior at longer times. By fitting the experimental data in the initial linear stage it is possible to estimate the interfacial tension of the

PLA1/PA11 blends as 0.9 ± 0.2 mN/m. This value is even lower than the 3.2 ± 0.3 mN/m obtained by the Neumann triangle method. Again, it is important to underline that this annealing study is undertaken on a PLA/PA11 50/50 vol% blend that had been previously prepared by dynamic melt mixing. Note also that although the term quiescent annealing is used here, significant coalescence of the highly interconnected co-continuous polymer blend clearly indicates that this type of annealing generates flow within the interconnected structure.

4.4.4 Thermal Behavior of PLA/PA11 Blends

The variation of the PLA1 and PA11 degree of crystallinity (%), for different blend compositions prepared by melt mixing, is presented in Table 4.1. Interestingly the degree of crystallinity of

Table 4.1. DSC characteristics of PLA1/PA11 blends.

PLA/PA11	$T_{cc,\ PLA}$ (ºC)	$\Delta H_{c,PLA1}$ (J/g)	$\Delta H_{m,PLA1}$ (J/g)	X_c PLA1(%)	X_c PA11(%)
100/0	109	34	36	2.6	----
90/10	100	27	40	15	15.5
80/20	100	20	34	19	17
70/30	101	18	31	20	18
60/40	102	17	29	22	19.5
50/50	102	11	23	26	20
40/60	94	9	22	35	21.5
30/70	91	5	17	42	21
20/80	89	3	10.5	40	21.5
0/100	---	---	---	---	24

PA11 diminishes with increasing PLA1 concentration in the blend. The degree of crystallinity of PLA1, however, increases with increasing PA11 concentration in the blends. In PLA1/PA11 blends PA11 crystals (PA11 crystallizes first) supply a surface where heterogeneous nucleation can occur. That is expected to result in higher nucleation rates and higher crystallinity levels for PLA1 [41]. A similar observation for blends of polyamide with PET or PBT has been reported in the literature and was attributed to an ester-amide interchange reaction between the polyester and polyamide [42–44].

The isothermal crystallization of the PLA1-major phase and the PA11-major phase were also studied by DSC. Figure 4.10 shows that the half-time crystallization of PLA1 decreases by

addition of PA11 while the half-time crystallization of PA11 increases with increasing PLA1 content. The decrease in the half time of crystallization for PLA is clearly related to the nucleation effect of PA11 crystals as also discussed above. However, the decrease in the half time of crystallization of PA11 in the presence of PLA can be attributed to an interfacial

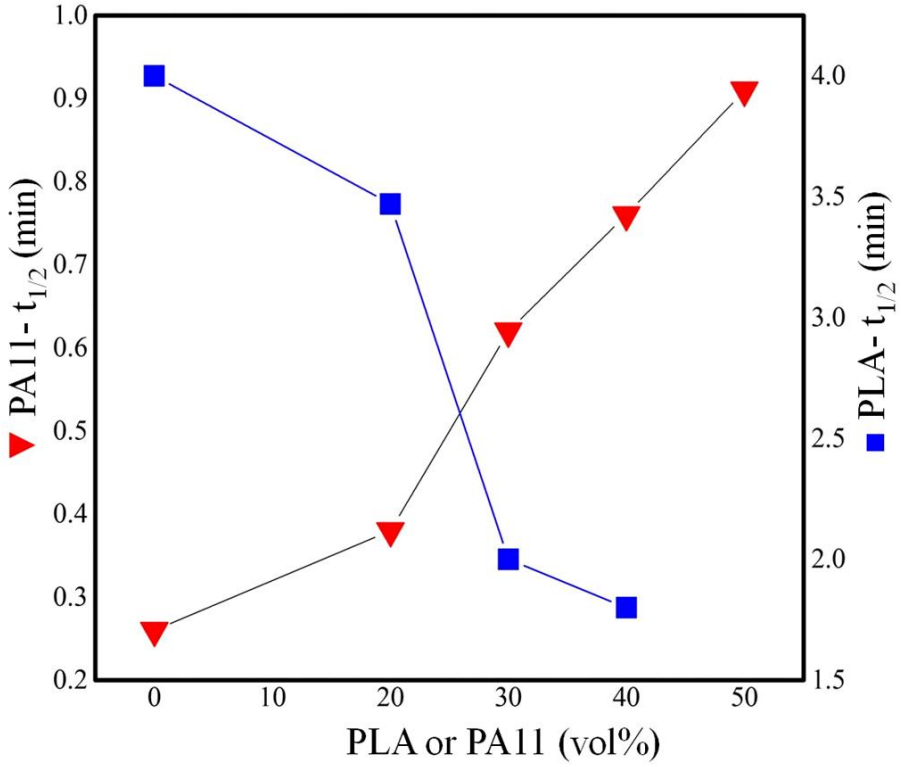

Figure 4.10. The effect of the PLA1/PA11 blend composition on the half time crystallization of PLA1 and PA11, ▼) PA11 isothermally crystallized at 165 ºC and ■) PLA1 isothermally crystallized at 110 ºC.

reaction. This reaction makes it difficult for PA11 chains to find their way to the PA11 crystal surface. A number of cases for immiscible blends have shown this behavior [45,46]. Muller et al. [47] studied the crystallization behavior of functionalized PE/PA reactive blends. The low crystallization rate of PA within the blend compared to the neat PA was attributed to the topological restriction imposed on the PA phase resulting from the interfacial reaction. A slower crytallization rate of PA, resulting from interfacial reactions, has also been reported for PA/PET [7] and PA/functionalized polysulfone (PSU) [48] blends.

Overall, these crystallization studies are another indication that the PLA/PA11 blend during melt mixing is apparently behaving as a highly interacting interfacially modified system.

4.4.5 Interfacial Reaction in PLA/PA11 Binary Blends

When the concentration of functional groups is low, it is generally recognized that it is difficult to detect an interfacial reaction using standard methods such as NMR and FTIR [26]. Moreover in our system detecting the reaction by measuring the mass of formed copolymer is difficult due to the lack of selective solvents for PA11. Although it was not possible to directly detect an ester-amide exchange reaction between PLA and PA11, indirect support for such a reaction has been widely reported in polyester/polyamide blends [6,7,43,49–52]. Changes in the thermophysical characteristics of annealed PET/PA/PBT blends was attributed to exchange reactions by Fakirov et al. [7]. In many other studies changes in mechanical properties [7,51], crystallinity [50], compatibility [44,49] or rheological behavior [53] of polyerster/polyamide blends were related to ester-amide chemical reactions.

In this work, although definitive ester-amide exchange reactions could not be established, our FTIR analysis did demonstrate a hydrogen bonding interaction between PLA and PA11 (data not shown here). Despite this, the morphological observations of this work point to the formation of an interfacial modifier. Hydrogen bonding on its own between the two base polymers would not be expected to have produced the observed morphological features of this work.

The above cited works demonstrate the clear possibility of an interfacial amide-ester exchange reaction for the systems studied in this work however, it does not explain why the measured static interfacial tension values are so high for this system. In the next section, the influence of chain mobility will be explored.

4.4.6 Effect of Chain Mobility on Interfacial Tension

It is well-known that the intrinsic polymer chain stiffness, expressed as the characteristic ratio and molecular entanglement, are key parameters influencing chain mobility in polymers [24,54]. The brittle nature of poly(lactic acid) has been demonstrated experimentally in the literature [55]. The characteristic ratio of PLA and PA11 from Van Krevelen group contributions [56] can be estimated as 10.5 and 6, respectively. These values are in good agreement with theoretical and experimental values reported in the literature [24,55]. Joziasse et al. [24] determined the characteristic ratio of PLA with D-lactide content in the range of 0-50 mol% and found that the

characteristic ratio for PLA varies between 9.5 to 11.8 for racemic PDLLA and isotactic PLLA, respectively. As a reference, note that stiff polystyrene chains have a characteristic ratio of 10.8 while flexible polyethylene has a characteristic ratio of 5.7 [57]. The entanglement molecular weight can also be determined based on the group contribution method [56] as 8283 g/mol and 2003 g/mol for PLA and PA11, respectively. Polystyrene and polyethylene entanglement molecular weights are reported as 13500 [58] and 1760 [59] g/mol, respectively. Thus, clearly, PLA falls into the category of a stiff polymer chain while PA11 is a flexible chain.

To have a better understanding of the effect of chain mobility on interfacial tension, PLA1 was plasticized with 5% polyethylene oxide (PEO) (PLA1-5PEO) and in another experiment, PA11 was plasticized with 5% N-Butylbenzene sulfonamide (BBSA) (PA11-5BBSA). Note that both of these plasticizers are very specific for their respective phases. In the case of the breaking thread experiment with PLA1-5PEO and PA11, remarkably the PA11 thread in the PLA1-5PEO

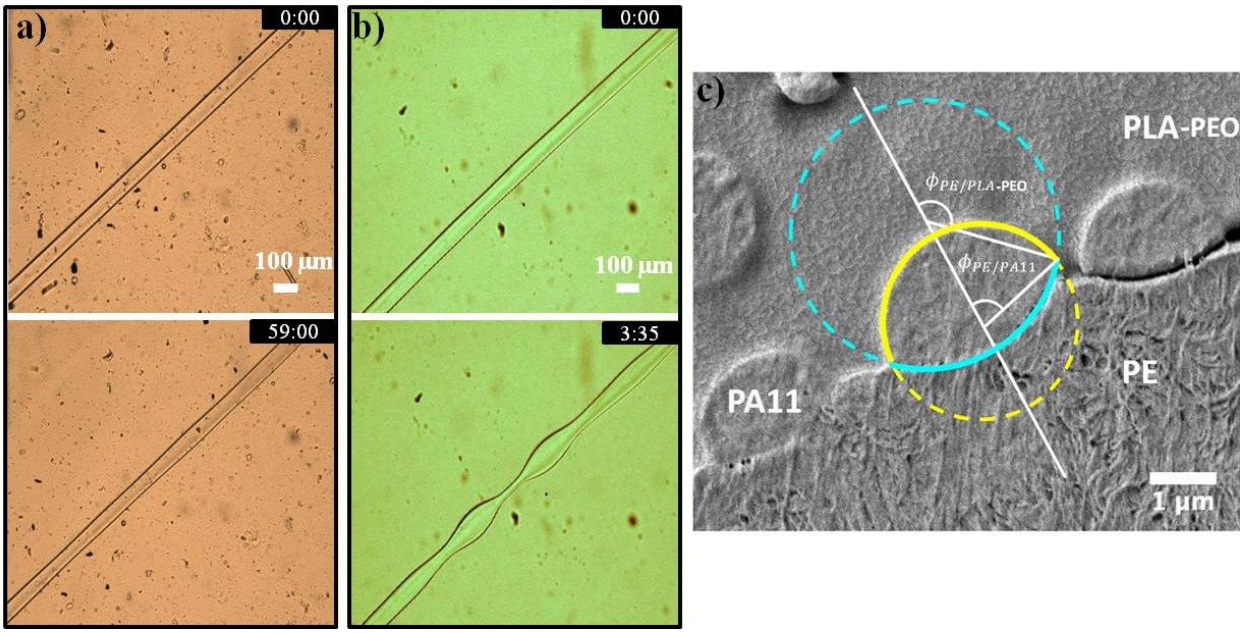

Figure 4.11. a) PA11 thread does not break up in PLA1-5PEO matrix even after several hours, b) PA11-5BBSA thread in PLA1 matrix breaks in several minutes, c) PLA1-5PEO/PA11 interfacial tension obtained by in-situ Neumann triangle method (2.1 ± 0.3 mN//m).

matrix does not break up even after several hours as shown in Figure 4.11-a. This very stable thread behavior indicates a low interfacial tension between PA11 and PLA1-5PEO. However, for the PA11-5BBSA thread in the unplasticized PLA1 matrix a typical sinusoidal thread distortion

(see Figure 4.11-b) is observed leading to the same interfacial tension values as reported earlier in this paper for PLA/PA11 by breaking thread, Figure 4.11-b.

The interfacial tension of PLA1-5PEO with PA11 was also determined by the in-situ Neumann-triangle method in partially wet PLA1-5PEO/PA11/PE 45/10/45 (%vol) system as 2.1 ± 0.3 mN/m as shown in Figure 4.11c. These large variations in interfacial tension upon addition of PEO plasticizer in PLA1 are an indication of PLA-PA11 interfacial interactions that are PLA chain mobility dependent. The interfacial tension values of the PLA/PA11 blend with and without plasticizer are summarized in Table 4.2. As expected the addition of BBSA plasticizer to PA11 has very little effect on the interfacial tension with PLA since the PA11 chains are already quite flexible.

Table 4.2. Interfacial tension values (mN/m) of PLA/PA11 blend with and without plasticizer.

Method	**BT**	**NT**
PLA1/PA11	5.8 ± 0.6	3.2 ± 0.3
PLA1-5PEO/PA11	No break up	2.1 ± 0.3
PLA1/PA11-5BBSA	5.3 ± 0.5	-

It has been shown that polymer rigidity, chain mobility, chain connectivity, intra-molecule interactions and steric crowding are essential factors that affect functional group accessibility and thus the extent of inter-molecular reactions between polymers [60–64]. Thus, depending on the above, not all functional groups in a blend system can participate in interfacial interactions. Radmard et al. [60] studied the effect of the rigidity of the aromatic polyether chains on the formation of interfacial interactions between polyether and poly(styrene-co-vinyl phenol) (PS-co-VPh). They showed that the extent of inter-molecular interactions increases with increasing flexibility of the polyether chains. Interfacial reactions in polymer blends have been studied theoretically in the literature [12,65]. Fredrickson [12] predicted that interfacial interactions in a polymer blend are described by a reaction rate constant:

$$k \approx DR_g((2R_g S_V) / \ln N) \tag{4.7}$$

in which D is the diffusion coefficient, R_g is the radius of gyration, N is the degree of polymerization and S_V is the ratio of interfacial area to total volume. Accordingly the interfacial reaction in polymer blends is controlled by the diffusion of the center of mass of functional chains in the polymer bulk towards the interface [66]. Increasing the diffusivity through an

increase in the chain mobility may thus influence interfacial reactions. In the current study the addition of PEO plasticizer to PLA in blends with PA11 would be expected to increase the chain diffusivity through an increase in the free volume. Bhadane et al. [36] studied the interfacial reaction of brominated poly(isobutylene-co-p-methylstyrene) (BIMSM) and PA reactive blends with and without plasticizer. They found that the reaction initiation temperature decreases with increasing plasticizer concentration.

4.4.7 Effect of Chain Mobility on Morphology

Figure 4.12 shows the dispersed phase size of the (PLA1-5PEO)/PA11 blends. Plasticized and unplasticized PLA1/PA11 blends have similar diameters at low concentrations (up to 20 vol%

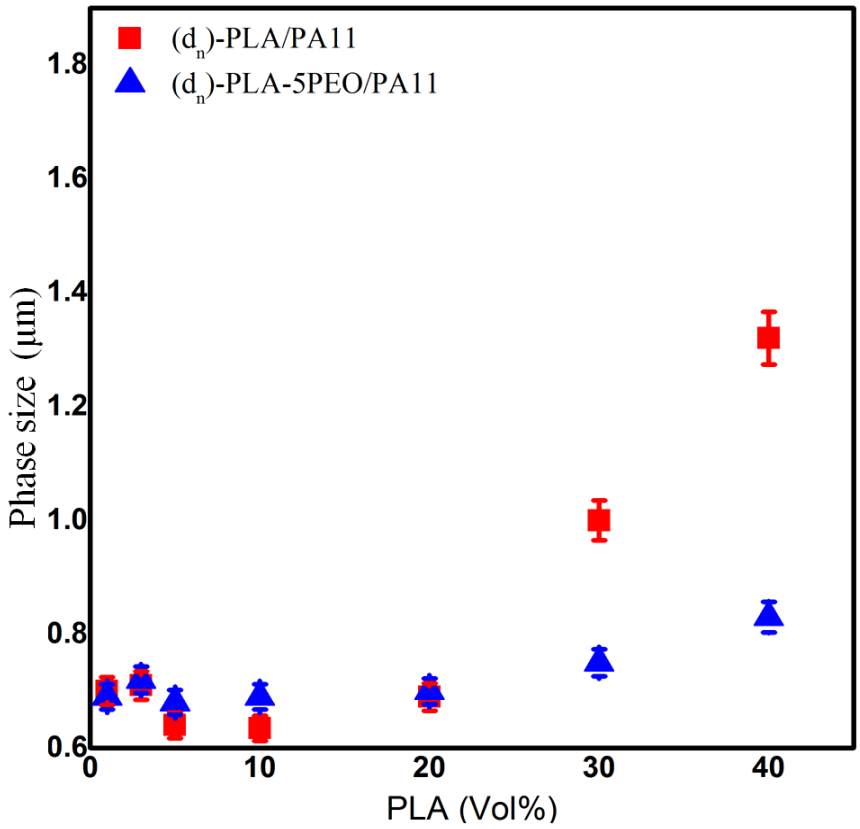

Figure 4.12. Effect of PLA chain mobility on coalescence in the PLA1/PA11 blend. All the PLA1/PA11 blends have similar diameters at low concentrations (up to 20 vol% PLA1), but adding 5% PEO suppresses coalescence at the higher compositions.

PLA), however, adding 5% PEO to the PLA1 phase clearly decreases the dispersed phase size at higher PLA1 compositions. This effect is not related to changes in the viscosity ratio since it has

already been shown earlier that viscosity ratio has very little effect on the morphology of these systems. The increased chain mobility of PLA, and hence increased interfacial interactions with PA11, are now so significantly improved that even the region of high continuity development shows a decrease in coalescence behavior.

4.5 Conclusion

It is shown that the interfacial tension in poly(lactic acid)/polyamide11 blends measured under static conditions by the breaking thread (BT) and imbedded fiber retraction (IFR) methods is 5.8 mN/m and 5.4 mN/m, respectively. Such high values are an indication of a highly immiscible system with poor interfacial interactions. However, when the PLA/PA11 interfacial tension is measured by the Neuman triangle technique under dynamic conditions, the interfacial tension is significantly lower at 3.2 mN/m. Furthermore, under conditions of dynamic mixing, the phase size/composition dependence, continuity studies, viscosity ratio dependence, annealing behavior and half time of crystallization results unambiguously indicate that the PLA/PA11 system is behaving as a highly interacting interfacially compatibilized system. It is shown that this discrepancy between the static and dynamic behavior of PLA /PA11 blends is related to the limited chain mobility of the stiff PLA chains. The addition of 5% of a PEO plasticizer to PLA results in significantly lower interfacial tension values and even further diminished coalescence under dynamic mixing at 30 and 40 vol% minor phase. These results on PLA/PA11 highlight that, even if polymers may have the potential for interfacial interactions, sufficient chain mobility is necessary in order for those interactions to come into play.

4.6 Acknowledgements

The authors would like to thank the NSERC Network for Innovative Plastic Materials and Manufacturing Processes (NIPMMP) for their financial support.

4.7 References

[1] K. Hashima, S. Nishitsuji, T. Inoue, Structure-properties of super-tough PLA alloy with excellent heat resistance, Polymer. 51 (2010) 3934–3939.

[2] H. Liu, W. Song, F. Chen, L. Guo, J. Zhang, Interaction of Microstructure and Interfacial Adhesion on Impact Performance of Polylactide (PLA) Ternary Blends, Macromolecules. 44 (2011) 1513–1522.

[3] G. Stoclet, R. Seguela, J.-M. Lefebvre, Morphology, thermal behavior and mechanical properties of binary blends of compatible biosourced polymers: Polylactide/polyamide11, Polymer. 52 (2011) 1417–1425.

[4] R. Patel, D.A. Ruehle, J.R. Dorgan, P. Halley, D. Martin, Biorenewable blends of polyamide-11 and polylactide, Polym. Eng. Sci. 54 (2014) 1523–1532.

[5] W. Dong, X. Cao, Y. Li, High-performance biosourced poly(lactic acid)/polyamide 11 blends with controlled salami structure, Polym. Int. 63 (2013) 1094–1100.

[6] T.L. Boykin, R.B. Moore, The role of specific interactions and transreactions on the compatibility of polyester ionomers with poly(ethylene terephthalate) and nylon 6,6, Polym. Eng. Sci. 38 (1998) 1658–1665.

[7] S. Fakirov, M. Evstatiev, S. Petrovich, Microfibrillar Reinforced Composites from Binary and Ternary Blends of Polyesters and Nylon 6, Macromolecules. 26 (1993) 5219–5226.

[8] D.J. Ihm, J.L. White, Interfacial tension of polyethylene/polyethylene terephthalate with various compatibilizing agents, J. Appl. Polym. Sci. 60 (1996) 1–7.

[9] J.C. Lepers, B.D. Favis, R.J. Tabar, The relative role of coalescence and interfacial tension in controlling dispersed phase size reduction during the compatibilization of polyethylene terephthalate/polypropylene blends, J. Polym. Sci. Part B-Polymer Phys. 35 (1997) 2271–2280.

[10] X. Zhang, J.K. Kim, Interfacial tension measurement with the Neumann triangle method, Macromol. Rapid Commun. 19 (1998) 499–504.

[11] J.K. Kim, W.Y. Jeong, J.M. Son, H.K. Jeon, Interfacial tension measurement of a reactive polymer blend by the Neumann triangle method, Macromolecules. 33 (2000) 9161–9165.

[12] G.H. Fredrickson, Diffusion-Controlled Reactions at Polymer-Polymer Interfaces, Phys. Rev. Lett. 76 (1996) 3440–3443.

[13] Z.H. Yuan, B.D. Favis, Coarsening of immiscible co-continuous blends during quiescent annealing, AIChE J. 51 (2005) 271–280.

[14] J.J. Elmendorp, A.K. Van Der Vegt, A study on polymer blending microrheology: Part IV. The influence of coalescence on blend morphology origination, Polym. Eng. Sci. 26 (1986) 1332–1338.

[15] U. Sundararaj, C.W. Macosko, Drop Breakup and Coalescence in Polymer Blends: The Effects of Concentration and Compatibilization, Macromolecules. 28 (1995) 2647–2657.

[16] D.Y. Kwok, A.W. Neumann, Contact angle measurement and contact angle interpretation, Adv. Colloid Interface Sci. 81 (1999) 167–249.

[17] P. Xing, M. Bousmina, D. Rodrigue, M.R. Kamal, Critical Experimental Comparison between Five Techniques for the Determination of Interfacial Tension in Polymer Blends: Model System of

Polystyrene/Polyamide-6, Macromolecules. 33 (2000) 8020–8034.

[18] M. Bousmina, A. Ait-Kadi, J.B. Faisant, Determination of shear rate and viscosity from batch mixer data, J. Rheol. (N. Y. N. Y). 43 (1999) 415–433.

[19] A.-L. Esquirol, P. Sarazin, N. Virgilio, Tunable Porous Hydrogels from Cocontinuous Polymer Blends, Macromolecules. 47 (2014) 3068–3075.

[20] J.M. Li, P.L. Ma, B.D. Favis, The role of the blend interface type on morphology in cocontinuous polymer blends, Macromolecules. 35 (2002) 2005–2016.

[21] Q. Zhang, Z. Mo, S. Liu, H. Zhang, Influence of Annealing on Structure of Nylon 11, Macromolecules. 33 (2000) 5999–6005.

[22] A. Nuzzo, E. Bilotti, T. Peijs, D. Acierno, G. Filippone, Nanoparticle-induced co-continuity in immiscible polymer blends – A comparative study on bio-based PLA-PA11 blends filled with organoclay, sepiolite, and carbon nanotubes, Polymer. 55 (2014) 1–12.

[23] H. Vanoene, Modes of dispersion of viscoelastic fluids in flow, J. Colloid Interface Sci. 40 (1972) 448–467.

[24] C.A.P. Joziasse, H. Veenstra, D.W. Grijpma, A.J. Pennings, On the chain stiffness of poly(lactide)s, Macromol. Chem. Phys. 197 (1996) 2219–2229.

[25] L.H. Sperling, Introduction to Physical Polymer Science, John Wiley & Sons, Inc., Hoboken, NJ, USA, 2005.

[26] C.W. Macosko, H.K. Jeon, T.R. Hoye, Reactions at polymer–polymer interfaces for blend compatibilization, Prog. Polym. Sci. 30 (2005) 939–947.

[27] H.K. Jeon, C.W. Macosko, B. Moon, T.R. Hoye, Z. Yin, Coupling Reactions of End- vs Mid-Functional Polymers, Macromolecules. 37 (2004) 2563–2571.

[28] J. Jiao, E.J. Kramer, S. De Vos, M. Möller, C. Koning, Morphological changes of a molten polymer/polymer interface driven by grafting, Macromolecules. 32 (1999) 6261–6269.

[29] F. Mathilde, I. Iliopoulos, M. Milléquant, J.J. Flat, L. Leibler, Graft copolymers of poly(methyl methacrylate) and polyamide-6: Synthesis by reactive blending and characterization, Macromolecules. 39 (2006) 6905–6912.

[30] T.D. Jones, J.S. Schulze, C.W. Macosko, T.P. Lodge, Effect of thermodynamic interactions on reactions at polymer/polymer interfaces, Macromolecules. 36 (2003) 7212–7219.

[31] Z. Yin, C. Koulic, C. Pagnoulle, R. Jérôme, Probing of the reaction progress at a PMMA/PS interface by using anthracene-labeled reactive PS chains, Langmuir. 19 (2003) 453–457.

[32] W. Zhao, X. Zhao, M.H. Rafailovich, J. Sokolov, R.J. Composto, S.D. Smith, T.P. Russell, W.D. Dozier, T. Mansfield, M. Satkowski, Segregation of chain ends to polymer melt surfaces and interfaces, Macromolecules. 26 (1993) 561–562.

[33] J.S. Schulze, J.J. Cernohous, A. Hirao, T.P. Lodge, C.W. Macosko, Reaction kinetics of end-functionalized chains at a polystyrene/poly(methyl methacrylate) interface, Macromolecules. 33 (2000) 1191–1198.

[34] B. Majumdar, D.R. Paul, A.J. Oshinski, Evolution of morphology in compatibilized vs uncompatibilized polyamide blends, Polymer. 38 (1997) 1787–1808.

[35] N.C. Beck Tan, S.-K. Tai, R.M. Briber, Morphology control and interfacial reinforcement in reactive polystyrene/amorphous polyamide blends, Polymer. 37 (1996) 3509–3519.

[36] P.A. Bhadane, A.H. Tsou, J. Cheng, M.D. Ellul, B.D. Favis, Enhancement in interfacial reactive compatibilization by chain mobility, Polymer. 55 (2014) 3905–3914.

[37] P. Guegan, C.W. Macosko, T. Ishizone, A. Hirao, S. Nakahama, Kinetics of Chain Coupling at Melt Interfaces, Macromolecules. 27 (1994) 4993–4997.

[38] J.C. Angola, Y. Fujita, T. Sakai, T. Inoue, Compatibilizer-aided toughening in polymer blends consisting of brittle polymer particles dispersed in a ductile polymer matrix, J. Polym. Sci. Part B Polym. Phys. 26 (1988) 807–816.

[39] G. Wildes, H. Keskkula, D.R. Paul, Morphology of PC/SAN blends: effect of reactive compatibilization, SAN concentration, processing, and viscosity ratio, J. Polym. Sci. Part B Polym. Phys. 37 (1999) 71–82.

[40] Z.H. Yuan, B.D. Favis, Influence of the efficacy of interfacial modification on the coarsening of cocontinuous PS/HDPE blends during quiescent annealing, J. Polym. Sci. Part B-Polymer Phys. 44 (2006) 711–721.

[41] C. Li, Q. Kong, J. Zhao, D. Zhao, Q. Fan, Y. Xia, Crystallization of partially miscible linear low-density polyethylene/poly(ethylene-co-vinylacetate) blends, Mater. Lett. 58 (2004) 3613–3617.

[42] L.Z. Pillon, J. Lara, D.W. Pillon, On the crystallinity and some structure/property relationships of poly(ethylene terephthalate)?poly(amide-6,6) blends, Polym. Eng. Sci. 27 (1987) 984–989.

[43] L.Z. Pillon, L.A. Utracki, D.W. Pillon, Spectroscopic study of poly(ethylene terephthalate)/poly(amide-6,6) blends, Polym. Eng. Sci. 27 (1987) 562–567.

[44] M.R. Kamal, M.A. Sahto, L.A. Utracki, Some solid-state properties of blends of polyethylene terephthalate and polyamide-6,6, Polym. Eng. Sci. 22 (1982) 1127–1137.

[45] D. Newman, E. Laredo, A. Bello, A. Grillo, J.L. Feijoo, A.J. Müller, Molecular Mobilities in Biodegradable Poly(dl-lactide)/Poly(ε-caprolactone) Blends, Macromolecules. 42 (2009) 5219–5225.

[46] A.J. Müller, V. Balsamo, M.L. Arnal, Nucleation and crystallization in diblock and triblock copolymers, Adv. Polym. Sci. 190 (2005) 1–63.

[47] M.E. Córdova, A.T. Lorenzo, A.J. Müller, L. Gani, S. Tencé-Girault, L. Leibler, The Influence of

Blend Morphology (Co-Continuous or Sub-Micrometer Droplets Dispersions) on the Nucleation and Crystallization Kinetics of Double Crystalline Polyethylene/Polyamide Blends Prepared by Reactive Extrusion, Macromol. Chem. Phys. 212 (2011) 1335–1350.

[48] P. Charoensirisomboon, H. Saito, T. Inoue, M. Weber, E. Koch, Crystallization in Polyamide 6/Polysulfone Blends: Effect of Polysulfone Particle Size., Macromolecules. 31 (1998) 4963–9.

[49] T. Serhatkulu, B. Erman, I. Bahar, S. Fakirovf, A. Polymeric, D. Sapundjieva, Dynamic mechanical study of amorphous phases in poly (ethylene terephthalate)/ nylon-6 blends, Polymer. 36 (1995) 2371–2377.

[50] M. Evstatiev, N. Nicolov, S. Fakirov, Morphology of microfibrillar reinforced composites PET/PA 6 blend, Polymer. 37 (1996) 4455–4463.

[51] C.K. Samios, N.K. Kalfoglou, Compatibilization of poly(ethylene terephthalate)/polyamide-6 alloys: Mechanical, thermal and morphological characterization, Polymer. 40 (1999) 4811–4819.

[52] J. Gug, M.J. Sobkowicz, Improvement of the mechanical behavior of bioplastic poly(lactic acid)/polyamide blends by reactive compatibilization, J. Appl. Polym. Sci. 133 (2016) 1–12.

[53] L.A. Utracki, A.M. Catani, G.L. Bata, M.R. Kamal, V. Tan, Melt rheology of blends of semicrystalline polymers. I. Degradation and viscosity of poly(ethylene terephthalate)–polyamide-6,6 mixtures, J. Appl. Polym. Sci. 27 (1982) 1913–1931.

[54] J. Qin, S.T. Milner, Tubes, Topology, and Polymer Entanglement, Macromolecules. 47 (2014) 6077–6085.

[55] K.S. Anderson, M.A. Hillmyer, Melt Chain Dimensions of Polylactide, Macromolecules. 37 (2004) 1857–1862.

[56] S. Wu, Predicting chain conformation and entanglement of polymers from chemical structure, Polym. Eng. Sci. 32 (1992) 823–830.

[57] S. Wu, Control of intrinsic brittleness and toughness of polymers and blends by chemical structure: A review, Polym. Int. 29 (1992) 229–247.

[58] Y.H. Lin, Entanglement and the molecular weight dependence of polymer glass transition temperature, Macromolecules. 23 (1990) 5292–5294.

[59] V.M. Litvinov, M.E. Ries, T.W. Baughman, A. Henke, P.P. Matloka, Chain Entanglements in Polyethylene Melts. Why Is It Studied Again?, Macromolecules. 46 (2013) 541–547.

[60] B. Radmard, M.. Dadmun, The accessibility of functional groups to intermolecular hydrogen bonding in polymer blends containing a liquid crystalline polymer, Polymer. 42 (2001) 1591–1600.

[61] M.M. Coleman, G.J. Pehlert, P.C. Painter, Functional Group Accessibility in Hydrogen Bonded Polymer Blends, Macromolecules. 29 (1996) 6820–6831.

[62] G.J. Pehlert, P.C. Painter, B. Veytsman, M.M. Coleman, Functional Group Accessibility in Hydrogen-Bonded Polymer Blends. 2. Miscibility Map of 2,3-Dimethylbutadiene- stat -vinylphenol Blends with Ethylene- stat -vinyl acetate, Macromolecules. 30 (1997) 3671–3677.

[63] Y. Hu, P.C. Painter, M.M. Coleman, R.J. Butera, Ramifications of Chain Connectivity in Hydrogen-Bonded Polymer Solutions, Macromolecules. 31 (1998) 3394–3396.

[64] M.M. Coleman, P.C. Painter, Hydrogen bonded polymer blends, Prog. Polym. Sci. 20 (1995) 1–59.

[65] B. O'Shaughnessy, U. Sawhney, Polymer Reaction Kinetics at Interfaces, Phys. Rev. Lett. 76 (1996) 3444–3447.

[66] Jie Song;, PhD dissertation on: Interfacial Coupling Between Immiscible Polymers : Flow Accelerates Reaction and Improves Adhesion, University of Minnesota, 2011.

CHAPTER 5 ARTICLE 2: HIGH PERFORMANCE POLY (LACTIC ACID)/BIO-POLYAMIDE11 THROUGH CONTROLLED CHAIN MOBILITY[2]

Vahid Heshmati and Basil D. Favis

CREPEC, Dept of Chemical Engineering, École Polytechnique de Montréal, Montreal, Canada

5.1 Abstract

This study shows that controlled PLA chain mobility in poly (lactic acid)/polyamide11 (PLA/PA11) blends can lead to high performance materials. The addition of an appropriate amount of polyethylene oxide (PEO) or polyethylene glycol (PEG) to a PLA/PA11 blend reduces the interfacial tension and increases the interfacial interactions due to an increase in the PLA chain mobility. The mechanical properties of (PLA-PEO)/PA11 50/50 systems are highly dependent on the PEO composition and at an optimal PEO concentration show a remarkable improvement in the Izod impact strength with specimens demonstrating 17.5 times the impact strength of the neat PLA and 3 times that of neat PA11. Also, these same blends show exceptional ductility with an elongation at break of 275% as compared to 5% for the neat PLA and 6% for PLA/PA11 without added PEO. Analysis of the fracture surface of the tough blends after impact indicates controlled interfacial debonding/cavitation at the continuous PLA/PA11 interface which leads to extensive shear yielding in the surrounding matrices. An excellent correlation is found between the optimal PEO composition for high performance properties and PEO limited miscibility in the PLA phase. When PEO phase separates in the PLA it tends towards the PLA/PA11 interface and provides a locus of failure for interfacial debonding. PEG, is not as effective as PEO and it has virtually no effect on the mechanical properties of the PLA/PA11 blend since it phase separates at lower concentrations thus limiting its effect on PLA mobility and ultimately providing insufficient plastic deformation to the PLA matrix. These results indicate that controlled PLA chain mobility through the use of an optimal concentration of an appropriate plasticizer is a highly effective approach towards the development of high performance PLA/PA11 blends.

[2] Submitted to Polymer.

5.2 Introduction

The development of high performance bio-materials has made important inroads as a replacement of commodity polymers in recent years [1,2]. Poly (lactic acid) (PLA) is a compostable biobased polymer and has significant potential due to its high tensile strength and modulus [1,3]. However, PLA suffers from inherent brittleness which limits its application [1,4]. Different strategies including blending with flexible polymers, plasticization and copolymerization have been employed to compensate for its mechanical property deficiencies [1,5–9]. Blending with various bio and synthetic polymers such as poly(butylene-succinate) [5,10], poly(butylene adipate-co-terephtalate) [9], thermoplastic starch [8], polycaprolactone [11], polycarbonate [6] and polyethylene [7] have been used to toughen PLA. However, finding a biobased polymer that enhances PLA mechanical properties has always been a challenge.

Polyamide11 (PA11), derived from castor oil, is an interesting biobased polymer with some physical similarities to PLA (T_g = 45 ºC and T_m = 187 ºC) yet shows a high thermal-mechanical performance, interesting elongation at break and impact strength [12,13]. Only a few studies have been carried out so far on PLA/PA11 blends [2,13–15]. In a previous work [15] on PLA/PA11 blends, a very fine dispersed phase size, high level of morphology stability and delayed PA11 crystallization behavior was related to significant PLA/PA11 interfacial reactions. A self-compatibilization behavior resulting from interfacial interactions in PLA/PA11 blends was reported by Stoclet et al. [13]. Although they did not observe a significant improvement in the mechanical properties of PLA/PA11 blends at room temperature, the PA11 dispersed phase provides a reinforcing effect to the rubbery PLA matrix at temperatures higher than the T_g of PLA. Thus, a reduction in the T_g of PLA, could be an approach to enhance the performance of PLA based blends with a proper level of interfacial adhesion.

A common approach to improve the flexibility of glassy polymers is the plasticization of the amorphous phase. Poly(ethylene glycol) (PEG) [16], poly(ethylene oxide) [17,18], citrate esters [19] and triacetine [20] are the most efficient plasticizers for PLA. Among the most interesting results, it has been shown that in most plasticized PLA systems, increasing the plasticizer concentration results in phase separation at a certain plasticizer concentration depending on the plasticizer molecular weight and chain architecture [21–23]. Pillin et al. [22] studied the miscibility of PLA and PEGs with different molecular weights. They showed that phase

separation is caused by the PLA crystallization which increases for PEGs with lower molecular weight. Depletion of an excessive amount of plasticizer from the growing PLA spherulites increases stiffness and decreases the strain at break of plasticized PLA [23].

Only a few studies have rigorously investigated the effect of enhanced chain mobility and flexibility on the morphology/mechanical properties relationship in polymer blends [3,6,24]. In a previous work from this laboratory the role of polymer chain mobility, through PA plasticization in reactive brominated poly(isobutylene-co-p-methylstyrene) BIMSM/PA blends was studied [24]. The enhancement of the PA chain mobility upon addition of an optimum content of 5-10% plasticizer was found to significantly affect the extent of reaction, the overall dynamics and dispersed phase size of the BIMSM/PA blend. Recently Hillmyer et al. [3] studied the effect of the addition of polyalkylene glycol liquid (PAG) plasticizer on the stress-strain behavior of reactively compatibilized PLA/polypropylene-based elastomer (PBE) blends. They used an epoxy-functionalized terpolymer (PEGMMA) as a reactive compatibilizer for the PLA/PBE blend. They demonstrated that PAG was formed as small droplets (200-400 nm) dispersed in the PLA phase and that PAG did not significantly restrict the compatibilizing ability of the PEGMMA. Their quaternary systems of PLA/PBE/PEGMMA/PAG showed an increase in the elongation at break to 110% as compared to 7% for pure PLA which was attributed to the improved interfacial adhesion and micro-void initiating effects associated with the PAG plasticizer. Hashima et al. [6] studied the mechanical properties of PLA/PC/SEBS/EGMA quaternary blends. They used poly(ethylene-co-glycidyl methacrylate) (EGMA) as a reactive compatibilizer for the SEBS/PLA pair. They suggested that an exchange reaction occurs between the polycarbonate (PC) and the PLA phase. Their TEM results reveal that SEBS droplets do not disperse in the PC, but rather preferentially in the PLA phase. The increase in the impact strength to 63 kJ/m^2 of the quaternary blend compared to pure PLA (5 kJ/m^2) and binary PLA/PC blends was attributed to the enhanced local segmental mobility of the PLA matrix in the presence of SEBS rubber particles.

The objective of this work is to examine the potential of enhanced PLA chain mobility, through addition of plasticizers, as a route to yield high performance mechanical properties in PLA/PA11 blends. This work will examine the effect of plasticizer type and concentration on the morphology/mechanical properties relationship.

5.3 Experimental

5.3.1 Materials

PA11 (Rilsan BMNO TL) and PLA (PLA 3001D), were obtained from Arkema and Natureworks, respectively. Poly(ethylene glycol) (PEG) with a molecular weight of 4000 g/mol and Poly(ethylene) oxide (PEO) water-soluble polymer (POLYOX™ WSR-N10) with a molecular weight of 10^5 g/mol were produced by Aldrich and Dow, respectively. PEO and PEG were dried at 40 °C and PLA and PA11 were dried at 70 °C under vacuum for 48 h before use.

5.3.2 Interfacial Tension

The Neumann triangle (NT) approach was used as an in-situ measurement of interfacial tension of PLA-PEO and PLA-PEG with PA11 at different PEO and PEG concentrations. This method is applied on a ternary immiscible system demonstrating a partial wet morphology at equilibrium with a three phase contact line [25]. In this study PE was used as the third component to prepare a partially wet (PLA-plasticizer)/PA11/PE ternary blend. Although the NT method gives relative values, it is possible to calculate the absolute value of interfacial tensions when the magnitude of at least one pair of the components is known [25]. The contact angle values ($\theta_{PLA\text{-}plasticizer}$, θ_{PA11} and θ_{PE}) and also the relative interfacial tensions ($\gamma_{(PA11/PLA\text{-}plasticizer)}/\gamma_{(PA11/PE)}$, $\gamma_{(PA11/PLA\text{-}plasticizer)}/\gamma_{(PLA\text{-}plasticizer/PE)}$, $\gamma_{(PLA\text{-}plasticizer/PE)}/(\gamma_{PA11/PE})$) were determined for at least 20 partially wet droplets at the interface by applying the NT method on the micrographs of the (PLA-plasticizer)/PA11/PE blend morphology. The detailed procedure for the NT method is described elsewhere [25].

5.3.3 Blend Preparation

PLA and PA11 were dried at 70 °C and PEO was dried at 40 °C in a vacuum oven for 48h before mixing. All samples used for the study of the effect of plasticizer on morphology and the PLA/PA11 interfacial tension were prepared in an internal batch mixer (Plasti-Corder, Brabender, with a total volume of 30 ml) with roller blades, under nitrogen atmosphere. The rotor speed was maintained at 50 rpm and the processing temperature was set at 200 °C. All samples used for mechanical analysis were prepared with a Leistritz ZSE 18HP co-rotation twin screw extruder equipped with a pelletizer. A screw with a L/D ratio of 40 and a speed of 100 rpm were employed. For the ternary (PLA-PEO)/PA11 blends, first a PLA/PEO masterbatch was

prepared and then this was melt blended with PA11. All the blend components were first dried mixed and subsequently added to the extruder for melt mixing. The processing temperature was controlled at the different zones of the extruder in order to obtain an ascending temperature profile from 180 at zone x to 200 °C at the die. After exiting the extruder, the extrudate samples were quenched in a water bath and granulated with a pelletizer. The granulated samples were dried at 80 °C in a vacuum oven for 24 hours before injection molding. Type I dog-bone samples (ASTM D638) and impact test specimens with dimensions of 63.5*12.7*3.2 mm were prepared with a Sumimoto SE50S injection molding machine with an average temperature of 200 °C and a screw speed of 100 rpm.

5.3.4 Polarized and Optical Microscopy (POM)

A Nikon Optiphot-2 microscope equipped with a light polarizer was used to examine the nucleation and growth of PLA/PEO, PLA/PEG and PLA-PEO/PA11 blends during iso-thermal crystallization. Under the microscope, thin film of each sample, sandwiched between two microscope slide cover glasses, was heated at a rate of 20 °C/min to 200 °C in a Mettler FP-82HT hot-stage equipped with a Mettler FP-90 central processor. The samples were cooled down subsequently to the desired temperature and micrographs were taken with a CCD camera. Streampix v.III and Visilog v.6.3 software were used to analyze the micrographs.

5.3.5 Microtomy and Scanning Electron Microscopy (SEM)

Prior to pelletizing the samples, 1 cm long cylinders were cut out from some strands. Blends were then cryo-microtomed using a leica-Jung RM2065 microtome equipped with a liquid nitrogen cryo-chamber and a glass knife. PLA was extracted with chloroform and in ternary samples PEO was extracted with water. The samples were then coated with a 15 nm thick gold layer and a Field Emission scanning electron microscope SEM (JSM 7600F, JEOL) at a voltage of 5kV was used for morphology observation.

5.3.6 Atomic Force Microscopy (AFM)

All the blends were cut and then cryo-microtomed using the same protocol described for the SEM sample preparation. The prepared surface was directly analyzed by atomic force microscopy, AFM, (MultiMode Nanoscope IIIa with extender, Digital instrument, Santa Barbara, CA). ACTA-W AppNano silicon tips with a radius of around 10 nm were used. As PLA, PA11 and PEO all have different modulus, AFM-tapping was conducted on the samples

and the phase mode was used to analyse the blend morphology.

5.3.7 Image Analysis

Dispersed phase size and PLA spherulite size were measured with an image analyzer (SigmaScan Pro.V.5) equipped with a digitizing table (Wacom). For each sample, the number average diameter, d_n, and volume average diameter, d_v, were calculated based on approximately 400 droplets from different SEM micrographs.

5.3.8 Temperature Modulated Differential Scanning Calorimetry (TMDSC)

Thermal characterization of the blends were carried out in a DSC Q1000, TA instruments. Temperature Modulated DSC (TMDSC) was used to determine the glass transition temperature (T_g) of the PLA phase in the (PLA-PEO)/PA11 blend. Heat capacity calibration was carried out with a standard sapphire sample. Moreover, calibrations of the melting temperature and cell constant were performed using a standard indium sample and an empty pan. TMDSC tests were carried out in the temperature range of -90 °C to 70 °C with a oscillation period of 60s and oscillation amplitude of ±1.27 °C at a heating rate of 2 °C/min.

5.3.9 Dynamic Mechanical Thermal Analysis (DMTA)

Dynamic mechanical thermal analysis were carried out on Izod specimens on a 2980 DMA, TA instruments. The dual cantilever clamp mode with a frequency of 1 Hz and an amplitude of 30 μm was used. The experiment was conducted at a scanning rate of 3 °C/min in the range of -100 °C to 110 °C. TA instruments universal analysis 2000 software was used to determine the thermal transitions based on the maximum of tanδ peaks.

5.3.10 Mechanical Tests

Tensile tests were carried out using a universal testing machine (Instron 4400R) at a cross-head speed of 5 mm/min according to the ASTM D638 standard. The initial strain was recorded using an extensometer. Notched Izod impact strength was performed according to the ASTM D256 standard using a CS-137C-176 CSI Custom Scientific Instrument impact machine. Five specimens were examined for each sample.

5.4 Results and Discussion

5.4.1 Effect of Plasticizer Concentration on Morphology and Interfacial Tension

The number average diameter (d_n) and volume average diameter (d_v) of the PLA dispersed phase size in the (PLA-PEO)/PA11 70/30 and 30/70 vol% blends with different PEO concentrations are summarized in Table 5.1 and in Figure 5.1. The addition of 5% PEO to the

Table 5.1. Number average dn (μm) and volume average dv (μm) diameter of the PLA dispersed phase in the (PLA-PEO)/PA11 ternary blends.

PEO content (%)	**0**		**5**		**10**		**15**		**25**	
	d_v	d_n	d_v	d_n	d_v	d_n	d_v	d_n	d_v	d_n
(PLA-PEO)/PA11 30/70	1.2	1	0.8	0.7	0.72	0.65	0.71	0.7	1.4	1.1
(PLA-PEO)/PA11 70/30	1.5	1	0.9	0.8	1	0.7	1	0.7	1.7	1.2

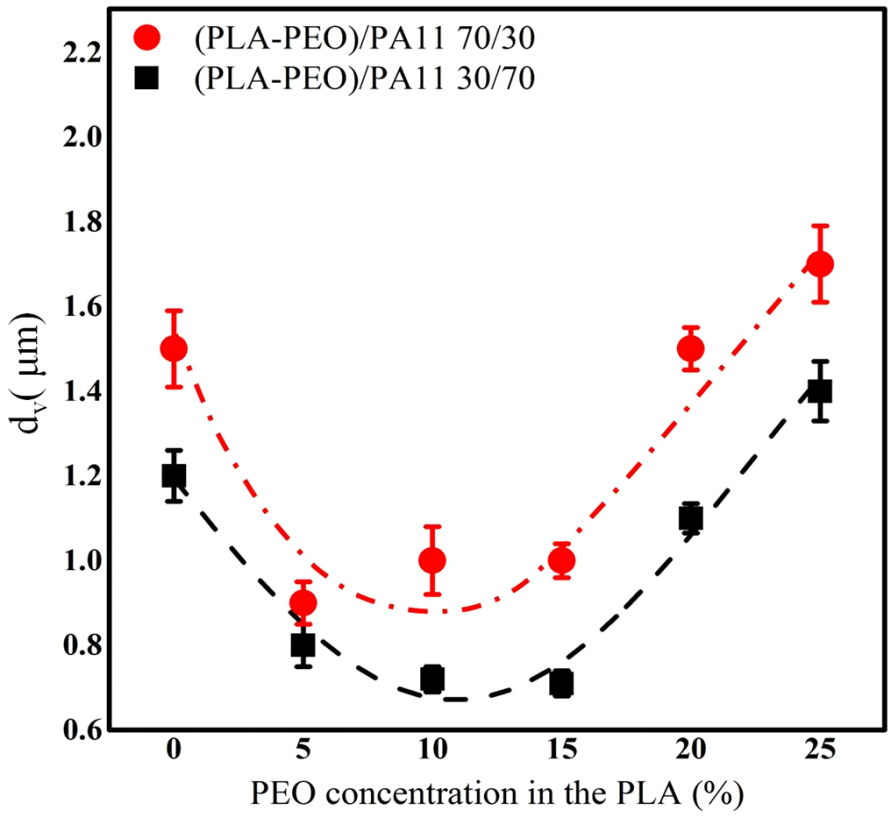

Figure 5.1. The effect of PEO concentration on the volume average d_v (μm) diameter of the PLA dispersed phase in (PLA-PEO)/PA11 blends

PLA phase significantly decreases the dispersed phase size in both blend compositions. Further increase of the PEO concentration to 10 and 15% does not significantly change the dispersed phase size. However, the blends with 20 and 25% plasticizer concentration in the PLA phase demonstrate an unexpected increase in the phase size. It is quite clear in Figure 5.1 that the lowest volume average dispersed phase for the (PLA-PEO)/PA11 70/30 and 30/70 vol% blends is observed at a concentration of 5-15% PEO.

These effects are not related to changes in the viscosity ratio since in a previous work [15] we have shown that the viscosity has virtually no effect on the PLA/PA11 blend morphology. It was shown in that work that the PLA/PA11 blend behaves as an interacting system in which increasing PLA chain mobility through plasticization leads to more efficient interfacial interactions, lower coalescence and smaller phase size. What is unusual here is that, after a significant reduction, the dispersed phase size increases once again at a certain PEO concentration. This change can be seen visually from SEM micrographs in Figure 5.2 for the PLA/PA11 30/70 vol% blend.

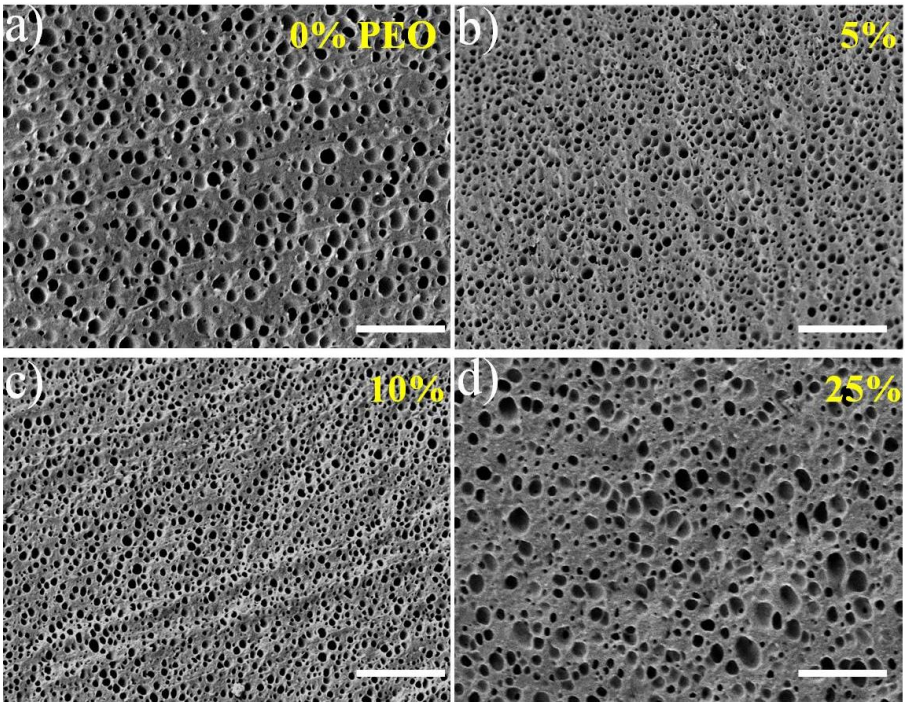

Figure 5.2. The effect of PEO concentration on the dispersed phase size of the (PLA-PEO)/PA11 30/70 vol% blends a) PLA/PA11 b) (PLA-5PEO)/PA11 c) (PLA-10PEO)/PA11 and d) (PLA-25PEO)/PA11. The scale bar is 10 μm.

In order to have a better understanding of the effect of PEO on the morphology of the PLA/PA11 blends, the interfacial tension of the PLA/PA11, with and without plasticizer was measured by the in-situ Neumann triangle (NT) method for a (PLA-plasticizer)/PA11/PE blend and the results are shown in Figure 5.3. The NT method is applied to ternary immiscible blends which show a partially wet morphology at equilibrium with a common line of contact.[25] In the NT method when the magnitude of the interfacial tension of at least one pair of the three components is known it is possible to calculate the interfacial tension of the desired pair. In this case, the interfacial tension of the PLA/PE pair was measured by the breaking thread method as 5 ± 0.4 mN/m. Figure 5.3 shows the PLA/PA11 interfacial tension for two different plasticizers, PEO and PEG. For the system plasticized with PEO, Figure 5.3 shows that the interfacial tension drops with added plasticizer and a minimum interfacial tension is achieved at 5-15% PEO. However at 25% PEO, the PLA/PA11 interfacial tension increases significantly. These

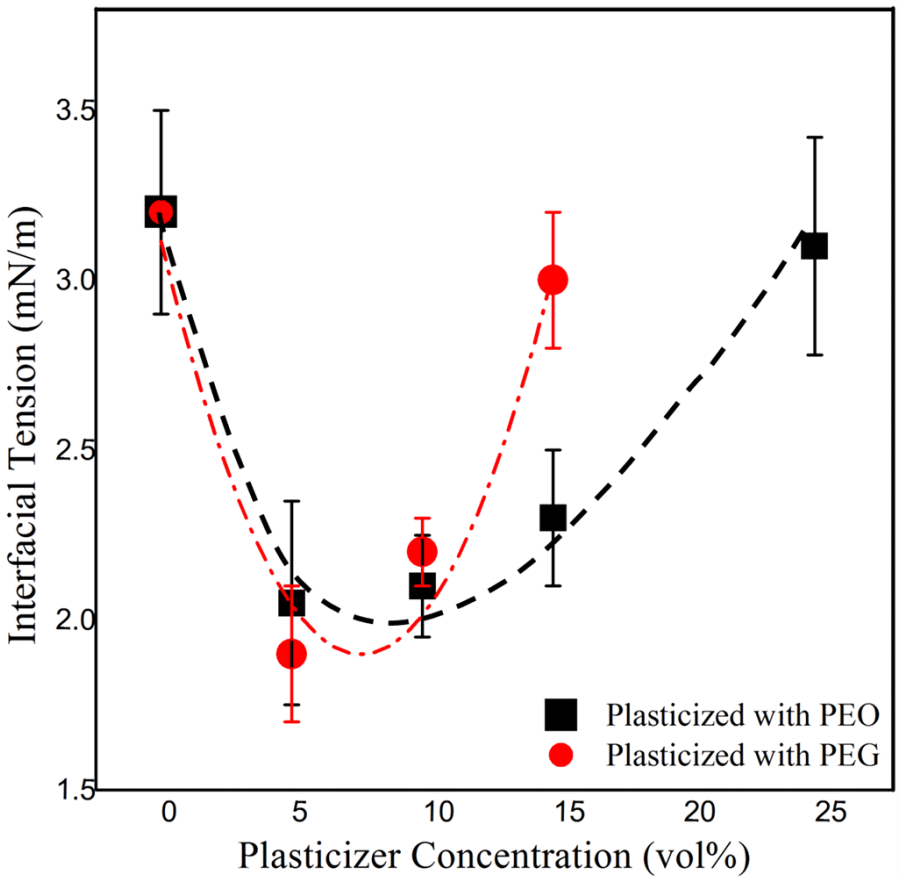

Figure 5.3. The effect of PEO and PEG concentration on the PLA/PA11 interfacial tension obtained by the in-situ Neumann triangle method.

results show a similar tendency to the morphology data for (PLA-PEO)/PA11 70/30 and 30/70 vol% shown in Figure 5.1. In the PEG plasticized blends, a similar decrease in the PLA/PA11 interfacial tension is observed, but in this case the interfacial tension shows a significant increase at a lower concentration, 15% PEO. As discussed above, the decrease in interfacial tension can be explained by the role of chain mobility on interfacial interactions as reported previously [15], however, the increase in interfacial tension at higher plasticizer content shown here is a unique observation.

5.4.2 PLA/PEO and PLA/PEG Miscibility

In order to better understand the change in the morphology and interfacial tension of PLA/PA11 blends with added PEO plasticizer, the thermal properties of the blend were examined. Table 5.2 shows the effect of PEO on the PLA glass transition temperature in the (PLA-PEO)/PA11 50/50 and 70/30 vol% blends. Pure PLA has a T_g of 61 °C which remains unchanged in binary PLA/PA11 blends. Upon addition of PEO in the (PLA-PEO)/PA11 50/50 and 70/30 vol% ternary blends the T_g of PLA decreases significantly at 5% and 15% PEO showing the well known plasticization/miscibility effect of PEO with PLA. However, at 20% PEO, both ternary (PLA-PEO)/PA11 blends show a glass transition temperature which is significantly higher than the counterpart ternary systems with 5-15% PEO. This observation clearly points to diminished miscibility and a phase separation effect at the high PEO content.

Table 5.2. PLA glass transition temperature (°C) in the (PLA-PEO)/PA11 blends with different PEO content.

PEO (%)	(PLA/PEO)/PA11 (vol%)	
	50/50	70/30
0	61	61
5	37	37
15	34	35
20	54	52

PLA/PEO miscibility as a binary mixture was also studied by DMTA. The temperature dependence of tanδ at various PEO concentrations is shown in Figure 5.4. Up to the 20% PEO composition one single transition is observed, however at 25% PEO an additional broad peak is observed. This additional peak can be attributed to PLA/PEO phase separation [26]. The DMTA

studies confirm the PLA-PEO phase separation effects at higher PEO concentrations, but in the T_g studies above phase separation appears to occur at 20% PEO rather than at 25%. This is an indication that the presence of PA11 also enhances the PLA-PEO phase separation effect at higher PEO concentrations.

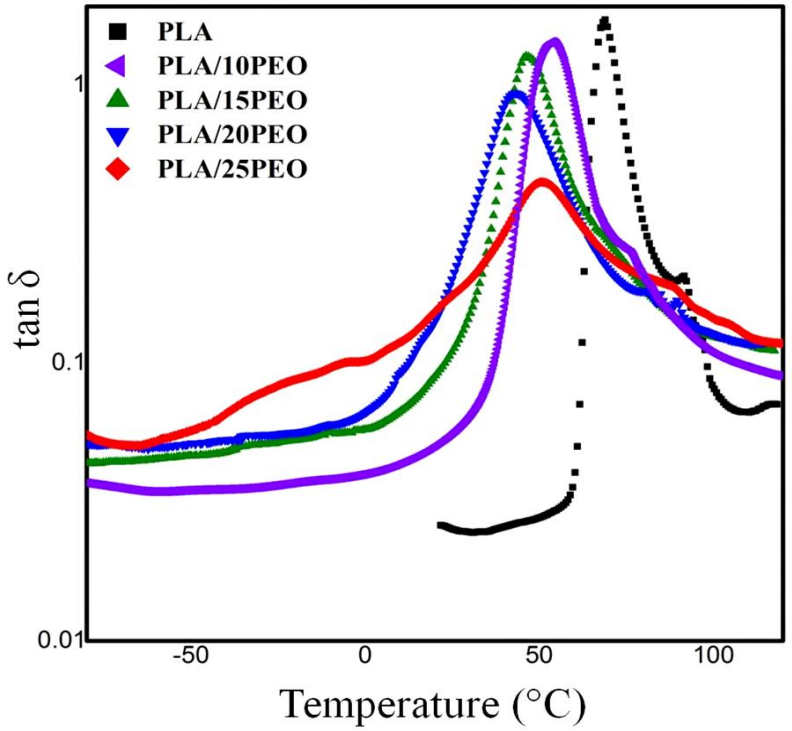

Figure 5.4. Tan δ as a function of temperature for PLA and PLA/PEO blends with different concentrations.

PLA/PEG miscibility as a binary mixture was also studied by DSC (not shown here). Although the blend with up to 10% PEG demonstrated miscibility, PEG melting peak around 60 °C was detected for the blends containing 12.5 and 15 vol% PEG indicating phase separation.

Taking the morphology, interfacial tension and thermal data results all together shows that improved PLA chain mobility due to plasticization enhances interfacial interactions between PLA and PA11 which reduces the interfacial tension and thus diminishes the dispersed phase size as also reported previously [15]. The addition of amounts in excess of 15% PEO results in a PLA-PEO phase separation and diminished PLA chain mobility which leads to higher interfacial tension and thus increased dispersed phase size. The interfacial tension data for PEG plasticized ternary blends indicate that PEG plasticizer is also able to reduce the interfacial tension through

enhanced PLA chain mobility, but undergoes phase separation at lower PEG concentrations.

5.4.3 Mechanical Properties

The mechanical properties of (PLA-PEO)/PA11 and (PLA-PEG)/PA11 50/50 vol% ternary blends with different PEO and PEG contents are presented in Table 5.3. Data is also presented

Table 5.3. Mechanical properties of neat PLA, neat PA11 and PLA/PA11 50/50 blends with and without PEO and PEG plasticizer.

Sample	Izod Impact (J/m)	ε* (%)	σ* (MPa)	E* (GPa)
PLA	12.1 ± 3	5 ± 3	65 ± 1	4.3 ± 0.2
PA11	69.4 ± 4.6	235 ± 40	41 ± 2	1.4 ± 0.1
PLA/PA11 50/50	11 ± 2	6 ± 1	50 ± 2	2.7 ± 0.2
PLA-15PEO	14 ± 3	300 ± 40	27 ± 1	2.0 ± 0.1
(PLA-10PEO)/PA11 50/50	40 ± 8	100 ± 20	34 ± 3	1.8 ± 0.1
(PLA-15PEO)/PA11 50/50	212 ± 20	275 ± 32	31 ± 1	1.6 ± 0.2
(PLA-20PEO)/PA11 50/50	62 ± 10	25 ± 10	20 ± 3	1.3 ± 0.2
(PLA-10PEG)/PA11 50/50	15 ± 2	8 ± 2	28 ± 2	1.7 ± 0.3
(PLA-15PEG)/PA11 50/50	18 ± 1	12 ± 3	23 ± 3	1.4 ± 0.1
(PLA-20PEG)/PA11 50/50	16 ± 4	10 ± 5	18± 1	1.1 ± 0.1

* ε: Elongation at break, σ: Tensile Strength and E: Young's Modulus

for neat PLA, neat PA11 and the binary PLA/PA11 blend. In all the ternary (PLA-PEO)/PA11 blends, the tensile strength decreases with increasing PEO concentration indicating a lower onset of plastic deformation. The enhancement in the blend deformability leads to a considerable improvement in the notched impact properties and elongation at break as presented in Table 5.3. The (PLA-15PEO)/PA11 50/50 vol% system has an impact strength that is 17.5 times higher than that of neat PLA and 3 times higher that of PA11. That same blend shows an elongation at break of 275% as compared to 4% for neat PLA and 235% for neat PA11. An expected corresponding decrease in the elastic modulus for these ternary systems is also observed in Table 5.3. It is interesting to note that PEG has no significant effect on the mechanical properties of the

PLA/PA11 blends.

Relationship between Mechanical Properties and PEO Concentration. The PEO concentration has a crucial effect on the toughening of PLA/PA11 blends. The Izod impact strength of (PLA-PEO)/PA11 50/50 and 70/30 vol% blends at different PEO concentrations is shown graphically in Figure 5.5. The addition of 2.5-10% PEO to the PLA phase in the blends results in only a minor improvement in the impact strength. However, 15% PEO brings about a dramatic improvement in the blend ductility with an impact strength of 212 J/m for the (PLA-PEO)/PA11 50/50 vol% and 105 J/m for the (PLA-PEO)/PA11 70/30 vol% as compared to 12.1 J/m for the neat PLA and 69.4 J/m for the neat PA11. A further increase in the PEO concentration to 20% leads to a substantial drop in the impact strength to 62 J/m for (PLA-PEO)/PA11 50/50 vol% and 45 J/m for (PLA-PEO)/PA11 70/30 vol%. Clearly, an optimal PEO plasticizer concentration of about 15% is required to maximize the impact strength. Figure 5.5 also clearly demonstrates that the 50/50 (PLA-15PEO)/PA11 blend has a much higher impact strength than the 70/30 (PLA-15PEO)/PA11 blend. This is a clear indication of the importance of a co-continuous morphology [2]. Although it is not possible to selectively extract the PA11,

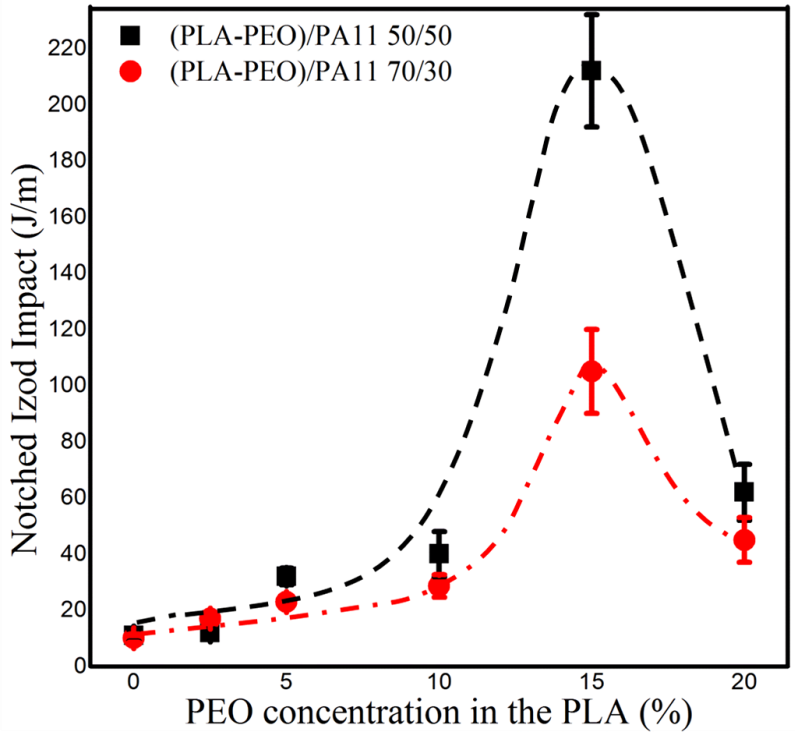

Figure 5.5. Impact strength of the (PLA-PEO)/PA11 50/50 vol% and (PLA-PEO)/PA11 70/30 vol% blends as a function PEO concentration in the PLA phase.

selective extraction of the PLA indicates that the 70/30 (PLA-15PEO)/PA11 blend forms a matrix/dispersed phase type morphology. Selective gravimetric extraction of PLA in the 50/50 (PLA-15PEO)/PA11 blend estimates the PLA-PEO continuity at 102%. This 50/50 ternary blend is thus co-continuous.

The effect of PEO composition on the elongation at break of the ternary 50/50 and 70/30 (PLA-PEO)/PA11 blends is shown in Figure 5.6. Similar tendencies as shown in Figure 5.5 are observed here with dramatic increases in the elongation at break for both blend compositions observed at 15% PEO. The (PLA-15PEO)/PA11 70/30 vol% has an elongation at break of 240% while (PLA-15PEO)/PA11 50/50 has an elongation of 275% as compared to 5% for PLA, 235% for PA11 and 6% for PLA/PA11. It is interesting to note that the co-continuous morphology is

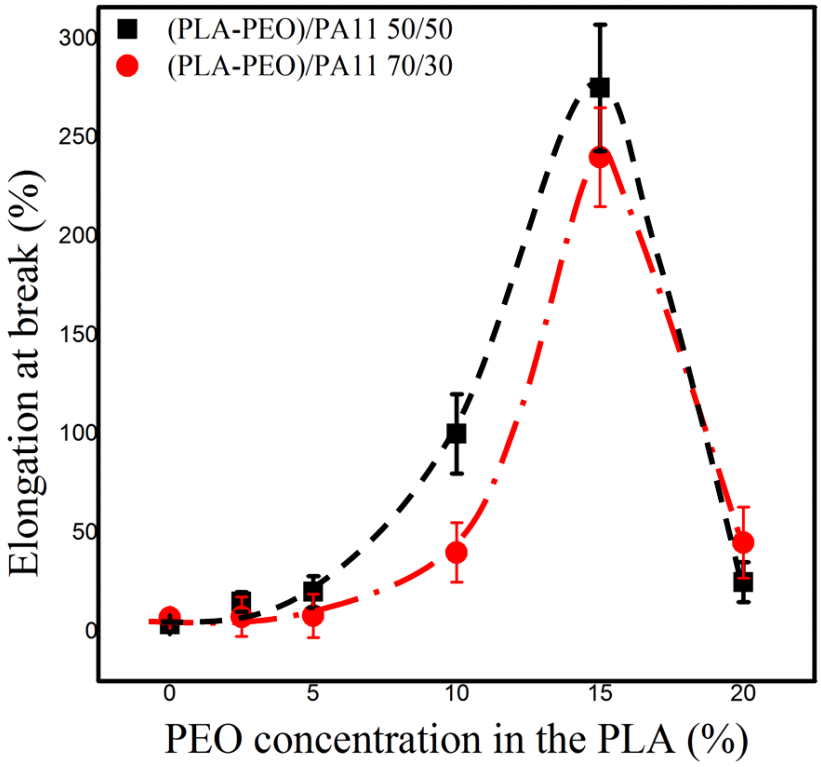

Figure 5.6. Elongation at break of the (PLA-PEO)/PA11 50/50 vol% and (PLA-PEO)/PA11 70/30 vol% blends as a function of PEO concentration in the PLA phase.

less critical to the improvement of elongation at break than for impact strength. It will be shown later in this paper that maximized impact strength is dependent on debonding cavitation across a continuous interface and is the principal energy dissipation mechanism for these systems.

5.4.4 Toughening Mechanism

Fracture Surface. SEM micrographs of the impact fracture surface of PLA, PLA/PA11, PLA/PEO and ternary (PLA-PEO)/PA11 blends are shown in Figure 5.7. Pure PLA, PLA/15PEO, PLA/PA11 50/50 vol% and PLA/PA11 70/30 vol% blends exhibit classic brittle fracture surfaces with little or no plastic deformation. However, addition of 15% PEO to the PLA phase in (PLA-PEO)/PA11 50/50 and 70/30 vol% results in massive tearing and deformation

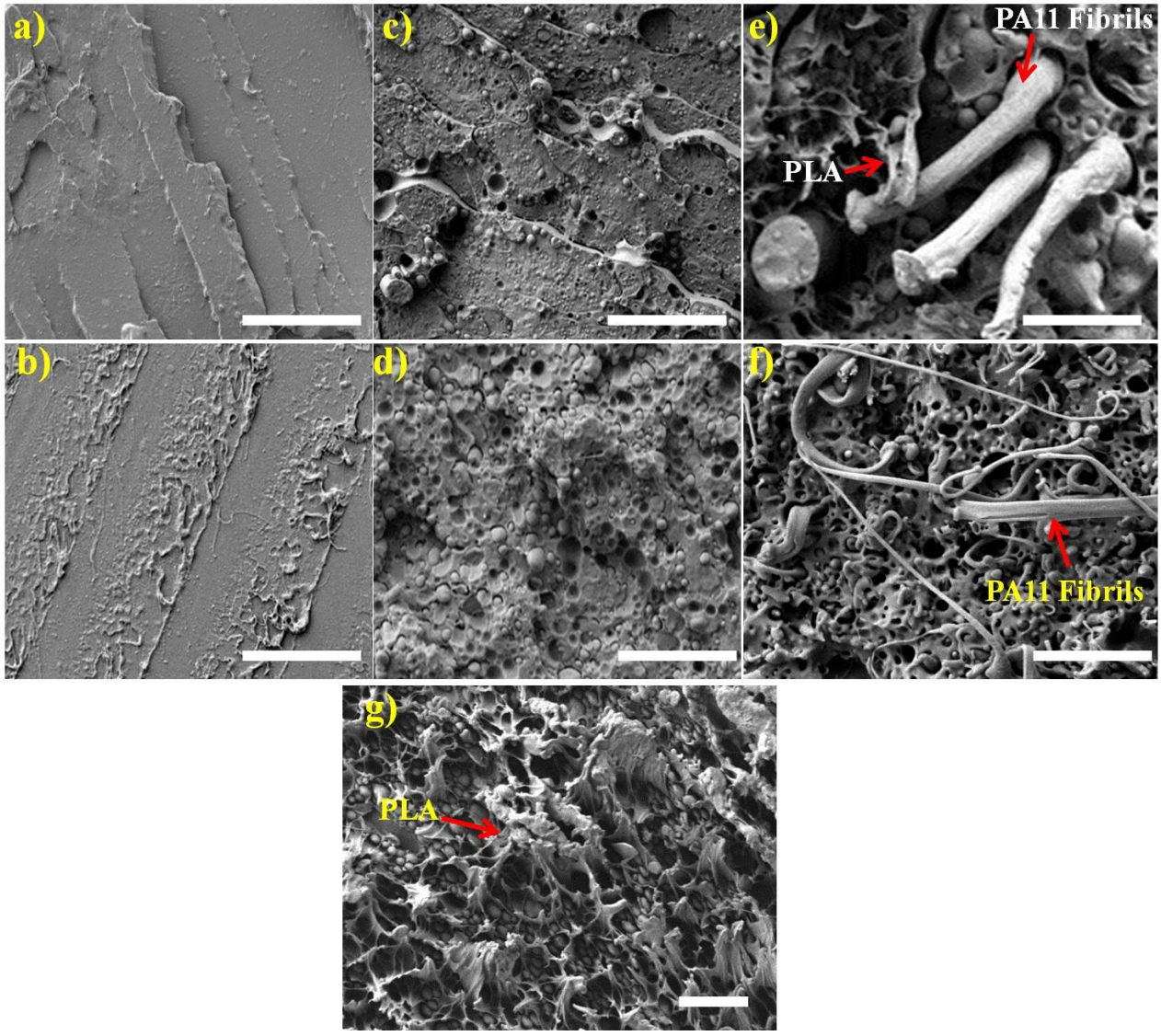

Figure 5.7. SEM images of the impact fracture surface adjacent to the notch of a) PLA, b) PLA/15PEO, c) PLA/PA11 50/50 vol%, d) PLA/PA11 70/30 vol%, e) (PLA-15PEO)/PA11 50/50 vol% and f, g) (PLA-15PEO)/PA11 70/30 vol%. The scale bar indicates 10 μm.

over the entire impact fracture surfaces as shown in Figure 5.7 (e, f). These results are clearly in line with the impact data.

Mechanism. Crazing and shear yielding are two major energy dissipation mechanisms which depend on the matrix properties [11,27]. It is also well known that microvoiding is a critical step in triggering matrix shear yielding in polymer blends, thereby enhancing energy dissipation [28–33]. Internal cavitation inside rubber particles and debonding cavitation at the interface are considered as the two main mechanisms of microvoiding [28,31–33]. In our system, as shown in Table 3, the yield stress of PLA-15PEO is much lower than that for PA11. In such a case it can be expected that the PA11 phase will act as a stress concentrator [29,30]. This stress concentration results in the development of a triaxial tension in the PA11 domains and microvoiding occurs through a debonding process at the (PLA-PEO)/PA11 interface as is shown in Figure 5.8. Figure 5.8 shows SEM images of the cross sections underneath the impact fractured surfaces of (PLA-PEO)/PA11 50/50 vol% blends. Microvoiding by interfacial debonding is indicated by arrows. Once debonding cavitation takes place, the triaxial stress is locally relived in the surrounding voids [29,32]. As controlled debonding progresses, due to the good level of PLA/PA11 interfacial adhesion, PA11 domains are fibrillated and simultaneously shear yielding is triggered in the (PLA-PEO) matrix. Extensive shear yielding of the PLA along with significant fibrillation of the PA11 domains can be clearly observed in Figure 5.7 (e, f, g). Clearly PEO lowers the yield strength of the PLA which is expected to facilitate the dilatational

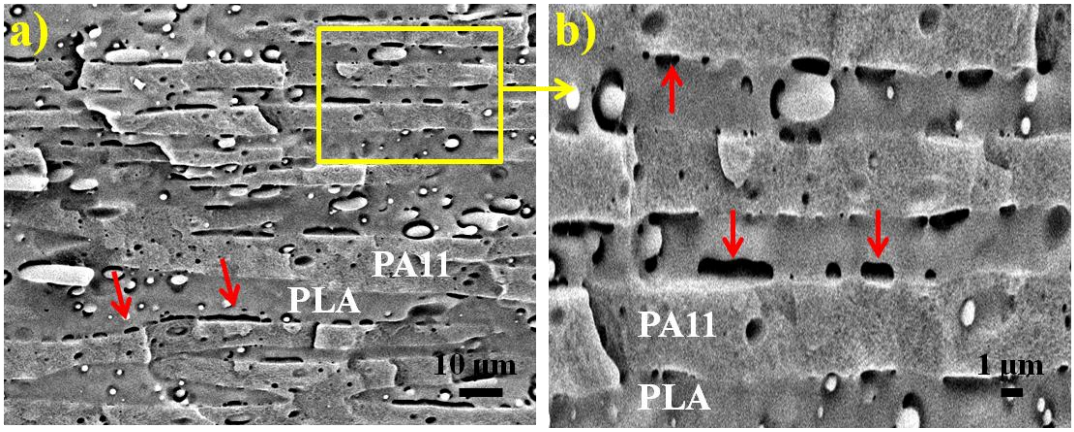

Figure 5.8. SEM images of the cryo-fractured surface of a cross section underneath the impact fracture surface of the (PLA-15PEO)/PA11 50/50 vol% blend representing interfacial cavitations. The arrows indicate the resulted microvide at the interface.

deformation of the PLA phase as is observed in Figure 5.7-g. This effect is clearly shown in Table 5.3 where the elongation of break of PLA-15PEO is 300%. The role of PA11 domains in generating microvoids under the high velocity-high strain conditions of the Izod impact test is also an important step in generating high impact (PLA-PEO)/PA11 blends.

In co-continuous (PLA-PEO)/PA11 50/50 vol% blends a percolated stress field forms along the continuous interface due to the interfacial debonding cavitation which results in the propagation of shear yielding over the entire surrounding matrices (See Figure 5.8). Thus, the co-continuous morphology is also critical to the optimized improvement of impact strength.

5.4.5 Morphology/Mechanical Properties Relationship

Figures 5.5 and 5.6 clearly show that when the PEO plasticizer concentration is reduced below 15% or increased above that value, a sharp drop in mechanical properties is observed. Earlier in this paper it was shown that sufficient PLA chain mobility is necessary in order for PLA/PA11 interfacial interactions to come into play. Figure 5.3 shows that at 5-15% plasticizer a minimum PLA/PA11 interfacial tension is observed. However, the mechanical property results in Figures 5.5 and 5.6 show that at 5 and 10% plasticizer, the properties do not show any substantial improvement. These results point to the conclusion that in addition to effective interfacial interactions, a higher mobility of PLA polymer chains is necessary in order to realize the potential of significant shear yielding which is displayed directly in the elongation at break data in Figure 5.6.

Also, earlier in this paper it was shown that above 15% PEO, PEO starts to phase separate out of PLA. The effect of this phase separation is evident in Figures 5.5 and 5.6 with a significant drop in impact and elongation at break properties observed when the PEO concentration is increased to 20%. SEM and AFM micrographs of (PLA-PEO)/PA11 50/50 vol% blend with 15 and 20% PEO are shown in Figure 5.9. In blends with 15% PEO, PLA/PEO are miscible and PEO cannot be distinguished as a separate phase as shown in Figure 5.9 (a, c). However, at 20% PEO concentration, a significant quantity of PEO has been depleted from the PLA phase. In Figure 5.9-b the PEO phase is extracted and it can be clearly seen that the depleted PEO situates itself between the PLA and PA11 phases. This result is also confirmed by AFM in Figure 5.9-d where PEO is identified as the darkest phase at the PLA/PA11 interface. Not surprisingly, for the 20% PEO sample, an accumulation of PEO at the PLA/PA11 boundary weakens that interface.

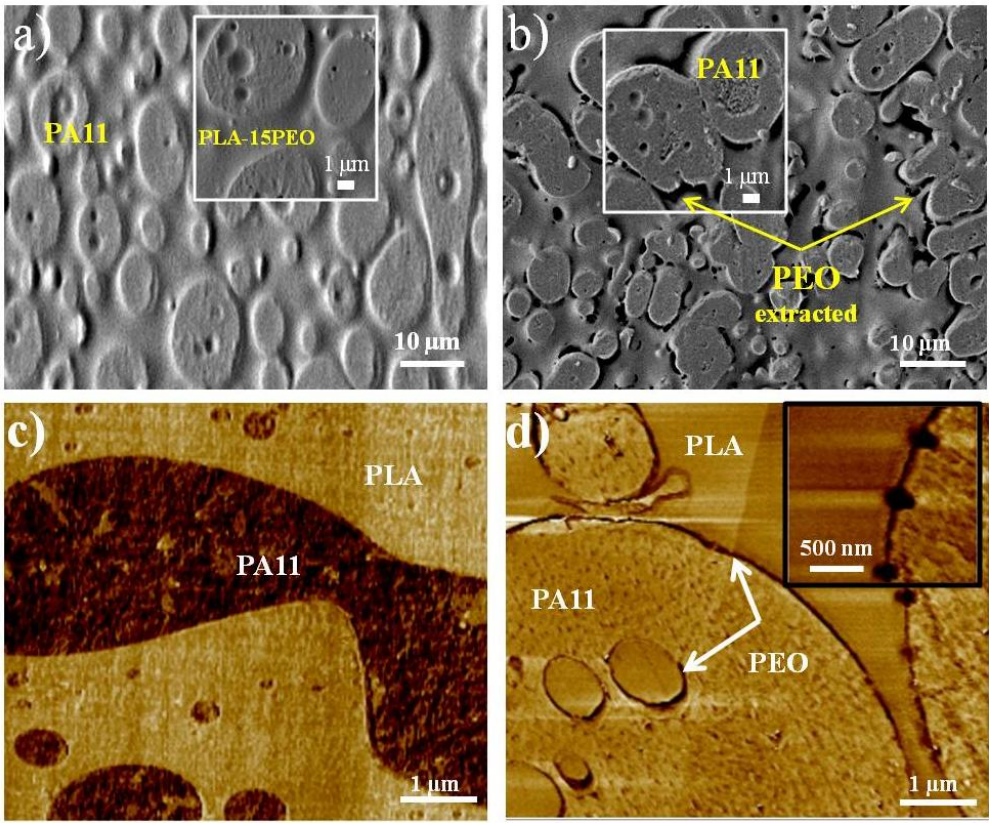

Figure 5.9. SEM (a, b) and AFM (c, d) micrographs of the (PLA-PEO)/PA11 50/50 vol% with a, c) 15% PEO and b, d) 20% PEO, PEO was extracted with water in SEM images.

The PEO phase separation at high plasticizer concentration can also be observed in the spherulitic development of PLA/PEO blends as shown in Figure 5.10 by polarized optical microscopy (POM) and SEM. In the POM images of PLA and PLA/15PEO blends, micrographs (a, b) in Figure 5.10, all the spherulites are closely packed. However, in the sample with 25% PEO almost all the PLA spherulites are separated with a thick layer (4.87 ± 0.3 µm) of PEO phase. In the SEM images the PEO has been extracted with water, Figure 5.10-c. No inter-spherulitic PEO is observed in the SEM image of pure PLA spherulites or in the PLA/15PEO blends. In the latter case, the PEO phase is evident as small voids and crevices within the PLA spherulites.

Earlier in this work we showed that although PEG decreases the interfacial tension of PLA/PA11 at an optimal concentration, it does not improve the mechanical properties of the blend (see Table 5.3). In these systems because of the PEG lower molecular weight, crystallization induced

phase separation occurs at lower PEG concentrations before providing sufficient plastic deformation to the PLA phase.

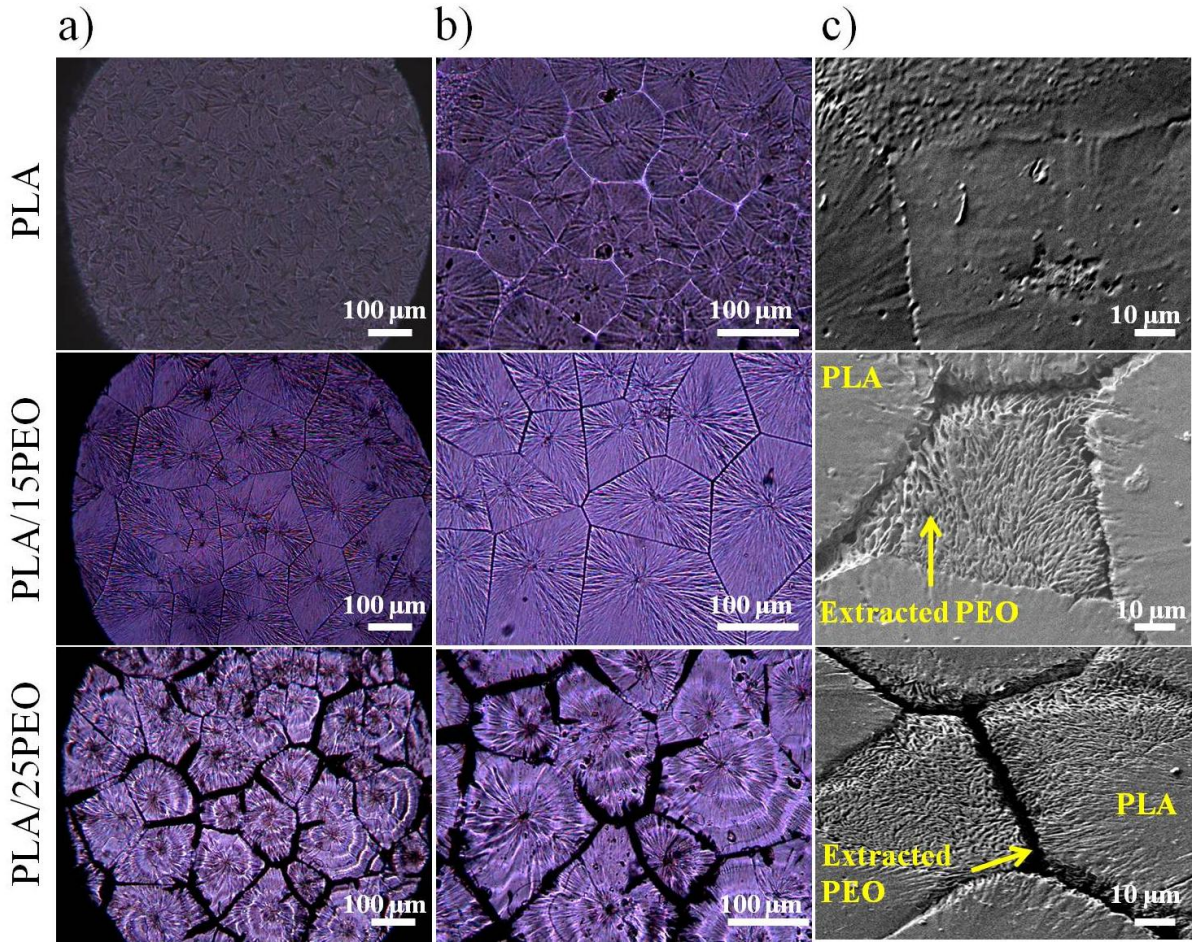

Figure 5.10. Assembly of the PLA spherulites in the PLA/PEO blends with different PEO content isothermally crystallized at 130 °C; a), b) POM and c) SEM micrographs (PEO phase was extracted with water before SEM).

5.5 Conclusion

This study reports on the role of controlled PLA chain mobility in developing high performance PLA/PA11 blends. It is shown that enhanced PLA chain mobility due to the addition of an optimal amount of PEO or PEG to the PLA, increases the interfacial interactions and reduces PLA/PA11 interfacial tension. The mechanical properties of the ternary (PLA-PEO)/PA11 blends strongly depends on PEO concentration. In the (PLA-15PEO)/PA11 50/50 vol% blend a

remarkable improvement in mechanical properties is observed with specimens demonstrating 17.5 times the impact strength of the neat PLA and 3 times that of neat PA11. Also an exceptional improvement in elongation at break at 275% is found, as compared to 5% for the PLA and 6 % for PLA/PA11. The fracture surfaces analysis indicate that the toughening mechanism is controlled interfacial debonding/cavitation at the continuous PLA/PA11 interface, which relieves the hydrostatic tension, followed by the massive shear yielding of the surrounding PLA-PEO and PA11 matrices. The dependence of the mechanical properties on PEO concentration is found to correlate with the limited miscibility of PEO in the PLA phase. At high concentrations of PEO the PEO phase separates from PLA and accumulates at the PLA/PA11 interface and at the inter-spherulitic boundaries providing a locus of failure. In contrast to PEO, PEG as a plasticizer has no effect on the toughening of PLA/PA11. This is attributed to PLA/PEG phase separation at lower PEG concentrations than for PEO. These findings demonstrate a new strategy to generate high impact performance PLA/PA11 blends through controlled PLA chain mobility via an optimal concentration of an appropriate plasticizer.

5.6 Acknowledgements

The authors would like to thank the NSERC Network for Innovative Plastic Materials and Manufacturing Processes (NIPMMP) for their financial support. We would also like to thank Dr. Ali M. Zolali for his valuable insight and discussion.

5.7 References

[1] T. Li, J. Zhang, D.K. Schneiderman, L.F. Francis, F.S. Bates, Toughening Glassy Poly(lactide) with Block Copolymer Micelles, ACS Macro Lett. 5 (2016) 359–364.

[2] A.M. Zolali, V. Heshmati, B.D. Favis, Ultratough Co-Continuous PLA/PA11 by Interfacially Percolated Polyether-b-amide, Macromolecules. 50 (2016) 264–274.

[3] Y. Xu, P. Delgado, A.D. Todd, J. Loi, S.A. Saba, R.J. McEneany, T. Tower, V. Topolkaraev, C.W. Macosko, M.A. Hillmyer, Lightweight micro-cellular plastics from polylactide/polyolefin hybrids, Polymer. 102 (2016) 73–83.

[4] S.C. Mauck, S. Wang, W. Ding, B.J. Rohde, C.K. Fortune, G. Yang, S.-K. Ahn, M.L. Robertson, Biorenewable Tough Blends of Polylactide and Acrylated Epoxidized Soybean

Oil Compatibilized by a Polylactide Star Polymer, Macromolecules. 49 (2016) 1605–1615.

[5] K. Anderson, K. Schreck, M. Hillmyer, Toughening Polylactide, Polym. Rev. 48 (2008) 85–108.

[6] K. Hashima, S. Nishitsuji, T. Inoue, Structure-properties of super-tough PLA alloy with excellent heat resistance, Polymer. 51 (2010) 3934–3939.

[7] K.S. Anderson, M.A. Hillmyer, The influence of block copolymer microstructure on the toughness of compatibilized polylactide/polyethylene blends, Polymer. 45 (2004) 8809–8823.

[8] O. Martin, L. Avérous, Poly(lactic acid): plasticization and properties of biodegradable multiphase systems, Polymer. 42 (2001) 6209–6219.

[9] L. Jiang, M.P. Wolcott, J. Zhang, Study of biodegradable polylactide/poly(butylene adipate-co-terephthalate) blends, Biomacromolecules. 7 (2006) 199–207.

[10] M. Shibata, Y. Inoue, M. Miyoshi, Mechanical properties, morphology, and crystallization behavior of blends of poly(l-lactide) with poly(butylene succinate-co-l-lactate) and poly(butylene succinate), Polymer. 47 (2006) 3557–3564.

[11] H. Bai, C. Huang, H. Xiu, Y. Gao, Q. Zhang, Q. Fu, Toughening of poly(l-lactide) with poly(ε-caprolactone): Combined effects of matrix crystallization and impact modifier particle size, Polymer. 54 (2013) 5257–5266.

[12] T.D. Fornes, D.R. Paul, Structure and Properties of Nanocomposites Based on Nylon-11 and -12 Compared with Those Based on Nylon-6, Macromolecules. 37 (2004) 7698–7709.

[13] G. Stoclet, R. Seguela, J.-M. Lefebvre, Morphology, thermal behavior and mechanical properties of binary blends of compatible biosourced polymers: Polylactide/polyamide11, Polymer. 52 (2011) 1417–1425.

[14] W. Dong, X. Cao, Y. Li, High-performance biosourced poly(lactic acid)/polyamide 11 blends with controlled salami structure, Polym. Int. 63 (2013) 1094–1100.

[15] V. Heshmati, A.M. Zolali, B.D. Favis, Morphology Development in Poly (Lactic Acid)/ Polyamide11 Biobased Blends: Chain Mobility and Interfacial Interactions, (n.d.)

Submitted to “ Polymer” for publication.

[16] Y. Hu, Y.S. Hu, V. Topolkaraev, A. Hiltner, E. Baer, Crystallization and phase separation in blends of high stereoregular poly(lactide) with poly(ethylene glycol), Polymer. 44 (2003) 5681–5689.

[17] A.N. Gaikwad, E.R. Wood, T. Ngai, T.P. Lodge, Two Calorimetric Glass Transitions in Miscible Blends Containing Poly(ethylene oxide), Macromolecules. 41 (2008) 2502–2508.

[18] A.J. Nijenhuis, E. Colstee, D.W. Grijpma, A.J. Pennings, High molecular weight poly(l-lactide) and poly(ethylene oxide) blends: thermal characterization and physical properties, Polymer. 37 (1996) 5849–5857.

[19] L. V. Labrecque, R.A. Kumar, V. Dav, R.A. Gross, S.P. McCarthy, Citrate esters as plasticizers for poly(lactic acid), J. Appl. Polym. Sci. 66 (1997) 1507–1513.

[20] Z. Ren, H. Li, X. Sun, S. Yan, Y. Yang, Fabrication of High Toughness Poly(lactic acid) by Combining Plasticization with Cross-linking Reaction, Ind. Eng. Chem. Res. 51 (2012) 7273–7278.

[21] Y. Yang, Z. Xiong, L. Zhang, Z. Tang, R. Zhang, J. Zhu, Isosorbide dioctoate as a “green” plasticizer for poly(lactic acid), Mater. Des. 91 (2016) 262–268.

[22] I. Pillin, N. Montrelay, Y. Grohens, Thermo-mechanical characterization of plasticized PLA: Is the miscibility the only significant factor?, Polymer. 47 (2006) 4676–4682.

[23] Z. Kulinski, E. Piorkowska, K. Gadzinowska, M. Stasiak, Plasticization of Poly (l-lactide) with Poly (propylene glycol), Biomacromolecules. 7 (2006) 2128–2135.

[24] P.A. Bhadane, A.H. Tsou, J. Cheng, M.D. Ellul, B.D. Favis, Enhancement in interfacial reactive compatibilization by chain mobility, Polymer. 55 (2014) 3905–3914.

[25] J.K. Kim, W.Y. Jeong, J.M. Son, H.K. Jeon, Interfacial tension measurement of a reactive polymer blend by the Neumann triangle method, Macromolecules. 33 (2000) 9161–9165.

[26] M. Pluta, M.-A. Paul, M. Alexandre, P. Dubois, Plasticized polylactide/clay nanocomposites. I. The role of filler content and its surface organo-modification on the physico-chemical properties, J. Polym. Sci. Part B Polym. Phys. 44 (2006) 299–311.

[27] A.C. Renouf-Glauser, J. Rose, D.F. Farrar, R.E. Cameron, The effect of crystallinity on the deformation mechanism and bulk mechanical properties of PLLA, Biomaterials. 26 (2005) 5771–5782.

[28] R. Dou, C. Shen, B. Yin, M. Yang, B. Xie, Tailoring the impact behavior of polyamide 6 ternary blends via a hierarchical core–shell structure in situ formed in melt mixing, RSC Adv. 5 (2015) 14592–14602.

[29] G.-M. Kim, G.. Michler, Micromechanical deformation processes in toughened and particle filled semicrystalline polymers: Part 2. model representation for micromechanical deformation processes, Polymer. 39 (1998) 5699–5703.

[30] G.-M. Kim, G.. Michler, Micromechanical deformation processes in toughened and particle-filled semicrystalline polymers: Part 1. Characterization of deformation processes in dependence on phase morphology, Polymer. 39 (1998) 5689–5697.

[31] D. Dompas, G. Groeninckx, M. Isogawa, T. Hasegawa, M. Kadokura, Cavitation versus debonding during deformation of rubber-modified poly(vinyl chloride), Polymer. 36 (1995) 437–441.

[32] Y. Li, H. Shimizu, Toughening of Polylactide by Melt Blending with a Biodegradable Poly(ether)urethane Elastomer, Macromol. Biosci. 7 (2007) 921–928.

[33] H.-J. Sue, J. Huang, A.. Yee, Interfacial adhesion and toughening mechanisms in an alloy of polycarbonate/polyethylene, Polymer. 33 (1992) 4868–4871.

CHAPTER 6 ARTICLE 3: CELLULOSE NANOCRYSTAL IN POLY (LACTIC ACID)/POLYAMIDE11 BLENDS: PREPARATION, MORPHOLOGY AND CO-CONTINUITY[3]

Vahid Heshmati[a], Musa R. Kamal[b] and Basil D. Favis[a]

a. CREPEC, Dept of Chemical Engineering, École Polytechnique de Montréal, Montreal, Canada

b. CREPEC, Dept of Chemical Engineering, McGill university, Montreal, Canada

6.1 Abstract

In this work, for the first time, cellulose nanocrystal (CNC) is incorporated into poly (lactic acid)/bio-polyamide11 (PA11) blends at different loadings through a combination of solvent dissolution, casting and melt mixing. Atomic force microscopy (AFM) and rheology analysis demonstrate an exceptional level of CNC dispersion using this technique. CNC is fed into the blends through prepared PLA/CNC or PA11/CNC mixtures via melt mixing in an internal mixer. In the PLA/PA11/CNC system, the CNC particles perfectly segregate into the PA11 phase at all compositions, after mixing, irrespective of whether the PLA/CNC or the PA11/CNC mixture is used. These findings are supported by thermodynamic predictions based on interfacial energy. There is virtually no influence of CNC content on the PLA/PA11 morphology when it is in a matrix/dispersed phase form. This is attributed to the already low level of coalescence resulting from the low interfacial tension between PLA and PA11. However, when coalescence phenomena are fully maximized through the preparation of a co-continuous system (PLA/PA11 50/50), then CNC addition dramatically diminishes coalescence even at values as low as 1 wt% CNC. It is suggested that the retarded relaxation of the CNC filled PA11 domains is the main mechanism governing this coalescence reduction.

[3] Submitted to Carbohydrate Polymers

6.2 Introduction

Increasing environmental concerns over pollution caused by non-degradable petroleum based polymers has driven the development of more eco-friendly products [1–3]. Poly(lactic acid) (PLA) is one of the most promising bio-plastics and has received particular attention [1,4]. Despite a high tensile strength and modulus, the inherent brittleness of PLA limits its application [1,5]. Among different strategies used for PLA toughening, polymer blending is a practical and widely used approach and allows for the tuning of the mechanical properties [1,5–9].

Polyamide11 (PA11) is a high-performance bio-polymer with high impact strength and elongation at break [10]. Since these properties are just those lacking in PLA, a PLA/PA11 blend has the potential to generate a new bio-product with unique advantages [10,11]. In previous work from this laboratory [12] the morphology and mechanical performance of PLA/PA11 blends has been systematically studied. It was shown that PLA/PA11 system behaves as a highly interacting system and controlled PLA chain mobility through addition of an appropriate amount of PEO plasticizer leads to significant enhancement in mechanical properties of the blend.

The study of the localization of nanoparticles in polymer-polymer blends is still an emerging field. The thermodynamically stable localization of solid nanoparticles in melt mixed polymer-polymer blends and their influence on morphology is essential in determining the ultimate performance of such multiphase systems [13,14]. In a thermodynamically stable localization, which is expected to stay unchanged even after reprocessing, nanoparticles migrate to the phase to which they have the higher affinity in order to diminish the system free energy [15–17]. Goldel et al.[17] reported on the selective localization of carbon nano-tubes in the PC phase in PC/SAN blends either by pre-compounding with one of the components or by one step melt mixing. The selective localization of nanoparticles can also significantly affects the morphology of polymer blends [13,18–20]. Filippone et al. [20] showed that selective localization of organomodified clay in the PA6 phase in PA6/HDPE blends substantially diminishes the HDPE dispersed phase size. They suggested that organoclay platelets act as solid barriers and suppress the coalescence by preventing the collision of HDPE droplets during melt mixing. In another study Lee et al. [21] reported that addition of silica nanoparticles to co-continuous PP/polyolefin elastomer (POE) blends, in the presence of maleated-PP as a compatibilizer, results in a finer morphology consisting of elongated POE domains within the PP phase. They attributed this

change to the increase in the elasticity of the PP phase with silica loading.

Cellulose nanocrystal (CNC) has many advantages including superior mechanical properties, low density, biodegradability, renewability and low cost. Thus, they offer significant potential in generating new materials when well dispersed in polymers [22–24]. High strength cellulose nanocrystal (CNC) is typically obtained from acid hydrolysis of cellulosic fibers and has a rod-like shape with a length of tens to hundreds of nanometers and a thickness of four to tens nanometers [22,25,26]. In recent years CNC has been successfully added to different polymers improving their thermo-mechanical performances [2,25,27–30]. Only a few studies, however, have examined the effect of incorporation of CNC particles into polymer-polymer blends [6,31]. Bitinis et al. [31] demonstrated that the localization of CNC particles in the PLA phase diminishes the size of the natural rubber (NR) dispersed phase in PLA/NR blends. This was attributed to the increased PLA viscosity and to coalescence suppression of the NR droplets. In another study it was found that CNC particles increase the interfacial adhesion and thermal stability of PLA/PHB blends [6].

The main challenge associated with polymer/CNC systems is obtaining a proper homogenous level of CNC dispersion within polymer matrices due to the highly hydrophilic character of CNC particles [22,32]. There are limited methods for dispersion of CNC in a polymeric matrix [33]. Typically, solvent dissolution is known to be the most effective method for CNC dispersion within a single polymer matrix [22,33]. However this approach becomes very limited when applied to polymer-polymer blending due to the lack of common solvents. The direct melt mixing of CNC into polymers, on the other hand, is significantly less effective at generating well dispersed CNC.

The objective of this work is to develop a technique to generate well dispersed cellulose nanocrystal (CNC) in PLA/PA11 bio-blends through melt mixing and to examine the effect of CNC on the blend morphology. Both dispersed phase and co-continuous morphologies will be examined. Special attention will be given to examining the localization of the CNC in the PLA/PA11 blend system.

6.3 Experimental Section

6.3.1 Materials

PLA 3001D with 1.8%-D isomer, M_w = 142000 and M_n = 72000 and PA11 (Rilsan BMNO TL) with M_w = 25000 and M_n = 12000 were obtained from Natureworks and Arkema, respectively. The PLA and PA11 materials were dried at 70 °C under vacuum for 48h before use. Spray dried cellulose nanocrystal (CNC) particles were obtained from Alberta Innovates Technology Futures.

6.3.2 Surface Tension Measurements

For surface tension measurements, PLA and PA11 films with 1mm thickness were prepared by compression molding. The prepared films were rinsed with ethanol and distilled water and then dried under vacuum. The CNC film was obtained by casting an aqueous CNC suspension. Contact angle and surface tension measurements of the PLA, PA11 and CNC films were performed by the contact angle method with probe liquids. The details of the method are presented elsewhere [34]. Briefly, the PLA, PA11 or CNC film were placed in the test chamber. A drop, about 4-7 µl, of liquid probe was then placed gently on the prepared film. The drop development was recorded by a CCD camera. Images were taken every 40s until a stable drop shape was obtained.

6.3.3 PLA/CNC and PA11/CNC Mixture Preparation

For the PLA/CNC mixture preparation, a homogenous CNC suspension in DMF was first prepared by dispersing a desired amount of the CNC particles in the DMF medium with the aid of a water-bath sonicator (FS30 100 Watts Ultrasonic Cleaner, Fisher Scientific). Then, a PLA/DMF solution with a desired PLA concentration was added to the suspension while stirring with a magnetic stirrer for 2h at 50 °C. The PLA/CNC mixture was obtained by casting/evaporation of the prepared suspension in a vacuum oven at 80 °C for 48h. The mixture was put into powder form afterwards with a grinder and kept in the vacuum oven at 60 °C for another 48h to make sure that final traces of the solvent are removed. For the PA11/CNC mixture the same procedure was applied except that formic acid was used as the suspension medium.

6.3.4 Melt Mixing Blend Preparation

PLA/PA11/CNC ternary systems were prepared in two steps. For the ternary system in which CNC was fed into the blends through the PLA/CNC mixture, neat PLA and the mixture were first melt mixed in an internal mixer (Plasti-Corder, Brabender, with a total volume of 30 ml).

Once the torque reached a plateau, the desired amount of the PA11 was fed into the chamber and mixed for 6 minutes. The processing temperature and rotor speed were fixed at 200 °C and 50 rpm, respectively. For the ternary systems in which CNC was added to the blends via the PA11/CNC mixture, neat PA11 and the materbatch were first mixed in the internal mixer and after reaching the plateau of the torque, PLA was fed into the mixer. Essentially, the same procedures were applied here. Three different compositions of PLA/PA11, i.e. 30/70, 50/50 and 70/30 vol% with 0.5, 1, 2 and 3 wt% of CNC (based on the entire blend) were prepared.

6.3.5 Rheology

A constant stress rheometer (Physica MCR 301, Anton Paar) in a parallel plate geometry with a 1 mm gap and a diameter of 25 mm was used for the rheological characterization. The test was carried out at 200 °C and under a nitrogen atmosphere. Disk-shaped samples with a diameter of 25 mm and a thickness of 1 mm were prepared by compression molding in a Carver hot plate hydraulic press at 300 kPa and 200 °C under a constant flow of dry nitrogen. All samples were dried in a vacuum oven at 80 °C for 24 h before compression molding or the rheological test.

6.3.6 Microtomy and Scanning Electron Microscopy (SEM)

As-prepared samples from the internal mixer were cut and then microtomed using a Leica-Jung RM 2065 microtome equipped with a liquid nitrogen cryo-chamber and a glass knife. PLA was first selectively extracted from the blend with chloroform. The samples were then coated with a gold layer (15 nm thickness) and a field emission scanning electron microscope (FESEM) (JSM 7600F, JEOL) at a voltage of 1-5 kV was employed for the morphology characterization.

6.3.7 Atomic Force Microscopy (AFM)

All the samples were cut and cryo-microtomed according to the same protocol reported for the SEM sample preparation. The prepared plane surface was directly examined by AFM (MultiMode Nanoscope IIIa with extender, Digital instrument, Santa Barbara, CA) without any further preparation. ACTA-W AppNano silicon tips with a radius of 10 nm were employed. For the analysis of the as-received CNC, a droplet of well dispersed CNC aqueous suspension was dried on a mica surface prior to AFM examination. The films were analyzed directly very shortly after solvent evaporation.

6.3.8 Image Analysis

An image analyzer (SigmaScan Pro.V.5) equipped with a digitizing table (Wacom) was used to analyze SEM images in order to determine the volume average diameter, d_v, the number average diameter, d_n, of the dispersed phase and the specific interfacial area of the PLA/PA11 50/50 vol% blends at different CNC contents. The specific interfacial area , S, of the co-continuous PLA/PA11 50/50 vol% blends was estimated using the following equation [35]:

$$S = P / A \tag{6.1}$$

in which A is the area of the examined image and P is the interfacial perimeter of the PLA/PA11 interface. The pore diameter was then calculated using equation 6.2:

$$d = 4\emptyset_p/S \tag{6.2}$$

in which *d* is the pore diameter, $\emptyset_p$ is the porous volume fraction and *S* is the specific interfacial area.

6.3.9 Quiescent Annealing

In order to study the effect of the selective localization of CNC particles on the static coalescence of the PLA/PA11 50/50 vol% co-continuous blend, quiescent annealing was carried out on some samples. The tests were carried out at 200 °C for up to 80 min using a hot plate hydraulic press without applied pressure and under a constant flow of dry nitrogen.

6.4 Results and Discussion

6.4.1 Surface Tension

The total surface tension, including the polar and dispersive components of PLA, PA11 and CNC particles at room temperature measured by the contact angle technique, are presented in Table 6.1. The surface tension data at the processing temperature were calculated by considering the thermal coefficients of the surface tension obtained from the literature [25,36]. PLA has a surface tension of $\gamma = 33.6 \pm 0.3$ mN/m at 200 °C with dispersive and polar contributions of $\gamma^d = 26.5 \pm 0.2$ and $\gamma^p = 7.1 \pm 0.1$, respectively. The surface tension of PA11 was found to be $\gamma = 25.6 \pm 0.2$ mN/m at 200 °C with dispersive and polar contributions of $\gamma^d = 13 \pm 0.1$ and $\gamma^p = 12.6 \pm 0.1$, respectively. CNC has a surface tension of $\gamma = 20 \pm 0.3$ mN/m at 200 °C with dispersive and polar components of $\gamma^d = 11.8 \pm 0.1$ and $\gamma^p = 8.2 \pm 0.2$, respectively. Similar results were reported for CNC film prepared by solvent casting [25] and CNC pellets [37] while a higher

value was reported for an CNC film prepared by spin coating [38]. It has to be noted that CNC surface tension data measured with the contact angle technique strongly depend on their hydrolysis process, surface charges, surface roughness and also sample preparation [25,34].

Table 6.1. Surface tension parameters of the PLA, PA11 and CNC at 25 and 200 ºC.

	T (º C)	γ (mN/m)	γ^d (mN/m)	γ^p (mN/m)	$\frac{d\gamma}{dT}$ (m/mK)
PLA	25	45 ± 0.3	35.5 ± 0.2	9.50 ± 0.1	-0.065 [25]
	200	33.6 ± 0.3	26.5 ± 0.2	7.1 ± 0.1	
PA11	25	37 ± 0.2	18.9 ± 0.1	18.1 ± 0.1	-0.065 [36]
	200	25.6 ± 0.2	13 ± 0.1	12.6 ± 0.1	
CNC	25	55 ± 0.3	32.5 ± 0.1	22.5 ± 0.2	-0.2 [25]
	200	20 ± 0.3	11.8 ± 0.1	8.2 ± 0.2	

6.4.2 CNC Microstructure

The SEM image of the as-received spray dried CNC powder is shown in Figure 6.1-a. The spray dried powder demonstrates highly agglomerated particles with a size distribution of between 5 to 25 µm. AFM images of non-agglomerated single CNC particles obtained from an aqueous suspension are shown in Figures 6.1 (b, c). The CNC clearly has a rod-like structure with an average length of 195 ± 40 nm. The height difference between the particles and the mica surface can be considered as the particle thickness which is around 15 ± 5 nm. This value also correlates with the thickness value obtained from image analysis. These dimensions are in good agreement with the literature [22,25,26,39].

6.4.3 CNC Dispersion in PLA or PA11

FESEM images of directly melt mixed PLA/2 wt% CNC and PA11/2 wt% CNC are shown in Figure 6.2. The presence of large CNC aggregates in both images shows that the direct melt processing of the spray dried CNC powder is not effective in de-agglomeration or in achieving CNC dispersion in PLA or PA11. However, due to its higher polarity, the PA11 provides a somewhat better de-agglomeration than PLA.

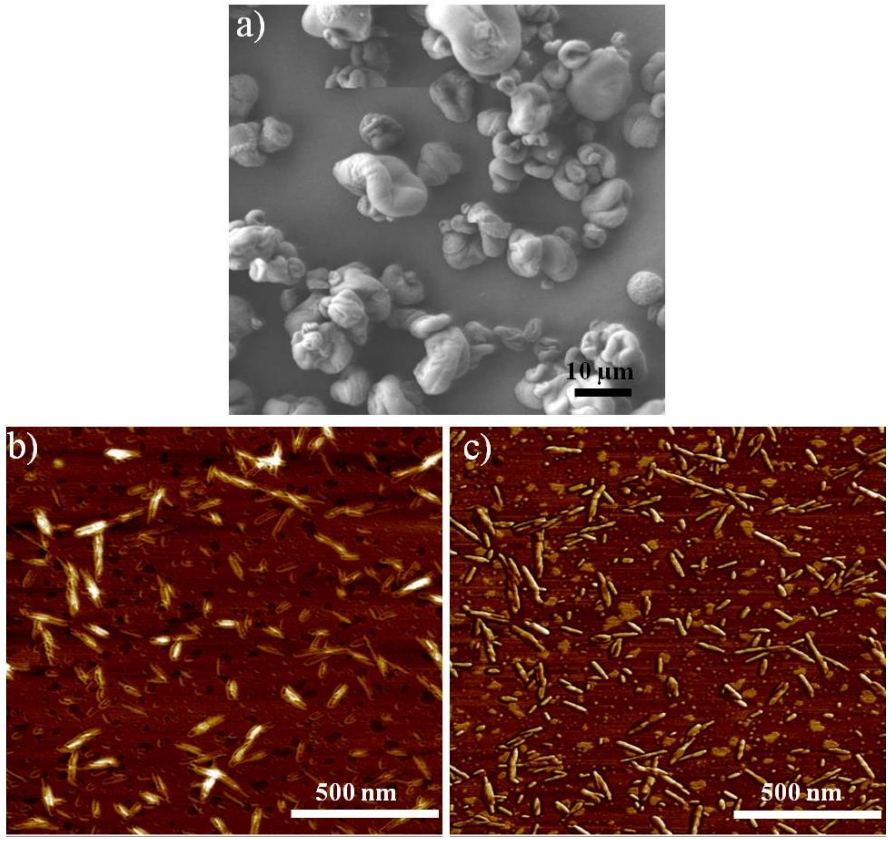

Figure 6.1. a) SEM micrograph of spray dried CNC agglomerates, b) AFM height and c) AFM phase topographies of a dried drop of an aqueous CNC suspension deposited over a mica surface.

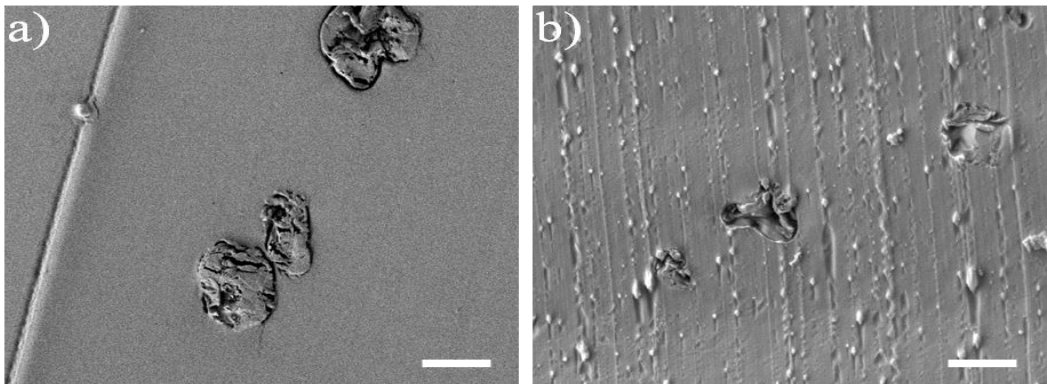

Figure 6.2. FE-SEM images of melt mixed a) PLA and b) PA11 with 2 wt% CNC. The scale bars indicate 10 µm.

Micrographs of 2 wt% CNC in PLA and PA11 prepared by the combined solvent dissolution/melt mixing method are presented in Figure 6.3. Although some agglomeration can

be seen in the FESEM images on the left, the AFM images on the right show a substantially homogeneous CNC dispersion for both the PLA and PA11 matrix materials. The CNC appears as white dots and are easily identified. These dots correlate to the transverse section of the CNC particles. The diameter/thickness of the CNC particles based on AFM topography images ranges from 15 to 50 nm. This indicates the significant presence of individual CNC particles as well as small aggregates well distributed within the PLA and PA11 matrices. It has to be noted that CNC particles appears as dots in SEM and AFM micrographs because the samples are microtomed to a plane face before microscopic observation. Individual particle CNC dispersion in a polymer matrix has rarely been achieved [25,27].

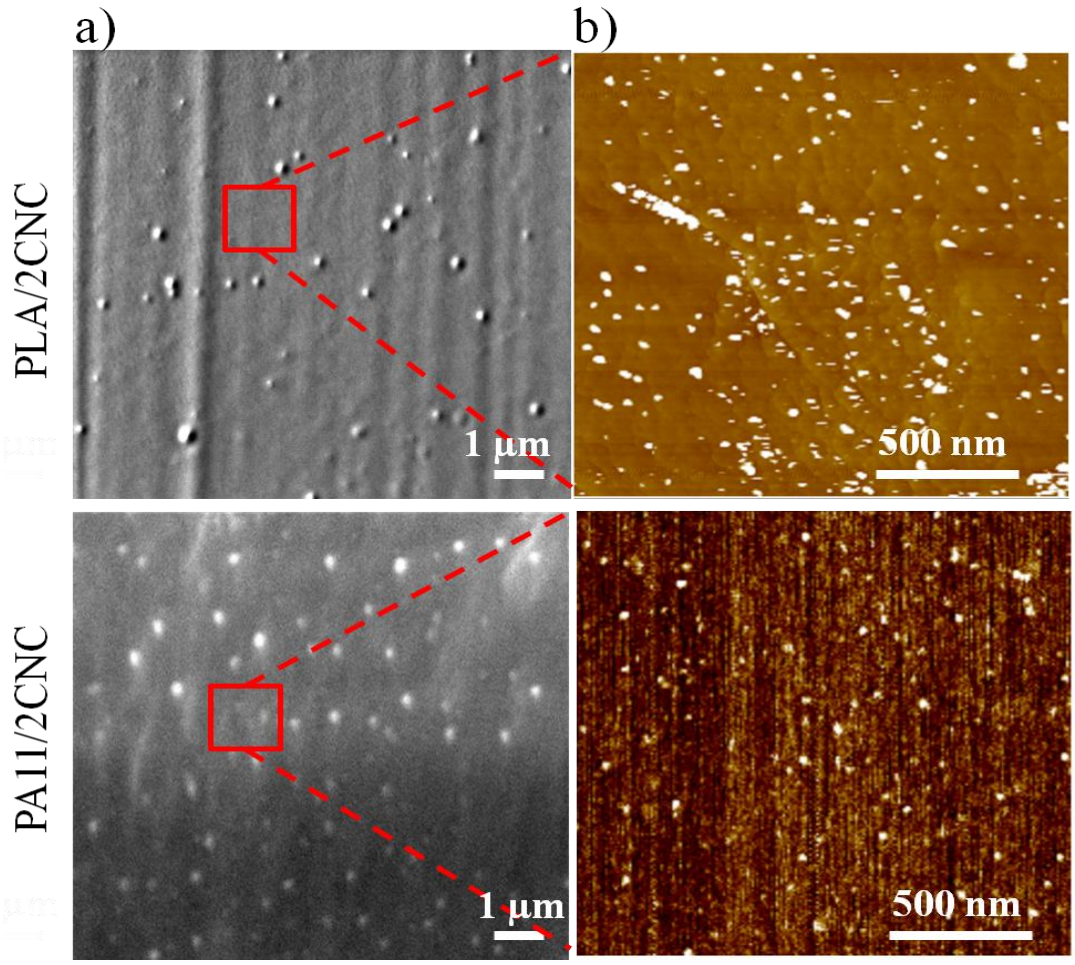

Figure 6.3. FE-SEM images (left) and AFM phase micrographs (right) of 2wt% CNC in PLA and 2wt% CNC in PA11 prepared by solvent dissolution/melt mixing.

6.4.4 Rheological Analysis of CNC/PLA and CNC/PA11

Rheology has been shown to be an effective indirect method to analyze the quality of nanoparticle dispersion in polymers [14,40,41]. Figure 6.4-a shows the change in complex viscosity (η*) versus angular frequency (ω) in PLA containing different CNC loadings. For the lower CNC concentrations, although the complex viscosity increases, no significant shear thinning behavior is observed. At high CNC concentration, however, an increase in the complex viscosity along with shear thinning behavior at low frequencies is evident. Similar behavior has

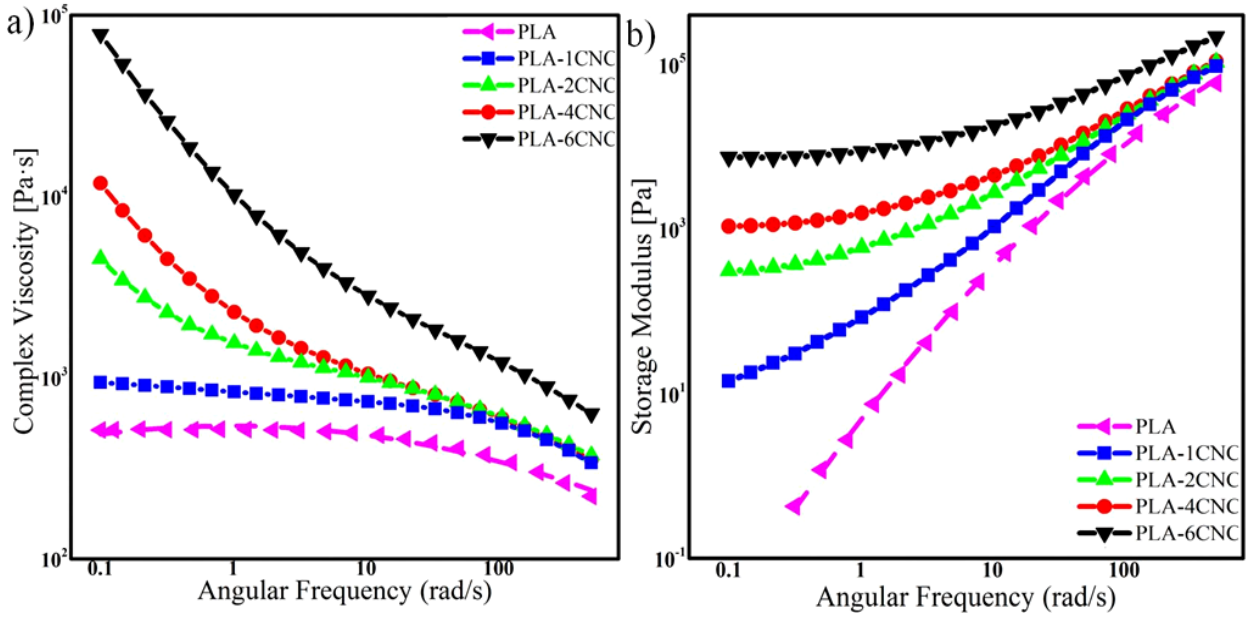

Figure 6.4. a) Complex viscosity (η^*) and b) Storage modulus (G') versus angular frequency (ω) for PLA and PLA/CNC nanocomposites.

been observed for polymers that are highly loaded (more than 30 wt %) with microfillers [42]. Thus, the increase in complex viscosity combined with highly shear thinning behavior in the PLA/CNC system, with the onset already observed at even 1 wt% CNC, can be most likely attributed to the onset of network formation of the CNC particles. For this effect to be observed at 1 wt% CNC is an indication of a high level of CNC dispersion [2,28,29,43]. Moreover it is shown in Figure 6.4-b that the slope of the storage modulus (G') versus angular frequency (ω) at low frequencies decreases from 1.5 for the PLA to 0.12 for nanocomposites containing 6 wt% CNC. At low frequencies, polymer chains have enough time to disentangle and any changes in

the storage modulus, including the slope, can also be related to the effect of the CNC dispersion. Thus, the plateau of G' at low frequencies for PLA containing greater than 1 wt% CNC concentration indicates that the PLA/CNC nanocomposite attains a pseudo solid-like behavior due to network formation.

The viscoelastic properties of neat PA11 and PA11/CNC systems are shown in Figure 6.5. The complex viscosity (η*) of neat PA11 shows a wide plateau in Figure 6.5-a. For PA11 nanocomposites with an CNC concentration of 0.5 wt% or greater, the complex viscosity exhibits a similar shear thinning behavior with no plateau region as observed above for PLA. The even lower onset concentration is likely an indication of an even lower percolation network threshold and thus better dispersion of CNC in PA11 than in PLA [2,28,29,43]. Also, the PA11 storage modulus (G') exhibits the general behavior of polymer melts with a terminal behavior ($G' \sim \omega^2$) as shown in Figure 6.5-b. The frequency dependence of G' of the CNC filled PA11 samples progressively weakens with increasing CNC concentration similar to what is observed for PLA in Figure 6.4-b. In contrast to PLA/CNC nanocomposites, however, a lower onset concentration between 0.5-1 wt% CNC is observed for PA11/CNC system which again highlights the better CNC dispersion in PA11 and stronger interactions between PA11 and CNC particles.

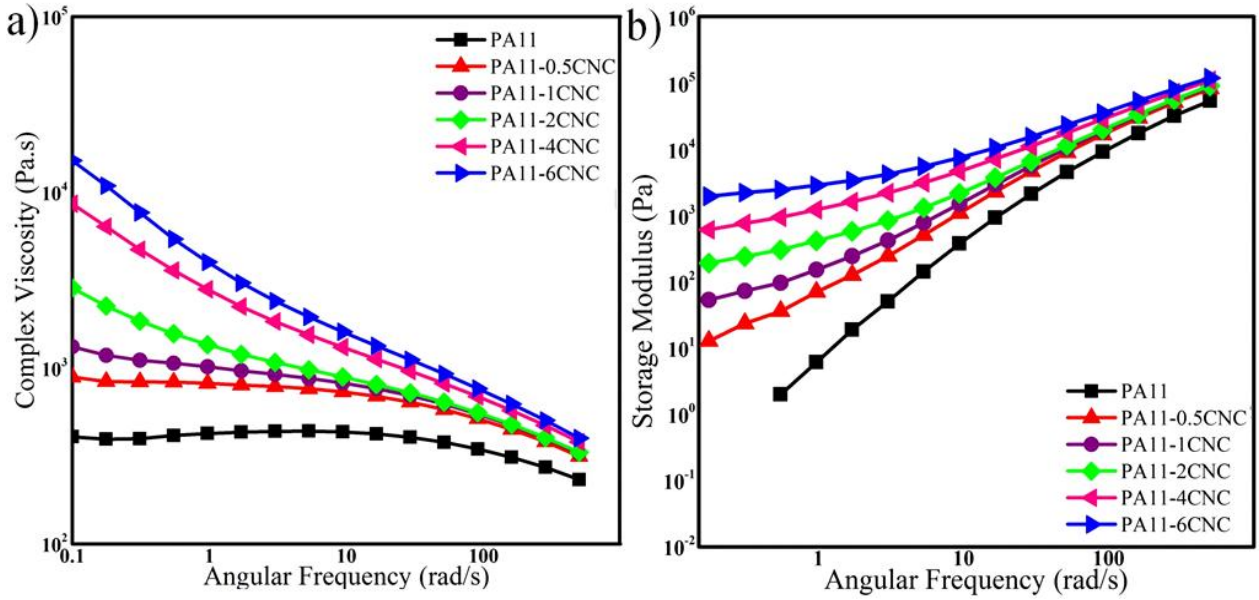

Figure 6.5. a) Complex viscosity (η^*) and b) Storage modulus (G') versus angular frequency (ω) for PA11 and PA11/CNC nanocomposites.

6.4.5 CNC Localization in PLA/PA11 Blends.

Morphology. Figure 6.6 shows AFM phase micrographs of three blend compositions (30/70, 70/30 and 50/50 vol%) of PLA/PA11 blends without and with 2wt% CNC particles in which CNCs were fed into the system through the PA11/CNC mixture. In all three blends compositions, CNC particles appear as white dots located in the PA11 phase. The morphological stability was confirmed by annealing selected samples. The same localization of nanoparticles as seen in Figure 6.6 was observed for the samples after annealing.

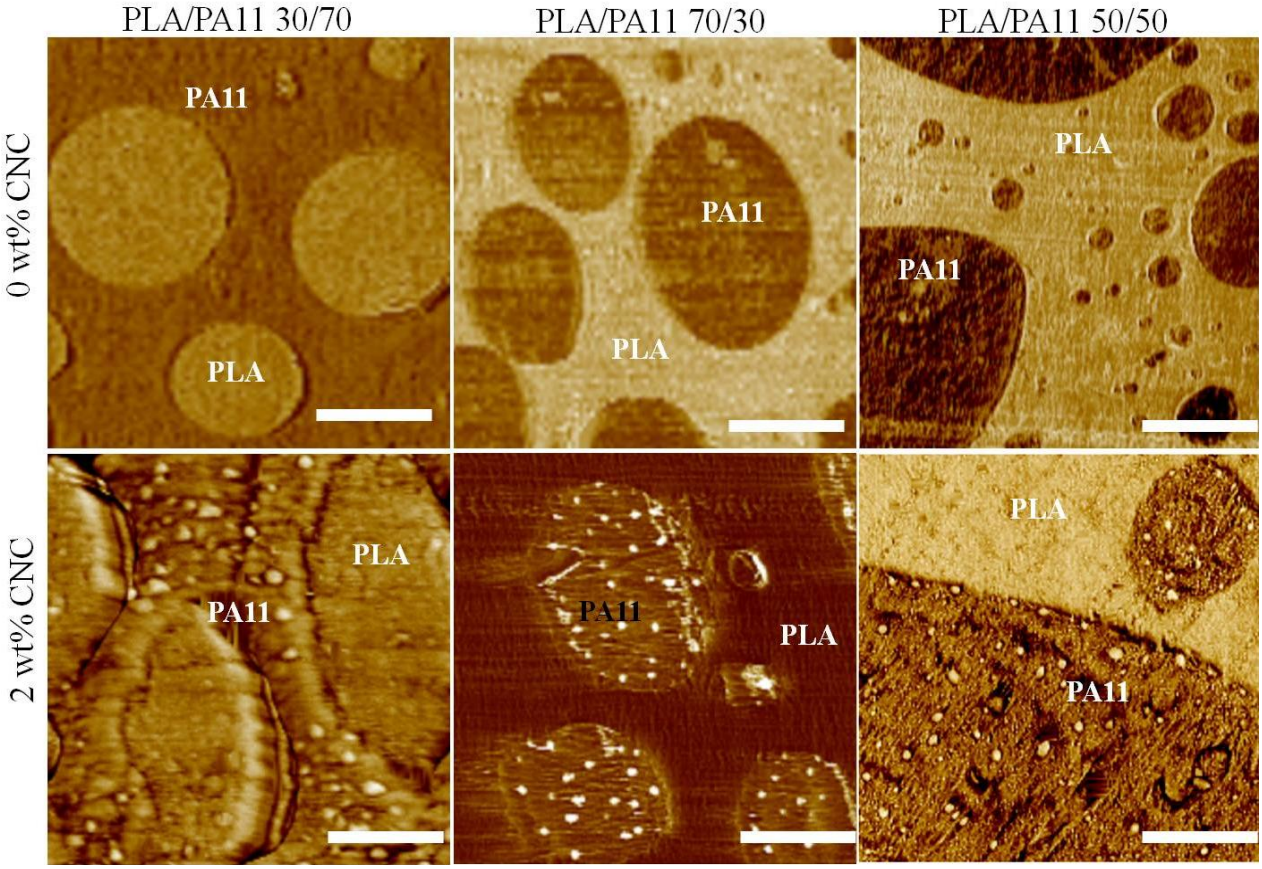

Figure 6.6. AFM phase micrographs of the PLA/PA11 blends with and without CNC particles. CNC was fed into the blend through the PA11/CNC mixture. The scale bars indicate 500 nm.

The state of the localization of CNC particles in the PLA/PA11 blends at three different compositions (30/70, 70/30 and 50/50 vol %) containing 2wt% CNC, prepared using the PLA/CNC mixture, are presented in Figure 6.7. According to Figure 6.7, the CNC particles have clearly migrated from the PLA phase towards the PA11 phase during processing irrespective of

whether the PA11 is the matrix phase (PLA/PA11 30/70 vol%), or the dispersed phase (PLA/PA11 70/30 vol %), or is forming a co-continuous morphology with PLA (PLA/PA11 50/50 vol%).

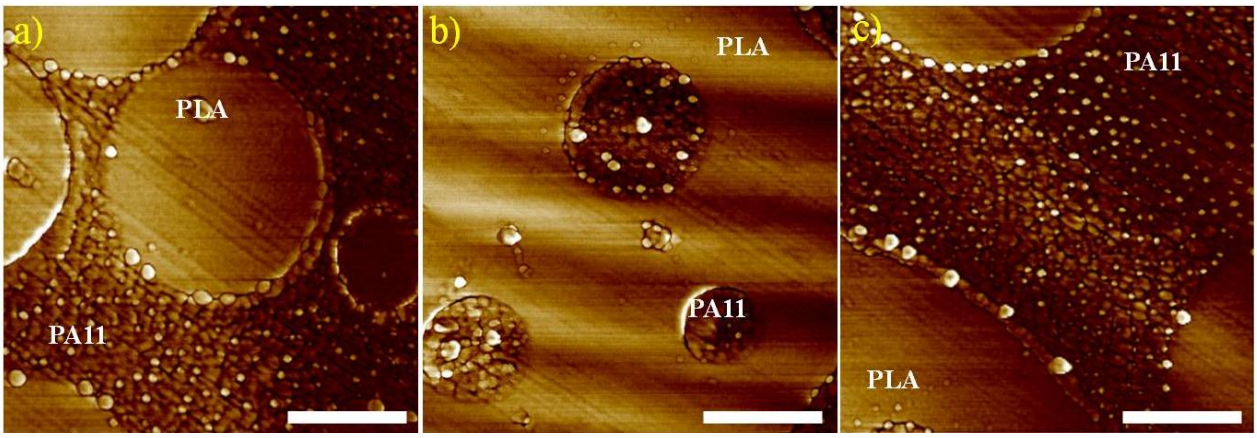

Figure 6.7. AFM phase micrographs of 2 wt% CNC particles in PLA/PA11: a) 30/70 b) 70/30 and c) 50/50 vol% blends. CNC was fed into the blend through the PLA/CNC mixture. The scale bars indicate 500 nm.

Theoretical Analysis. From a thermodynamic point of view, the localization of solid nano-inclusions can qualitatively be estimated by comparing the interfacial tension of polymer components and nanoparticles. Ideally, the CNC is localized in the phase with which it has the lower interfacial tension in order to minimize the interfacial free energy. This will result in a thermodynamically stable localization, which is expected to stay unchanged even after reprocessing. This can be predicted by Young's equation which represents the ability of polymer 1 or polymer 2 to wet the CNC particle [41]:

$$\omega = \frac{\gamma_{NCC-2} - \gamma_{NCC-1}}{\gamma_{12}} \tag{6.3}$$

where γ_{NCC-i} is the interfacial tension between nano-inclusion and polymer i, γ_{12} is the interfacial tension between the two polymers and ω is the wetting coefficient. When < -1, CNCs are only found in polymer 2. For values of $\omega > 1$, CNC particles reside in polymer 1. If $-1 < \omega < 1$, CNC particles locate at the interface of the two polymers.

The PLA/CNC and PA11/CNC interfacial tension data are calculated using the surface tension data from Table 6.1 and the harmonic-mean equation which is valid for the calculation of the

interfacial tension between low surface tension materials:

$$\gamma_{12} = \gamma_1 + \gamma_2 - 4\left[\frac{\gamma_1^d \gamma_2^d}{\gamma_1^d + \gamma_2^d} + \frac{\gamma_1^p \gamma_2^p}{\gamma_1^p + \gamma_2^p}\right] \quad (6.4)$$

in which, γ_i is the surface energy, γ_1^p is the polar component and γ_1^d is dispersive component of surface energy. In a previous work [12], it was demonstrated that the contact angle and harmonic mean approach does not provide an accurate value of the interfacial tension between PLA and PA11 because of the interfacial interactions between the two polymers that occur during dynamic mixing. In that work using the in-situ Neumann triangle method, the real in-situ interfacial tension of the PLA/PA11 pair during mixing was found to be 3.2 mN/m. Therefore, taking PLA as phase 1 and PA11 as phase 2, the wetting parameter in the PLA/PA11/CNC system is estimated as -1.47, as is summarized in Table 6.2. This value of ω predicts the thermodynamic equilibrium localization of the CNC particles in the PA11 phase, which is in agreement with the experimental results.

Table 6.2. Interfacial tension data (mN/m) for the three possible interfaces and wetting coefficient for the PLA/PA11/CNC system.

PLA/PA11	3.2
PLA/CNC	5.7
PA11/CNC	1
ω	- 1.47
Prediction	PA11 phase

6.4.6 The Effect of CNC on PLA/PA11 Blend Morphology

Matrix/Dispersed Phase Morphology. The volume average (d_v) and number average (d_n) diameter of the dispersed phase in the PLA/PA11 30/70 and 70/30 vol% blends with different CNC contents are presented in Table 6.3. Interestingly, the dispersed phase size does not change even after addition of 3 wt% CNC into the blend. This effect can be seen visually from the SEM micrographs in Figure 6.8 for both blend compositions without and with 3 wt% CNC particles. According to Figures 6.4 and 6.5, the viscosity ratio (viscosity of the dispersed phase to that of the matrix) at the processing conditions changes from 1 to 0.4 for PLA/PA11 30/70 vol% and from 1 to 2.6 for PLA/PA11 70/30 vol% blend after addition of 3 wt% CNC as is presented in Table 6.3. Although it has been reported that the viscosity ratio has a significant influence on the dispersed phase size in immiscible polymer blends, it is well known that interacting systems

demonstrate much less dependency on this parameter [12,44].

Table 6.3. Dispersed phase size (μm) and viscosity ratio of CNC filled PLA/PA11 blends.

CNC (wt%)	**0**			**1**			**3**		
	d_v	d_n	η_d/η_m	d_v	d_n	η_d/η_m	d_v	d_n	η_d/η_m
PLA/PA11 30/70	1.2	1	1	1.2	0.9	0.7	1.3	0.9	0.4
PLA/PA11 70/30	1.5	1	1	1.5	1.1	1.5	1.6	1.2	2.6

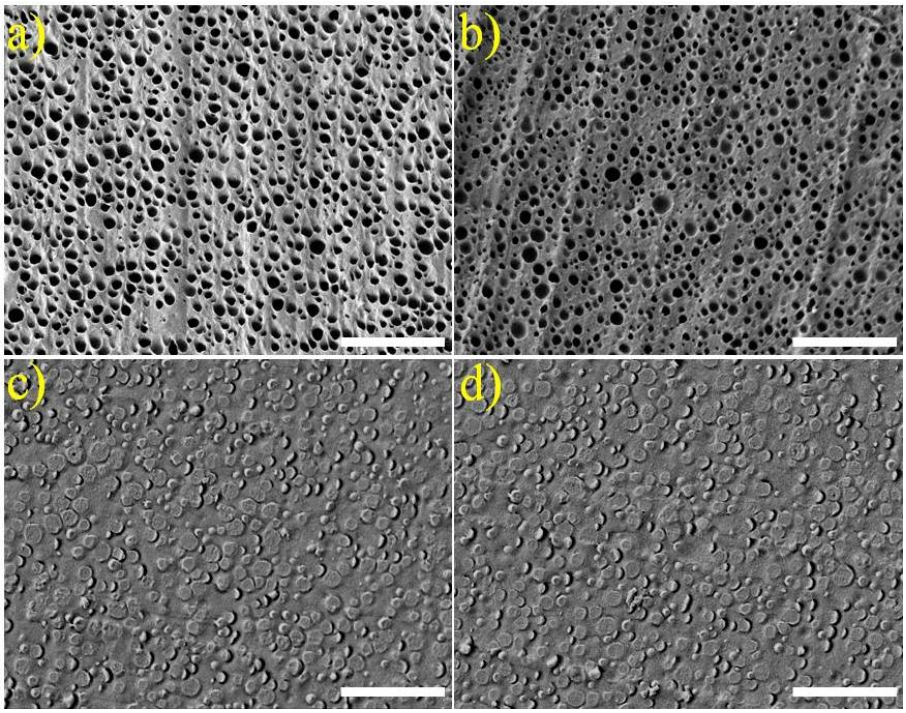

Figure 6.8. SEM images of PLA/PA11 30/70 blends with a) 0 wt% CNC, b) 3 wt% CNC and PLA/PA11 70/30 blends with c) 0 wt% CNC and d) 3 wt% CNC. The scale bars indicate 10 μm.

Previous studies from this laboratory [12] point to a high level of interfacial interactions between PLA and PA11. In the PLA/PA11/CNC system with a dispersed/phase morphology, it appears that the dispersed phase morphology is dominated by the high level of interactions between PLA and PA11 and any changes in the viscoelastic properties of the PA11 phase resulting from the addition of CNC particles have virtually no effect on the dispersed phase size at this level of coalescence.

Co-Continuous Morphology. Due to the interconnected nature of co-continuous systems, they are known to demonstrate the most severe levels of phase coalescence. In this case, the addition of even 1wt% of CNC particles to PLA/PA11 50/50 vol% blends in Figure 6.9 results in a much finer co-continuous network morphology. The pore size diameter of PLA/PA11 50/50 vol% substantially decreases from 13 to 3 μm in the presence of only 1wt% CNC particles located in the continuous PA11 phase. This is a very significant observation considering the very low concentration of CNC particles and the very fine network pore size diameter (only 3 μm).

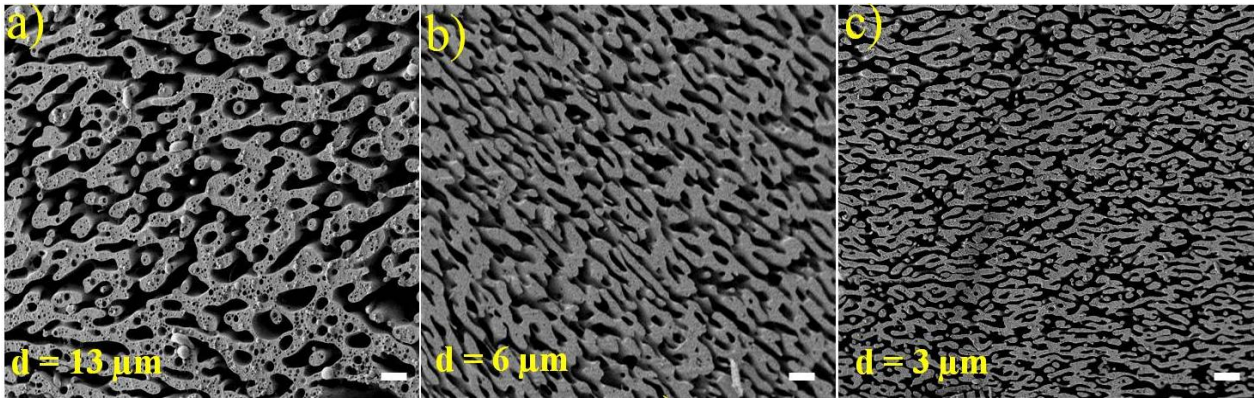

Figure 6.9. Morphology evolution of the PLA/PA11 50/50 vol% blend in the presence of CNC particles: a) 0 wt % CNC, b) 0.5 wt% CNC, c) 1wt% CNC. The scale bars indicate 10 μm and *d* is the pore diameter.

Annealing. Besides the finer morphology, the phase coarsening of the co-continuous PLA/PA11 50/50 vol% blend is diminished and morphological stability of the blends is improved in the presence of CNC particles. The coarsening behavior of the co-continuous PLA/PA11 blends without and with 1 wt% CNC under quiescent annealing at the processing temperature are shown in Figure 6.10. After 80 minutes of annealing, the pore size in the PLA/PA11 50/50 vol % blends without CNC particles increases from 13 to 46 μm while in the presence of only 1 wt% CNC the pore size increases from 3 to 10 μm.

Coalescence Reduction Mechanism for CNC in Co-Continuous PLA/PA11. Generally, solid inclusions influence the morphology of polymer blends by increasing the compatibility of blends components by localizing at the interface [45–47], through a solid barrier effect on coalescence [20,48,49] or by changing the viscoelastic properties [14,20,41,48]. In this study, the decrease in the pore size by the addition of CNC particles cannot be attributed to the enhanced compatibility

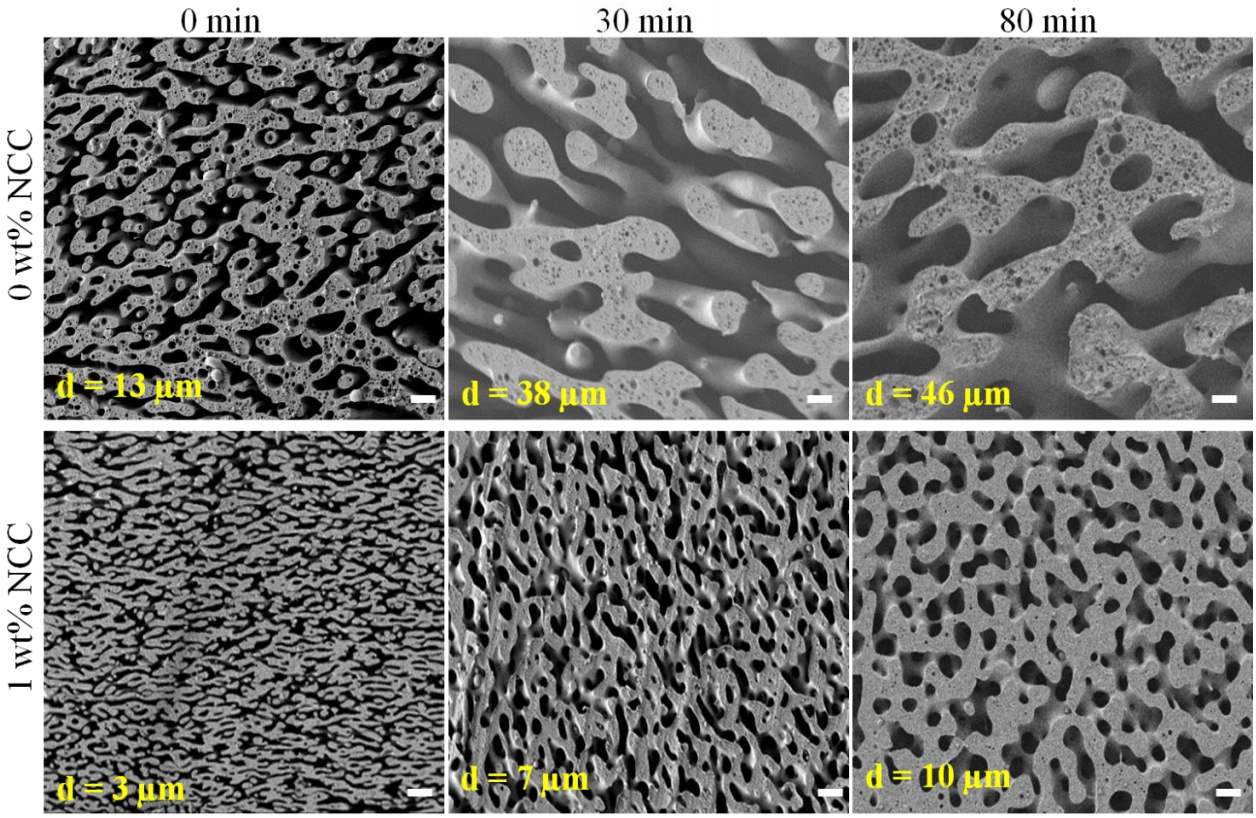

Figure 6.10. The effect of quiescent annealing at 200 ºC on the morphology of PLA/PA11 50/50 vol% co-continuous blend without and with CNC. The scale bars indicate 10 µm and *d* is the pore diameter.

between PLA and PA11 as AFM images reveal that CNC localizes in the PA11 phase and not at the interface. For the solid barrier effect, its influence on morphology is principally related to the fact that nanoparticles can act as physical barriers inhibiting the coalescence of the colliding droplets during melt processing. In that case, when the matrix containing nanoparticles tries to drain as droplets of the dispersed phase come together, the solid particles do not allow them to meet and the droplets recoil. This elastic recoil separates the dispersed droplets during the initial collision step and inhibits coalescence. However, diminished coalescence in the present work is only observed for co-continuous systems which are already fully interconnected, thus a barrier effect on matrix drainage cannot be an explanation for the observed effect. Furthermore, the localization of CNC is restricted to only one phase, PA11. For these reasons, we will focus the discussion related to the mechanism of co-continuous coalescence reduction on the viscoelastic mechanism.

Changes in the PA11 viscoelastic behavior resulting from the selective localization of CNC

particles are an important consideration. Due to their stiff nature, rod like shape, high specific surface area [50] of 150-200 m^2/g and high self-networking ability [51], well segregated CNC particles can easily form a 3D network structure at very low concentrations [28,51]. The percolation threshold is the concentration of nanoparticles above which the rheological properties of the nanocomposite increases exponentially [28]. This value can be measured by fitting the following power law function to the experimental data of the PA11 storage modulus (G') at the frequency of 0.1 rad/s, versus CNC content [28]:

$$G' = \beta_c G \left(\frac{m - m_c G}{m_c G}\right)^n \qquad \text{for} \quad m > m_c G \tag{6.7}$$

in which $\beta_c G$ and n are power law constants, m is the CNC content (wt%) and $m_c G$ is the percolation threshold. A value of 0.9 wt% is obtained for the PA11/CNC nanocomposites examined in this work. Kamal et al. [2,27] reported a rheological percolation threshold of 2.5 and 3 wt% for PP/CNC and PLA/CNC, respectively. The lower rheological percolation threshold in this study can be most likely related to high level of CNC dispersion and/or the higher interactions between PA11 and CNC as compared to those of PP/CNC and PLA/CNC systems. In fact CNC particles disperse into the PA11 phase very effectively creating a very high surface area interaction with PA11. Since PA11 and CNC have a very low interfacial tension of 1 mN/m (see Table 6.2), PA11 becomes highly immobilized at the nanoparticle surface. The dynamics of the PA11 chains is thus retarded by chain confinement between the nanoparticles resulting from PA11/CNC interactions. This immobilization is reflected in the retarded relaxation of CNC filled PA11 domains as shown in the storage modulus in Figure 6.5-b. It should be noted that since the CNC is exclusively localized within the PA11 phase, the effective concentration of CNC for a PLA/PA11 50/50 blend doubles. In other words, 1 wt% CNC in the blend actually represents 2 wt% CNC in the PA11 phase. An examination of 2 wt% CNC in PA11 shows a very strong retarded relaxation effect as evidenced by the plateau in the storage modulus in Figure 6.5-b. As was mentioned earlier, neat PA11 fully relaxes and approaches terminal behavior, while in the PA11/CNC nanocomposite the relaxation spectrum widens gradually with increasing CNC concentration which is an indication of a transition from liquid- to solid-like behavior (see Figure 6.5-b).

Figure 6.11 schematically illustrates the suppression effect of CNC particles on the coalescence of the co-continuous PLA/PA11 blend. For a co-continuous blend, coalescence occurs through

the retraction and break-up of elongated domains which is quite closely related to the dynamics of polymer chains. For pure PLA/PA11 blends due to the relatively high level dynamics of the PA11 chains, a quick retraction process of the elongated PA11 domains occurs. However, when well segregated CNC particles form an interconnected network structure in the PA11 phase, the dynamics of PA11 chains is dramatically delayed due to confinement between CNC particles, a high surface area of CNC particles and strong interactions between CNC and PA11. This makes it difficult for the elongated PA11 domains to relax and the retraction of elongated PA11, necessary for co-continuous coalescence, is inhibited. Due to the interconnected structure of the co-continuous morphology, the suppressed retraction of PA11 domains results in an overall suppression of phase coalescence.

Figure 6.11. Schematic illustrating the effect of the retarded relaxation of CNC filled PA11 domains, resulting from diminished dynamics of PA11 chain, on the coalescence of co-continuous PLA/PA11 blends.

Since it has been shown that phase growth during static annealing is directly related to the retraction of elongated domains followed by the coalescence of the retracted domains, diminished phase coarsening under quiescent annealing as is shown in Figure 6.10 is another indication of the suppressed coalescence and delayed relaxation of PA11 domain in the co-continuous PLA/PA11 blend in the presence of CNC particles.

6.5 Conclusion

A novel approach based on a combination of solvent dissolution, casting and melt mixing

process is used to incorporate cellulose nanocrystal (CNC) particles into an entirely bio-based PLA/PA11 blend. PLA/CNC or PA11/CNC mixtures with a solid homogeneous dispersion of CNC particles are first prepared by solvent dissolution followed by casting/evaporation. A high level of CNC dispersion in each polymer is confirmed with atomic force microscopy (AFM) and rheology analysis. CNC is then fed into the blends through the prepared PLA/CNC or PA11/CNC mixture in an internal mixer. AFM analysis demonstrates the selective localization of CNC particles with a thickness of 15-50 nm in the PA11 phase irrespective of whether the PLA/CNC or the PA11/CNC mixture is used. This indicates a strong affinity of the CNC particles for the PA11 phase. The CNC is shown to be located in the PA11 phase regardless of whether PA11 is the dispersed phase (PLA/PA11 70/30) or the matrix phase (PLA/PA11 30/70) or the system is co-continuous (PLA/PA11 50/50). This observation is in line with the prediction from the Young's model based on interfacial energy. The dispersed phase size in the PLA/PA11 30/70 and 70/30 vol% does not change even in the presence of 3 wt% CNC particles which is attributed to the low level of coalescence in these dispersed phase compositions resulting from the low interfacial tension between PLA and PA11. This result implies generally that nanoparticles have little influence on the dispersed phase/matrix morphology in low interfacial tension polymer blend systems. However, for co-continuous PLA/PA11 50/50 vol%, the addition of only 1 wt% of CNC particles results in a dramatic coalescence suppression effect with the co-continuous phase thickness dropping from 13 to 3 μm. This coalescence reduction effect is attributed to the delayed relaxation of the CNC filled PA11 domains as demonstrated in the rheology data.

6.6 Acknowledgements

The authors would like to gratefully acknowledge the NSERC Network for Innovative Plastic Materials and Manufacturing Processes (NIPMMP) for supporting this project.

6.7 References

[1] T. Li, J. Zhang, D.K. Schneiderman, L.F. Francis, F.S. Bates, Toughening Glassy Poly(lactide) with Block Copolymer Micelles, ACS Macro Lett. 5 (2016) 359–364.

[2] M.R. Kamal, V. Khoshkava, Effect of cellulose nanocrystals (CNC) on rheological and mechanical properties and crystallization behavior of PLA/CNC nanocomposites,

Carbohydr. Polym. 123 (2015) 105–114.

[3] N. Bitinis, E. Fortunati, R. Verdejo, J. Bras, J.M. Kenny, L. Torre, M.A. López-Manchado, Poly(lactic acid)/natural rubber/cellulose nanocrystal bionanocomposites. Part II: properties evaluation., Carbohydr. Polym. 96 (2013) 621–7.

[4] Y. Xu, P. Delgado, A.D. Todd, J. Loi, S.A. Saba, R.J. McEneany, T. Tower, V. Topolkaraev, C.W. Macosko, M.A. Hillmyer, Lightweight micro-cellular plastics from polylactide/polyolefin hybrids, Polymer. 102 (2016) 73–83.

[5] A.M. Zolali, V. Heshmati, B.D. Favis, Ultratough Co-Continuous PLA/PA11 by Interfacially Percolated Polyether-b-amide, Macromolecules. 50 (2016) 264–274.

[6] M.P. Arrieta, E. Fortunati, F. Dominici, E. Rayón, J. López, J.M. Kenny, Multifunctional PLA–PHB/cellulose nanocrystal films: Processing, structural and thermal properties, Carbohydr. Polym. 107 (2014) 16–24.

[7] K. Anderson, K. Schreck, M. Hillmyer, Toughening Polylactide, Polym. Rev. 48 (2008) 85–108.

[8] K. Hashima, S. Nishitsuji, T. Inoue, Structure-properties of super-tough PLA alloy with excellent heat resistance, Polymer. 51 (2010) 3934–3939.

[9] K.S. Anderson, M.A. Hillmyer, The influence of block copolymer microstructure on the toughness of compatibilized polylactide/polyethylene blends, Polymer. 45 (2004) 8809–8823.

[10] T.D. Fornes, D.R. Paul, Structure and Properties of Nanocomposites Based on Nylon-11 and -12 Compared with Those Based on Nylon-6, Macromolecules. 37 (2004) 7698–7709.

[11] G. Stoclet, R. Seguela, J.-M. Lefebvre, Morphology, thermal behavior and mechanical properties of binary blends of compatible biosourced polymers: Polylactide/polyamide11, Polymer. 52 (2011) 1417–1425.

[12] V. Heshmati, A.M. Zolali, B.D. Favis, Morphology Development in Poly (Lactic Acid)/ Polyamide11 Biobased Blends: Chain Mobility and Interfacial Interactions, (2017) Submitted to “ Polymer” for publication.

[13] A. Nuzzo, S. Coiai, S.C. Carroccio, N.T. Dintcheva, C. Gambarotti, G. Filippone, Heat-Resistant Fully Bio-Based Nanocomposite Blends Based on Poly(lactic acid), Macromol. Mater. Eng. 299 (2014) 31–40.

[14] A. Nuzzo, E. Bilotti, T. Peijs, D. Acierno, G. Filippone, Nanoparticle-induced co-

continuity in immiscible polymer blends – A comparative study on bio-based PLA-PA11 blends filled with organoclay, sepiolite, and carbon nanotubes, Polymer. 55 (2014) 1–12.

[15] A. Taghizadeh, B.D. Favis, Carbon nanotubes in blends of polycaprolactone/thermoplastic starch., Carbohydr. Polym. 98 (2013) 189–98.

[16] E. Jalali Dil, B.D. Favis, Localization of micro- and nano-silica particles in heterophase poly(lactic acid)/poly(butylene adipate-co-terephthalate) blends, Polymer. 76 (2015) 295–306.

[17] A. Göldel, A. Marmur, G.R. Kasaliwal, P. Pötschke, G. Heinrich, Shape-Dependent Localization of Carbon Nanotubes and Carbon Black in an Immiscible Polymer Blend during Melt Mixing, Macromolecules. 44 (2011) 6094–6102.

[18] L. As'habi, S.H. Jafari, B. Baghaei, H.A. Khonakdar, P. Pötschke, F. Böhme, Structural analysis of multicomponent nanoclay-containing polymer blends through simple model systems, Polymer. 49 (2008) 2119–2126.

[19] M. Zhang, Y. Huang, M. Kong, H. Zhu, G. Chen, Q. Yang, Morphology and rheology of poly(l-lactide)/polystyrene blends filled with silica nanoparticles, J. Mater. Sci. 47 (2012) 1339–1347.

[20] G. Filippone, N.T. Dintcheva, F.P. La Mantia, D. Acierno, Using organoclay to promote morphology refinement and co-continuity in high-density polyethylene/polyamide 6 blends – Effect of filler content and polymer matrix composition, Polymer. 51 (2010) 3956–3965.

[21] S.H. Lee, M. Kontopoulou, C.B. Park, Effect of nanosilica on the co-continuous morphology of polypropylene/polyolefin elastomer blends, Polymer. 51 (2010) 1147–1155.

[22] M.A.S. Azizi Samir, F. Alloin, A. Dufresne, Review of Recent Research into Cellulosic Whiskers, Their Properties and Their Application in Nanocomposite Field, Biomacromolecules. 6 (2005) 612–626.

[23] S.J. Eichhorn, Cellulose nanowhiskers: promising materials for advanced applications, Soft Matter. 7 (2011) 303–315.

[24] K. Ben Azouz, E.C. Ramires, W. Van den Fonteyne, N. El Kissi, A. Dufresne, Simple Method for the Melt Extrusion of a Cellulose Nanocrystal Reinforced Hydrophobic Polymer, ACS Macro Lett. 1 (2012) 236–240.

[25] V. Khoshkava, M.R. Kamal, Effect of surface energy on dispersion and mechanical properties of polymer/nanocrystalline cellulose nanocomposites., Biomacromolecules. 14 (2013) 3155–63.

[26] I. Kvien, B.S. Tanem, K. Oksman, Characterization of cellulose whiskers and their nanocomposites by atomic force and electron microscopy, Biomacromolecules. 6 (2005) 3160–3165.

[27] V. Khoshkava, M.R. Kamal, Effect of Cellulose Nanocrystals (CNC) Particle Morphology on Dispersion and Rheological and Mechanical Properties of Polypropylene/CNC Nanocomposites, ACS Appl. Mater. Interfaces. 6 (2014) 8146–8157.

[28] D. Bagheriasl, P.J. Carreau, B. Riedl, C. Dubois, W.Y. Hamad, Shear rheology of polylactide (PLA)–cellulose nanocrystal (CNC) nanocomposites, Cellulose. 23 (2016) 1–13.

[29] D. Bagheriasl, P.J. Carreau, C. Dubois, B. Riedl, Properties of polypropylene and polypropylene/poly(ethylene-co-vinyl alcohol) blend/CNC nanocomposites, Compos. Sci. Technol. 117 (2015) 357–363.

[30] R. Nasseri, N. Mohammadi, Starch-based nanocomposites: A comparative performance study of cellulose whiskers and starch nanoparticles, Carbohydr. Polym. 106 (2014) 432–439.

[31] N. Bitinis, R. Verdejo, J. Bras, E. Fortunati, J.M. Kenny, L. Torre, M.A. López-Manchado, Poly(lactic acid)/natural rubber/cellulose nanocrystal bionanocomposites Part I. Processing and morphology, Carbohydr. Polym. 96 (2013) 611–620.

[32] S.J. Eichhorn, A. Dufresne, M. Aranguren, N.E. Marcovich, J.R. Capadona, S.J. Rowan, C. Weder, W. Thielemans, M. Roman, S. Renneckar, W. Gindl, S. Veigel, J. Keckes, H. Yano, K. Abe, M. Nogi, A.N. Nakagaito, A. Mangalam, J. Simonsen, A.S. Benight, A. Bismarck, L.A. Berglund, T. Peijs, Review: current international research into cellulose nanofibres and nanocomposites, J. Mater. Sci. 45 (2010) 1–33.

[33] M. Mariano, N. El Kissi, A. Dufresne, Cellulose nanocrystals and related nanocomposites: Review of some properties and challenges, J. Polym. Sci. Part B Polym. Phys. 52 (2014) 791–806.

[34] D.Y. Kwok, A.W. Neumann, Contact angle measurement and contact angle interpretation, Adv. Colloid Interface Sci. 81 (1999) 167–249.

[35] A.-L. Esquirol, P. Sarazin, N. Virgilio, Tunable Porous Hydrogels from Cocontinuous Polymer Blends, Macromolecules. 47 (2014) 3068–3075.

[36] A.-C. Baudouin, J. Devaux, C. Bailly, Localization of carbon nanotubes at the interface in blends of polyamide and ethylene–acrylate copolymer, Polymer. 51 (2010) 1341–1354.

[37] N. Lin, J. Huang, P.R. Chang, J. Feng, J. Yu, Surface acetylation of cellulose nanocrystal and its reinforcing function in poly(lactic acid), Carbohydr. Polym. 83 (2011) 1834–1842.

[38] T. a. Dankovich, D.G. Gray, Contact Angle Measurements on Smooth Nanocrystalline Cellulose (I) Thin Films, J. Adhes. Sci. Technol. 25 (2011) 699–708.

[39] A. Arias, M.C. Heuzey, M.A. Huneault, G. Ausias, A. Bendahou, Enhanced dispersion of cellulose nanocrystals in melt-processed polylactide-based nanocomposites, Cellulose. 22 (2015) 483–498.

[40] P. Cassagnau, Melt rheology of organoclay and fumed silica nanocomposites, Polymer. 49 (2008) 2183–2196.

[41] F. Fenouillot, P. Cassagnau, J.C. Majesté, Uneven distribution of nanoparticles in immiscible fluids: Morphology development in polymer blends, Polymer. 50 (2009) 1333–1350.

[42] H. Sojoudiasli, M.-C. Heuzey, P.J. Carreau, Rheological, morphological and mechanical properties of flax fiber polypropylene composites: influence of compatibilizers, Cellulose. 21 (2014) 3797–3812.

[43] C. Xu, J. Chen, D. Wu, Y. Chen, Q. Lv, M. Wang, Polylactide/acetylated nanocrystalline cellulose composites prepared by a continuous route: A phase interface-property relation study, Carbohydr. Polym. 146 (2016) 58–66.

[44] G. Wildes, H. Keskkula, D.R. Paul, Morphology of PC/SAN blends: effect of reactive compatibilization, SAN concentration, processing, and viscosity ratio, J. Polym. Sci. Part B Polym. Phys. 37 (1999) 71–82.

[45] M. Si, T. Araki, H. Ade, A.L.D. Kilcoyne, R. Fisher, J.C. Sokolov, M.H. Rafailovich, Compatibilizing Bulk Polymer Blends by Using Organoclays, Macromolecules. 39 (2006) 4793–4801.

[46] L. Elias, F. Fenouillot, J.C. Majesté, P. Alcouffe, P. Cassagnau, Immiscible polymer blends stabilized with nano-silica particles: Rheology and effective interfacial tension, Polymer. 49 (2008) 4378–4385.

[47] L. Elias, F. Fenouillot, J.C. Majeste, P. Cassagnau, Morphology and rheology of immiscible polymer blends filled with silica nanoparticles, Polymer. 48 (2007) 6029–6040.

[48] G. Filippone, N.T. Dintcheva, D. Acierno, F.P. La Mantia, The role of organoclay in promoting co-continuous morphology in high-density poly(ethylene)/poly(amide) 6 blends, Polymer. 49 (2008) 1312–1322.

[49] Y. Li, H. Shimizu, Novel morphologies of poly(phenylene oxide) (PPO)/polyamide 6 (PA6) blend nanocomposites, Polymer. 45 (2004) 7381–7388.

[50] L. Pranger, R. Tannenbaum, Biobased Nanocomposites Prepared by In Situ Polymerization of Furfuryl Alcohol with Cellulose Whiskers or Montmorillonite Clay, Macromolecules. 41 (2008) 8682–8687.

[51] V. Favier, H. Chanzy, J.Y. Cavaille, Polymer Nanocomposites Reinforced by Cellulose Whiskers, Macromolecules. 28 (1995) 6365–6367.

CHAPTER 7 ARTICLE 4: TUNING THE LOCALIZATION OF FINELY DISPERSED CELLULOSE NANOCRYSTAL IN POLY (LACTIC ACID)/BIO-POLYAMIDE11 BLENDS[4]

Vahid Heshmati[a], Musa R. Kamal[b] and Basil D. Favis[a]

a. CREPEC, Dept of Chemical Engineering, École Polytechnique de Montréal, Montreal, Canada

b. CREPEC, Dept of Chemical Engineering, McGill university, Montreal, Canada

7.1 Abstract

In this study, for the first time, a versatile approach to control the stable localization of finely dispersed cellulose nanocrystal (CNC) in the PLA phase in melt mixed poly (lactic acid) (PLA)/bio-polyamide11 (PA11) blends is presented. A novel approach combining high pressure homogenization and freeze-drying is employed in order to prepare poly (ethylene oxide) (PEO)/CNC mixture with a high level of CNC dispersion. The prepared PEO/CNC mixture is then incorporated into the PLA/PA11 blends using two different processing strategies. Atomic force microscopy (AFM) demonstrates that individually dispersed, non-agglomerated, CNCs with a thickness of 10-20 nm are obtained in the PEO, PLA-PEO and (PLA-PEO)/PA11 blends. Typically for CNC/PLA/PA11 the CNC particles selectively localize in the PA11 phase. However, when the CNC particles are coated with PEO, SEM and AFM analysis unambiguously show that the CNC particles almost exclusively segregate into the PLA phase irrespective of whether the PEO/CNC mixture is premixed with PLA or PA11. It is suggested that a strong interaction between PEO and CNC particles combined with the PLA/PEO miscibility facilitates the localization of PEO-coated CNC in the PLA phase. The localization of PEO-coated CNC in the PLA phase has no effect on the morphology of the PLA-5PEO/PA11 blend when it is in a matrix/dispersed phase form. However, the presence of 1 wt % PEO-coated CNC in the co-continuous (PLA-5PEO)/PA11 50/50 vol% blend diminishes the phase thickness from 11 to 7 μm. This is attributed to a retarded relaxation phenomena for the PLA phase. The degree of

[4] Submitted to J. Polym. Sci. B Polym. Phys

coalescence reduction is directly attributed to the rheological percolation threshold value and the onset of CNC network formation within the given phase. This work outlines a strategy for the control of the localization of individually dispersed CNC particles in the PLA phase in PLA/PA11 blends.

7.2 Introduction

The development of bio-based polymeric materials as a replacement for commodity plastics has gathered significant interest in recent years [1,2]. Furthermore, there is definite need to develop biobased materials for high performance applications. Poly(lactic acid) (PLA) is a promising biobased polymer with high tensile strength and modulus [3–5]. It suffers, however, from an inherent brittleness [4,6]. Different strategies for improving PLA properties such as plasticization, copolymerization and polymer blending have been employed in the literature [4,7–9]. The blending of PLA with other bioplastics is a strategy that allows for the tuning of the mechanical properties while still maintaining a bioproduct [10].

Polyamide11 (PA11), is a high-performance bio-polymer with high impact strength and elongation at break [11]. Since PA11 has highly complementary properties to PLA, a PLA/PA11 blend has the potential to generate a new bio-material with unique advantages [11,12]. In previous works [6,13] it was shown that controlled PLA chain mobility through the addition of an optimal amount of PEO plasticizer leads to significant enhancement in the impact strength and elongation at break of the blend. However, a drop in the modulus and tensile strength compared to neat PLA was observed. Developing an approach to selectively improve the stiffness of PLA in the (PLA-PEO)/PA11 system would be very beneficial.

The incorporation of solid nanoinclusions within polymer blends has been considered as a route towards improving the toughness/stiffness balance[5,14]. However, the effect on blend properties is significantly related to the localization of nanoparticles in one of the two phases or at the interface [15]. Controlling the stable localization of nanoparticles is very essential in achieving the desired properties. Gultner et al.[16] showed that CNTs are selectively located in the PC phase in PC/SAN blends while after addition of N-phenylmaleimide styrene maleic anhydride (N-PSMA), all the nanoparticles are found in the miscible SAN/N-PSMA phase. This was attributed to the strong interaction between N-PSMA and CNTs and miscibility of N-PSMA with SAN. Li et al. [17] studied the effect of PP-g-maleic anhydride (PP-g-MA) on the

localization of Tio_2 nanoparticles in PP/PET blends. Their theoretical analysis predicted the stable localization of Tio_2 in the PET phase in PP/PET blends without PP-g-MA. However, in the presence of PP-g-MA, the preferred localization of Tio_2 particles was found in the PP phase which was attributed to the adsorption of PP-g-MA on the Tio_2 surface. The stable localization of nanoparticles in PLA, in particular, could present a number of advantages such as higher levels of crystallization resulting in enhanced thermomechanical (e.g. heat deflection temperature) and barrier properties [18].

Among nanoparticles generally, cellulose nanocrystal (CNC) is known for its superior mechanical properties, low cost, low density, abundance and renewability and is a promising candidate for generating new materials [19–21]. In recent years numerous studies have been undertaken to prepare CNC nanocomposites employing melt mixing, solvent casting or a combination of both [2,22–26]. Only a very few studies, however, have been conducted so far on the incorporation of CNCs into heterophase polymer-polymer systems [1,10]. Bitinis et al. [1] studied the localization of CNC particles in PLA/natural rubber (NR) blends. They showed that CNC particles were selectively located in the PLA phase. In another study addition of CNC particles enhanced the thermal stability and processability of PLA/PHB blends [10].

The main challenge associated with polymer/CNC systems is related to the highly hydrophilic character of CNC particles which limits its dispersion in non-polar polymer matrices [19,27,28]. However, a proper level of dispersion of CNC particles in water-soluble polymers such as polyethylene oxide (PEO) and polyvinyl alcohol (PVOH) through the casting/evaporation method has been reported [28–30]. Incorporating CNC particles into melt processed thermoplastics through a carrier mixture, prepared by the casting/evaporation of water-soluble polymers, is a versatile processing approach [21,28,31,32]. Bondeson et al.[31] used a PVOH/CNC mixture to add CNC particles to a PLA matrix prepared by melt mixing. They achieved a reasonable level of dispersion of agglomerated CNC in PVOH, but were not able to disperse CNC in PLA due to the immiscibility of PLA and PVOH. Jiang et al. [33] added CNC particles into a PHBV matrix in a twin-screw extruder by using PEO as the CNC carrier. A high level of CNC agglomeration, however, was observed.

The objectives of this work are to develop a strategy to generate finely dispersed cellulose nanocrystal (CNC) in PLA/PA11 bio-blends through melt mixing and to control the localization

of the CNC in the blend. Both matrix/dispersed phase and co-continuous morphologies will be examined. Special attention will be given to examine the effect of CNC localization on the blend morphology.

7.3 Experimental Section

7.3.1 Materials and Formulations

PA11 (Rilsan BMNO TL) with M_n = 12000 and M_w = 25000 and PLA 3001D with 1.8%-D isomer, M_n = 72000 and M_w = 142000 were obtained from Arkema and Natureworks, respectively. Poly(ethylene) oxide (PEO) water-soluble polymer (POLYOX™ WSR-N10) with molecular weight of 10^5 g/mol was produced by Dow. PLA and PA11 materials were dried at 70 °C and PEO was dried at 40 °C under vacuum for 48 h before use. Spray dried CNC particles were obtained from Alberta Innovates Technology Futures. As received spray dried CNC powder consists of highly agglomerated particles with a size distribution of between 5 to 25 µm.
In all the studied samples, the composition of PLA and PA11 are reported as parts based on volume. Since PLA/PEO miscibility is composition dependent, the PEO content in PLA was maintained at 5 volumetric parts based on the PLA. Since PLA and PEO are miscible at this composition, (PLA-5PEO) is shown as one single phase in all the studied systems. CNC content (wt%) is expressed based on the total weight of the blend for all the studied systems. Hence 1% CNC in (PLA-5PEO)/PA11 50/50 indicates 50 volumetric parts of (PLA-PEO), 50 volumetric parts PA11, 5 volumetric parts of PEO based on PLA and 1 weight percent of CNC based on the total weight of all the components.

7.3.2 Rheology

All the rheological characterization was performed in a constant stress rheometer (Physica MCR 301, Anton Paar) with a parallel plate geometry (a 1mm gap and a 25 mm plate diameter). A Carver hydraulic press, under a nitrogen atmosphere, was used to prepare disk samples of 1 mm thickness and 25 mm diameter. A pressure of 300 kPa was applied and the temperature was set at 200 °C. PLA composites with PEO-coated CNC particles and PEO/CNC nanocomposites were dried at 70 °C and 40 °C under vacuum for 48 h before the compression molding or the rheological test.

7.3.3 PEO/CNC Mixture Preparation

PEO/CNC mixture used in the study was prepared using a new approach. A three-step strategy was followed to homogenously disperse individual CNC particles in the PEO. In the first step, aqueous suspensions of CNC particles with different concentrations of CNCs were prepared. A PEO solution in water with the desired concentrations was then added to the CNC aqueous suspensions and stirred for two hours. In the second step, the prepared PEO/CNC mixture was homogenized by a series of successive passes through a laboratory high pressure homogenizer (EmulsiFlex-C3, Avestin) operated at 500 bars and at room temperature to obtain well dispersed CNC suspensions in the PEO solution. In the final step, the prepared PEO/CNC suspension was frozen rapidly in liquid nitrogen and PEO/CNC mixture was subsequently obtained by freeze-drying for 72h at -50 °C. It is important to note that the casting/evaporation of aqueous CNC/PEO suspensions at room temperature results in a high level of CNC aggregation. The major advantage of freeze-drying is to prevent CNC agglomeration as water is removed. It guarantees a homogeneous dispersion of CNC particles in the PEO matrix. Throughout this paper, CNC particles prepared with the PEO/CNC mixture are called "PEO-coated-CNC".

7.3.4 Preparation of PLA/CNC and PLA/PA11/CNC Systems

In order to prepare PLA nanocomposites containing PEO-coated CNC, PLA and PEO/CNC mixture were melt mixed in an internal mixer (Plasti-Corder, Brabender, with a total volume of 30 ml). The processing temperature and rotor speed were fixed at 200 °C and 50 rpm, respectively. Two different mixing strategies were employed for the preparation of ternary PLA/PA11/CNC multiphase systems. In procedure 1, the PEO/CNC mixture was first melt mixed with PLA in an internal mixer and PA11 was then added to the blend. In procedure 2, the PEO/CNC mixture was first melt mixed with PA11 and PLA was then added into the internal mixer. Using the same processing conditions as mentioned above, three different compositions of (PLA-PEO)/PA11, i.e. 30/70, 50/50 and 70/30 vol% with different CNC concentrations (wt%) were prepared.

7.3.5 Microtomy and Scanning Electron Microscopy (SEM)

In order to analyze the dispersion quality of CNC particles in the PEO/CNC mixture, a thin film of the PEO/CNC mixture was prepared with a hot press. A small section of the prepared film (3 cm*1 cm) was cut and imbedded in an epoxy mold. The PEO/CNC embedded film, as-prepared PLA and PLA/PA11 blends containing different content of PEO-coated CNC particles were cut

and then microtomed using a microtome (Leica-Jung RM 2065) equipped with a glass knife and a liquid nitrogen cryo-chamber. A gold coated layer of 15 nm thickness was then applied on the samples. Morphology characterization was carried out on a field emission scanning electron microscope (FESEM) (JSM 7600F, JEOL) at a voltage of 5kV. In order to analyze the dispersion of CNC particles in aqueous suspension, a droplet of the CNC aqueous suspension was dried on a carbon tape surface (on a copper substrate) prior to SEM examination.

7.3.6 Atomic Force Microscopy (AFM)

For the AFM analysis, microtoming and surface preparation was performed according to the same protocol reported for the previous section. The prepared plane surface was directly characterized by AFM (MultiMode Nanoscope IIIa with extender, Digital instrument, Santa Barbara, CA) without any additional preparation. Silicon tips (ACTA-W AppNano) with a 10 nm radius were used. In order to characterize the CNC particles, a droplet of the CNC aqueous suspension was dried on a mica surface prior to AFM analysis. The films were examined directly very shortly after water elimination.

7.3.7 Image Analysis

The volume average diameter, d_v, and the number average diameter, d_n, of the dispersed phase and the specific interfacial area of the PLA/PA11 50/50 vol% blends containing different PEO-coated CNC contents were measured with an image analyzer (SigmaScan Pro.V.5) equipped with a digitizing table (Wacom). The specific interfacial area, S, of the co-continuous PLA/PA11 50/50 vol% blends was estimated using the following equation [34]:

$$S = P / A \tag{7.1}$$

in which A is the area of the examined image and P is the interfacial perimeter of the PLA/PA11 interface. The pore diameter was then calculated using equation 7.2:

$$d = 4\emptyset_p / S \tag{7.2}$$

in which *d* is the pore diameter, $\emptyset_p$ is the porous volume fraction and *S* is the specific interfacial area.

7.4 Results and discussion

7.4.1 High Pressure Homogenization (HPH) of CNC Aqueous Suspension

A high level of dispersion of CNC particles in water soluble polymers such as PEO requires the

homogenization of a concentrated CNC aqueous-suspension which is found to be problematic. We found that although sonication has been widely used in dispersing different nanoparticles in polymers [15,35], it significantly degrades CNC particles. High pressure homogenization (HPH) is an innovative method for achieving a highly stable nano-emulsions or nano-dispersions [36]. HPH has also been employed in cellulose microfibril preparation [37–39]. However, to the best of our knowledge no studies has utilized the HPH approach for the dispersion of CNC particles in hydrophobic polymer matrices. This technique can effectively break down CNC agglomerates without any CNC degradation as compared to the sonication method. Figure 7.1 shows the

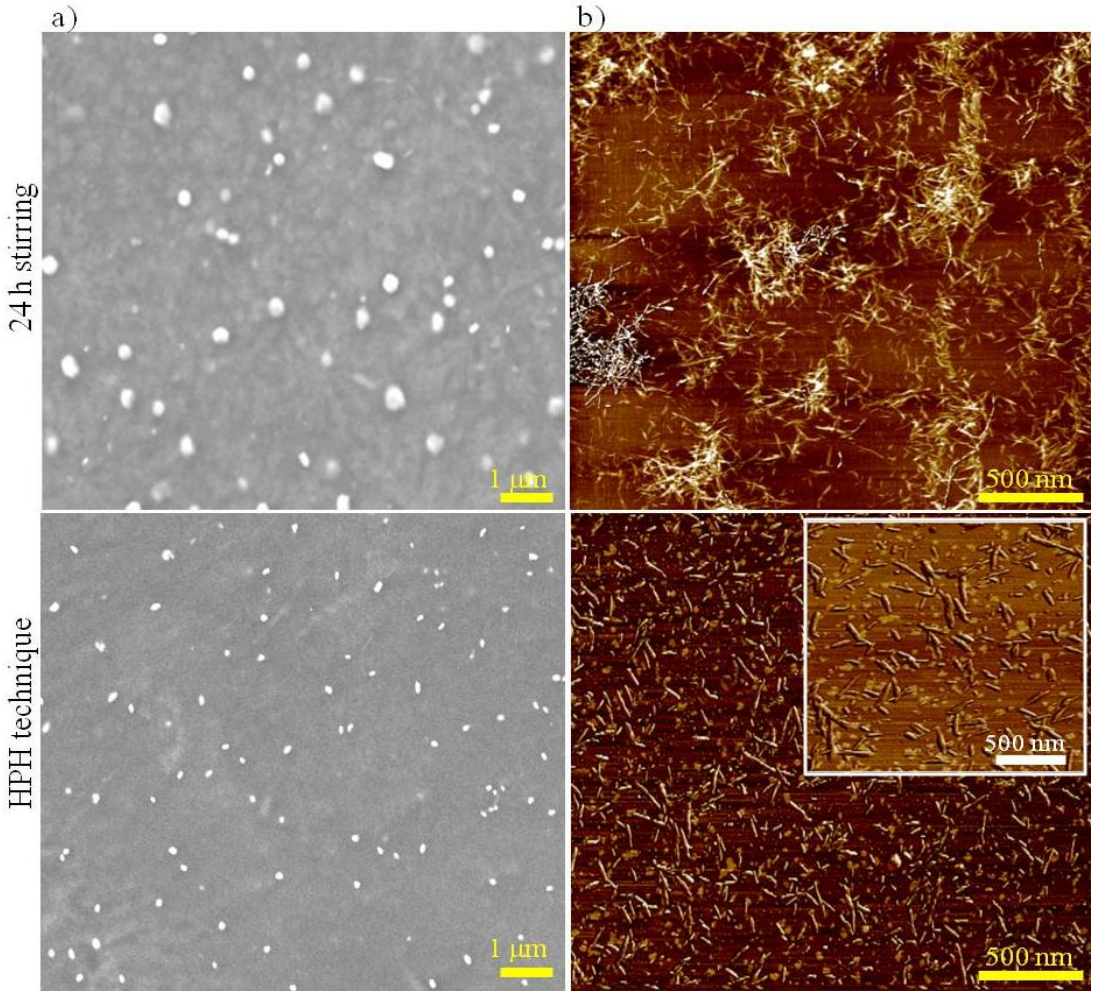

Figure 7.1. CNC dispersion in an aqueous suspension prepared with 24 h magnetic stirring compared to the high pressure homogenization (HPH) technique: a) SEM images of a dried drop of the suspensions deposited on a carbon tape very shortly after water elimination and b) AFM micrographs of a dried drop of the suspensions deposited on a mica surface very shortly after water evaporation.

dispersion quality of a 2 wt% CNC aqueous suspension prepared by 24 h magnetic stirring as compared with the HPH technique. SEM micrographs of a dried drop of CNC aqueous suspensions deposited over a carbon tape are shown in Figure 7.1-a. Clearly CNC particles obtained after high pressure homogenization have a much smaller size as compared to those prepared by magnetic stirring. AFM micrographs of a dried drop of CNC aqueous suspensions on a mica surface in Figure 7.1-b show that in the suspension prepared by stirring, CNC particles form large agglomerates with a size of 300-500 nm. In the suspensions prepared by the high pressure homogenization process, however, individual cellulose nanocrystals are evident. Analysis of the shape and size of the individual CNC particles prepared by the HPH process was carried out by AFM phase and the height topography demonstrates a rod-shape structure with an average length of 190 ± 45 nm based on 200 measurements. CNC particle thickness is considered as the height difference between the mica surface and the particles which is 15 ± 5 nm. The HPH process is thus highly effective in deagglomerating CNC particles.

7.4.2 CNC Dispersion in PEO

FESEM micrographs of the PEO/CNC mixture containing 2 wt% CNC prepared by the HPH/freeze drying technique are presented in Figure 7.2-a. A homogeneous CNC dispersion of CNC particles in the PEO matrix is observed. CNC appears as white dots in the SEM image which correlates to the transverse section of the CNC particles. The AFM analysis of the bulk of

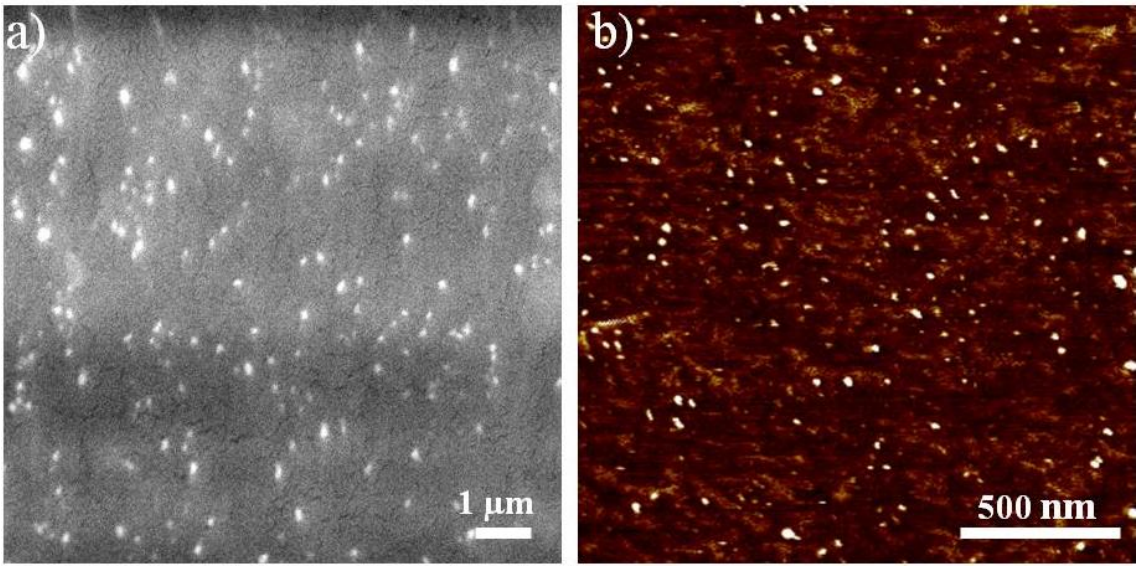

Figure 7.2. a) SEM image and b) AFM phase topography of PEO/2 wt% CNC nanocomposites.

the PEO/CNC film prepared with a cryo-microtome provides more detailed information of the CNC dispersion in PEO as is shown in Figure 7.2-b. The observation of CNC as dots in the blend system as observed by SEM and AFM is expected since the samples are microtomed to a plane face prior to microscopic observation. All CNC rod orientations, except that perfectly parallel to the surface, would be expected to present as circles or as slightly deformed ellipsoids at the surface. However, it should also be noted that some CNC particles can be seen to partially protrude from the surface in the AFM micrograph. In the cases where CNC particles are encapsulated with PEO, this protrusion from the surface is due to the difficulty of the knife to cut through soft PEO during microtoming. A homogenous nanoscale dispersion of CNC in the PEO matrix was obtained. The thickness of the CNC particles based on the AFM phase images ranges from 10 to 20 nm which is in the same range as the individual CNC particles.

In order to evaluate the efficacy of the HPH/freeze drying process in the dispersion of CNC particles in the PEO matrix, rheological characterization was also carried out. Figure 7.3 shows the viscoelastic properties of PEO and PEO/CNC nanocomposites with different CNC content. The complex viscosity (η*) versus angular frequency (ω) of PEO exhibits shear thinning behavior with a short plateau at low frequencies as shown in Figure 7.3-a. The addition of CNC

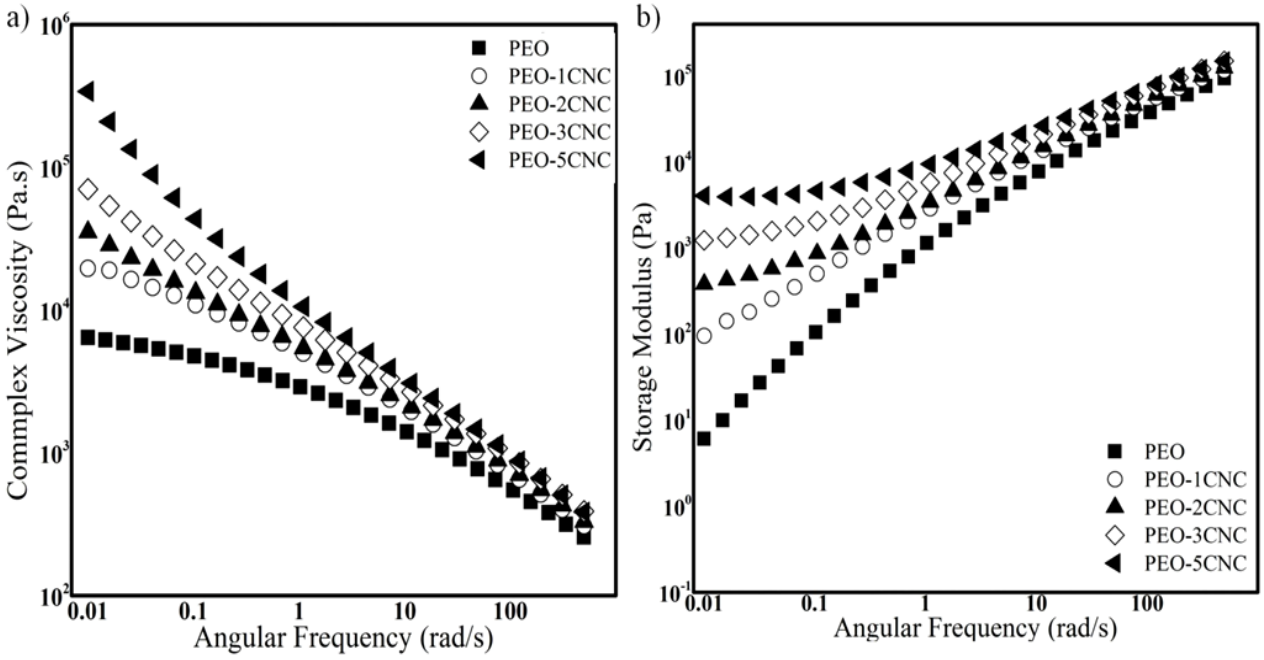

Figure 7.3. a) Complex viscosity (η^*) and b) Storage modulus (G') versus angular frequency (ω) for PEO and PEO/CNC nanocomposites.

particles results in an increase in the complex viscosity of the PEO/CNC nanocomposites with a significant shear thinning behavior at CNC concentrations of 2 wt% or greater. Moreover, as is shown in Figure 7.3-b, while neat PEO shows a non-terminal behavior at low frequencies, the storage modulus (G') versus frequency (ω) of the PEO/CNC nanocomposites increases gradually and becomes less dependent on shear rate at CNC concentrations of 2 wt% or greater. These observations indicate a transition from liquid- to gel-like behavior for PEO/CNC nanocomposites at high CNC concentrations due to the formation of a space-spanning CNC-network in the PEO matrix resulting from the good quality of CNC dispersion [2,23]. This is another indication of the efficacy of the HPH technique in attaining a high level of CNC dispersion in water soluble polymers such as PEO.

7.4.3 Dispersion of PEO-coated CNC particles in PLA

In a previous work [40], it has been shown that direct melt processing is not effective in achieving the de-agglomeration of hydrophilic CNC in hydrophobic PLA. Since PEO possesses hydrophobic and hydrophilic moieties, it has been used as a compatibilizing agent for melt mixed polymer nanocomposites [32,41,42]. An interesting approach would be to coat the CNC with PEO prior to mixing with PLA. Furthermore, in another work from this laboratory, it has been shown that PEO has a substantial effect on the interfacial tension, morphology and mechanical properties of PLA/PA11 blends when PEO and PLA are in the concentration range for miscibility. In order to maintain miscibility with PLA, throughout this study, the PEO concentration is maintained at 5 vol% of the PLA phase. Also, as PEO and PLA are miscible at 5 vol% PEO, (PLA-5PEO) is shown as one single phase in all the studied nanocomposites.

The effect of the CNC concentration on the quality of the dispersion of CNC in the PLA-5PEO matrix is studied by SEM and AFM. SEM and AFM phase topography of the (PLA-5PEO)/2wt% CNC system prepared by the combined (HPH-freeze drying)/melt mixing method are presented in Figure 7.4. In the SEM image, CNC particles are clearly seen as white dots. Some of the PEO-coated CNC particles can also be seen to protrude from the surface of the sample in the AFM micrograph. As discussed earlier, this is due to the difficulty of the knife to cut through the soft PEO phase during microtoming. Interestingly, this effect serves to even more easily identify the CNC particles and also highlights the high level of individual CNC dispersion. Individual CNC particles with a thickness of 10-20 nm, similar to those observed in Figure 7.1,

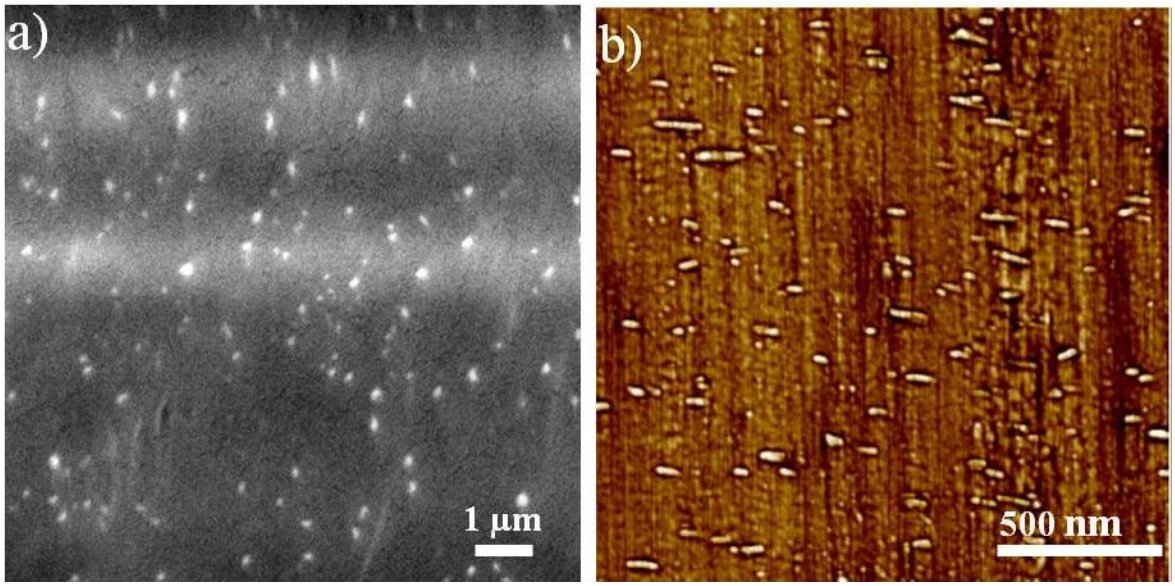

Figure 7.4. a) SEM and b) AFM phase micrographs of (PLA-5PEO)/2 wt% CNC. Some PEO coated CNC particles can be seen to protrude from the surface in the AFM micrograph.

can be easily identified in the AFM micrograph. This is an indication that coating CNC with PEO promotes interactions between PLA and CNC which leads to a high level of CNC dispersion. It has to be noted that increasing the CNC content to 5% does not affect the quality of the CNC dispersion (not shown here). Individual CNC dispersion in a melt mixed polymer matrix has rarely been achieved [22,23].

7.4.4 Localization of PEO-coated CNC in PLA/PA11 Blend.

Changing the surface characteristics of nanoparticles is a reliable approach in tuning the localization of nanoparticles in melt mixed polymer-polymer blends [16]. In a previous work [40], it was demonstrated both theoretically and experimentally that CNC particles localize selectively in the PA11 phase of a PLA/PA11 blend. In this work, the effect of the encapsulation of CNC particles with PEO, a polymer miscible with PLA at certain concentrations, on CNC localization in the blend is investigated. In order to study the effect of kinetic parameters on the localization of PEO-coated CNC, two different mixing strategies are used. In one case, the PEO/CNC mixture is first premixed with PLA and in the other case it is premixed with PA11.

Procedure 1: *premixing of the PEO/CNC mixture with PLA.* FESEM is used as a first step to analyze the dispersion and localization of the CNC particles in the PLA/PA11 polymer blend.

Figure 7.5 shows SEM images of co-continuous (PLA-5PEO)/PA11 50/50 vol% blends with different CNC contents prepared by procedure 1. It is evident that PEO-coated CNC particles are almost exclusively locate in the PLA phase and are clearly observed as white dots. These dots are associated with the cross section of the CNC particles. The high contrast observed in Figure 7.5 is because PLA has a very low stability to radiolysis resulting from electron exposure in FESEM and the PLA surface is etched with high accelerating voltage [43]. Thus the PLA and

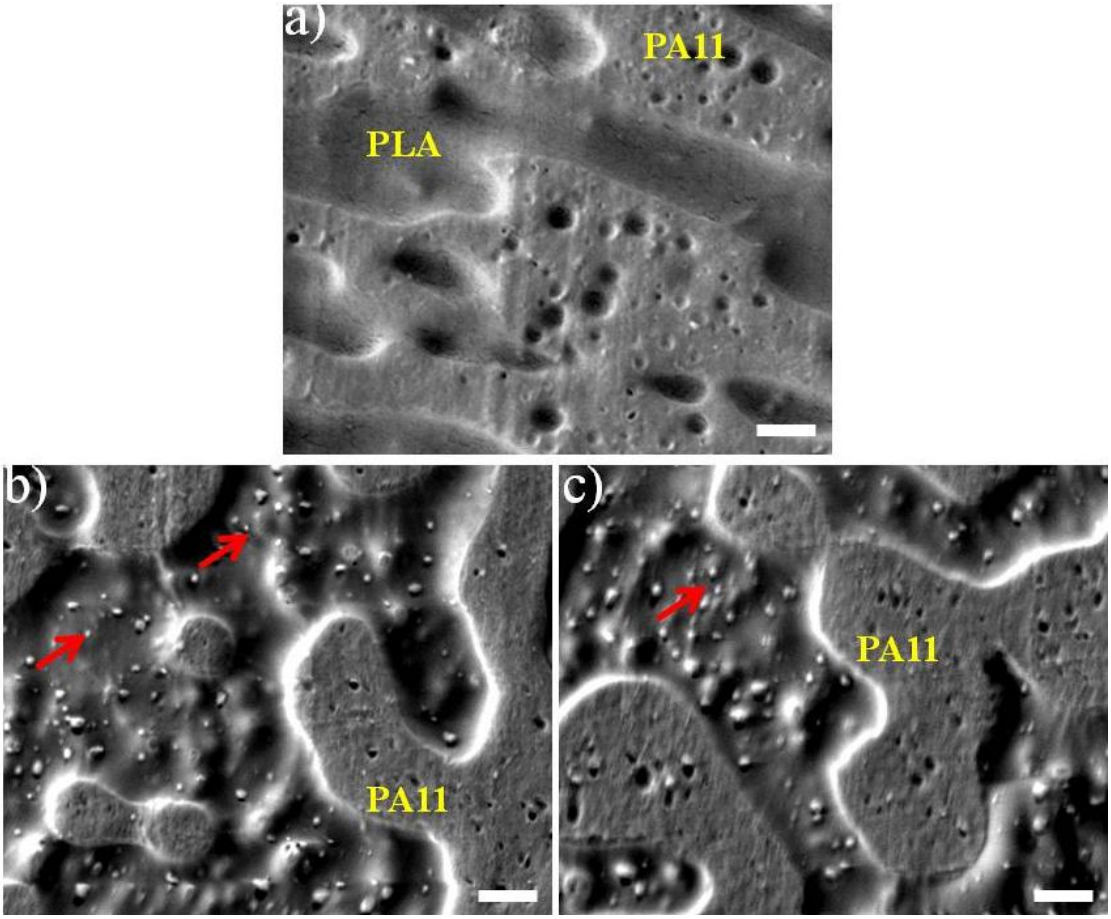

Figure 7.5. SEM images of (PLA-5PEO)/PA11 50/50 vol% blends with a) 0 wt% b) 1 wt% and c) 2 wt% CNC particles. The PEO/CNC mixture was first premixed with the PLA phase. The scale bar indicates 1 µm.

PA11 phases in Figure 7.5 are easily distinguishable due to the height difference while the CNC particles partly stick out of the PLA phase after radiolysis of the surrounding PLA chains. The holes observed in the PA11 phase are the PLA dispersed phase which are etched due to high

accelerating voltage.

SEM can certainly provide valuable information on the morphology and localization of CNC particles. However, the actual size of nanoparticles measured from SEM images is not very precise due to the charge concentration effect [19,29]. Figure 7.6 shows the AFM phase topography images of the same co-continuous (PLA-5PEO)/PA11 50/50 vol% blend with 0, 1 and 2 wt% CNC particles prepared with procedure 1. Individual PEO-coated CNC particles with an average thickness of 15 nm, similar to the individual CNC particles observed in Figure 7.1, are selectively located in the PLA phase.

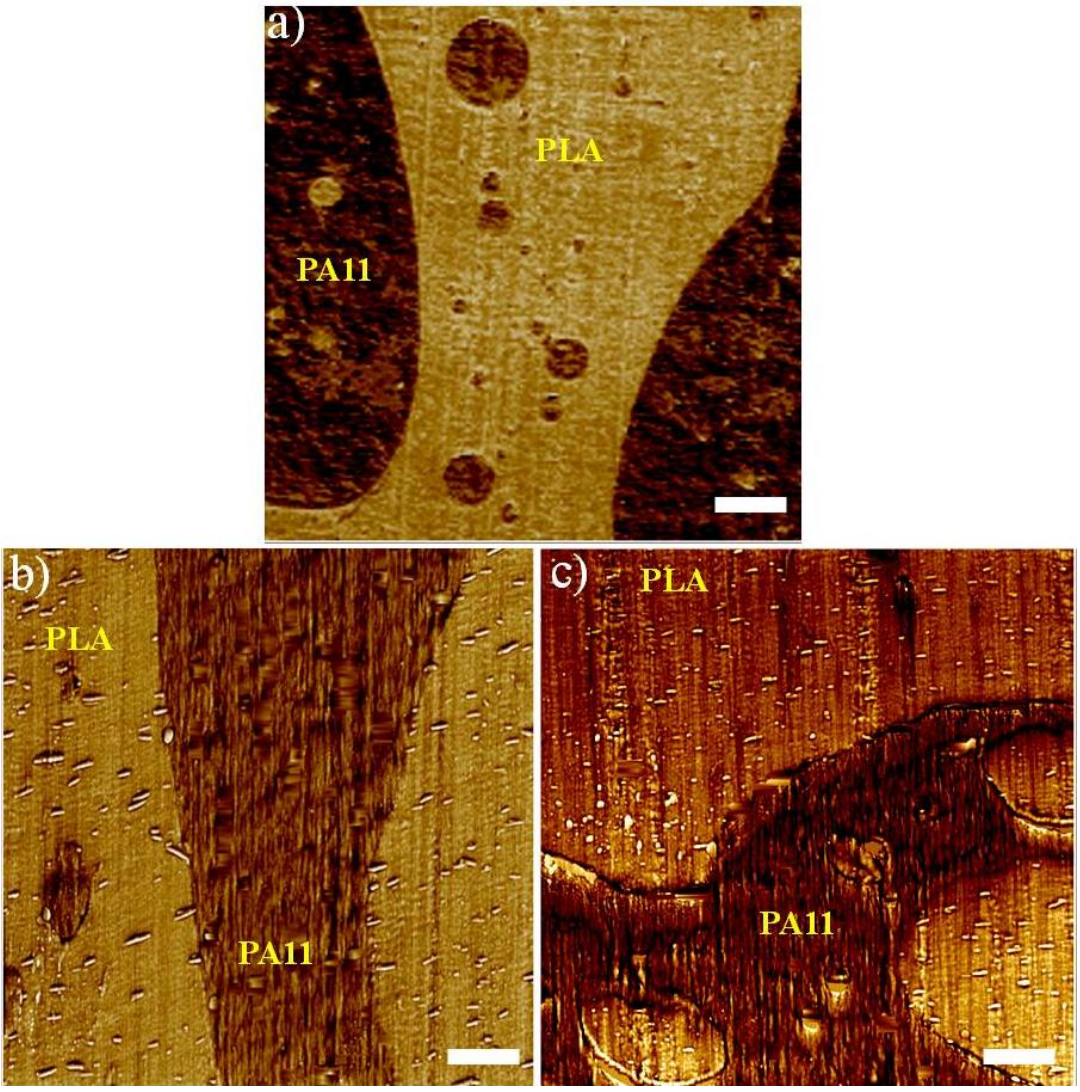

Figure 7.6. AFM phase micrographs of (PLA-5PEO)/PA11 50/50 vol% blends with a) 0 wt% b) 1 wt% and c) 2 wt% CNC particles. The PEO/CNC mixture was first premixed with the PLA phase. The scale bar indicates 500 nm.

The same localization state of the PEO-coated CNC in the PLA phase is observed for the (PLA-PEO)/PA11 70/30 vol% blends containing 2 wt% CNC particles prepared with procedure 1 as shown in Figure 7.7. The efficacy of PEO in achieving an individual nanoscale dispersion of CNC in the PLA/PA11blend is also evident here.

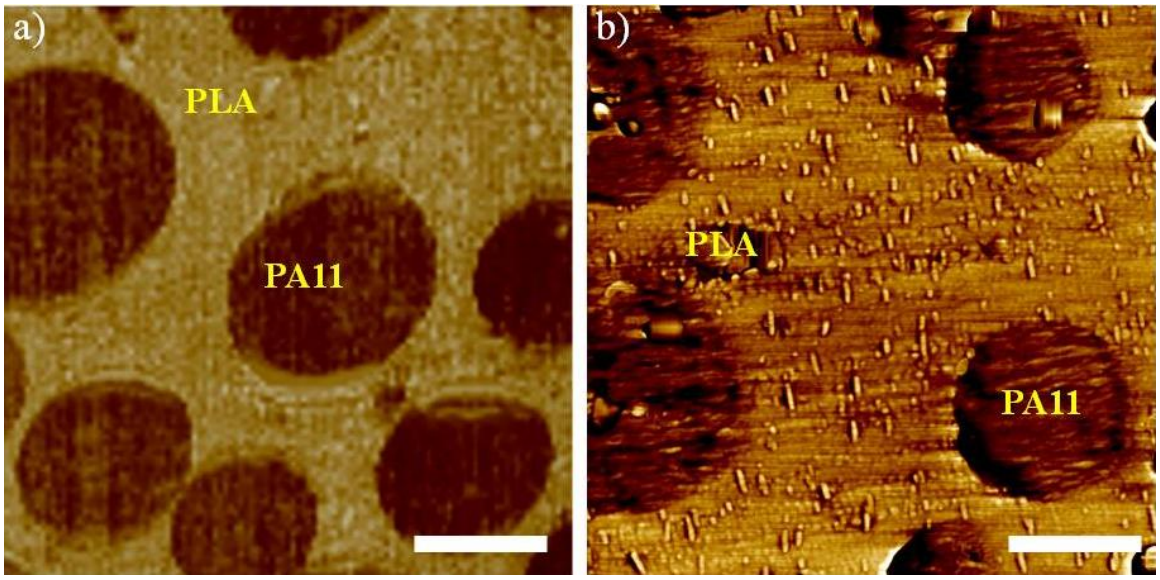

Figure 7.7. AFM phase micrographs of (PLA-5PEO)/PA11 70/30 vol% blends with a) 0 wt% b) 2 wt%, CNC particles. The PEO/CNC mixture was first premixed with the PLA phase. The scale bar indicates 500 nm.

Procedure 2: *premixing of the PEO/CNC mixture with PA11*. The effect of the procedure 2 mixing strategy on the localization of the PEO-coated CNC particles in PLA/PA11 50/50 vol% blends are shown in Figure 7.8. It is clear in AFM micrographs in Figure 7.8 that PEO-coated CNC particles have migrated from the PA11 phase towards the PLA phase during processing. This indicates the very high affinity of the PEO-coated CNC particles for the PLA phase.

These results confirm the thermodynamically stable localization of PEO-coated CNC particles in the PLA phase irrespective of whether the PEO/CNC mixture is first premixed with PLA or PA11. This observation also appears to be independent of PLA composition and CNC is found in the PLA phase when the system is co-continuous (PLA/PA11 50/50), when PLA is the matrix (PLA/PA11 70/30) or when it is the dispersed phase (PLA/PA11 30/70). Moreover, this localization is stable over a range of CNC contents. As mentioned earlier, in previous work on

PLA/PA11 blends, in the absence of PEO, CNC segregates into the PA11 phase [40]. The results in this paper now indicates a strategy for the almost exclusive segregation of CNC into PLA. Thus, it is possible to have a high degree of control over CNC localization in PLA/PA11 blends.

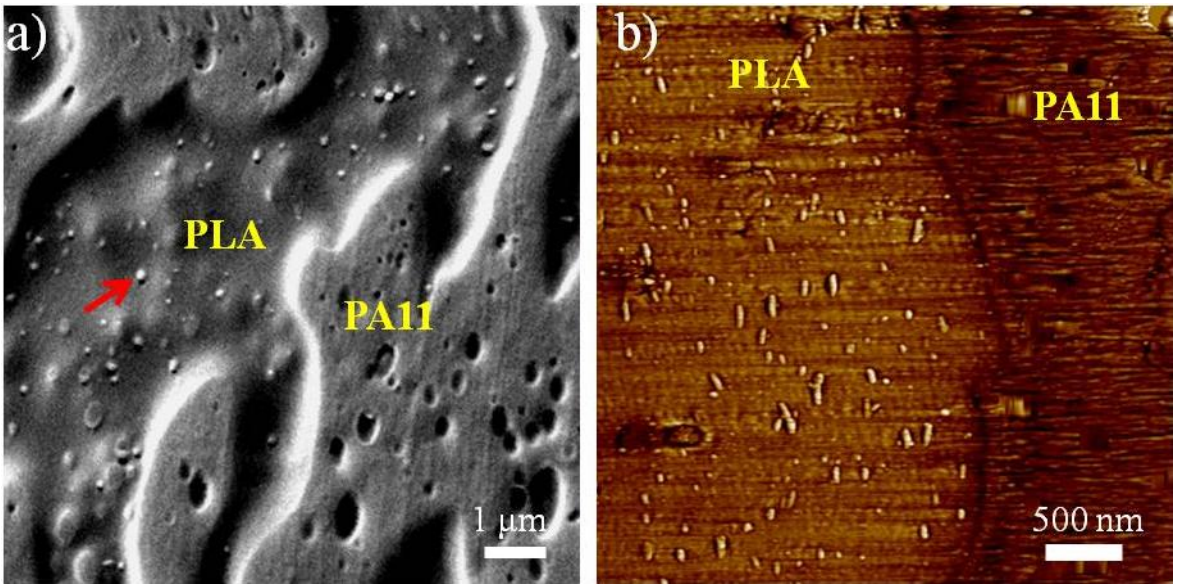

Figure 7.8. a) SEM and b) AFM phase micrographs of (PLA-5PEO)/PA11 50/50 vol% blends with 2 wt% CNC. The PEO/CNC mixture was first premixed with the PA11 phase.

PEO-coated CNC particles locate in the PLA phase due to the strong interactions between CNC and PEO combined with the PLA/PEO miscibility in the studied composition range. Strong interactions between CNC and PEO have been reported [29,32,44]. A specific interaction between CNC particles and PEO chains was reported by Dufresne et al. [32]. Samir et al. [29] quantified the interactions between PEO and CNC particles by using heat flow micro-calorimetery. Significant interactions between the hydroxyl end groups and ether oxygen groups of PEO with the hydroxyl groups of the CNC were reported. PLA-PEO miscibility was also studied in a previous work [13] and it was shown that melt mixed PLA and PEO are miscible up to 25 vol% PEO composition. Thus, the combination of stable interactions between PEO and CNC followed by PEO miscibility with PLA results in the stable localization of CNC particles in the PLA phase. The strong interaction between PEO and CNC particles and PEO/PLA is evidently dominant in the blend when it is considered that in procedure 2, the PEO/CNC mixture is first added into the PA11 phase.

7.4.5 The Effect of PEO-coated CNC on PLA/PA11 Blend Morphology

Matrix-Dispersed Phase Morphology. The addition of up to 3 wt% CNC particles through the PEO/CNC mixture to the PLA/PA11 70/30 vol% blends does not significantly change the dispersed phase size as compared to the (PLA-5PEO)/PA11 70/30 vol% blends without CNC (not shown here). Although the viscosity ratio (viscosity of the dispersed phase to that of the matrix) at the processing conditions changes from 1.6 to 0.4 after addition of 3 wt% CNC, (PLA-5PEO)/PA11 70/30 vol% blends with and without 3 wt% CNC demonstrate a dispersed phase morphology with almost the same volume average diameter (d_v) and number average (d_n) diameter of 0.9 and 0.8 μm, respectively. In previous works from this laboratory it was shown that the dispersed/phase morphology in PLA/PA11 blends is dominated by the low interfacial tension between PLA and PA11 and any changes in the viscoelastic properties of the blend components due to CNC addition do not significantly affect the dispersed phase size [45]. Since the coalescence in the matrix/dispersed phase PLA/PA11 system is already low due to the low interfacial tension, further addition of PEO-coated CNC to the PLA phase has little influence on the coalescence.

Co-continuous Morphology. Co-continuous polymer blends are known to show the highest level of coalescence due to their interconnected structure. The co-continuous blend of (PLA-5PEO)/PA11 50/50 vol%, shown in Figure 7.9, after selective extraction of PLA-5PEO by chloroform, does show a significant reduction in coalescence when PEO-coated CNC particles are added. The selective localization of the PEO-coated CNC in the PLA phase results in a substantial decrease in the pore size diameter from 11 μm for (PLA-5PEO)/PA11 50/50 vol% to 4 μm for (PLA-5PEO)/PA11 50/50 containing 2 wt% CNC particles as shown in Figure 7.9.

In a previous work [40] on the PLA/PA11 blend, where the CNC selectively localized in the PA11 phase, a more significant reduction in coalescence was observed. Table 7.1 compares the data from the two experiments and it is evident that when CNC is selectively localized in the PA11 phase a more than double effect of reduced coalescence is observed. The localization of 1 wt% PEO-coated CNC in the PLA phase diminishes the blend pore size from 11 to 7 μm, while in the case of the localization of 1 wt% CNC in the PA11 phase the pore size decreases from 13 to 3 μm. In that previous work [40] the reduction in coalescence was attributed to an increase in the elasticity of the PA11 domains due to the selective localization of CNC particles, which eventually prevents the retraction and breakup phenomena of the elongated PA11 domains

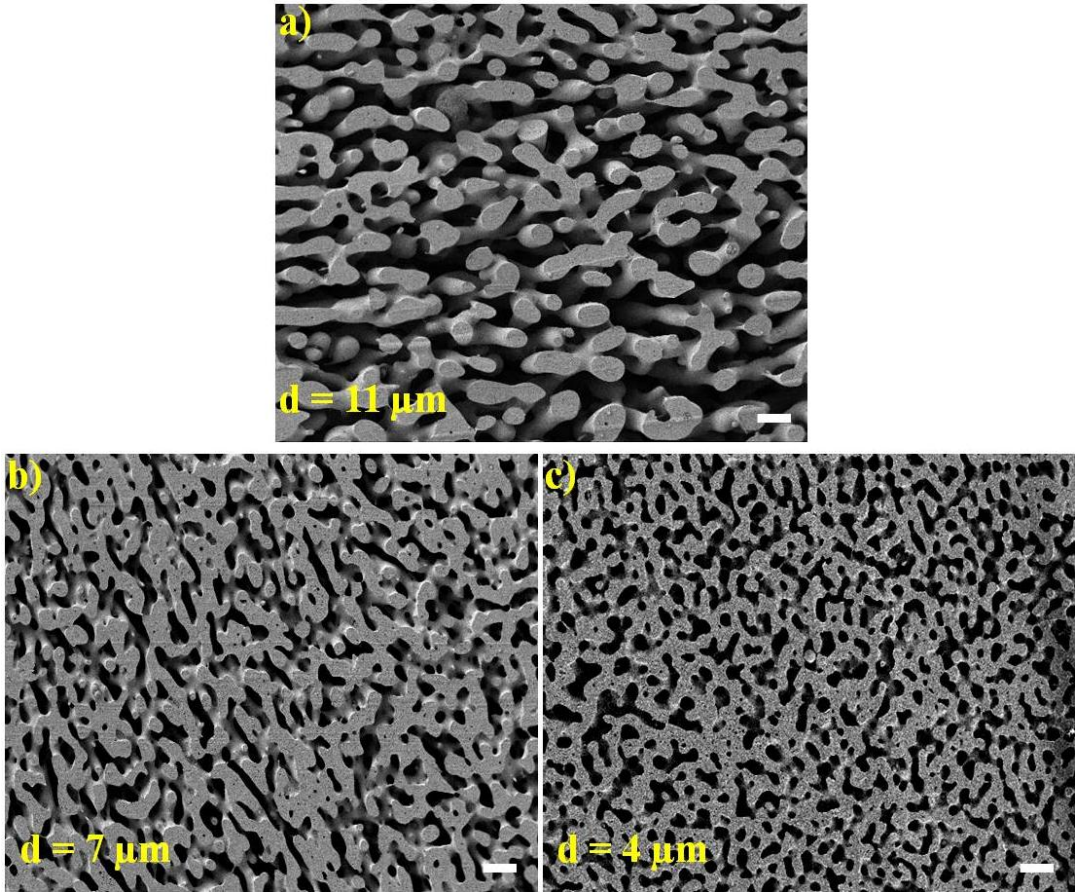

Figure 7.9. Morphology evolution of the (PLA-5PEO)/PA11 50/50 vol% in the presence of CNC particles: a) 0 wt % CNC, b) 1 wt% CNC, c) 2 wt% CNC. The scale bars indicate 10 µm. The (PLA-5PEO) phase was selectively extracted with chloroform.

Table 7.1. The effect of different localization of CNC in PLA/PA11 blends on the pore size.

	CNC (wt%)	Pore size (µm)
CNC Localization in the PA11 phase [a]	0	13
	1	3
CNC Localization in the PLA-5PEO phase	0	11
	1	7

a. Data obtained from a previous work [40].

formed during melt processing. A retarded relaxation mechanism of the co-continuous structure, due to a confinement effect of PA11 chains between the CNC particles, was suggested and was

supported by rheological data.

In this work less coalescence reduction is observed when the CNC is selectively localized in the PLA phase in the (PLA-5PEO)/PA11 blend. This difference cannot be related to the changes in the viscosity of the systems, as the complex viscosity of the PLA with PEO-coated CNC at the processing conditions is about the same as that of the PA11 with CNC (not shown here). Therefore, it is important to focus more on the elastic behavior of the systems. The frequency dependence of the storage modulus (G') of (PLA-5PEO)/CNC nanocomposites with different contents of CNC particles is shown in Figure 7.10-a. The frequency dependence of the storage modulus (G') of PLA containing PEO-coated CNC particles decreases progressively with increasing PEO-coated CNC concentration, indicating delayed dynamic relaxations in the studied frequency range [2,23]. Compared to the previous work [40], where CNC is localized in PA11, the storage modulus of that system at 2 wt% CNC is 2.5 times greater than that for CNC in PLA-5PEO at the frequency closest to the processing conditions as is shown in Figure 7.10-b.

The loss tangent, tan δ, is also usually used to study the viscoelastic behavior of polymer melts [46]. As shown in Figure 7.10-c, the PLA-5PEO system shows a typical behavior of a viscoelastic polymer with tan δ decreasing as a function of frequency. For the nanocomposites with an CNC concentration of 1 wt% or greater, the tan δ demonstrates frequency independence indicating increasing elastic behavior of the nanocomposites [23,25,46]. This increased elasticity of PLA confined between PEO-coated CNC leads to a retarded relaxation of the PLA domains and contributes to the coalescence suppression of the blend which is in consistent with the previous work [40].

Using the storage modulus data in Figure 7.10-a and a power law function [46], a rheological percolation threshold of 1.5 wt% CNC is determined for the (PLA-5PEO)/CNC nanocomposite which is much higher than that of PA11/CNC system (0.9 wt%) in the previous study [40]. Since 1 wt % CNC, based on the total weight of the blend, actually corresponds to 2 wt% CNC when it is localized in the PLA phase in (PLA-5PEO)/PA11 50/50 vol%, the system studied here is always above the rheological percolation threshold. Thus, it can be concluded that the retarded relaxation of the PLA domains in the presence of PEO-coated CNC particles is the result of a CNC network structure (overlapping or physical touching of CNC particles). The higher level of coalescence reduction observed in the previous work [40], for the case of CNC localization in

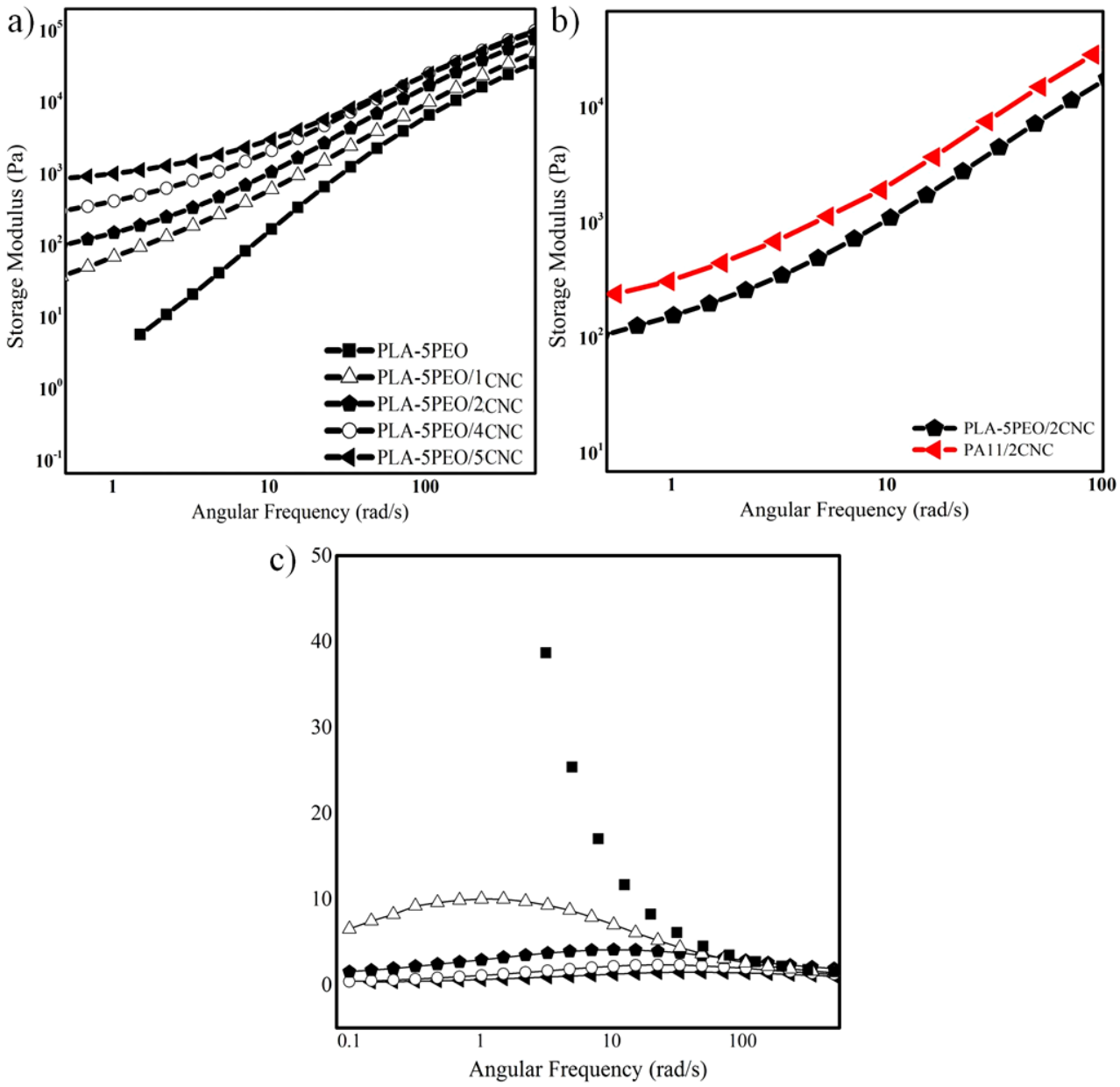

Figure 7.10. a, b) storage modulus (G') and c) tan δ versus angular frequency (ω) for PLA-5PEO and PLA-5PEO/CNC and PA11/2CNC nanocomposites. The storage modulus data for PA11/2CNC nanocomposite are obtained from a previous work [40].

PA11, is the result of a more highly developed CNC network structure for that system at the same CNC concentration as reflected in its lower rheological percolation threshold value. In the present case, PEO-coated CNC particles are much more likely to be separated by PLA due to the high PLA/PEO interaction and this delays CNC-CNC network formation. CNC particles have a

very high level of attraction to each other and the PEO coating influences that interaction. Thus, PEO coated CNC localized in PLA has a less developed CNC network structure than CNC localized in PA11. The present system thus presents less retarded relaxation phenomena and hence less coalescence reduction.

7.5 Conclusion

This study reports on the control of the stable localization of finely dispersed cellulose nanocrystals (CNC) within the PLA phase in melt processed poly (lactic acid) (PLA)/bio-polyamide11 (PA11) blends. A high pressure homogenization technique followed by freeze drying is used to prepare a PEO/CNC mixture. The prepared PEO/CNC mixture is then added into PLA/PA11 blends via two different processing strategies. Atomic force microscopy (AFM) shows a homogenous nanoscale dispersion of CNC particles with a thickness in the same range of individual CNC particles, 10-20 nm, in PEO, PLA-PEO and (PLA-PEO)/PA11 blends. Although CNC particles preferentially localize in the PA11 phase in a typical PLA/PA11/CNC system, PEO-coated CNC selectively locates in the PLA phase, irrespective of whether the PEO/CNC mixture is premixed with PLA or PA11. This observation is attributed to the strong interaction between PEO and CNC combined with the PLA/PEO miscibility in the studied composition range. The localization of PEO-coated CNC in the PLA phase has no effect on the morphology of the PLA-5PEO/PA11 blend when it is in a matrix/dispersed phase form. However, the localization of 1 wt% PEO-coated CNC in the PLA phase in co-continuous (PLA-5PEO)/PA11 50/50 vol% diminishes the blend pore size from 11 to 7 μm. This is attributed to retarded relaxation of PLA resulting from the development of a percolated CNC network structure. It is shown that the degree of coalescence reduction in the co-continuous blend can be directly related to the onset of CNC network formation. This work outlines a strategy for the almost exclusive segregation of CNC particles into PLA in PLA/PA11 blends. It should be noted though, that due to the high affinity of PEO to PLA, this approach should be applicable to virtually any polymer-polymer blend mixture involving PLA. Since CNC can directly affect PLA crystallinity and subsequently its heat deflection temperature this approach has significant potential.

7.6 Acknowledgements

The authors would like to gratefully acknowledge the NSERC Network for Innovative Plastic Materials and Manufacturing Processes (NIPMMP) for supporting this project.

7.7 References

[1] N. Bitinis, R. Verdejo, J. Bras, E. Fortunati, J.M. Kenny, L. Torre, M.A. López-Manchado, Poly(lactic acid)/natural rubber/cellulose nanocrystal bionanocomposites Part I. Processing and morphology, Carbohydr. Polym. 96 (2013) 611–620.

[2] M.R. Kamal, V. Khoshkava, Effect of cellulose nanocrystals (CNC) on rheological and mechanical properties and crystallization behavior of PLA/CNC nanocomposites, Carbohydr. Polym. 123 (2015) 105–114.

[3] Y. Xu, P. Delgado, A.D. Todd, J. Loi, S.A. Saba, R.J. McEneany, T. Tower, V. Topolkaraev, C.W. Macosko, M.A. Hillmyer, Lightweight micro-cellular plastics from polylactide/polyolefin hybrids, Polymer. 102 (2016) 73–83.

[4] T. Li, J. Zhang, D.K. Schneiderman, L.F. Francis, F.S. Bates, Toughening Glassy Poly(lactide) with Block Copolymer Micelles, ACS Macro Lett. 5 (2016) 359–364.

[5] A. Nuzzo, S. Coiai, S.C. Carroccio, N.T. Dintcheva, C. Gambarotti, G. Filippone, Heat-Resistant Fully Bio-Based Nanocomposite Blends Based on Poly(lactic acid), Macromol. Mater. Eng. 299 (2014) 31–40.

[6] A.M. Zolali, V. Heshmati, B.D. Favis, Ultratough Co-Continuous PLA/PA11 by Interfacially Percolated Polyether-b-amide, Macromolecules. 50 (2016) 264–274.

[7] K. Anderson, K. Schreck, M. Hillmyer, Toughening Polylactide, Polym. Rev. 48 (2008) 85–108.

[8] K. Hashima, S. Nishitsuji, T. Inoue, Structure-properties of super-tough PLA alloy with excellent heat resistance, Polymer. 51 (2010) 3934–3939.

[9] K.S. Anderson, M.A. Hillmyer, The influence of block copolymer microstructure on the toughness of compatibilized polylactide/polyethylene blends, Polymer. 45 (2004) 8809–8823.

[10] M.P. Arrieta, E. Fortunati, F. Dominici, E. Rayón, J. López, J.M. Kenny, Multifunctional PLA–PHB/cellulose nanocrystal films: Processing, structural and thermal properties, Carbohydr. Polym. 107 (2014) 16–24.

[11] T.D. Fornes, D.R. Paul, Structure and Properties of Nanocomposites Based on Nylon-11 and -12 Compared with Those Based on Nylon-6, Macromolecules. 37 (2004) 7698–7709.

[12] G. Stoclet, R. Seguela, J.-M. Lefebvre, Morphology, thermal behavior and mechanical properties of binary blends of compatible biosourced polymers: Polylactide/polyamide11, Polymer. 52 (2011) 1417–1425.

[13] V. Heshmati, B.D. Favis, High Performance Poly (Lactic Acid)/Bio-Polyamide11 through Controlled Chain Mobility, (2017) Submitted.

[14] A. Nuzzo, E. Bilotti, T. Peijs, D. Acierno, G. Filippone, Nanoparticle-induced co-continuity in immiscible polymer blends – A comparative study on bio-based PLA-PA11 blends filled with organoclay, sepiolite, and carbon nanotubes, Polymer. 55 (2014) 1–12.

[15] A. Taghizadeh, B.D. Favis, Carbon nanotubes in blends of polycaprolactone/thermoplastic starch., Carbohydr. Polym. 98 (2013) 189–98.

[16] M. Gültner, A. Göldel, P. Pötschke, Tuning the localization of functionalized MWCNTs in SAN/PC blends by a reactive component, Compos. Sci. Technol. 72 (2011) 41–48.

[17] W. Li, J. Karger-Kocsis, A.K. Schlarb, Dispersion of TiO_2 Particles in PET/PP/TiO_2 and PET/PP/PP -*g*- MA/TiO_2 Composites Prepared with Different Blending Procedures, Macromol. Mater. Eng. 294 (2009) 582–589.

[18] J.-M. Raquez, Y. Habibi, M. Murariu, P. Dubois, Polylactide (PLA)-based nanocomposites, Prog. Polym. Sci. 38 (2013) 1504–1542.

[19] M.A.S. Azizi Samir, F. Alloin, A. Dufresne, Review of Recent Research into Cellulosic Whiskers, Their Properties and Their Application in Nanocomposite Field, Biomacromolecules. 6 (2005) 612–626.

[20] S.J. Eichhorn, Cellulose nanowhiskers: promising materials for advanced applications,

Soft Matter. 7 (2011) 303–315.

[21] K. Ben Azouz, E.C. Ramires, W. Van den Fonteyne, N. El Kissi, A. Dufresne, Simple Method for the Melt Extrusion of a Cellulose Nanocrystal Reinforced Hydrophobic Polymer, ACS Macro Lett. 1 (2012) 236–240.

[22] V. Khoshkava, M.R. Kamal, Effect of surface energy on dispersion and mechanical properties of polymer/nanocrystalline cellulose nanocomposites., Biomacromolecules. 14 (2013) 3155–63.

[23] V. Khoshkava, M.R. Kamal, Effect of Cellulose Nanocrystals (CNC) Particle Morphology on Dispersion and Rheological and Mechanical Properties of Polypropylene/CNC Nanocomposites, ACS Appl. Mater. Interfaces. 6 (2014) 8146–8157.

[24] D. Bagheriasl, P.J. Carreau, C. Dubois, B. Riedl, Properties of polypropylene and polypropylene/poly(ethylene-co-vinyl alcohol) blend/CNC nanocomposites, Compos. Sci. Technol. 117 (2015) 357–363.

[25] D. Bagheriasl, P.J. Carreau, B. Riedl, C. Dubois, W.Y. Hamad, Shear rheology of polylactide (PLA)–cellulose nanocrystal (CNC) nanocomposites, Cellulose. 23 (2016) 1–13.

[26] H. Sojoudiasli, M.-C. Heuzey, P.J. Carreau, Mechanical and morphological properties of cellulose nanocrystal-polypropylene composites, Polym. Compos. (2017).

[27] S.J. Eichhorn, A. Dufresne, M. Aranguren, N.E. Marcovich, J.R. Capadona, S.J. Rowan, C. Weder, W. Thielemans, M. Roman, S. Renneckar, W. Gindl, S. Veigel, J. Keckes, H. Yano, K. Abe, M. Nogi, A.N. Nakagaito, A. Mangalam, J. Simonsen, A.S. Benight, A. Bismarck, L.A. Berglund, T. Peijs, Review: current international research into cellulose nanofibres and nanocomposites, J. Mater. Sci. 45 (2010) 1–33.

[28] A. Arias, M.C. Heuzey, M.A. Huneault, G. Ausias, A. Bendahou, Enhanced dispersion of cellulose nanocrystals in melt-processed polylactide-based nanocomposites, Cellulose. 22 (2015) 483–498.

[29] M.A.S. Azizi Samir, F. Alloin, J.Y. Sanchez, A. Dufresne, Cellulose nanocrystals

reinforced poly(oxyethylene), Polymer. 45 (2004) 4149–4157.

[30] M. Roohani, Y. Habibi, N.M. Belgacem, G. Ebrahim, A.N. Karimi, A. Dufresne, Cellulose whiskers reinforced polyvinyl alcohol copolymers nanocomposites, Eur. Polym. J. 44 (2008) 2489–2498.

[31] D. Bondeson, K. Oksman, Polylactic acid/cellulose whisker nanocomposites modified by polyvinyl alcohol, Compos. Part A Appl. Sci. Manuf. 38 (2007) 2486–2492.

[32] M. Pereda, N. El Kissi, A. Dufresne, Extrusion of Polysaccharide Nanocrystal Reinforced Polymer Nanocomposites through Compatibilization with Poly(ethylene oxide), ACS Appl. Mater. Interfaces. 6 (2014) 9365–9375.

[33] Long Jiang, E. Morelius, Jinwen Zhang, M. Wolcott, J. Holbery, Study of the Poly(3-hydroxybutyrate-co-3-hydroxyvalerate)/Cellulose Nanowhisker Composites Prepared by Solution Casting and Melt Processing, J. Compos. Mater. 42 (2008) 2629–2645.

[34] A.-L. Esquirol, P. Sarazin, N. Virgilio, Tunable Porous Hydrogels from Cocontinuous Polymer Blends, Macromolecules. 47 (2014) 3068–3075.

[35] A.-C. Baudouin, J. Devaux, C. Bailly, Localization of carbon nanotubes at the interface in blends of polyamide and ethylene–acrylate copolymer, Polymer. 51 (2010) 1341–1354.

[36] S.M. Jafari, Y. He, B. Bhandari, Optimization of nano-emulsions production by microfluidization, Eur. Food Res. Technol. 225 (2007) 733–741.

[37] A. Ferrer, I. Filpponen, A. Rodríguez, J. Laine, O.J. Rojas, Valorization of residual Empty Palm Fruit Bunch Fibers (EPFBF) by microfluidization: Production of nanofibrillated cellulose and EPFBF nanopaper, Bioresour. Technol. 125 (2012) 249–255.

[38] T. Zimmermann, E. Pöhler, T. Geiger, Cellulose Fibrils for Polymer Reinforcement, Adv. Eng. Mater. 6 (2004) 754–761.

[39] S.-Y. Lee, S.-J. Chun, I.-A. Kang, J.-Y. Park, Preparation of cellulose nanofibrils by high-pressure homogenizer and cellulose-based composite films, J. Ind. Eng. Chem. 15 (2009) 50–55.

[40] V. Heshmati, M.R. Kamal, B.D. Favis, Cellulose Nanocrystal in Poly (Lactic acid)/Polyamide11 Blends: Preparation, Morphology and Co-continuity, (n.d.) Sbmitted.

[41] Y. Song, Q. Zheng, Concepts and conflicts in nanoparticles reinforcement to polymers beyond hydrodynamics, Prog. Mater. Sci. 84 (2016) 1–58.

[42] Q. Zhang, L.A. Archer, Poly(ethylene oxide)/Silica Nanocomposites: Structure and Rheology, 18 (2002) 10435–10442.

[43] R.F. Egerton, P. Li, M. Malac, Radiation damage in the TEM and SEM, Micron. 35 (2004) 399–409.

[44] T. Kondo, C. Sawatari, Intermolecular hydrogen bonding in cellulose/poly(ethylene oxide) blends: thermodynamic examination using 2,3-di-O- and 6-O-methylcelluloses as cellulose model compounds, Polymer. 35 (1994) 4423–4428.

[45] V. Heshmati, A.M. Zolali, B.D. Favis, Morphology Development in Poly (Lactic Acid)/ Polyamide11 Biobased Blends: Chain Mobility and Interfacial Interactions, (2017) Submitted to “ Polymer” for publication.

[46] S. Abbasi, P.J. Carreau, A. Derdouri, M. Moan, Rheological properties and percolation in suspensions of multiwalled carbon nanotubes in polycarbonate, Rheol. Acta. 48 (2009) 943–959.

CHAPTER 8 GENERAL DISCUSSION

In this research the morphology and interfacial development in PLA/PA11 blends was first studied. PLA/PA11 blend demonstrated a high interfacial tension under static conditions. High interfacial tension is an indication of a highly immiscible system with large dispersed phase size and high coarsening level. Morphology analysis, however, revealed very fine dispersed phase morphology and low level of coalescence. The discrepancy between the interfacial tension obtained under static conditions and morphology characterization observed for PLA/PA11 was puzzling. Therefore interfacial tension under dynamic conditions was measured. Surprisingly a lower interfacial tension value was obtained indicating that the PLA/PA11 blend behaves as a low interfacial tension system during dynamic mixing. A possible explanation is that an interfacial reaction is taking place between PLA and PA11 under dynamic conditions that is not observed under static conditions. However, due to the low concentration of functional groups in PLA and PA11 it was not possible to detect the interfacial reaction between PLA and PA11 with standard methods such as NMR and FTIR as they did show enough sensitivity. Moreover in our system detecting the reaction by measuring the mass of the formed copolymer was impossible due to the lack of a mutual solvent for PLA and PA11. Therefore indirect methods including crystallinity and chain mobility were examined. It is well known that PLA is a stiff chain while PA is more mobile. The validity of this latter explanation was explored by enhancing the PLA or PA11 chain mobility through plasticization. Plasticized PLA in PLA/PA11 blends was shown to significantly diminishes the static interfacial tension as well as the phase size and coalescence in the dynamically mixed system at high PLA concentrations. Another important difficulty in analyzing the morphology of PLA/PA11 blends was the lack of selective solvent for PA11. In this study a good level of contrast between PLA and PA11 in SEM analysis in the blends with PA11 as the dispersed phase was obtained by etching the PLA surface with high accelerating voltage under electron exposure in FESEM resulting from low stability of PLA to radiolysis.

In the second step, attempt was made to produce a high performance PLA/PA11 based blends. From the first part of the project it is realized that PLA/PA11 has a good level of interfacial adhesion and thus the ability of the PA11 phase to enhance the PLA mechanical properties is affected by the brittle nature of the PLA phase itself. In order to solve this issue plasticization of the PLA phase with PEO (two different molecular weight) was considered. High molecular weight PEO was chosen to limit the plasticizer migration toward the surface. In order to make

sure of a high level of mixing between PLA and PEO, a PLA/PEO mixture was first extruded. The prepared PLA/PEO pellets were then dried and melt mixed with PA11 in a subsequent extrusion process. It was found that humidity significantly affect the mechanical properties of the final product. The first set of experimental data revealed that drying of the material at 60 °C for 24 h before extrusion was not enough. Therefore all the materials were dried under vacuum at 80 °C for 48-72 h. The same drying step was applied on the obtained pellets before injection molding. Examining the miscibility of PLA/PEO by analyzing the T_g of the phases was also challenging. It was found that the regular DSC cannot provide a good reproducibility to determine the PLA/PEO miscibility. Therefore MDSC were employed and a compositional dependent miscibility of PLA/PEO system was observed.

In the third part of the project, CNC particles are incorporated into the PLA/PA11 blend. One of the main problem at the beginning of this part of the project was to obtain CNC particles. Because of intellectual property issues, FPInnovations could not provide us with the nanoparticles. After about two and a half years, CNC particles were obtained from Alberta Innovates Technology Futures. Another problem associate with CNC particles was measuring the surface tension because surface roughness higher than 0.5 µm influences the contact angle measurements. To solve this problem a thin CNC film was prepared with solvent casting/evaporation of a CNC aqueous suspension and its surface tension was obtained with the contact angle technique. The main challenge associated with polymer/CNC systems is obtaining a proper homogenous level of CNC dispersion within polymer matrices due to the highly hydrophilic character of CNC particles. In this work a high level of CNC dispersion in both PLA and PA11 through solvent/evaporation technique was obtained. Dimethylformamide (DMF) and formic acid are among the few organic solvents which provide stable homogenous CNC suspensions. On the other hand DMF and formic acid are good solvents for PLA and PA11, respectively. Therefore a homogenous dispersion of CNC in either PLA or PA11 through solvent casting was obtained. It has to be noted that DMF is known as a toxic solvent, therefore a lot of care was taken during work with DMF. All the mixing, casting and evaporation processes were carried out under the hood and a safety mask was used during the experiment. Although experimental observations demonstrated the localization of CNC particles in the PA11 phase, theoretical consideration based on the surface tension data obtained with the contact angle technique predicts the localization of the CNC particles at the PLA/PA11 interface. This

discrepancy was solved by using the accurate value of the PLA/PA11 interfacial tension obtained by the Neumann triangle technique in the first part of this research. Our observation thus indicates that thermodynamic analysis based on the surface tensions of neat PLA and PA11 is not sufficient to predict the CNC localization in PLA/PA11 blends.

Finally control of the localization of CNC in the blend was studied. Although water has been reported to be a good suspension medium for CNC particles, it requires a post homogenization process. We found that mechanical homogenization and sonication process lead to a significant degradation of CNC particles. To solve this problem we employed a high pressure homogenizer which proved to be very effective in breaking down the CNC agglomerates without any CNC degradation. After a longtime searching for a high pressure homogenizer equipment, we found an EmulsiFlex-C3, Avestin model at the pharmacy department at Université de Montréal. Due to the pharmaceutical applications, it was only dedicated to aqueous suspensions. It is important to note that the casting/evaporation of aqueous CNC/PEO suspensions, obtained after homogenization, results in a high level of CNC aggregation. The major advantage of freeze-drying is to prevent CNC agglomeration as water is removed. It guarantees a homogeneous dispersion of CNC particles in the PEO matrix. Protrusion of PEO-coated CNC particles due to the difficulty of the knife to cut through soft PEO during microtoming was an another problem in this part of the project. It is recommended to set the microtoming temperature much lower than PEO glass transition temperature.

CHAPTER 9 CONCLUSION AND RECOMMENDATIONS

9.1 Conclusion

In this dissertation, the morphology and mechanical properties of PLA/PA11 blends and the localization of crystalline nanocellulose (CNC) particles in the blend are investigated. The first part of this work underlines the importance of PLA chain mobility on the interfacial properties of binary PLA/PA11 blends. This blend combines the very unusual characteristics of high static interfacial tension, 5.8 ± 0.6 mN/m and 5.4 ± 0.4 mN/m as measured by the breaking thread (BT) and fiber retraction (FR) methods respectively, with the fine dispersed morphology and low level coalescence of a highly interacting system after melt mixing. It is shown that this discrepancy between the static interfacial tension and the observed morphology after dynamic mixing can be attributed directly to the limited chain mobility of the stiff PLA molecule, particularly under quiescent conditions, which inhibits the available functional groups from reacting at the interface. Enhancing the PLA chain mobility through the addition of 5% PEO plasticizer results in a significantly lower interfacial tension and even further suppressed coalescence under dynamic mixing at 30 and 40 vol% minor phase.

In the second part, attempt are made to improve the mechanical properties of the PLA/PA11 blends. Enhancing PLA ductility by using an optimum concentration of PEO plasticizer was significantly effective in improving the Impact strength and elongation at break of the interacting PLA/PA11 system. In some samples exceptional ductility with an elongation at break of 275% as compared to 5% for PLA and also significant improvement in the Izod impact strength with 17.5 in the impact strength of PLA and 3 times that of PA11 are observed. These finding were well correlated with the PEO limited miscibility in the PLA phase. PEG, however, had substantially lower toughening efficiency compared to PEO. This was attributed to the PLA/PEG phase separation at lower PEG concentration before providing enough ductility to the PLA phase. Analysis of the fracture surface of the tough blends after Impact indicates that interfacial debonding/cavitation in conjunction with the very large PLA phase yielding due to the PEO plasticization are the main toughening mechanisms. These insight demonstrated a new strategy on the efficient toughening and increasing the application window of PLA/PA11 blends.

In the third part of this work, PLA/PA11/Cellulose nanocrystal (CNC) multiphase system is investigated for the first time. An exceptional level of CNC dispersion in the blend is achieved. CNC in the melt mixed PLA/PA11 blends perfectly segregates into the PA11 phase even when the blend is prepared from a PLA/CNC mixture. This is a result of a very low interfacial tension of 1 mN/m between CNC and PA11. There is virtually no influence of CNC content on the PLA/PA11 morphology when it is in a matrix/dispersed phase form. This indicates that the morphology under those conditions is controlled by the PLA/PA11 interfacial tension and this result has important consequences for nanoparticles in low interfacial tension blend systems in general. When coalescence phenomena are fully maximized through the preparation of co-continuous systems, then CNC dramatically diminishes coalescence even at values as low as 1 wt% CNC. It is postulated that the co-continuous coalescence reduction is due to a retarded relaxation process, as demonstrated in the rheology results, resulting from PA11 confinement between CNC particles and the high level of interaction between PA11 and CNC. These results are of significant importance since they clearly reveal the stable localization of well segregated CNC particles in the PA11 phase for PLA/PA11 blends and a significant phase coalescence reduction of the co-continuous blend at a very low CNC concentration.

Finally, the control of the stable localization of cellulose nanocrystal (CNC) in the PLA phase in melt mixed PLA/PA11 blends is presented for the first time. A versatile processing strategy is optimized combining homogenization-freeze drying in order to prepare a PEO/CNC mixture. An exceptional CNC dispersion in the same range of individual CNC particles is achieved. Typically, CNC in melt mixed PLA/PA11 blends, selectively localizes in the PA11 phase. Significantly, when CNC is coated with PEO, it segregates in the PLA phase even when PEO/CNC mixture is premixed with PA11. It is suggested that the strong interactions between PEO and CNC particles combined with PLA/PEO miscibility facilitate the localization of PEO-coated CNC in the PLA phase. The phase coalescence of the co-continuous blend substantially decreases in the presence of PEO-coated CNC particles. This is attributed to a retarded relaxation of the PLA phase resulting from the development of a percolated CNC network structure. Interestingly, when CNC is selectively localized in PA11, a more than double effect of reduced coalescence is observed. The degree of coalescence reduction is directly related to the rheological percolation threshold value and the onset of CNC network formation within the given phase.

9.2 Original Contributions

The major scientific contributions of this work are:

- For the first time, a systematic study of the morphology, coalescence, continuity development and interfacial properties of PLA/PA11 blends is presented.
- It is demonstrated that PLA/PA11 blend behaves as a highly interacting interfacially compatibilized system. This interfacial interaction is shown to depend strongly on the PLA chain mobility.
- It is shown that in intefacially interactive polymer blends, static methods such IFR and BT may not provide a precise value of the interfacial tension.
- It is reported that even if polymers may have the potential for interfacial interactions, sufficient chain mobility is necessary in order for those interactions to come into play.
- Profound impact of controlled PLA chain mobility on the interfacial tension, morphology and mechanical properties is presented.
- By using an appropriate amount of a proper PLA plasticizer, it is shown that PA11 ability to enhance PLA mechanical properties is affected by the brittle nature of the PLA phase itself. This might be the case in many other polymer-polymer blends with good interfacial adhesion.
- It is shown that the co-continuous morphology is less critical to the improvement of elongation at break than for impact strength. It is demonstrated that maximized impact strength is dependent on debonding cavitation across a continuous interface and is the principal energy dissipation mechanism for (PLA-PEO)/PA11 systems.
- Selective localization of cellulose nanocrystal (CNC) in PLA/PA11 blends is reported for the first time.
- An exceptional CNC dispersion in PLA, PA11 and PLA/PA11 is presented. It is the first time PA11/CNC nanocomposite reported in the literature.
- A substantial suppression in phase coalescence of co-continuous polymer blend in the presence of only 1 wt% nanoparticle is reported.
- A versatile processing strategy is optimized combining homogenization-freeze drying in order to prepare a PEO/CNC mixture.
- The control of the stable localization of cellulose nanocrystal (CNC) in the PLA phase in melt mixed PLA/PA11 blends is presented for the first time.

- A high level of control over CNC localization in PLA/PA11 blend is demonstrated.

9.3 Recommendations for Future Works

Based on the obtained results in this dissertation, the following recommendations are proposed for future works:

- The obtained results indicate the possibility of enhancing the compatibility of polyester/polyamide blends in general with plasticization of the polyester component. It will be interesting to study this approach in improving the mechanical properties of another polyester/polyamide blend in order to generalize this idea.
- A high level of control over CNC localization in either PLA or PA11 phase in PLA/PA11 blend was presented in this work. It will be interesting to control the localization of CNC particles at the PLA/PA11 interface. Premixing of CNC particles with a polymer that would partially wet (PBAT) or completely wet (PEBA) this system would be a starting point.
- Due to the high level of interactions between PEO and PLA, the approach presented in the last part of this work has the potential to localize CNC into PLA for virtually any polymer-polymer blend system. It will be interesting to study this approach in another PLA based blend in order to generalize the idea.
- Any other nanoparticle (nanosilica for example) which has good level of interaction with PEO can be exclusively segregated in the PLA phase for any PLA based blends. This would be another idea to follows up in systems that localization of nanoparticles in the PLA phase is an objective
- Study the effect of the selective localization of the CNC particle on the mechanical properties of the PLA/PA11 blend could be another interesting subject. Localization of CNC in the PLA phase, in particular can be very effective in improving the stiffness/toughness balance and increasing thermomechanical properties (HDT) of (PLA-PEO)/PA11 blends.

BIBLIOGRAPHY

[1] K. Madhavan Nampoothiri, N. R. Nair, and R. P. John, "An overview of the recent developments in polylactide (PLA) research," *Bioresour. Technol.*, vol. 101, no. 22, pp. 8493–8501, 2010.

[2] T. Li, J. Zhang, D. K. Schneiderman, L. F. Francis, and F. S. Bates, "Toughening Glassy Poly(lactide) with Block Copolymer Micelles," *ACS Macro Lett.*, vol. 5, no. 3, pp. 359–364, Mar. 2016.

[3] "Biodegradable Plastics Market by Type PLA, PHA, PBS, Starch-Based Plastics, Regenerated Cellulose, PCL), by Application (Packaging, Fibers, Agriculture, Injection Molding, and Others) - Global Trends & Forecasts to 2020."

[4] M. K. P. L. Shen, J. Haufe, "Product overview and market projection of emerging biobased plastics PRO-BIT 2009," Utrecht University, Utrecht, Netherlands, 2009.

[5] R. A. Auras, L. T. Lim, S. E. M. Selke, and H. Tsuji, *Poly(lactic Acid): Synthesis, Structures, Properties, Processing, and Applications*. John Wiley & Sons, 2010.

[6] A. M. Zolali, V. Heshmati, and B. D. Favis, "Ultratough Co-Continuous PLA/PA11 by Interfacially Percolated Polyether-b-amide," *Macromolecules*, vol. 50, no. 1, pp. 264–274, Dec. 2016.

[7] K. Anderson, K. Schreck, and M. Hillmyer, "Toughening Polylactide," *Polym. Rev.*, vol. 48, no. 1, pp. 85–108, 2008.

[8] R. M. Rasal, A. V Janorkar, and D. E. Hirt, "Poly(lactic acid) modifications," *Prog. Polym. Sci.*, vol. 35, no. 3, pp. 338–356, 2010.

[9] Y. Xu, P. Delgado, A. D. Todd, J. Loi, S. A. Saba, R. J. McEneany, T. Tower, V. Topolkaraev, C. W. Macosko, and M. A. Hillmyer, "Lightweight micro-cellular plastics from polylactide/polyolefin hybrids," *Polymer.*, vol. 102, pp. 73–83, 2016.

[10] H. Liu and J. Zhang, "Research progress in toughening modification of poly(lactic acid)," *J. Polym. Sci. Part B Polym. Phys.*, vol. 49, no. 15, pp. 1051–1083, 2011.

[11] M. Shibata, Y. Inoue, and M. Miyoshi, "Mechanical properties, morphology, and crystallization behavior of blends of poly(l-lactide) with poly(butylene succinate-co-l-lactate) and poly(butylene succinate)," *Polymer.*, vol. 47, no. 10, pp. 3557–3564, 2006.

[12] E. Jalali Dil, P. J. Carreau, and B. D. Favis, "Morphology, miscibility and continuity development in poly(lactic acid)/poly(butylene adipate-co-terephthalate) blends," *Polymer.*, vol. 68, pp. 202–212, Jun. 2015.

[13] P. Sarazin, G. Li, W. J. Orts, and B. D. Favis, "Binary and ternary blends of polylactide, polycaprolactone and thermoplastic starch," *Polymer.*, vol. 49, no. 2, pp. 599–609, 2008.

[14] K. Hashima, S. Nishitsuji, and T. Inoue, "Structure-properties of super-tough PLA alloy

with excellent heat resistance," *Polymer.*, vol. 51, no. 17, pp. 3934–3939, 2010.

[15] K. S. Anderson and M. A. Hillmyer, "The influence of block copolymer microstructure on the toughness of compatibilized polylactide/polyethylene blends," *Polymer.*, vol. 45, no. 26, pp. 8809–8823, 2004.

[16] C. M. Thurber, Y. Xu, J. C. Myers, T. P. Lodge, and C. W. Macosko, "Accelerating Reactive Compatibilization of PE/PLA Blends by an Interfacially Localized Catalyst," *ACS Macro Lett.*, vol. 4, no. 1, pp. 30–33, Jan. 2015.

[17] M. P. Arrieta, E. Fortunati, F. Dominici, E. Rayón, J. López, and J. M. Kenny, "Multifunctional PLA–PHB/cellulose nanocrystal films: Processing, structural and thermal properties," *Carbohydr. Polym.*, vol. 107, pp. 16–24, Jul. 2014.

[18] E. Landreau, L. Tighzert, C. Bliard, F. Berzin, and C. Lacoste, "Morphologies and properties of plasticized starch/polyamide compatibilized blends," *Eur. Polym. J.*, vol. 45, no. 9, pp. 2609–2618, 2009.

[19] T. D. Fornes and D. R. Paul, "Structure and Properties of Nanocomposites Based on Nylon-11 and -12 Compared with Those Based on Nylon-6," *Macromolecules*, vol. 37, no. 20, pp. 7698–7709, Oct. 2004.

[20] T. L. Boykin and R. B. Moore, "The role of specific interactions and transreactions on the compatibility of polyester ionomers with poly(ethylene terephthalate) and nylon 6,6," *Polym. Eng. Sci.*, vol. 38, no. 10, pp. 1658–1665, 1998.

[21] S. Fakirov, M. Evstatiev, and S. Petrovich, "Microfibrillar Reinforced Composites from Binary and Ternary Blends of Polyesters and Nylon 6," *Macromolecules*, vol. 26, no. 19, pp. 5219–5226, 1993.

[22] G. Stoclet, R. Seguela, and J.-M. Lefebvre, "Morphology, thermal behavior and mechanical properties of binary blends of compatible biosourced polymers: Polylactide/polyamide11," *Polymer.*, vol. 52, no. 6, pp. 1417–1425, Mar. 2011.

[23] W. Dong, X. Cao, and Y. Li, "High-performance biosourced poly(lactic acid)/polyamide 11 blends with controlled salami structure," *Polym. Int.*, vol. 63, no. 16, pp. 1094–1100, 2013.

[24] R. Patel, D. A. Ruehle, J. R. Dorgan, P. Halley, and D. Martin, "Biorenewable blends of polyamide-11 and polylactide," *Polym. Eng. Sci.*, vol. 54, no. 7, pp. 1523–1532, Jul. 2014.

[25] A. Nuzzo, S. Coiai, S. C. Carroccio, N. T. Dintcheva, C. Gambarotti, and G. Filippone, "Heat-Resistant Fully Bio-Based Nanocomposite Blends Based on Poly(lactic acid)," *Macromol. Mater. Eng.*, vol. 299, no. 1, pp. 31–40, Jan. 2014.

[26] A. Nuzzo, E. Bilotti, T. Peijs, D. Acierno, and G. Filippone, "Nanoparticle-induced co-continuity in immiscible polymer blends – A comparative study on bio-based PLA-PA11 blends filled with organoclay, sepiolite, and carbon nanotubes," *Polymer.*, vol. 55, no. 19, pp. 1–12, Aug. 2014.

[27] E. Jalali Dil and B. D. Favis, “Localization of micro- and nano-silica particles in heterophase poly(lactic acid)/poly(butylene adipate-co-terephthalate) blends,” *Polymer.*, vol. 76, pp. 295–306, 2015.

[28] E. Jalali Dil and B. D. Favis, “Localization of micro and nano- silica particles in a high interfacial tension poly(lactic acid)/low density polyethylene system,” *Polymer.*, vol. 77, pp. 156–166, 2015.

[29] E. Jalali Dil, N. Virgilio, and B. D. Favis, “The effect of the interfacial assembly of nano-silica in poly(lactic acid)/poly(butylene adipate-co-terephthalate) blends on morphology, rheology and mechanical properties,” *Eur. Polym. J.*, vol. 85, pp. 635–646, 2016.

[30] A. Taghizadeh and B. D. Favis, “Carbon nanotubes in blends of polycaprolactone/thermoplastic starch.,” *Carbohydr. Polym.*, vol. 98, no. 1, pp. 189–98, Oct. 2013.

[31] M. A. S. Azizi Samir, F. Alloin, and A. Dufresne, “Review of Recent Research into Cellulosic Whiskers, Their Properties and Their Application in Nanocomposite Field,” *Biomacromolecules*, vol. 6, no. 2, pp. 612–626, 2005.

[32] S. J. Eichhorn, “Cellulose nanowhiskers: promising materials for advanced applications,” *Soft Matter*, vol. 7, no. 2, pp. 303–315, 2011.

[33] K. Ben Azouz, E. C. Ramires, W. Van den Fonteyne, N. El Kissi, and A. Dufresne, “Simple Method for the Melt Extrusion of a Cellulose Nanocrystal Reinforced Hydrophobic Polymer,” *ACS Macro Lett.*, vol. 1, no. 1, pp. 236–240, Jan. 2012.

[34] M. R. Kamal and V. Khoshkava, “Effect of cellulose nanocrystals (CNC) on rheological and mechanical properties and crystallization behavior of PLA/CNC nanocomposites,” *Carbohydr. Polym.*, vol. 123, pp. 105–114, Jun. 2015.

[35] V. Khoshkava and M. R. Kamal, “Effect of surface energy on dispersion and mechanical properties of polymer/nanocrystalline cellulose nanocomposites.,” *Biomacromolecules*, vol. 14, no. 9, pp. 3155–63, Sep. 2013.

[36] V. Khoshkava and M. R. Kamal, “Effect of Cellulose Nanocrystals (CNC) Particle Morphology on Dispersion and Rheological and Mechanical Properties of Polypropylene/CNC Nanocomposites,” *ACS Appl. Mater. Interfaces*, vol. 6, no. 11, pp. 8146–8157, Jun. 2014.

[37] D. Bagheriasl, P. J. Carreau, C. Dubois, and B. Riedl, “Properties of polypropylene and polypropylene/poly(ethylene-co-vinyl alcohol) blend/CNC nanocomposites,” *Compos. Sci. Technol.*, vol. 117, pp. 357–363, 2015.

[38] D. Bagheriasl, P. J. Carreau, B. Riedl, C. Dubois, and W. Y. Hamad, “Shear rheology of polylactide (PLA)–cellulose nanocrystal (CNC) nanocomposites,” *Cellulose*, vol. 23, no. 3, pp. 1–13, 2016.

[39] S. J. Eichhorn, A. Dufresne, M. Aranguren, N. E. Marcovich, J. R. Capadona, S. J. Rowan, C. Weder, W. Thielemans, M. Roman, S. Renneckar, W. Gindl, S. Veigel, J.

Keckes, H. Yano, K. Abe, M. Nogi, A. N. Nakagaito, A. Mangalam, J. Simonsen, A. S. Benight, A. Bismarck, L. A. Berglund, and T. Peijs, “Review: current international research into cellulose nanofibres and nanocomposites,” *J. Mater. Sci.*, vol. 45, no. 1, pp. 1–33, Jan. 2010.

[40] A. Arias, M. C. Heuzey, M. A. Huneault, G. Ausias, and A. Bendahou, “Enhanced dispersion of cellulose nanocrystals in melt-processed polylactide-based nanocomposites,” *Cellulose*, vol. 22, no. 1, pp. 483–498, Feb. 2015.

[41] D. Bondeson and K. Oksman, “Polylactic acid/cellulose whisker nanocomposites modified by polyvinyl alcohol,” *Compos. Part A Appl. Sci. Manuf.*, vol. 38, no. 12, pp. 2486–2492, 2007.

[42] M. Pereda, N. El Kissi, and A. Dufresne, “Extrusion of Polysaccharide Nanocrystal Reinforced Polymer Nanocomposites through Compatibilization with Poly(ethylene oxide),” *ACS Appl. Mater. Interfaces*, vol. 6, no. 12, pp. 9365–9375, Jun. 2014.

[43] M. A. S. Azizi Samir, F. Alloin, J. Y. Sanchez, and A. Dufresne, “Cellulose nanocrystals reinforced poly(oxyethylene),” *Polymer.*, vol. 45, no. 12, pp. 4149–4157, 2004.

[44] M. Roohani, Y. Habibi, N. M. Belgacem, G. Ebrahim, A. N. Karimi, and A. Dufresne, “Cellulose whiskers reinforced polyvinyl alcohol copolymers nanocomposites,” *Eur. Polym. J.*, vol. 44, no. 8, pp. 2489–2498, 2008.

[45] K. Van de Velde and P. Kiekens, “Biopolymers: overview of several properties and consequences on their applications,” *Polym. Test.*, vol. 21, no. 4, pp. 433–442, 2002.

[46] M. Jamshidian, E. A. Tehrany, M. Imran, M. Jacquot, and S. Desobry, “Poly-Lactic Acid: Production, Applications, Nanocomposites, and Release Studies,” *Compr. Rev. Food Sci. Food Saf.*, vol. 9, no. 5, pp. 552–571, 2010.

[47] L. T. Lim, R. Auras, and M. Rubino, “Processing technologies for poly(lactic acid),” *Prog. Polym. Sci.*, vol. 33, no. 8, pp. 820–852, 2008.

[48] O. Martin and L. Avérous, “Poly(lactic acid): plasticization and properties of biodegradable multiphase systems,” *Polymer.*, vol. 42, no. 14, pp. 6209–6219, 2001.

[49] G. Perego and G. D. Cella, “Mechanical Properties,” in *Poly(lactic acid) : synthesis, structures, properties, processing, and applications*, R. Auras, L. T. Lim, S. E. M. Selke, and H. Tsuji, Eds. Hoboken, New Jersey: John Wiley & Sons, Inc., 2010.

[50] I. Engelberg and J. Kohn, “Physicomechanical properties of degradable polymers used in medical applications - A comparative-study,” *Biomaterials*, vol. 12, no. 3, pp. 292–304, 1991.

[51] M. Ajioka, K. Enomoto, K. Suzuki, and A. Yamaguchi, “Basic properties of polylactic acid produced by the direct condensation polymerization of lactic-acid,” *Bull. Chem. Soc. Jpn.*, vol. 68, no. 8, pp. 2125–2131, 1995.

[52] A. Sodergard and M. Stolt, “Properties of lactic acid based polymers and their correlation

with composition," *Prog. Polym. Sci.*, vol. 27, no. 6, pp. 1123–1163, 2002.

[53] R. Rulkens and C. Koning, "Chemistry and Technology of Polyamides," in *Polymer Science: A Comprehensive Reference, 10 Volume Set*, vol. 5, 2012, pp. 431–467.

[54] C. W. Macosko, "Morphology development and control in immiscible polymer blends," *Macromol. Symp.*, vol. 149, no. 1, pp. 171–184, Jan. 2000.

[55] S. Wu, "Polymer interface and adhesion," *M. Dekker*, 1982.

[56] L. A. Girifalco and R. J. Good, "A Theory for the Estimation of Surface and Interfacial Energies. I. Derivation and Application to Interfacial Tension," *J. Phys. Chem.*, vol. 61, no. 7, pp. 904–909, Jul. 1957.

[57] S. Wu, "Calculation of interfacial tension in polymer systems," *J. Polym. Sci. Part C Polym. Symp.*, vol. 34, no. 1, pp. 19–30, Mar. 1971.

[58] P. Xing, M. Bousmina, D. Rodrigue, and M. R. Kamal, "Critical Experimental Comparison between Five Techniques for the Determination of Interfacial Tension in Polymer Blends: Model System of Polystyrene/Polyamide-6," *Macromolecules*, vol. 33, no. 21, pp. 8020–8034, 2000.

[59] P. H. M. Elemans, J. M. H. Janssen, and H. E. H. Meijer, "The measurement of interfacial tension in polymer/polymer systems: The breaking thread method," *J. Rheol. (N. Y. N. Y).*, vol. 34, no. 8, pp. 1311–1325, 1990.

[60] S. Tomotika, "On the Instability of a Cylindrical Thread of a Viscous Liquid Surrounded by Another Viscous Fluid," *Proc. R. Soc. London Ser. A*, vol. 150, no. 870, pp. 322–337, 1935.

[61] N. R. Demarquette, "Evaluation of experimental techniques for determining interfacial tension between molten polymers," *Int. Mater. Rev.*, vol. 48, no. 4, pp. 247–269, Aug. 2003.

[62] C. J. Carriere, A. Cohen, and C. B. Arends, "Estimation of Interfacial Tension Using Shape Evolution of Short Fibers," *J. Rheol. (N. Y. N. Y).*, vol. 33, no. 5, pp. 681–689, 1989.

[63] A. Cohen and C. J. Carriere, "Analysis of a retraction mechanism for imbedded polymeric fibers," *Rheol. Acta*, vol. 28, no. 3, pp. 223–232, 1989.

[64] J. K. Kim, W. Y. Jeong, J. M. Son, and H. K. Jeon, "Interfacial tension measurement of a reactive polymer blend by the Neumann triangle method," *Macromolecules*, vol. 33, no. 25, pp. 9161–9165, 2000.

[65] X. Zhang and J. K. Kim, "Interfacial tension measurement with the Neumann triangle method," *Macromol. Rapid Commun.*, vol. 19, no. 9, pp. 499–504, 1998.

[66] N. Virgilio, P. Desjardins, G. L'Espérance, and B. D. Favis, "Modified interfacial tensions measured in situ in ternary polymer blends demonstrating partial wetting," *Polymer.*, vol.

51, no. 6, pp. 1472–1484, Mar. 2010.

[67] P. Pötschke and D. R. Paul, “Formation of Co-continuous Structures in Melt-Mixed Immiscible Polymer Blends,” *J. Macromol. Sci. Part C Polym. Rev.*, vol. 43, no. 1, pp. 87–141, 2003.

[68] B. D. Favis, C. Lavallee, and A. Derdouri, “PREPARATION OF COMPOSITE DISPERSED PHASE MORPHOLOGIES IN INCOMPATIBLE AND COMPATIBLE BLENDS DURING MELT PROCESSING,” *J. Mater. Sci.*, vol. 27, no. 15, pp. 4211–4218, 1992.

[69] S. Ravati and B. D. Favis, “Morphological states for a ternary polymer blend demonstrating complete wetting,” *Polymer.*, vol. 51, no. 20, pp. 4547–4561, 2010.

[70] B. D. Favis, “The effect of processing parameters on the morphology of an immiscible binary blend,” *J. Appl. Polym. Sci.*, vol. 39, no. 2, pp. 285–300, 1990.

[71] B. D. Favis, “POLYMER ALLOYS AND BLENDS - RECENT ADVANCES,” *Can. J. Chem. Eng.*, vol. 69, no. 3, pp. 619–625, 1991.

[72] B. D. Favis and J. P. Chalifoux, “Influence of composition on the morphology of polypropylene/polycarbonate blends,” *Polymer.*, vol. 29, no. 10, pp. 1761–1767, 1988.

[73] B. D. Favis and J. M. Willis, “Phase size composition dependence in immiscible blends - experimental and theoretical considerations,” *J. Polym. Sci. Part B-Polymer Phys.*, vol. 28, no. 12, pp. 2259–2269, 1990.

[74] J. Li and B. D. Favis, “Characterizing co-continuous high density polyethylene/polystyrene blends,” *Polymer.*, vol. 42, no. 11, pp. 5047–5053, 2001.

[75] N. Mekhilef, B. D. Favis, and P. J. Carreau, “Morphological stability, interfacial tension, and dual-phase continuity in polystyrene-polyethylene blends,” *J. Polym. Sci. Part B-Polymer Phys.*, vol. 35, no. 2, pp. 293–308, 1997.

[76] A. T. Hedegaard, L. Gu, and C. W. Macosko, “Effect of extensional viscosity on cocontinuity of immiscible polymer blends,” *J. Rheol. (N. Y. N. Y).*, vol. 59, no. 6, pp. 1397–1417, 2015.

[77] S. Huang, L. Bai, M. Trifkovic, X. Cheng, and C. W. Macosko, “Controlling the Morphology of Immiscible Cocontinuous Polymer Blends via Silica Nanoparticles Jammed at the Interface,” *Macromolecules*, vol. 49, no. 10, pp. 3911–3918, May 2016.

[78] G. I. Taylor, “The Viscosity of a Fluid Containing Small Drops of Another Fluid,” *Proc. R. Soc. London. Ser. A, Contain. Pap. a Math. Phys. Character*, vol. 138, no. 834, pp. 41–48, 1932.

[79] G. I. Taylor, “The Formation of Emulsions in Definable Fields of Flow,” *Proc. R. Soc. A Math. Phys. Eng. Sci.*, vol. 146, no. 858, pp. 501–523, Oct. 1934.

[80] H. P. GRACE†, “DISPERSION PHENOMENA IN HIGH VISCOSITY IMMISCIBLE

FLUID SYSTEMS AND APPLICATION OF STATIC MIXERS AS DISPERSION DEVICES IN SUCH SYSTEMS," *Chem. Eng. Commun.*, vol. 14, no. 3–6, pp. 225–277, Mar. 1982.

[81] B. D. Favis and J. P. Chalifoux, "The effect of viscosity ratio on the morphology of polypropylene/polycarbonate blends during processing," *Polym. Eng. Sci.*, vol. 27, no. 21, pp. 1591–1600, Nov. 1987.

[82] S. Wu, "Formation of dispersed phase in incompatible polymer blends: Interfacial and rheological effects," *Polym. Eng. Sci.*, vol. 27, no. 5, pp. 335–343, Mar. 1987.

[83] G. Wildes, H. Keskkula, and D. R. Paul, "Morphology of PC/SAN blends: effect of reactive compatibilization, SAN concentration, processing, and viscosity ratio," *J. Polym. Sci. Part B Polym. Phys.*, vol. 37, no. 1, pp. 71–82, Jan. 1999.

[84] P. A. Bhadane, M. F. Champagne, M. A. Huneault, F. Tofan, and B. D. Favis, "Continuity development in polymer blends of very low interfacial tension," *Polymer.*, vol. 47, no. 8, pp. 2760–2771, 2006.

[85] B. D. Favis and D. Therrien, "FACTORS INFLUENCING STRUCTURE FORMATION AND PHASE SIZE IN AN IMMISCIBLE POLYMER BLEND OF POLYCARBONATE AND POLYPROPYLENE PREPARED BY TWIN-SCREW EXTRUSION," *Polymer.*, vol. 32, no. 8, pp. 1474–1481, 1991.

[86] U. Sundararaj and C. W. Macosko, "Drop Breakup and Coalescence in Polymer Blends: The Effects of Concentration and Compatibilization," *Macromolecules*, vol. 28, no. 8, pp. 2647–2657, 1995.

[87] Z. H. Yuan and B. D. Favis, "Coarsening of immiscible co-continuous blends during quiescent annealing," *AIChE J.*, vol. 51, no. 1, pp. 271–280, 2005.

[88] G. Li and B. D. Favis, "Morphology Development and Interfacial Interactions in Polycaprolactone/Thermoplastic-Starch Blends," *Macromol. Chem. Phys.*, vol. 211, no. 3, pp. 321–333, 2010.

[89] R. González-Nuñez, M. Arellano, F. J. Moscoso, V. M. González-Romero, and B. D. Favis, "Determination of a limiting dispersed phase concentration for coalescence in PA6/HDPE blends under extensional flow," *Polymer.*, vol. 42, no. 12, pp. 5485–5489, Jun. 2001.

[90] N. Tokita, "Analysis of Morphology Formation in Elastomer Blends," *Rubber Chem. Technol.*, vol. 50, no. 2, pp. 292–300, May 1977.

[91] J. C. Lepers, B. D. Favis, and R. J. Tabar, "The relative role of coalescence and interfacial tension in controlling dispersed phase size reduction during the compatibilization of polyethylene terephthalate/polypropylene blends," *J. Polym. Sci. Part B-Polymer Phys.*, vol. 35, no. 14, pp. 2271–2280, 1997.

[92] J. C. Lepers and B. D. Favis, "Interfacial tension reduction and coalescence suppression in compatibilized polymer blends," *AIChE J.*, vol. 45, no. 4, pp. 887–895, 1999.

[93] J. J. Elmendorp and A. K. Van Der Vegt, “A study on polymer blending microrheology: Part IV. The influence of coalescence on blend morphology origination,” *Polym. Eng. Sci.*, vol. 26, no. 19, pp. 1332–1338, Oct. 1986.

[94] S. Ravati and B. D. Favis, “Morphological states for a ternary polymer blend demonstrating complete wetting,” *Polymer.*, vol. 51, no. 20, pp. 4547–4561, 2010.

[95] D. R. Paul and J. W. Barlow, “Polymer Blends,” *J. Macromol. Sci. Part C Polym. Rev.*, vol. 18, no. 1, pp. 109–168, 1980.

[96] A. Luciani and J. Jarrin, “Morphology development in immiscible polymer blends,” *Polym. Eng. Sci.*, vol. 36, no. 12, pp. 1619–1626, 1996.

[97] D. Bourry and B. D. Favis, “Cocontinuity and phase inversion in HDPE/PS blends: Influence of interfacial modification and elasticity,” *J. Polym. Sci. Part B-Polymer Phys.*, vol. 36, no. 11, pp. 1889–1899, 1998.

[98] S. Steinmann, W. Gronski, and C. Friedrich, “Quantitative rheological evaluation of phase inversion in two-phase polymer blends with cocontinuous morphology,” *Rheol. Acta*, vol. 41, no. 1–2, pp. 77–86, 2002.

[99] R. C. Willemse, A. Posthuma de Boer, J. van Dam, and A. D. Gotsis, “Co-continuous morphologies in polymer blends: a new model,” *Polymer.*, vol. 39, no. 24, pp. 5879–5887, 1998.

[100] S. Steinmann, W. Gronski, and C. Friedrich, “Cocontinuous polymer blends: Influence of viscosity and elasticity ratios of the constituent polymers on phase inversion,” *Polymer.*, vol. 42, no. 15, pp. 6619–6629, 2001.

[101] R. C. Willemse, A. Posthuma de Boer, J. van Dam, and A. D. Gotsis, “Co-continuous morphologies in polymer blends: the influence of the interfacial tension,” *Polymer.*, vol. 40, no. 4, pp. 827–834, 1999.

[102] J. M. Li, P. L. Ma, and B. D. Favis, “The role of the blend interface type on morphology in cocontinuous polymer blends,” *Macromolecules*, vol. 35, no. 6, pp. 2005–2016, 2002.

[103] R. C. Willemse, E. J. J. Ramaker, J. Van Dam, and A. P. De Boer, “Coarsening in molten quiescent polymer blends: The role of the initial morphology,” *Polym. Eng. Sci.*, vol. 39, no. 9, pp. 1717–1725, 1999.

[104] J. K. Lee and C. D. Han, “Evolution of polymer blend morphology during compounding in an internal mixer,” *Polymer.*, vol. 40, no. 23, pp. 6277–6296, 1999.

[105] H. Veenstra, B. J. J. van Lent, J. van Dam, and A. P. de Boer, “Co-continuous morphologies in polymer blends with SEBS block copolymers,” *Polymer.*, vol. 40, no. 24, pp. 6661–6672, 1999.

[106] H. Veenstra, J. Van Dam, and A. P. de Boer, “On the coarsening of co-continuous morphologies in polymer blends: effect of interfacial tension, viscosity and physical cross-links,” *Polymer.*, vol. 41, no. 8, pp. 3037–3045, 2000.

[107] T. S. Omonov, C. Harrats, G. Groeninckx, and P. Moldenaers, “Anisotropy and instability of the co-continuous phase morphology in uncompatibilized and reactively compatibilized polypropylene/polystyrene blends,” *Polymer.*, vol. 48, no. 18, pp. 5289–5302, 2007.

[108] Z. H. Yuan and B. D. Favis, “Influence of the efficacy of interfacial modification on the coarsening of cocontinuous PS/HDPE blends during quiescent annealing,” *J. Polym. Sci. Part B-Polymer Phys.*, vol. 44, no. 4, pp. 711–721, 2006.

[109] C. R. López-Barrón and C. W. Macosko, “A new model for the coarsening of cocontinuous morphologies,” *Soft Matter*, vol. 6, no. 12, p. 2637, Jun. 2010.

[110] J. R. Bell, K. Chang, C. R. López-Barrón, C. W. Macosko, and D. C. Morse, “Annealing of Cocontinuous Polymer Blends: Effect of Block Copolymer Molecular Weight and Architecture,” *Macromolecules*, vol. 43, no. 11, pp. 5024–5032, Jun. 2010.

[111] H. Veenstra, J. Van Dam, and A. Posthuma de Boer, “On the coarsening of co-continuous morphologies in polymer blends: effect of interfacial tension, viscosity and physical cross-links,” *Polymer.*, vol. 41, no. 8, pp. 3037–3045, Apr. 2000.

[112] T. S. Omonov, C. Harrats, P. Moldenaers, and G. Groeninckx, “Phase continuity detection and phase inversion phenomena in immiscible polypropylene/polystyrene blends with different viscosity ratios,” *Polymer.*, vol. 48, no. 20, pp. 5917–5927, 2007.

[113] P. Sarazin and B. D. Favis, “Morphology control in co-continuous poly(L-lactide)/polystyrene blends: A route towards highly structured and interconnected porosity in poly(L-lactide) materials,” *Biomacromolecules*, vol. 4, no. 6, pp. 1669–1679, 2003.

[114] C. W. Macosko, H. K. Jeon, and T. R. Hoye, “Reactions at polymer–polymer interfaces for blend compatibilization,” *Prog. Polym. Sci.*, vol. 30, no. 8, pp. 939–947, 2005.

[115] K. D. and and G. Groeninckx*, “Interfacial Graft Copolymer Formation during Reactive Melt Blending of Polyamide 6 and Styrene−Maleic Anhydride Copolymers,” 1999.

[116] N. C. Beck Tan, S.-K. Tai, and R. M. Briber, “Morphology control and interfacial reinforcement in reactive polystyrene/amorphous polyamide blends,” *Polymer.*, vol. 37, no. 16, pp. 3509–3519, 1996.

[117] H. K. J. and and J. K. Kim*, “Effect of Reaction Rate on Morphological Change of Reactive Blends,” 2000.

[118] P. Guegan, C. W. Macosko, T. Ishizone, A. Hirao, and S. Nakahama, “Kinetics of Chain Coupling at Melt Interfaces,” *Macromolecules*, vol. 27, no. 18, pp. 4993–4997, Aug. 1994.

[119] G. H. Fredrickson, “Diffusion-Controlled Reactions at Polymer-Polymer Interfaces,” *Phys. Rev. Lett.*, vol. 76, no. 18, pp. 3440–3443, Apr. 1996.

[120] B. O’Shaughnessy and U. Sawhney, “Polymer Reaction Kinetics at Interfaces,” *Phys. Rev. Lett.*, vol. 76, no. 18, pp. 3444–3447, Apr. 1996.

[121] H. K. Jeon, C. W. Macosko, B. Moon, T. R. Hoye, and Z. Yin, "Coupling Reactions of End- vs Mid-Functional Polymers," *Macromolecules*, vol. 37, no. 7, pp. 2563–2571, 2004.

[122] J. Jiao, E. J. Kramer, S. De Vos, M. Möller, and C. Koning, "Morphological changes of a molten polymer/polymer interface driven by grafting," *Macromolecules*, vol. 32, no. 19, pp. 6261–6269, 1999.

[123] F. Mathilde, I. Iliopoulos, M. Milléquant, J. J. Flat, and L. Leibler, "Graft copolymers of poly(methyl methacrylate) and polyamide-6: Synthesis by reactive blending and characterization," *Macromolecules*, vol. 39, no. 20, pp. 6905–6912, 2006.

[124] T. D. Jones, J. S. Schulze, C. W. Macosko, and T. P. Lodge, "Effect of thermodynamic interactions on reactions at polymer/polymer interfaces," *Macromolecules*, vol. 36, no. 19, pp. 7212–7219, 2003.

[125] C. E. Scott and C. W. Macosko, "Morphology development during the initial stages of polymer-polymer blending," *Polymer.*, vol. 36, no. 3, pp. 461–470, 1995.

[126] W. Zhao, X. Zhao, M. H. Rafailovich, J. Sokolov, R. J. Composto, S. D. Smith, T. P. Russell, W. D. Dozier, T. Mansfield, and M. Satkowski, "Segregation of chain ends to polymer melt surfaces and interfaces," *Macromolecules*, vol. 26, no. 3, pp. 561–562, May 1993.

[127] J. S. Schulze, J. J. Cernohous, A. Hirao, T. P. Lodge, and C. W. Macosko, "Reaction kinetics of end-functionalized chains at a polystyrene/poly(methyl methacrylate) interface," *Macromolecules*, vol. 33, no. 4, pp. 1191–1198, 2000.

[128] B. Moon, T. R. Hoye, and C. W. Macosko, "Synthesis and application of fluorescently labeled phthalic anhydride (PA) functionalized polymers by ATRP," *Polymer.*, vol. 43, no. 20, pp. 5501–5509, 2002.

[129] M. Hiljanen-Vainio, P. Varpomaa, J. Seppälä, and P. Törmälä, "Modification of poly(L-lactides) by blending: mechanical and hydrolytic behavior," *Macromol. Chem. Phys.*, vol. 197, no. 4, pp. 1503–1523, Apr. 1996.

[130] M. E. Broz, D. L. VanderHart, and N. R. Washburn, "Structure and mechanical properties of poly(d,l-lactic acid)/poly(ε-caprolactone) blends," *Biomaterials*, vol. 24, no. 23, pp. 4181–4190, 2003.

[131] G. Maglio, A. Migliozzi, R. Palumbo, B. Immirzi, and M. G. Volpe, "Compatibilized poly(ϵ-caprolactone)/poly(L-lactide) blends for biomedical uses," *Macromol. Rapid Commun.*, vol. 20, no. 4, pp. 236–238, 1999.

[132] L. Wang, W. Ma, R. A. Gross, and S. P. McCarthy, "Reactive compatibilization of biodegradable blends of poly(lactic acid) and poly(ε-caprolactone)," *Polym. Degrad. Stab.*, vol. 59, no. 1, pp. 161–168, 1998.

[133] L. Jiang, M. P. Wolcott, and J. Zhang, "Study of biodegradable polylactide/poly(butylene adipate-co-terephthalate) blends," *Biomacromolecules*, vol. 7, no. 1, pp. 199–207, 2006.

[134] M. Kumar, S. Mohanty, S. K. Nayak, and M. Rahail Parvaiz, “Effect of glycidyl methacrylate (GMA) on the thermal, mechanical and morphological property of biodegradable PLA/PBAT blend and its nanocomposites,” *Bioresour. Technol.*, vol. 101, no. 21, pp. 8406–8415, 2010.

[135] A. P. T. Pezzin, G. O. R. A. Van Ekenstein, C. A. C. Zavaglia, G. Ten Brinke, and E. A. R. Duek, “Poly(para-dioxanone) and poly(L-lactic acid) blends: thermal, mechanical, and morphological properties,” *J. Appl. Polym. Sci.*, vol. 88, no. 12, pp. 2744–2755, Jun. 2003.

[136] S. Ravati, C. Beaulieu, A. M. Zolali, and B. D. Favis, “High performance materials based on a self-assembled multiple-percolated ternary blend,” *AIChE J.*, vol. 60, no. 8, pp. 3005–3012, Aug. 2014.

[137] J.-S. Yoon, W.-S. Lee, K.-S. Kim, I.-J. Chin, M.-N. Kim, and C. Kim, “Effect of poly(ethylene glycol)-block-poly(L-lactide) on the poly[(R)-3-hydroxybutyrate]/poly(L-lactide) blends,” *Eur. Polym. J.*, vol. 36, no. 2, pp. 435–442, 2000.

[138] S. Iannace, L. Ambrosio, S. J. Huang, and L. Nicolais, “Poly(3-hydroxybutyrate)-co-(3-hydroxyvalerate)/Poly-L-lactide blends: Thermal and mechanical properties,” *J. Appl. Polym. Sci.*, vol. 54, no. 10, pp. 1525–1535, Dec. 1994.

[139] T. Semba, K. Kitagawa, U. S. Ishiaku, and H. Hamada, “The effect of crosslinking on the mechanical properties of polylactic acid/polycaprolactone blends,” *J. Appl. Polym. Sci.*, vol. 101, no. 3, pp. 1816–1825, Aug. 2006.

[140] H. Tsuji, T. Yamada, M. Suzuki, and S. Itsuno, “Part 7. Effects of poly(L-lactide-co-?-caprolactone) on morphology, structure, crystallization, and physical properties of blends of poly(L-lactide) and poly(?-caprolactone),” *Polym. Int.*, vol. 52, no. 2, pp. 269–275, Feb. 2003.

[141] G.-X. Chen and J.-S. Yoon, “Morphology and thermal properties of poly(L-lactide)/poly(butylene succinate-co-butylene adipate) compounded with twice functionalized clay,” *J. Polym. Sci. Part B Polym. Phys.*, vol. 43, no. 5, pp. 478–487, Mar. 2005.

[142] P. Choudhary, S. Mohanty, S. K. Nayak, and L. Unnikrishnan, “Poly(L-lactide)/polypropylene blends: Evaluation of mechanical, thermal, and morphological characteristics,” *J. Appl. Polym. Sci.*, vol. 121, no. 6, pp. 3223–3237, 2011.

[143] Y. Hu, Y. S. Hu, V. Topolkaraev, A. Hiltner, and E. Baer, “Crystallization and phase separation in blends of high stereoregular poly(lactide) with poly(ethylene glycol),” *Polymer.*, vol. 44, no. 19, pp. 5681–5689, Sep. 2003.

[144] A. N. Gaikwad, E. R. Wood, T. Ngai, and T. P. Lodge, “Two Calorimetric Glass Transitions in Miscible Blends Containing Poly(ethylene oxide),” *Macromolecules*, vol. 41, no. 7, pp. 2502–2508, Apr. 2008.

[145] A. J. Nijenhuis, E. Colstee, D. W. Grijpma, and A. J. Pennings, “High molecular weight poly(l-lactide) and poly(ethylene oxide) blends: thermal characterization and physical

properties," *Polymer.*, vol. 37, no. 26, pp. 5849–5857, Jan. 1996.

[146] L. V. Labrecque, R. A. Kumar, V. Dav, R. A. Gross, and S. P. McCarthy, "Citrate esters as plasticizers for poly(lactic acid)," *J. Appl. Polym. Sci.*, vol. 66, no. 8, pp. 1507–1513, Nov. 1997.

[147] Z. Ren, H. Li, X. Sun, S. Yan, and Y. Yang, "Fabrication of High Toughness Poly(lactic acid) by Combining Plasticization with Cross-linking Reaction," *Ind. Eng. Chem. Res.*, vol. 51, no. 21, pp. 7273–7278, May 2012.

[148] Z. Kulinski, E. Piorkowska, K. Gadzinowska, and M. Stasiak, "Plasticization of Poly (l-lactide) with Poly (propylene glycol)," *Biomacromolecules*, vol. 7, no. 7, pp. 2128–2135, Jul. 2006.

[149] Y. Yang, Z. Xiong, L. Zhang, Z. Tang, R. Zhang, and J. Zhu, "Isosorbide dioctoate as a 'green' plasticizer for poly(lactic acid)," *Mater. Des.*, vol. 91, pp. 262–268, Feb. 2016.

[150] I. Pillin, N. Montrelay, and Y. Grohens, "Thermo-mechanical characterization of plasticized PLA: Is the miscibility the only significant factor?," *Polymer.*, vol. 47, no. 13, pp. 4676–4682, 2006.

[151] S. Jacobsen and H. G. Fritz, "Plasticizing polylactide - The effect of different plasticizers on the mechanical properties," *Polym. Eng. Sci.*, vol. 39, no. 7, pp. 1303–1310, 1999.

[152] M. Baiardo, G. Frisoni, M. Scandola, M. Rimelen, D. Lips, K. Ruffieux, and E. Wintermantel, "Thermal and mechanical properties of plasticized poly(L-lactic acid)," *J. Appl. Polym. Sci.*, vol. 90, no. 7, pp. 1731–1738, 2003.

[153] Z. Kulinski and E. Piorkowska, "Crystallization, structure and properties of plasticized poly(l-lactide)," *Polymer.*, vol. 46, no. 23, pp. 10290–10300, Nov. 2005.

[154] D. R. Paul and L. M. Robeson, "Polymer nanotechnology: Nanocomposites," *Polymer.*, vol. 49, no. 15, pp. 3187–3204, Jul. 2008.

[155] F. Fenouillot, P. Cassagnau, and J. C. Majesté, "Uneven distribution of nanoparticles in immiscible fluids: Morphology development in polymer blends," *Polymer.*, vol. 50, no. 6, pp. 1333–1350, 2009.

[156] I. Kvien, B. S. Tanem, and K. Oksman, "Characterization of cellulose whiskers and their nanocomposites by atomic force and electron microscopy," *Biomacromolecules*, vol. 6, no. 6, pp. 3160–3165, 2005.

[157] N. Bitinis, R. Verdejo, J. Bras, E. Fortunati, J. M. Kenny, L. Torre, and M. A. López-Manchado, "Poly(lactic acid)/natural rubber/cellulose nanocrystal bionanocomposites Part I. Processing and morphology," *Carbohydr. Polym.*, vol. 96, no. 2, pp. 611–620, 2013.

[158] A.-C. Baudouin, J. Devaux, and C. Bailly, "Localization of carbon nanotubes at the interface in blends of polyamide and ethylene–acrylate copolymer," *Polymer.*, vol. 51, no. 6, pp. 1341–1354, 2010.

[159] L. Elias, F. Fenouillot, J. C. Majesté, G. Martin, and P. Cassagnau, "Migration of nanosilica particles in polymer blends," *J. Polym. Sci. Part B Polym. Phys.*, vol. 46, no. 18, pp. 1976–1983, 2008.

[160] W. Li, J. Karger-Kocsis, and A. K. Schlarb, "Dispersion of TiO_2 Particles in PET/PP/TiO_2 and PET/PP/PP -*g*- MA/TiO_2 Composites Prepared with Different Blending Procedures," *Macromol. Mater. Eng.*, vol. 294, no. 9, pp. 582–589, Sep. 2009.

[161] M. Gültner, A. Göldel, and P. Pötschke, "Tuning the localization of functionalized MWCNTs in SAN/PC blends by a reactive component," *Compos. Sci. Technol.*, vol. 72, no. 1, pp. 41–48, 2011.

[162] S. Bose, A. R. Bhattacharyya, P. V. Kodgire, and A. Misra, "Fractionated crystallization in PA6/ABS blends: Influence of a reactive compatibilizer and multiwall carbon nanotubes," *Polymer.*, vol. 48, no. 1, pp. 356–362, 2007.

[163] Y. Liu and M. Kontopoulou, "Effect of filler partitioning on the mechanical properties of TPO/nanosilica composites," *J. Vinyl Addit. Technol.*, vol. 13, no. 3, pp. 147–150, Sep. 2007.

[164] J. Chen, Y. Shi, J. Yang, N. Zhang, T. Huang, C. Chen, Y. Wang, and Z. Zhou, "A simple strategy to achieve very low percolation threshold via the selective distribution of carbon nanotubes at the interface of polymer blends," *J. Mater. Chem.*, vol. 22, no. 42, p. 22398, 2012.

[165] A. Göldel, A. Marmur, G. R. Kasaliwal, P. Pötschke, and G. Heinrich, "Shape-Dependent Localization of Carbon Nanotubes and Carbon Black in an Immiscible Polymer Blend during Melt Mixing," *Macromolecules*, vol. 44, no. 15, pp. 6094–6102, Aug. 2011.

[166] M. H. Al-Saleh and U. Sundararaj, "An innovative method to reduce percolation threshold of carbon black filled immiscible polymer blends," *Compos. Part A Appl. Sci. Manuf.*, vol. 39, no. 2, pp. 284–293, 2008.

[167] D. Wu, D. Lin, J. Zhang, W. Zhou, M. Zhang, Y. Zhang, D. Wang, and B. Lin, "Selective Localization of Nanofillers: Effect on Morphology and Crystallization of PLA/PCL Blends," *Macromol. Chem. Phys.*, vol. 212, no. 6, pp. 613–626, 2011.

[168] L. Elias, F. Fenouillot, J. C. Majesté, P. Alcouffe, and P. Cassagnau, "Immiscible polymer blends stabilized with nano-silica particles: Rheology and effective interfacial tension," *Polymer.*, vol. 49, no. 20, pp. 4378–4385, 2008.

[169] A. L. Persson and H. Bertilsson, "Viscosity difference as distributing factor in selective absorption of aluminium borate whiskers in immiscible polymer blends," *Polymer.*, vol. 39, no. 23, pp. 5633–5642, 1998.

[170] A. Göldel, G. Kasaliwal, and P. Pötschke, "Selective Localization and Migration of Multiwalled Carbon Nanotubes in Blends of Polycarbonate and Poly(styrene-acrylonitrile)," *Macromol. Rapid Commun.*, vol. 30, no. 6, pp. 423–429, Mar. 2009.

[171] L. Elias, F. Fenouillot, J. C. Majeste, and P. Cassagnau, "Morphology and rheology of

immiscible polymer blends filled with silica nanoparticles," *Polymer.*, vol. 48, no. 20, pp. 6029–6040, 2007.

[172] X. Zhao, J. Zhao, J.-P. Cao, D. Wang, G.-H. Hu, F. Chen, and Z.-M. Dang, "Effect of the selective localization of carbon nanotubes in polystyrene/poly(vinylidene fluoride) blends on their dielectric, thermal, and mechanical properties," *Mater. Des.*, vol. 56, pp. 807–815, 2014.

[173] S. H. Lee, M. Bailly, and M. Kontopoulou, "Morphology and Properties of Poly(propylene)/Ethylene-Octene Copolymer Blends Containing Nanosilica," *Macromol. Mater. Eng.*, vol. 297, no. 1, pp. 95–103, Jan. 2012.

[174] M. Bailly and M. Kontopoulou, "Preparation and characterization of thermoplastic olefin/nanosilica composites using a silane-grafted polypropylene matrix," *Polymer.*, vol. 50, no. 11, pp. 2472–2480, 2009.

[175] J. S. Hong, Y. K. Kim, K. H. Ahn, and S. J. Lee, "Shear-induced migration of nanoclay during morphology evolution of PBT/PS blend," *J. Appl. Polym. Sci.*, vol. 108, no. 1, pp. 565–575, Apr. 2008.

[176] M. Si, T. Araki, H. Ade, A. L. D. Kilcoyne, R. Fisher, J. C. Sokolov, and M. H. Rafailovich, "Compatibilizing Bulk Polymer Blends by Using Organoclays," *Macromolecules*, vol. 39, no. 14, pp. 4793–4801, 2006.

[177] G. Filippone, N. T. Dintcheva, F. P. La Mantia, and D. Acierno, "Using organoclay to promote morphology refinement and co-continuity in high-density polyethylene/polyamide 6 blends – Effect of filler content and polymer matrix composition," *Polymer.*, vol. 51, no. 17, pp. 3956–3965, 2010.

[178] G. Filippone, N. T. Dintcheva, D. Acierno, and F. P. La Mantia, "The role of organoclay in promoting co-continuous morphology in high-density poly(ethylene)/poly(amide) 6 blends," *Polymer.*, vol. 49, no. 5, pp. 1312–1322, 2008.

[179] Q. Zhang, H. Yang, and Q. Fu, "Kinetics-controlled compatibilization of immiscible polypropylene/polystyrene blends using nano-SiO2 particles," *Polymer.*, vol. 45, no. 6, pp. 1913–1922, 2004.

[180] L. As'habi, S. H. Jafari, B. Baghaei, H. A. Khonakdar, P. Pötschke, and F. Böhme, "Structural analysis of multicomponent nanoclay-containing polymer blends through simple model systems," *Polymer.*, vol. 49, no. 8, pp. 2119–2126, 2008.

[181] A. Taguet, P. Cassagnau, and J.-M. Lopez-Cuesta, "Structuration, selective dispersion and compatibilizing effect of (nano)fillers in polymer blends," *Prog. Polym. Sci.*, vol. 39, no. 8, pp. 1526–1563, Apr. 2014.

[182] B. B. Khatua, D. J. Lee, H. Y. Kim, and J. K. Kim, "Effect of Organoclay Platelets on Morphology of Nylon-6 and Poly(ethylene- r an -propylene) Rubber Blends," *Macromolecules*, vol. 37, no. 7, pp. 2454–2459, Apr. 2004.

[183] S. H. Lee, M. Kontopoulou, and C. B. Park, "Effect of nanosilica on the co-continuous

morphology of polypropylene/polyolefin elastomer blends," *Polymer.*, vol. 51, no. 5, pp. 1147–1155, Mar. 2010.

[184] G. Z. Wu, B. P. Li, and J. D. Jiang, "Carbon black self-networking induced co-continuity of immiscible polymer blends," *Polymer.*, vol. 51, no. 9, pp. 2077–2083, 2010.

[185] Z. Fang, Y. Xu, and L. Tong, "Effect of clay on the morphology of binary blends of polyamide 6 with high density polyethylene and HDPE-graft-acrylic acid," *Polym. Eng. Sci.*, vol. 47, no. 5, pp. 551–559, May 2007.

[186] R. Salehiyan, Y. Yoo, W. J. Choi, and K. Hyun, "Characterization of Morphologies of Compatibilized Polypropylene/Polystyrene Blends with Nanoparticles via Nonlinear Rheological Properties from FT-Rheology," *Macromolecules*, vol. 47, no. 12, pp. 4066–4076, Jun. 2014.

[187] S.-K. Lim, E.-P. Hong, Y.-H. Song, H. J. Choi, and I.-J. Chin, "Ternary Poly(styrene- *co* -acrylonitrile)/Poly(vinyl chloride) Blend Composites with Multi-Walled Carbon Nanotubes and Enhanced Physical Characteristics," *Macromol. Mater. Eng.*, vol. 295, no. 4, pp. 329–335, Apr. 2010.

[188] M. Trifkovic, A. T. Hedegaard, M. Sheikhzadeh, S. Huang, and C. W. Macosko, "Stabilization of PE/PEO Cocontinuous Blends by Interfacial Nanoclays," *Macromolecules*, vol. 48, no. 13, pp. 4631–4644, Jul. 2015.

[189] Y. Habibi, L. A. Lucia, and O. J. Rojas, "Cellulose Nanocrystals: Chemistry, Self-Assembly, and Applications," *Chem. Rev.*, vol. 110, no. 6, pp. 3479–3500, Jun. 2010.

[190] G. Siqueira, J. Bras, and A. Dufresne, "Cellulosic Bionanocomposites: A Review of Preparation, Properties and Applications," *Polymers (Basel).*, vol. 2, no. 4, pp. 728–765, 2010.

[191] D. Bondeson, A. Mathew, and K. Oksman, "Optimization of the isolation of nanocrystals from microcrystalline cellulose by acid hydrolysis," *Cellulose*, vol. 13, no. 2, pp. 171–180, Apr. 2006.

[192] S. Beck-Candanedo, Maren Roman, and D. G. Gray, "Effect of Reaction Conditions on the Properties and Behavior of Wood Cellulose Nanocrystal Suspensions," 2005.

[193] S. Elazzouzi-Hafraoui, Y. Nishiyama, J.-L. Putaux, L. Heux, F. Dubreuil, and C. Rochas, "The Shape and Size Distribution of Crystalline Nanoparticles Prepared by Acid Hydrolysis of Native Cellulose," *Biomacromolecules*, vol. 9, no. 1, pp. 57–65, Jan. 2008.

[194] M. Börjesson and G. Westman, "Crystalline Nanocellulose — Preparation , Modification , and Properties," *Cellul. - Fundam. Asp. Curr. Trends*, no. c, pp. 3–22, Dec. 2016.

[195] M. A. S. Azizi Samir, F. Alloin, J. Y. Sanchez, N. El Kissi, and A. Dufresne, "Preparation of Cellulose Whiskers Reinforced Nanocomposites from an Organic Medium Suspension," *Macromolecules*, vol. 37, no. 4, pp. 1386–1393, 2004.

[196] V. Khoshkava, "Ph. D. dessertation on Polypropylene (PP) nanocomposites

incorporating nanocrystalline cellulose (NCC),” Mcgill, 2013.

[197] V. Favier, H. Chanzy, and J. Y. Cavaille, “Polymer Nanocomposites Reinforced by Cellulose Whiskers,” *Macromolecules*, vol. 28, no. 18, pp. 6365–6367, Aug. 1995.

[198] A. Dufresne, “Nanocellulose: a new ageless bionanomaterial,” *Mater. Today*, vol. 16, no. 6, pp. 220–227, 2013.

[199] Long Jiang, E. Morelius, Jinwen Zhang, M. Wolcott, and J. Holbery, “Study of the Poly(3-hydroxybutyrate-co-3-hydroxyvalerate)/Cellulose Nanowhisker Composites Prepared by Solution Casting and Melt Processing,” *J. Compos. Mater.*, vol. 42, no. 24, pp. 2629–2645, 2008.

[200] A. C. Corrêa, E. de Morais Teixeira, V. B. Carmona, K. B. R. Teodoro, C. Ribeiro, L. H. C. Mattoso, and J. M. Marconcini, “Obtaining nanocomposites of polyamide 6 and cellulose whiskers via extrusion and injection molding,” *Cellulose*, vol. 21, no. 1, pp. 311–322, Feb. 2014.

[201] A. Pei, Q. Zhou, and L. A. Berglund, “Functionalized cellulose nanocrystals as biobased nucleation agents in poly(l-lactide) (PLLA) – Crystallization and mechanical property effects,” *Compos. Sci. Technol.*, vol. 70, no. 5, pp. 815–821, 2010.

[202] K. Oksman, A. P. Mathew, D. Bondeson, and I. Kvien, “Manufacturing process of cellulose whiskers/polylactic acid nanocomposites,” *Compos. Sci. Technol.*, vol. 66, no. 15, pp. 2776–2784, 2006.